

University of Alberta

High-Resolution Seismic and Electrical Resistivity Tomography techniques
applied to image and characterize a buried channel

by

Jawwad Ahmad

A thesis submitted to the Faculty of Graduate Studies and Research
in partial fulfillment of the requirements for the degree of

Master of Science

in

Geophysics

Department of Physics

Edmonton, Alberta

Fall 2006

University of Alberta

Library Release Form

Name of Author: Jawwad Ahmad

Title of Thesis: High-Resolution Seismic and Electrical Resistivity
Tomography techniques applied to image and characterize a buried channel

Degree: Master of Science

Year this Degree Granted: 2006

Permission is hereby granted to the University of Alberta Library to reproduce single copies of this thesis and to lend or sell such copies for private, scholarly or scientific research purposes only.

The author reserves all other publication and other rights in association with the copyright in the thesis, and except as herein before provided, neither the thesis nor any substantial portion thereof may be printed or otherwise reproduced in any material form whatsoever without the author's prior written permission.

Signature

Abstract

Buried channels are often filled with a variety of porous and permeable sediments which can act as water and hydrocarbon reservoirs. Ten kilometre long joint high resolution seismic reflection and DC resistivity profiles were acquired in northwest Alberta to better define the position and geological setting of a buried channel. Interpretation of both shows that at its deepest point the channel cuts more than 300-m of Cretaceous formations through a regional unconformity into higher velocity Paleozoic carbonates. The channel fill materials have generally lower seismic velocities and are more resistive than the flanking undisturbed Cretaceous formations. These contrasts allow the channel to be detected on the basis of both refraction and resistivity analysis. The resistivity profile further shows highly resistive zones that may be indicative of shallow gas which correspond to a known producing horizon of nearby wells. The gas zone may also be associated with strong seismic reflection.

University of Alberta

Faculty of Graduate Studies and Research

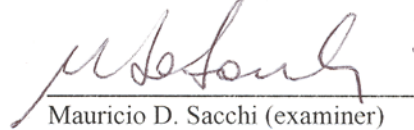
The undersigned certify that they have read, and recommend to the Faculty of Graduate Studies and Research for acceptance, a thesis entitled **High-Resolution Seismic and Electrical Resistivity Tomography techniques applied to image and characterize a buried channel** submitted by **Jawwad Ahmad** in partial fulfillment of the requirements for the degree of **Master of Science**.



Douglas R. Schmitt (supervisor)



Frances R. Fenrich (chair/examiner)



Mauricio D. Sacchi (examiner)



Octavian Catuneanu (examiner)

Date: Sept 7/2006

Acknowledgements

Author is thankful for the financial support received by various resources. Part of this research project was sponsored by NSERC discovery grant to Douglas R. Schmitt. This project was initiated by the Geological Survey of Canada (GSC) and funded through the 'Targeted Geoscience Initiative-2 (TGI-2)'. Thanks to the Department of Physics for giving me opportunity to work as Teaching Assistant (TA) and Research Assistant (RA). For software applications thanks to GEDCO, Calgary for providing seismic data processing software Vista[®] and Hampson-Russell, a Veritas Company, for their tomo-statics software GLI3D[®]. Thanks to Prof. John A. Hole (U of Tech. Virginia) for refraction tomography code and Dr. Barry C. Zelt (U of Hawaii) for visualization package for this. Thanks to Prof. Mauricio D. Sacchi for giving me opportunity to use SUN[®] Workstation, without that tomography was not possible.

I am very thankful to Prof. Doug Schmitt for his continuous technical and moral support throughout the course of the graduate study. I really enjoyed working with him. I was exposed to the industry and attended numerous scientific meeting which significantly improved my technical skills. The credit goes to Doug Schmitt. Without Doug's input in the thesis, his extensive review and addition of material including text and figures, this thesis was not at this current shape. Thank you very much Doug. I also want to acknowledge Prof. Mauricio Sacchi who taught me seismic inversion and tomography that opened a giant scientific field in front of me. Without his teaching that was not possible.

Thanks to Marek Welz and Len Tober for arranging and coordinating seismic acquisition. Also thanks to field crew without their hard work seismic data could not be recorded. Thanks to Alain Plouffe and John Pawlowicz for coordinating in this project from GSC and Alberta Geological Survey (AGS). Dean Rokosh's input in this project is also acknowledged. I am thankful to my fellow graduate

student for their help and cooperation during the course of graduate study. Thanks to Komex, Calgary for acquiring electrical resistivity tomography (ERT) data. Thanks to Jim Mackinnon and Jay Haverstock who were always available to fix computing problems.

In the end, I want to thank my wife Mubushrah, without her love and care I could not concentrate on the research. She always took care of me when I was busy doing research or just pretending to be busy. Moral support from my brothers Munib and Waqar Ji constantly boosted my moral during tough days. My parents and elders always remembered me in their prayers and their spiritual support was with me all the time.

Contents

Chapter 1: Introduction	1
Chapter 2: Literature Review.....	7
2.1. Geophysical Investigation of buried valleys.....	7
2.2. Near Surface Geophysical Techniques	11
2.2.1. Introduction to Seismic Method.....	12
2.2.2. Introduction to Resistivity Method	15
2.3. High Resolution Seismology	18
2.4. Electrical Resistivity Tomography (ERT)	21
2.5. Summary	24
Chapter 3: Geological Overview.....	25
3.1. Geological Setting.....	25
3.2. Gas in the Quaternary Sediments.....	34
3.3. Geophysical Log Response of Quaternary Sediments.....	40
3.4. Summary	50
Chapter 4: Seismic Methodology and Results.....	51
4.1. Seismic Data Acquisition.....	51
4.1.1. Introduction.....	51
4.1.2. Geodetic Surveying.....	57
4.1.3. Seismic Designing Consideration	58
4.1.3.1. Vertical Resolution	58
4.1.3.2. Lateral Resolution.....	60
4.1.3.3. Receiver Station Interval to avoid Aliasing	62
4.1.3.4. Fold	65
4.1.4. Vibroseis Source	67
4.1.5. Seismic Recording Instrument.....	68

4.2. Seismic Data Processing	75
4.2.1. Introduction.....	75
4.2.2. Editing.....	78
4.2.3. Sorting of Seismic Traces	78
4.2.4. Velocity analysis and Normal Moveout (NMO)	84
4.2.5. Static Corrections.....	91
4.2.6. Processing Pitfalls.....	96
4.2.7. Additional Processing Steps	100
4.2.7.1. Pre-stack.....	100
4.2.7.2. Post-stack	102
4.3. Summary	102
 Chapter 5: Electrical Resistivity Tomography (ERT) Methodology and Results	104
5.1. Introduction.....	104
5.2. ERT Acquisition	105
5.3. ERT Inversion.....	111
5.4. ERT Interpretation	112
5.5. Summary	118
 Chapter 6: Interpretation.....	119
6.1. Seismic Refraction Analysis	119
6.1.1 Conventional Refraction Interpretation	124
6.1.1.1. Methodology	125
6.1.1.2. Interpretation.....	129
6.1.2 Refraction Tomography	132
6.1.2.1. Methodology	134
6.1.2.2. Interpretation.....	136
6.2. Seismic Reflection Interpretation	142
6.3. Synthetic Seismogram	147
6.4. Integration Electrical Resistivity Tomography and Seismic	153
6.4.1. Gas Anomaly	154
6.4.2. Specialized Processing.....	158

6.4.2.1. Conventional Processing approach	158
6.4.2.2. Shift stack processing	161
6.5. Summary	164
Chapter 7: Conclusions and future work	167
7.1. Conclusions.....	167
7.2. Future work and Recommendations	171
References.....	175

List of Figures

Figure 2.1: Modified from Huuse et. al., (2003) shows Quaternary buried valley. (a) seismic section; (b) interpreted section.....	11
Figure 2.2: Cartoon showing Seismic reflected and refracted wave with simple two layer case..	14
Figure 2.3: Cartoon showing turning ray - continuously refracted ray over positive velocity gradient subsurface model.....	14
Figure 2.4: Cartoon showing different arrays in resistivity surveying. In the above diagrams C_1 & C_2 are current electrodes and	17
Figure 2.5: ERT sequence of measurements using Wenner array. C_1 , C_2 are current and P_1 , P_2 are potential electrodes.	23
Figure 3.1: Basemap showing location of seismic line, wells and two main Quaternary producing fields i.e. Rainbow and Sausa gas fields.....	30
Figure 3.2: Aerial photo mosaic showing location of seismic line and surface physiographic features.....	31
Figure 3.3: Bedrock topography map modified from Pawlowicz et. al. (2005c) showing location of seismic line, incised valleys.....	32
Figure 3.4: Stratigraphic column based on wells and regional correlation. Generalized Stratigraphic column is based.....	33
Figure 3.5: Geological log redrawn from paper copy of well: 07-25-110-04W-6 showing lithological description of till and	37
Figure 3.6: Photographs showing blow out wells in the Quaternary strata (<100 m). Photographs from	38
Figure 3.7: Geophysical log character of Quaternary sediments (Well: 102012011003W600). The zones.	45
Figure 3.8: Geophysical log of non-channel well (Well: 100112611004600) showing different character as compared to channel well.	46
Figure 3.9: Figure showing crossplot of gamma ray (GR) and density log and colour coded with density porosity. a) Crossplot of	47
Figure 3.10: Regional scale gamma ray (GR) based crossection showing paleo-valley and top of bedrock. Top of the bedrock picked	48

Figure 3.11: Gamma ray (GR) based crossection showing paleo-valley and top of bedrock. Top of the bedrock picked based	49
Figure 4.1: Seismic data acquisition geometry.	54
Figure 4.2: Shot point 360 showing field raw data. Shot point is in the eastern end of the seismic profile.....	55
Figure 4.3: Shot point 1914 showing raw data. Shot point is in the western end of the seismic profile.....	56
Figure 4.4 Wind noise test; also showing background noise level. Few stations are shaking due to noise.....	57
Figure 4.5: Elevation Profile along seismic line. On the top of the X-axis shot point and CMP numbers are marked.....	58
Figure 4.6: The radius of first Fresnel Zone for zero offset data i.e., source and receiver are at same location..	61
Figure 4.7: Bedrock depth crossection based on bedrock topography map of Pawlowicz et. al. (2005) along the seismic profile	61
Figure 4.8: Actual final acquisition Fold	66
Figure 4.9: U of Alberta vibrator working in the field. Photographs courtesy of Marek Welz.	70
Figure 4.10: (a) Vibroseis complete sweep 30 to 250 Hz; (b) early part of the sweep; (c) late part of the sweep.....	71
Figure 4.11: Analysis of pilot sweep; (a) frequency versus time during the linear sweep (see horizontal axis); (b) Amplitude distribution.....	72
Figure 4.12: Effective source Klauder wavelet after autocorrelation of the pilot sweep, mentioned in Figure 4.10.....	73
Figure 4.13: Amplitude spectrum of; (a) correlated pilot of Figure 4.10 and; (b) one trace from shot 690. In Fig-b offset of trace	74
Figure 4.14: Processing flow chart for final stack	77
Figure 4.15: (a) without scaling; (b) with RMS scaling. Correlated pilot trace is visible in extreme left (1 st channel) of Fig-a.	80
Figure 4.16: (a) after AGC 150 msec window, (b) bad traces are killed and ground roll is surgically muted. First break refraction pick.....	81

Figure 4.17: First arrival stretch mute is very important is shallow data processing but not very important in deep reflection.....	82
Figure 4.18: (a) CMP gather without stretch mute and; (b) CMP gather with NMO stretch (15% stretch mute).....	83
Figure 4.19: NMO (Normal moveout correction) principle on CMP gather. NMO hyperbolas are corrected using correct velocity and	85
Figure 4.20: Semblance display of; (a) CMP 750 and; (b) CMP 1825 showing picked velocities (black) and Dix interval velocities	88
Figure 4.21: Interval velocity 10 km. east-west profile	89
Figure 4.22: Mute function; values picked from NMO mute of shallow reflectors (< 200msec) and Top Devonian (~400msec).	90
Figure 4.23: Cartoon showing static correction procedure. After calculating weathering layer thickness and velocity, static correction.....	92
Figure 4.24: Refraction static correction calculated in Vista [®] with fixed datum using plus-minus method. Surface consistent residual static.....	94
Figure 4.25: Showing (top) weathering layer thickness and (bottom) refraction velocity of weathering layer. Replacement velocity.	95
Figure 4.26: (<50 m) velocity profile based on turning ray tomography calculated in GLI3D [®] . The input parameters are.....	96
Figure 4.27: Part of brute stack with; (a) 50 msec AGC; (b) 150 msec AGC; (c) 250 msec AGC window. Correct AGC window is important.	98
Figure 4.28: (a) shows clipping at very near offset traces. The preamplifier gain was set to 24 db to boost weak reflections at far offsets.....	99
Figure 4.29: Part of the brute stack showing stacked refractions as a result of improper first arrival mute. Stacked refractions visible	100
Figure 5.1: Map showing locations of two ERT profiles. Deep ERT profile is about 4 km long, whereas Shallow ERT profile is.....	106
Figure 5.2: ERT field photographs. Cold working conditions made working conditions difficult.	107
Figure 5.3: Shows two acquisition geometries of ERT survey; a) shallow ERT profile with a 15 m electrode spacing that would sense.....	110
Figure 5.4: Measured apparent resistivity section. (a) 15 m electrode spacing with total length of profile 10 km	115

Figure 5.5: Final invested shallow ERT section with; (a) block parameterization and; (b) smooth contouring display..	116
Figure 5.6: Final invested deep ERT section with; (a) block parameterization and; (b) smooth contouring display..	117
Figure 6.1: Cartoon showing refractions and time distance curve. b) Refractions from three horizontally stratified layers of.....	121
Figure 6.2: Shot point 360 showing two refraction layers. Here Quaternary strata are directly lying over Paleozoic Carbonates that gives	126
Figure 6.3: Shot point 1914 showing two layers on refraction. Here the Quaternary strata are overlies the Cretaceous bedrock.....	127
Figure 6.4: Shot point 1848 showing three layers. Here Quaternary strata are overlying Cretaceous sediments. Here the Paleozoic carbonate.....	128
Figure 6.5: Figure shows first arrivals on selected shots. Blue color arrivals are from eastern part of line where Quaternary strata are.....	129
Figure 6.6: Velocity profile after conventional refraction interpretation. '0' metres on depth axis is sea level and depths are positive above.....	131
Figure 6.7: Block diagram showing complete workflow of seismic travel time tomography.	138
Figure 6.8: Tomographic 1D velocity profile. Thick solid line is input velocity model. Medium thick solid line is 1D velocity profile.	139
Figure 6.9: Final complete (10 km east west) velocity model after tomographic inversion. X-axis is UTM easting in kilometres.....	140
Figure 6.10: Zoomed in tomographic velocity profile showing layer cake geology. Isolated velocities anomalies are visible in the profile.	141
Figure 6.11: Conventional time processed seismic reflection profile. Small arrows showing base of the Quaternary deposits.....	145
Figure 6.12: Part of the uninterpreted seismic section (top) and line drawing interpretation (bottom) (Profile from Figure 6.11)..	146
Figure 6.13: Log and synthetic seismogram of a Quaternary well. Synthetic trace is displayed after fix gain. Synthetic seismogram was.	150
Figure 6.14: Log response along with synthetic seismogram of non-Quaternary (Cretaceous) well. Synthetic seismogram was.....	151

Figure 6.15: Comparison of Synthetic trace (well/0829-110-W6 (600 m away from line) and seismic (CMP-450). Seismic trace is.....	152
Figure 6.16: Photograph of producing Quaternary gas well 07-25-110-04W-6. Well number is clearly visible in the photograph	155
Figure 6.17: (a) depth converted seismic section; (b) Electrical Resistivity Tomography (ERT) Profile showing high resistivity anomaly.....	156
Figure 6.18: (a) Seismic – tomographic velocity overlay; (b) seismic and ERT overlay showing channel and associated high resistivity	157
Figure 6.19: shot gather showing bright reflection at ~0.05 sec and offset 40 – 50 m. This reflection is from shallow gas reservoir.....	160
Figure 6.20: Conventional (NMO stack) reprocessed seismic section showing high amplitude reflections at <0.1 sec (small arrows).....	160
Figure 6.21: Shows step by step procedure of shift – stack technique. (a) Shows shot gather with maximum offset 150 m and time.....	162
Figure 6.22: Shift-stack processed seismic section (see text for details). (a) Maximum normalized instantaneous amplitude displayed	163

List of Tables

Table 2.1: Table showing key differences in exploration and near surface seismic reflection surveys	21
Table 3.1: Table showing gas properties in different Quaternary gas pools. Data compiled by Dr. C. D. Rokosh	39
Table 4.1: Seismic acquisition parameters.....	53
Table 4.2: Table shows the subsurface vertical Resolution (metres).....	59
Table 4.3: Table show the horizontal resolution (radius of the first Fresnel Zone)	62
Table 4.4: Table shows the expected bin size with varying geological dip and frequencies in order to avoid spatial aliasing	64
Table 4.5: Table shows theoretical maximum and minimum offset limits for imaging target reflector	66
Table 4.6: Table showing statistics of seismic data	76
Table 4.7: showing fold with respect to mute	90
Table 5.1: Acquisition parameters for ERT survey	106
Table 5.2: Final parameters used to invert ERT data. These parameters were selected after number of trial inversions with different	112
Table 6.1: Table showing statistics of resistivity anomalies observed in Figure 5.5	153

Chapter 1

Introduction

Buried channels exist in many of the recently glaciated regions of the world. Channels are former valleys that were then filled in with weakly consolidated sediments as result of the major surface disturbances of glacial retreat and advance and glacially produced lakes. Such features contain high porosity sands and gravels often saturated with fluids such as water but in many cases even natural gas. These are of course important natural resources. The need for clean ground waters makes these buried channels increasingly important in many part of the planet subject to high population growth and with pollution of existing surface sources. These buried valleys contain larger amounts of aggregate deposits, also an economically important construction material, especially in areas where these are not available at the surface and must otherwise be transported from long distances away. To learn more about how such buried channels, at least in Northern Alberta, may be distinguished a wide variety of information from well logs through to advanced geophysical analysis was used. A second major purpose of this study is to examine the role of different saturating fluids on the geophysical responses such that this might assist in the search for near surface reservoirs of methane or water.

Obviously, due to low drilling costs, natural gas is very economical if discovered at shallow depth ($<100\text{m}$). Most exploration for gas occurs at much greater depths as part of the overall exploration for hydrocarbons. However, it should not be surprising that such gas can be found in the near surface. Indeed, the history of shallow gas is interesting. For example, recent evidence acquired by de Boer and coworkers (2001) found reasonably high concentration of methane and heavier hydrocarbons in ground waters in the vicinity of the sanctuary of Delphi on the

Greek mainland. This site is famous as it housed for many hundred years the 'oracle of Delphi', a local woman called the Pythia who after being enclosed in a small room under the Temple of Apollo would 'assist' leaders in their decision making process. They suggested, also on the basis of a detailed examination of fractures in the area, that the state of intoxication, which according to Plutarch sometimes even led to the death of the Pythia, was induced by inhalation of sweet smelling ethylene which in sufficient concentration is known to hallucinatory effects such as out of body experiences.

More importantly, perhaps, is the fact that the Chinese have been producing near surface natural gas for more than 2000 years. They developed an advanced technology, much in advance of western drilling methods that included bamboo drill strings and pipelines as well as a large assortment of various tools for drilling through different rock types and for repairing the drilled holes. This natural gas, and later the brines associated with them, were used together in a large salt making industry in which the salt was obtained from large pots of brine boiled off using the natural gas as heat. Kuhn (2006) has provided a popular description of the drilling for such gas.

Typically, shallow gas is found in the paleo-valleys filled by glacial sediments. Economical quantities of gas have been found in Northern Alberta in the channel sand within the glacial sediments overlying bedrock. In the past movement of the Ice Age glaciers and ice sheets eroded the underlying bedrock and created low lands. The subglacial meltwater at high pressures is believed to be the main cause of glacial erosion. This water gouges incised or tunnel valleys which at some places are filled by up to 300 m of thick glacial coarse- and fine-grained sediments. Meltwater streams emerging from these glaciers also cut into the existing landform and created incised valleys that may be few hundred metres wide and several kilometres long. These incised valleys further filled by glacial material that may be transported from far away.

At the ice margin, where drainage is blocked and ice dammed lakes were created, and at the places of depressions or topographic lows small pounds or lakes were formed, providing suitable conditions for sediment depositions. The glacial sediments are of Quaternary age¹ and are the result of a few episodes of glaciation and deglaciation. Glacial sediments were deposited during different episodes of glacial advance, retreat and standstill conditions. In addition to this, sediments were also continuously deposited in glacial lake environments that were fed by meltwater streams. The Quaternary sediments consist of clay, sand, till, gravels and conglomerates. Pre-Quaternary landscape is important for establishing paleoenvironment and understanding sediment fill in different successions. The upper Cretaceous² landscape was fluvial to shallow marine in Northern Alberta. Cretaceous rivers were incised into the existing landscape which then covered by glacial episodes in Quaternary period. In order to understand these shallow gas reservoirs, the topography of bedrock surface and particularly location of buried valleys are important. These paleo-valleys are incised into the Cretaceous bedrock and at some places up to the Top Paleozoic³ and filled with up to 300 m of Quaternary sediments. It is usually not possible to locate these buried valleys on the basis of surficial deposits or surface topography; subsurface geophysical imaging techniques or borehole information is necessary to assist in locating and delineating them.

¹ The Quaternary Period is taken to begin ~1.8 Ma to present, and the last major pulses of the Wisconsin glaciation lasted from approximately 0.1 Ma to 10 ka. We will refer to the fill material and the channel as being of Quaternary origin throughout this thesis under that assumption that they resulted from this latest glaciation. However, to our knowledge at this time there have not been any studies that have examined in detail the time during which these channels and the later fill were actually formed. A longer history may not be surprising.

² The Cretaceous Period is currently set from 65 Ma to 114 Ma. Tertiary Period (1.8 Ma to 65 Ma) bedrock sediments do not exist in this area of Alberta.

³ The Paleozoic Era covers the period of early complex life on earth from 248 Ma to 543 Ma. Although the geology of this area will be discussed in more detail later, these older sedimentary layers consisting primarily of well indurated carbonates and shales laid down in a passive continental shelf environment underlie the Western Canada Sedimentary Basin. Throughout this thesis these rocks will variously be referred to as the Paleozoic. The major unconformity that marks the top of these rocks will be referred to as the pre-Cretaceous unconformity and may on occasion also be called the pre-Mannville unconformity.

There is one other important aspect to shallow gas that should not be overlooked. Pressurized shallow gas is also a safety hazard if it is accidentally drilled. It is associated with few blowouts of petroleum and water drilling rigs in the past. In fact, these near surface gas deposits were accidentally discovered through a water well drilling rig blowout in the study area. It is significant drilling hazard for oil and gas wells because it is very shallow ($< 60\text{m}$) and even less than the depth of first surface casing of wells.

In Canada, shallow gas in the glacial sediments was first discovered in Québec in early 50's which later on produced and supplied to the nearby communities. Since mid 90's industry is producing gas from shallow depth intervals ($<100\text{m}$) in the Northern Alberta. This gas is of thermogenic origin being sourced from deeper in the basin. However, some near surface gas deposits can be formed from biological activity. The heating values of thermogenic gas are much higher than swamp gas that makes it more economical because price of the natural gas is calculated based on its heating values. These gas reservoirs are very shallow and capital cost associated with these deposits is very low and that has attracted a good deal of attention. These shallow gas pools are confined to a small area in the Northern Alberta. Within the Quaternary deposits, channel sands serve as reservoir and impermeable clay provides excellent seal. Glacial sediments are deposited all over Canada and there is need to explore shallow gas everywhere. In the Western Canada Sedimentary Basin which is highly prolific for hydrocarbons, especially in the areas where deeper Cretaceous gas is present; the overlying Quaternary deposits might also be charged with natural gas. In the study area, there is possibility that gas is generated by Cretaceous source rock such as Shaftesbury Formation and where Quaternary sediments intersected this, it migrated upward and trapped in these. Other possibility is that gas is migrated upward from leaking Cretaceous reservoir such as Bluesky Formation and trapped in the overlying Quaternary sediments. For these prospects there might be no need to go for extensive studies for petroleum source and migration pathways. The only need is to find buried valleys and look for isolated pockets of channel sand. Wherever

buried valleys intersect the gas bearing Cretaceous sediments, there may be good potential for Quaternary gas because the gas may have migrated upward into the channel fill sediments within the glacial deposits.

To better understand the buried channels, the University of Alberta (U of A) in conjunction with Geological Survey of Canada (GSC) and the Alberta Geological Survey (AGS) initiated a project to acquire high resolution seismic data close to existing shallow Quaternary gas wells between Rainbow Lake and High Level, Northern Alberta. The objectives of the seismic survey were to: 1) to image the surface of Sub-Cretaceous unconformity upon which a maximum of about 300 metre of channel-fill sediments are deposited; 2) to image shallow Quaternary or Tertiary channels resting on and above unconformity and; 3) to create public geoscience information database. After the successful results of the seismic reflection survey, an electrical resistivity tomography (ERT) profile was also recorded at the same line. The objective of the ERT profile was to find resistive anomalies which can be used to identify locations of free gas and fresh water saturated zones.

The thesis starts by reviewing both the seismic and the ERT geophysical imaging methods in Chapter 2. This chapter also includes some case studies of the imaging of buried valleys using above mentioned techniques. Chapter 3 begins to focus on this project's geological setting, glacial deposits, and Quaternary gas potential. An important part of this chapter deals with the geophysical log responses of Quaternary deposits relative to the surrounding areas in which the bedrock is undisturbed. The details of the field seismic acquisition and processing schemes including results from intermediate steps are discussed in chapter 4. In chapter 5, ERT data acquisition, inversion and final results are presented. In chapter 6 seismic refraction and reflection interpretation along with integration of ERT with seismic reflection are discussed. Shallow gas signatures on ERT and seismic reflection profile are also presented here. Chapter 7 gives synoptic conclusions and future work recommendations.

The author has been involved in all aspects of this project right from the field acquisition of the seismic and the ERT data through to the final interpretations. The work has been progressively disseminated at various meetings which includes; 1) oral presentation at Canadian Society of Exploration Geophysicist (CSEG) annual meeting 2005 (Ahmad et. al. 2005a); 2) poster presentation at American Association of Petroleum Geologist (AAPG) annual meeting 2005 (Ahmad et. al. 2005b); 3) poster presentation at American Geophysical Union 2005 annual meeting (Ahmad and Schmitt 2005a); 4) CSEG 2006 annual meeting (Ahmad and Schmitt, 2006a); 5) upcoming Society of Exploration Geophysicist (SEG) 2006 annual meeting (Ahmad and Schmitt 2006b). At CSEG 2005 meeting the author was awarded 'Honorable Mention' on the oral presentation. Preliminary result of this project was also published as an article in the CSEG 'Recorder' (Ahmad and Schmitt, 2005b). Currently a manuscript of this work is in preparation for the Canadian Journal of Earth Science (CJES) special volume. As well, the seismic data will be published and publicly available in an anticipated report from the Geological Survey of Canada (GSC).

Chapter 2

Literature Review

In this chapter, geophysical investigations of buried valleys by seismic and electrical resistivity methods are reviewed. Buried-valleys are often filled with different kind of material including sand, aggregate and even clays. These materials are of economic importance for construction, engineering and hydrogeological purpose. These paleo-valleys/channels are masked under recent/Quaternary glacial material and may not be visible at all from the surface. So, often geophysical methods are required to see and locate these paleo-valleys/channels. The meltwater channel sand or sand lens trapped in these paleo-valleys/channels often contain hydrocarbon or water which are of economic importance. Part of this chapter provides a review of some case histories that use different geophysical techniques to locate these economical resources trapped within these paleo-valleys/channels. The rest of the chapter provides a review of the two geophysical techniques, seismic profiling and electrical resistivity tomography, used in this thesis to image paleo-valley/channels.

2.1. Geophysical Investigations of Buried Valleys

Buried paleo-valleys have great deal of economic importance especially as they contain ground water resources, hydrocarbons and aggregates. Different areas have different need for these resources. Even in Alberta, for example, there is a large need for aggregate materials for construction in the North while the hunt for aquifers is of a primary importance in the South. But for all parts of the world shallow hydrocarbons trapped in these buried valleys have more recently received a good deal of attention from industry and scientific community. Hence it is worthwhile to first see what the status of similar work is globally.

Incised valleys are common in Fennoscandia. These glacial structures contain ground water resources. Detailed study of their stratigraphy is also used in paleoclimate research. High resolution seismic reflection and refraction methods are commonly used to locate and image these glacial structures. Some authors used high resolution seismic techniques to image incised glacial structures for ground water exploration (Juhlin et. al., 2002; Wiederhold et. al., 1998; B ker et. al, 1998). Other authors used high resolution seismic surveying to image glacial deposits and glacial basins for geological purposes (Pugin and Rossetti, 1992; Musil et. al., 2002).

In the late 40's, different authors started studying buried valleys of Alberta and Saskatchewan using geophysical techniques. Stalker (1960) gives extensive details of the location and character of the numerous buried valleys of central and southern Alberta and correlates the current and preglacial drainage patterns. In a study by Hobson et. al. (1970) seismic refraction technique was used to investigate overburden material, stratification within the overburden, the surface of bedrock and elastic constants in the Suffield, Alberta. Lennox and Carlson (1967) used electrical resistivity and seismic refraction geophysical methods to locate buried valleys in the NE Alberta. The economic importance of these buried valleys was the sand and the gravel units that at some places hosted groundwater. The bedrock and glacial material showed variable resistivity contrast and identified on resistivity profiles. Whereas on seismic refraction profile bedrock showed high velocity as compared to the surficial material and this contrast decreased as the distance increased from foothills to the east. Hall and Hajnal (1962) used gravity method to locate and identify the buried valley of South Saskatchewan, in Saskatchewan, Canada. Variations in the density and thickness of the glacial material were the main cause of the gravity anomaly. In this study, trends in the gravity lows were directly corresponded to the buried valley.

Seismic reflection and refraction techniques are successfully used in delineating both the geometry and the depth of paleochannels. Holzschuh (2002) used

compressional (P) and shear (S) wave seismic reflection in combination with P-wave refraction techniques to image a paleochannel which contains ground water. Iaco et. al. (2003) used seismic reflection and refraction tomography to image a landfill and its host sediments. Combined P and S wave reflection and refraction methods were used to image top of the bedrock and reflections within the valley filled with unconsolidated Quaternary sediments (Benjumea et. al., 2003). In this study, the shear wave refraction method is used to mark paleoearthquake locations associated with disturbed zones.

Shallow seismic reflection techniques are also widely used in environmental studies. Boyce and Koseoglu (1996) used high resolution seismic reflection techniques to obtain critical information of a waste disposal site, i.e., on the lateral continuity and geometry of sediments and ground water contaminant pathways. Francese et. al. (2002) used high resolution seismic methods to image waste disposal site near a potash mine area in Western Canada. Different independent sandy-gravel aquifers were identified along this seismic profile. These authors developed a procedure of acquisition and processing of seismic data, which can be used as template to image glacial structures and buried channels in the Western Canada Sedimentary Basin. Groundwater reservoir characterization was carried out using high resolution seismic reflection technique (Olsen et. al., 1993). In this study, facies analysis, seismic and sequence stratigraphic interpretation incorporating well logs were carried out, that supplemented traditional drilling and logging methods and assisted in the development of a new hydrogeological framework.

Sharpe et. al. (2003) used seismic stratigraphy to correlate and map different lithological units of Quaternary age on a high resolution seismic line. Geostatistical analysis of the observed seismic amplitude was also used to identify heterogeneity in the glaciofluvial aquifer. High resolution seismology is sometimes also used in basin studies.

Small scale Cretaceous basins covered under thick glacial drift are identified on high resolution profiles Nova Scotia (Stea and Pullan, 2001). These obscured basins contains unconsolidated quartz-rich sand, kaolinitic clay and lignite, all of these have economic importance in that region. Huuse and Anderson (2000) extensively reviewed Quaternary buried valleys and described their morphology, origins, and the mechanisms associated with glacial erosion in the Danish North Sea. The origin of these valleys is repeated cycles of sub-glacial erosion and down cutting of meltwater channels and their closure followed by ice creep, ultimately generating incised valleys. Figure 2.1 shows classical example of a Quaternary buried valley exploited for groundwater in NW Europe.

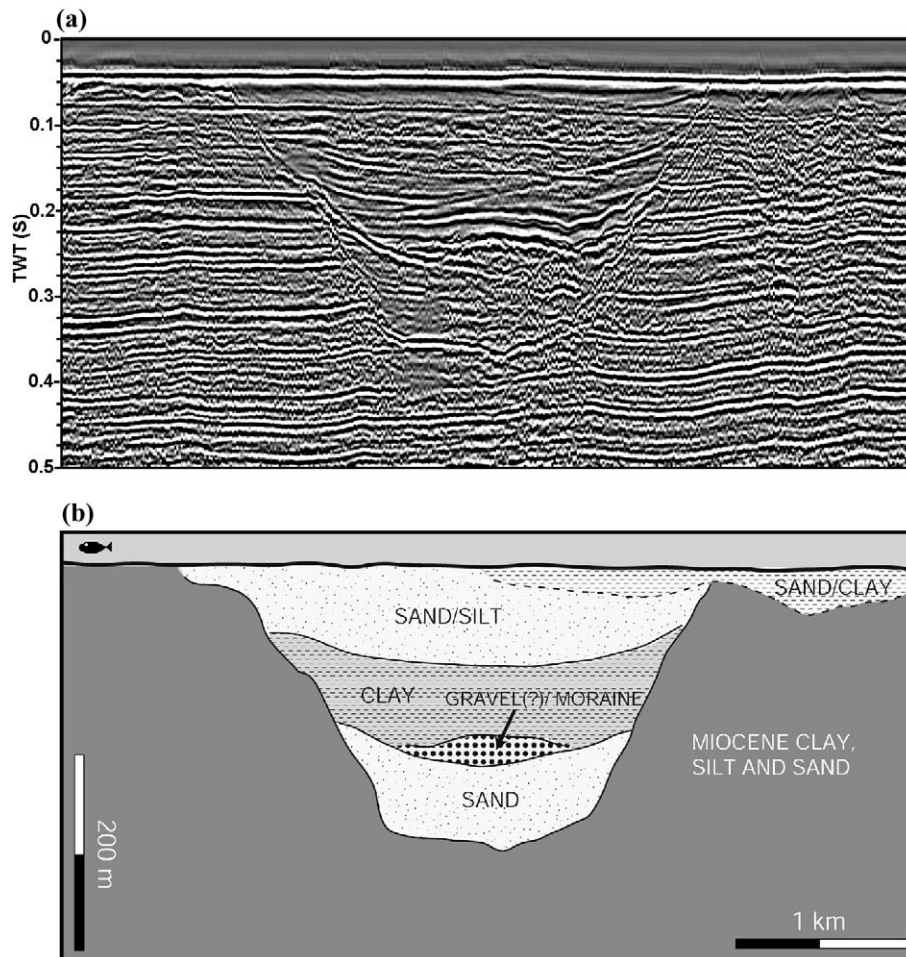


Figure 2.1: Modified from Huuse et. al., (2003) shows Quaternary buried valley. (a) seismic section; (b) interpreted section. This is representative section of Quaternary valleys of NW Europe. Reprinted with permission from Elsevier.

2.2. Near Surface Geophysical Techniques

Common geophysical techniques used in near surface exploration for environmental, natural resources and geotechnical evaluation are; 1) High resolution seismic; 2) Electrical Resistivity tomography (ERT); 3) Magnetic and; 4) Electromagnetic (EM) methods. Butler (2005) provides a good reference of these near surface geophysical techniques. In this chapter, only high resolution seismic and electrical resistivity tomography are reviewed as they are the methods employed in this thesis.

2.2.1. Introduction to Seismic Method

Seismic waves are elastic waves generated by sudden release of energy in the ground or in the water. These seismic waves are further classified as; 1) body waves and; 2) surface waves. Body waves are of two types; 1) compressional (P) waves and; 2) Shear (S) waves. Surface waves are of two types; 1) Love waves and; 2) and Raleigh waves. Surface waves travel along the surface of earth and create loss and damage during earthquake.

Within body waves, P-wave travel faster than S- waves. All of these waves are classified based on their particle motion. Particle motions of P-waves are in the direction of wave propagation whereas the particle motions of S-waves are perpendicular to the wave propagation. The particle motions of surface waves is more complex. At the surface, the particle motion in a Raleigh wave is elliptical and retrograde to the direction of wave propagation and in Love waves, particle motion is horizontal with no vertical motion. For definition of these waves and different terminology regarding exploration seismology refer to Sheriff (2002).

P-wave seismology is mainly used in exploration work. P-waves are the only mode that are employed to provide information about the subsurface in this thesis. With the advancement of seismic instruments and energy sources S-wave seismology is also increasingly used in exploration work. P-wave exploration seismic methods further fall into two broad categories of; 1) reflection seismology; 2) refraction seismology. The former essentially relies on the detection of weak echos from the contacts between differing types of rock in the earth with the final goal of imaging the subsurface structure. Making a reflection profile image requires that a series of corrections be applied to the data in order to increase the signal to the noise, this ‘processing’ of the seismic data will be discussed later. The latter, refraction, method Figure 2.2 and Figure 2.3 does not provide an image but does attempt to describe the geology in terms of the seismic wave speeds and thicknesses of layers. The basic input to this method is the travel times of the first arriving seismic waves from the source.

In seismic reflection, different seismic acquisition geometries can be adapted but basic concept remains the same for all. Essentially, in 2-D active source seismology, the acquisition geometry consists of a line of receivers along which the seismic source is activated. The receivers will in most cases, at least for land surveys, be geophones which provide a voltage proportional to the amplitude of the particle velocity of the ground motion as the wave passes. In the parlance of such exploration, the 'offset' refers to the distance of a given receiver from the seismic source along the surface of the earth. In seismic reflection, seismic energy is reflected back to the surface from underlying layer of higher density and velocity. Whereas in seismic refraction the wave is refracted back to the surface and recorded. For a typical seismic reflection acquisition, refractions are also unavoidably recorded. Hence, the refraction analysis essentially comes for free in the acquisition of high resolution seismic profiling, although their utility can be diminished by the use of geophone groups which average the response sometimes over many tens of metres.

Energy sources for generating seismic waves are of different types and most commonly used land energy sources are dynamite and seismic vibrators. The former gives a sharp and high energy pulse but for a variety of reasons including cost, environmental impact, and safety is often avoided. The latter seismic vibrators mainly consist of a heavy plate mounted on truck. This plate makes contact with the ground and is vibrated through a range of frequencies, called a sweep, which generates a seismic response into the earth that is extracted using knowledge of the input signal as will be described later. The current project employed the truck mounted U of Alberta vibrator.

As seismic waves travel from the source to the receiver their travel time is recorded. The distance between the source and the receiver is known and this travel time is used to calculate velocity of the subsurface material. Note that the term 'velocity' is often used in geophysical jargon, perhaps somewhat incorrectly, to describe the seismic wave speed; keeping with this naming convention this

thesis will employ the term ‘velocity’ throughout. The seismic velocity is an important physical property that can reveal a great deal about the compressibility of the rock and its fluid content.

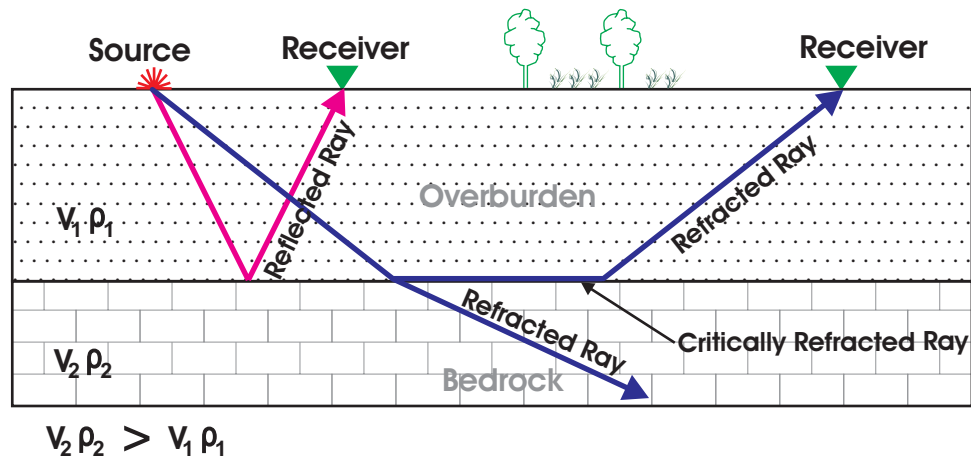


Figure 2.2: Cartoon showing seismic reflected and refracted wave with simple two layer case. Velocity (V_1) and density (ρ_1) of first layer (Overburden) is lower than the velocity (V_2) and density (ρ_2) of second layer (Bedrock).

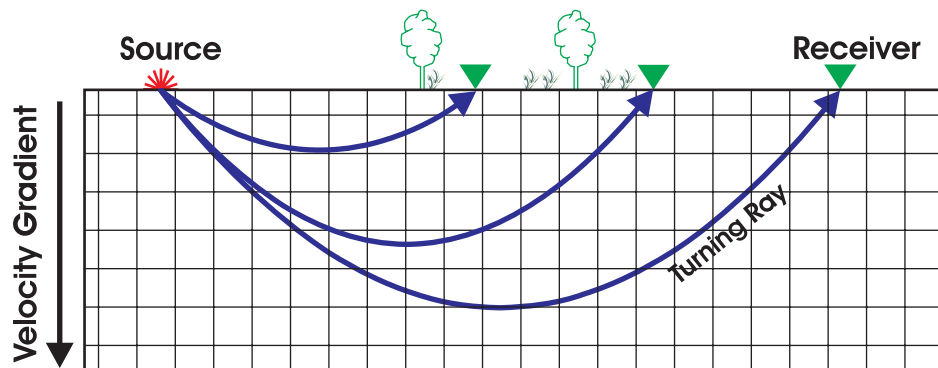


Figure 2.3: Cartoon showing turning ray - continuously refracted ray over positive velocity gradient subsurface model. Each block in this model has different velocity that allow wave to travel obeying Snell's law and turn back to surface. Turning waves are usually used in earthquake seismology but are beginning to find increasing use in near surface studies.

The seismic reflection method is mainly used to produce ‘images’ of the subsurface structure. Seismic refraction analyses, especially if the analysis

includes turning rays, are used to obtain the subsurface velocity information. Together, these methods provide complementary information useful for a geological interpretation.

2.2.2. Introduction to Resistivity Method

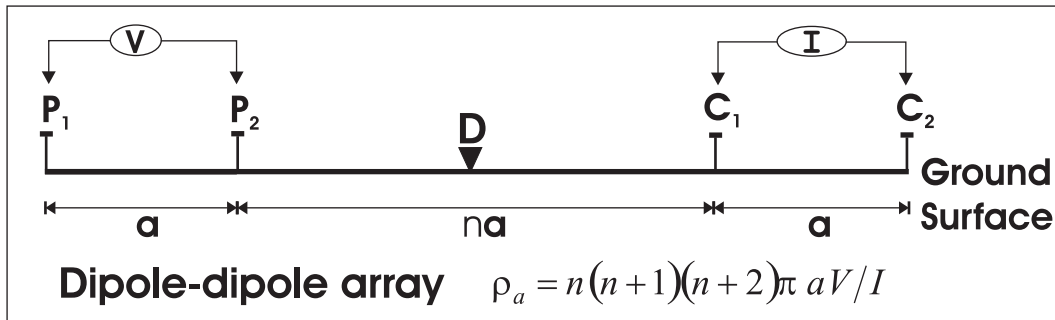
In the early 20th century, the resistivity method was introduced by developing wireline tools used in boreholes to detect and differentiate hydrocarbon from other borehole fluids. Later on, surface based electrical resistivity techniques were established and exclusively used for groundwater studies. Now, electrical resistivity method is widely used in environmental, engineering and ground water studies. In a typical DC electrical resistivity survey current (I) is induced into the ground by placing two current electrodes (C_1 & C_2) and potential difference is measured through two potential electrodes (P_1 & P_2). This technique can easily be employed in a variety of geometries that include: 1) on the ground surface; 2) in the bore holes; and 3) borehole to ground surface and vice versa. Different field arrays (i.e., arrangement of current and potential electrodes) are used to acquire resistivity data either in profiling or sounding mode. In traditional sounding or vertical electrical sounding (VES) mode, data is acquired as a function of depth for one surface location and it is called as depth probe. Whereas in profiling mode electrodes are moved along the profile line in order to measure lateral variation in the subsurface. Characteristically, depth of penetration for sounding is higher than for profiling. Recording of multiple data points at different surface locations gives profile of apparent resistivity values. Keeping in view geological objectives i.e., deeper target or to measure shallow lateral variation along profile, data can be acquired using sounding or profiling method.

The choice of array is a function of subsurface geological objective i.e., hydrocarbon reservoir, aquifer, and geological dykes etc., and ground conditions i.e., snow, marsh, desert etc. The controlling factor in each array is the spacing between the current and the potential electrodes and their relative spacing to each

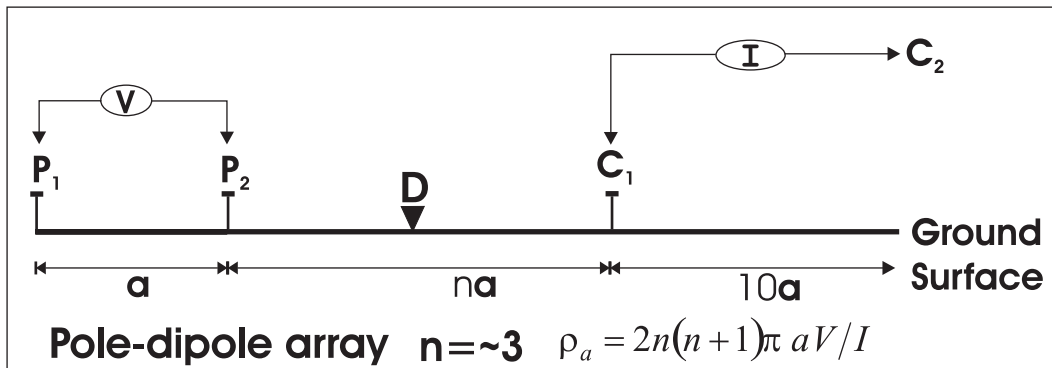
other (Figure 2.4). Wenner and Schlumberger arrays are the most commonly used geometries in conventional resistivity surveying.

The apparent resistivity of the subsurface for different arrays can be calculated using formulas given in the Figure 2.4. The data i.e., potential drop, measured using these arrays gives apparent resistivity value of the subsurface at the centre of the spread (point 'D' Figure 2.4) in Wenner and Schlumberger arrays with some variations for rest of arrays. Depth of investigation is associated with the spacing between these electrodes. Subsurface depth and true resistivities associated with this raw data (apparent resistivity) can be calculated using some kind of interpretation technique i.e., curve matching (curves derived from some analytical models). As this technique is quite old and mature; the variations in interpretation procedures exist that were developed over time.

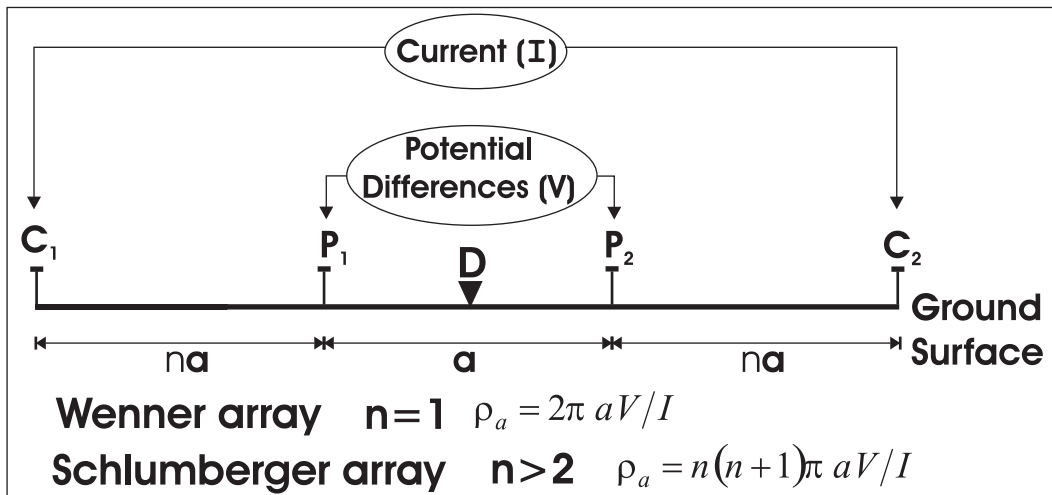
The latest interpretation technique is inversion that converts apparent resistivity section i.e., pseudosection, into true resistivity section. Apparent resistivity values along one profile i.e., as a function of position and electrode separation, can also be displayed in the form of pseudosection or quasi-section that gives general idea of the apparent resistivity variations with position and depth. For a brief description of the electrical resistivity method and practical application of different arrays, refer to Zonge et. al. (2005) and Loke (2004). A detailed description of the resistivity method including interpretation techniques may be found in the classic text by Telford et. al. (1991).



(c)



(b)



(a)

Figure 2.4: Cartoon showing different arrays in resistivity surveying. In the above diagrams C_1 & C_2 are current electrodes and P_1 & P_2 are potential electrodes. a) Wenner and Schlumberger arrays; b) Pole-dipole array; c) Dipole-dipole array. Different arrays are used for geological objectives and surface and subsurface conditions. Point 'D' in almost all figures give the surface location of data collected for particular array. Where ρ_a is apparent resistivity.

2.3. High resolution Seismology

High resolution seismology is a proven technique for imaging shallow geological targets for engineering, hydrogeological, and petroleum purposes. In order to get high spatial resolution closely spaced geophones are necessary while for high temporal resolution higher frequencies are required. High resolution seismic techniques are explained in detail in Brouwer and Helbig (1998) and acquisition and processing pitfalls are described by Steeples et. al. (1997). Processing techniques of near surface reflection data is described in Baker (1999). A free processing software 'Seismic Un*x' can also be used in processing seismic reflection data. Forel et. al. (2005) provides an excellent tutorial for processing and modeling seismic reflection data using Seismic Un*x.

The advancement of personal computers that are required to process seismic data as well as the increased dynamic range of digital seismographs made seismic reflection surveying highly cost effective method (Miller et. al., 1995). Seismic reflection is widely used technique for ground water exploration and engineering studies. During seismic reflection acquisition, the arrival times of refracted waves, often referred to as the 'first breaks', are also recorded and usually used to calculate near surface velocity structure for static correction (see Section 4.2.5). Travel time inversion of first break refraction using turning ray tomography gives an appropriate velocity model that can be used in depth migration. Usually in the presence of shallow water table seismic data deteriorate dramatically especially in the shallow part, because compressional wave velocity (V_p) increases by three to four times in the water-saturated aquifer (Bradford, 2002). Because of this effect conventional NMO velocity analysis fails to give accurate velocity model and prestack depth migration is required to get accurate results (Bradford and Sawyer, 2002; Bradford, 2002). Crosswell tomography and borehole to surface seismology was used to detect geometry of unconsolidated alluvial aquifer with weak lithological contrast among stratigraphic discontinuities (Moret et. al., 2006).

High resolution seismic techniques are widely used in hydrogeological studies. A technique developed in early 80's named 'optimum offset' or 'optimum window' is still very practical in less favorable conditions for seismic reflection acquisition when there is significant surface topography and other near surface problems exist (Whiteley et. al., 1998). In this method an 'optimum' source-receiver offset is selected in which the particular reflection of interest is not interfered with by other seismic arrivals such as the surface waves or the refraction; data acquisition is then restricted to this range of offsets for which the desired reflection is clearly separated from other arrivals. Only a little processing is required for this kind of acquisition geometry.

Pullan and Hunter (1985) described amplitude and phase variations of seismic reflection energy with increasing offset for simple overburden-bedrock interface i.e., change of reflection peak into trough at post critical offset distance - it is mainly dependent on velocity contrast between two layers. In a high resolution seismic survey Diago et. al. (2004) used post critical reflections to image bedrock using conventional reflection processing flow. The motivations of this study were; 1) reflections observed at large offsets are stronger and sharper than the near offset and; 2) reflections at near offset are masked under noise cone and selection of the optimum window is required to speed up acquisition procedure.

One aspect of reflection profiling is that the near surface of the earth is often composed of very slow materials with seismic velocities as low as a few hundred metres per second. Further, the near surface is complicated by both topography and the depth of what is often called the low velocity 'weathered' layer. This complexity causes the deeper seismic reflections to be shifted in time relative to one another; and 'static corrections' are carried out on raw seismic data in order to overcome this serious imaging problem. Static corrections play an important role in high resolution seismic imaging. If there are not much lateral velocity variations then refraction statics give good results. But in case of severe lateral velocity variations tomo-statics are required. Tomo-statics are calculated using

turning ray tomography and inversion procedure (Zhu et. al., 1992). The above mentioned procedures are standard for typical petroleum industry seismology in which the depth of interest is usually > 200 m. All available static correction techniques and their associated pitfalls are described in detail in Cox (1999). Different authors described specialized procedures for calculating static correction for shallow high resolution seismic surveys. Steeples et. al. (1990) described pitfalls and key point in calculating static correction for shallow reflection surveys. Brouwer and Helbig (1998) developed ‘ray tracing static correction’ method that gives better results for shallow structures in high resolution surveys. This technique is iterative process in which velocity model of near surface is known and some kind of comparison of ray traced results and known model is carried out to get final static correction. This method gives almost ‘true static correction’ for shallow datasets. Pugin and Pullan (2000) defined a new technique ‘first arrival alignments static correction’ which they applied on shallow high resolution reflection data. This technique calculates and takes care of short, medium and long wavelength statics (i.e., those that vary over short, intermediate, and far distances along the profile); and can easily be adapted and applied to the near surface seismic data. Any remaining error associate with static correction can be corrected by applying surface consistent residual static correction.

A brief comparison between seismic surveys used for deeper exploration in the Oil and Gas industry with those near surface seismology is shown in Table 2.1. Steeples (2004) explained differences between oil patch and near surface seismic in detail.

Oil Exploration	Near-Surface
Fold is High >30	Low fold is enough <~30
Mute Weathered zone	Use weathered zone
Refractions create no problem	Refractions create big problem
Airwave create no problem	Airwave create big problem
Sweep frequencies 10 – 100 Hz	Sweep frequencies >20 <500Hz
Depth 500 m to 6000m	Depth <100m to 500m
Two way travel time < 3 sec for targets	Two way travel time <400 msec
Geophone groups; 6, 12, 24 or 36 geophones	Usually single geophone
Geophone frequency 10 or 14 Hz	40 Hz or 100 Hz

Table 2.1: Table showing key differences in exploration and near surface seismic reflection surveys. Modified from Steeples (2004).

2.4. Electrical Resistivity Tomography (ERT)

Electrical resistivity tomography (ERT) is an emerging geophysical technique and is even being applied in the petroleum industry. ERT is widely used in engineering and groundwater industries. ERT is a simple technique that derives from standard DC (direct current) electrical resistivity measurements developed decades ago (section 2.2.2).

ERT imaging involves introducing current with two current electrodes and measuring potential difference with two potential electrodes across the surface of ground. The spacing between these electrodes is related with depth of investigation. There are different acquisition methods in ERT imaging. Most commonly used is almost same with standard Wenner profiling. In this technique 20 or more electrodes are placed in the ground with fixed distance, typically from 10 to 30 metres. These electrodes are connected to the recording instrument with multi-core cable. This is called one ‘spread’. The instrument is programmed in such a way that it automatically selects a number of differing sets of current and

potential electrode pairs and switches the distances between them. Hundreds of such measurements are taken in sequence at fixed spread location. Then the spread is laterally shifted and the electrodes are placed in a new location with the process being repeated (Figure 2.5). These immediate measurements of apparent resistivity are then fed to the tomographic inversion code which gives true resistivity of subsurface. Careful parameter selection is required for appropriate tomographic inversion results. In short ERT is combination of DC electrical measurements and tomographic inversion technique. Advancement of personal computers (PC) and tomographic inversion techniques made this technique more accessible and accurate. For detail description of ERT theory and inversion, along with case histories, refer to Daily et. al. (2005). Details of ERT imaging technique along with results will be discussed in Chapter 5.

ERT imaging technique is used to image channels and buried valleys. Baines et. al. (2002) used this technique to image buried channels and valley fill. These authors imaged and differentiated between; 1) buried channel in clay; 2) buried channel, clay and peat, and gravel; and 3) a buried gravel bed (valley fill) in shale bedrock, on ERT profiles. The ERT technique is also used in imaging 3 to 5 km deep geological targets i.e., sediments and metamorphic rocks (Storz et. al., 2000). Stratigraphic studies of recent valley fills give fluvial behavior over past that are used for paleoclimate and basin studies (Froese et. al., 2005). These authors used ground penetrating radar (GPR) and electrical resistivity tomography (ERT) to image present valley fill. Francese et. al. (2005) used high resolution seismic and ERT to image geometry of aquifer system. These authors used the results of ERT inversion i.e., depth of layers; in refraction tomography to obtain the near surface velocity model and using this data calculated the static corrections.

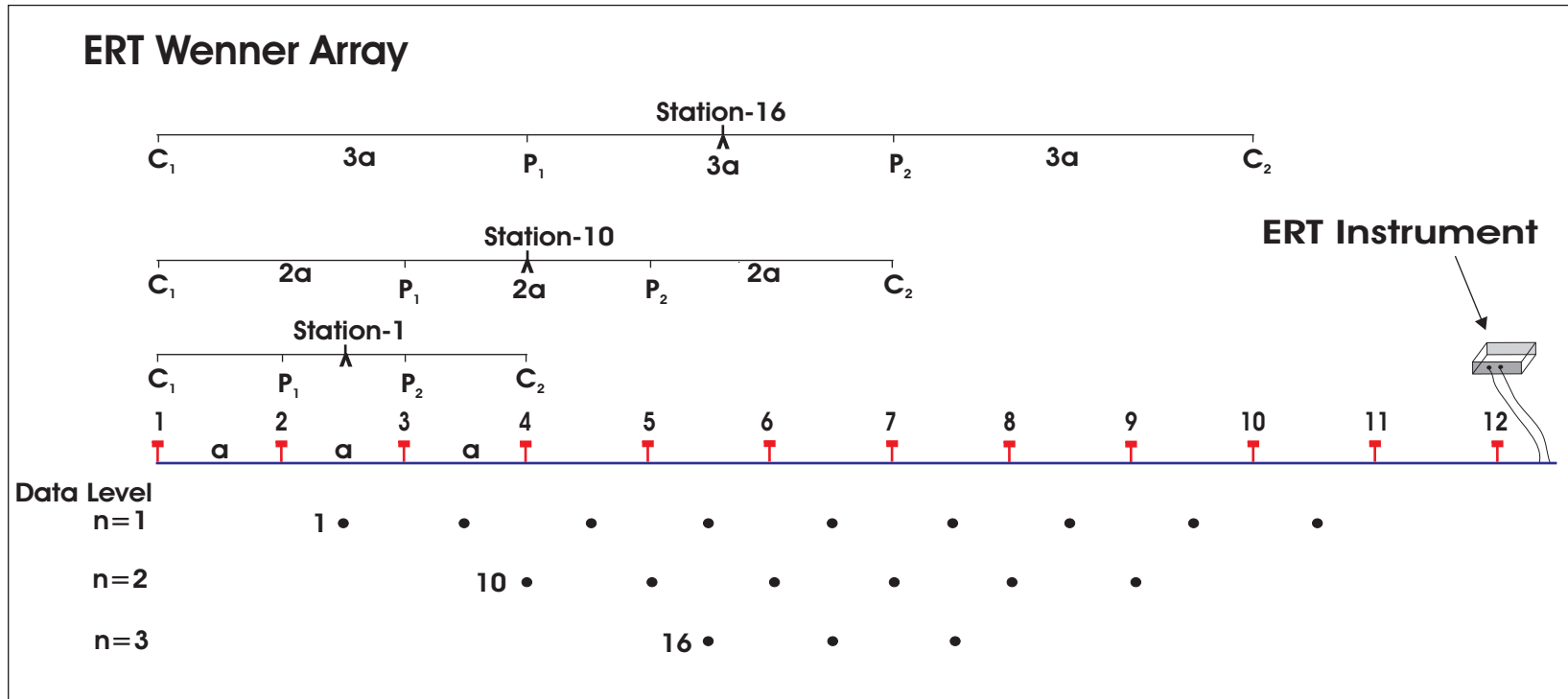


Figure 2.5: ERT sequence of measurements using Wenner array. C_1 , C_2 are current and P_1 , P_2 are potential electrodes. The distance between the electrodes remains the same. However, the symmetric Wenner array will expand in size to make numerous geometrical combinations the responses of which are fed to the inversion.

2.3. Summary

In this chapter different case studies associated with buried valleys and channels are discussed. Common geophysical techniques including seismic and electrical methods, required to image near surface geological targets are also reviewed here. Near surface seismic reflection technique requires careful field parameter selection which is dependent on the type of noise, the target depth, and the available instruments. Special skills are required to clean and process near surface seismic reflection data. Near surface seismology is not only scaling down of conventional exploration seismic but differs in many ways in acquisition and processing techniques. Electrical resistivity tomography (ERT) is slightly new geophysical technique and now widely used in near surface imaging. As ERT gives resistivities of the subsurface formations, one can easily interpret, correlate and link these with real geology/rock type. ERT data is also sensitive to the rock fluids and might be used as fluid indicator of the subsurface rocks. In next chapter high resolution seismic reflection data acquisition and processing is discussed that follows with ERT data acquisition, inversion and interpretation chapter.

Chapter 3

Geological Overview

In this chapter the geological setting, the shallow gas potential, and the geophysical signature of the Quaternary deposits are reviewed. Quaternary deposits in the study area are mainly covering Cretaceous bedrock which seldom is exposed at the surface. These Quaternary sediments are of great economic importance and host surprisingly large gas reservoirs at quite shallow depths in the study area. The reservoir sediments consist of coarse- to fine-grained sand trapped in the channels which are further capped by impermeable clays. The source of the gas appears to be from deeper strata. Deeper source rock, reservoir quality sand and highly impermeable clay completes the petroleum system and increases exploration potential for these small prospects. These Quaternary gas pools are as shallow as 50 metres and highly economical due to the extremely low drilling costs. Signatures of Quaternary and pre-Quaternary borehole geophysical logs are fairly different and Quaternary sediments can be clearly identified on these logs. Geophysical log correlations are made to see the character of these deposits. These correlation covers complete succession of Quaternary deposits within the channel and provides reference for identifying these deposits elsewhere.

2.1. Geological Setting

The study area is located in the extreme north-west corner of Alberta, Canada (~Lat. 58° 35' ~Long. 118° 31'; and according to the designation of the Dominion Land Survey (DLS) system lies within Townships 110 – 111 and Ranges 3 – 4 West of the 6th Meridian) (McKercher and Wolf, 1986) (Figure 3.1; Figure 3.2). The area falls between the present day lowlands bounded to the north by the Cameron hills, to the south by the Clear hills and in the east by Caribou Mountains. The bedrock topography and the surface elevation, the current and

ancient (Cretaceous times - ~100 Million (Ma) years ago) drainage pattern shows almost the same trends in this area (Fenton et. al., 1994). The present landforms in almost all of Northern Alberta consist of Quaternary deposits from the latest Pleistocene glaciations. The bedrock which is masked/covered by Quaternary deposits is rarely directly exposed. However, a large glacial meltwater channel and its tributaries are detected from the bedrock topography map of Pawlowicz et. al. (2004); with its lower end in the southeast direction having elevation difference between head and lower end > 100 m over few 10's of kilometre (Figure 3.3). A small local glacial lake was developed in the study area bounded to the north and the south by local high lands as clearly seen on the bedrock topography map (Pawlowicz et. al., 2004) (Figure 3.3).

Aside from the filled channels, the area is mostly blanketed at the surface with the glacial deposits likely left from the last retreat of the Wisconsin glaciation about 10,000 years ago. Beneath this, the pre-Quaternary succession consists of Cretaceous (~100 Ma) sand/shale, Mississippian/upper Devonian (~340 Ma) Carbonates underlain by thick succession of middle Devonian (~380 Ma) Shale (Figure 3.4). At the locations of the incised valleys, the Quaternary (<~2 Ma) sediments are cut the pre-Quaternary sediments, making the lower contact unconformable. Due to the valley incision different pre-Quaternary formations are eroded. Because of the angular unconformity at the base of Quaternary sediments, it underlies Cretaceous to Devonian age formations at different places within the study area. At different places pre-Quaternary strata (bedrock) consist of Cretaceous shale/sand of the Fort St. John Group, the Cretaceous Bullhead Group, the Mississippian Banff Formation and the Devonian Wabamun formation (Figure 3.4). The detailed overviews of these formations may be found in Mossop and Shetsen (1994). The whole pre-Quaternary package is truncated against the base of Quaternary deposits in the incised valleys (Pawlowicz et. al., 2004).

Paleo-valleys are deeply incised into the Cretaceous strata and even into the top of the Devonian Wabamun Formation. These channels are filled with up to 300 m or

more of what is thought to be Quaternary deposits, consisting of till, glaciolacustrine, and glaciofluvial sediments with interbeds of clay and preglacial fluvial sediments (Pawlowicz et. al., 2004). The Quaternary sediments in this region are dominated by glacial lake deposits (Canadian Discovery Digest, 2004). These glaciolacustrine deposits often consist of fine-grained sand almost absent of pebbles. Such types of materials can serve as good quality reservoirs i.e., the rock can both store substantial volumes of fluids and also allow these fluids to flow easily during production.

The Quaternary valley-fill sediments mainly consist of series of alternating layers of till and coarse grained stratified sediments; the former acts as an aquitard and latter as an aquifer (Fenton et. al., 1994). Also Quaternary sediments in this area are associated with a variety of different geological phenomena; 1) glacial thrusting and; 2) Normal Channel style deposition. Glacial thrusting in the Quaternary sediments have been observed further southeast in the Cold Lake area (Fennell et. al., 2001); and also reported in limited areas of Canadian plains (Klassen, 1989). During Quaternary time Laurentide ice sheet advanced across Alberta and British Columbia towards west and southwest direction (Fenton et. al., 2003). The advance of this thick ice sheet eroded and caused shear failure and near surface thrust faulting in some areas. Conversely, melt waters flowing from these glaciers cut channels into the Cretaceous and even Devonian bedrock. The retreat of the last ice sheet in northeast British Columbia and adjacent Alberta as well as the associated geomorphology of meltwater channels and ice dammed lakes are described in Mathews (1980). The retreat of the Laurentide ice sheet back to the north and northeast blocked local drainage patterns and produced a large ice dammed lake named 'Glacial Lake Peace' (Mathews et. al., 1980; Bednarski, 1999). The ice sheet advanced and retreated at least five times during the Quaternary period resulting alternating layers of glacial and non-glacial deposits (Fenton et. al., 1994). In this study region two different types of channel systems are identified; 1) preglacial channels that have broad shallow walled valleys and represent old Tertiary or Cretaceous river system and; 2) steep walled

meltwater channels during the Quaternary period of glaciations (Andriashek et. al., 2001). These horizontally isolated, vertically stacked meltwater channels are separated by layers of till and are good petroleum reservoirs because till provides an excellent low-permeability seal.

Not much detailed geological work has been done in Quaternary geology of northwest of Peace River, particularly in Rainbow Lake area focused on here. This lack of knowledge contrasts with the better understood Quaternary geology of Athabasca area in northeast Alberta is described in detail in Bednarski (1999) and Sand river area further to the southeast, by Andriashek et. al. (1989). Consequently, we look to these studies to provide some insight into possible Quaternary history in Northeastern Alberta. The Quaternary section in the Sand River area divided into eight different formations with each represent different period of glaciation and/or deglaciation. From the bottom to the top, older to younger, these are: 1) the Empress formation, 2) the Bronson Lake formation, 3) the Muriel Lake, 4) the Bonnyville Formation, 5) the Ethel Lake formation, 6) the Marie Creek Formation, 7) the Sand River Formation, and 8) the Grand Centre Formation (Andriashek, 1989; Fenton et. al., 1994). In a regional context, character and morphology of Quaternary deposits of the Canadian Plains and Cordillera, which includes morainal deposits (till), glacial lake deposits, glaciofluvial deposits and non-glacial deposits are described in Fulton (1989).

In comparison with European glaciated valleys, deeply incised valleys were produced in Canada by movement of Laurentide ice sheet and in Scandinavian countries by Fennoscandia ice sheet. The Quaternary buried valleys (100 – 350 m deep) in the Danish North Sea are deeply incised into the Cretaceous to Pleistocene strata, originated by repeated cycles of sub-glacial down cutting of meltwater channels and postdate glaciotectionic structures (Huuse et. al., 2000). The morphology and origin of the Quaternary valleys of northwest European lowlands are described in detail in articles by Huuse et. al. (2000) and Huuse et. al. (2003). In Canada Quaternary valleys have been identified in northwest,

central and south Alberta, northeast British Columbia, southwest of the Northwest Territories as well as in Québec (Bauman, 2005). In northwest Alberta and northeast British Columbia shallow Quaternary glacial sediments that fill these valleys can be of economic importance for; 1) aggregate sources; 2) diamonds in Kimberlite (Fenton et. al., 1994) and; 3) shallow gas. Bedrock topography and drift thickness maps have been used to identify buried valleys and exploration targets for shallow gas (Pawlowicz et. al., 2004; Pawlowicz et. al., 2005a & b).

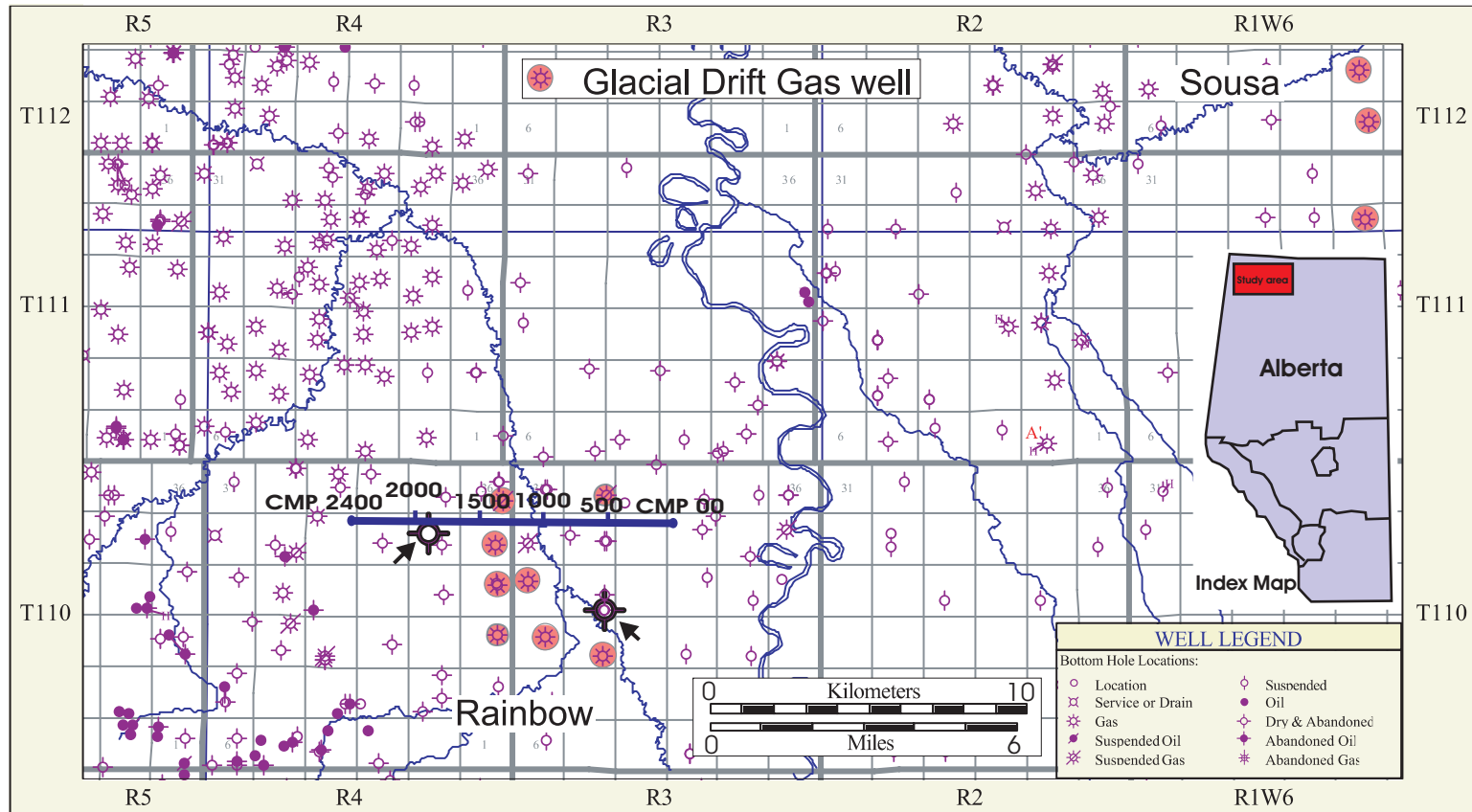


Figure 3.1: Basemap showing location of seismic line, wells and two main Quaternary producing fields i.e., Rainbow and Sousa gas fields (original map provided by Dr. C.D. Rokosh; Map created in Accumap[®]). Arrows in the map showing location of wells used in Figure 3.7 and Figure 3.8.

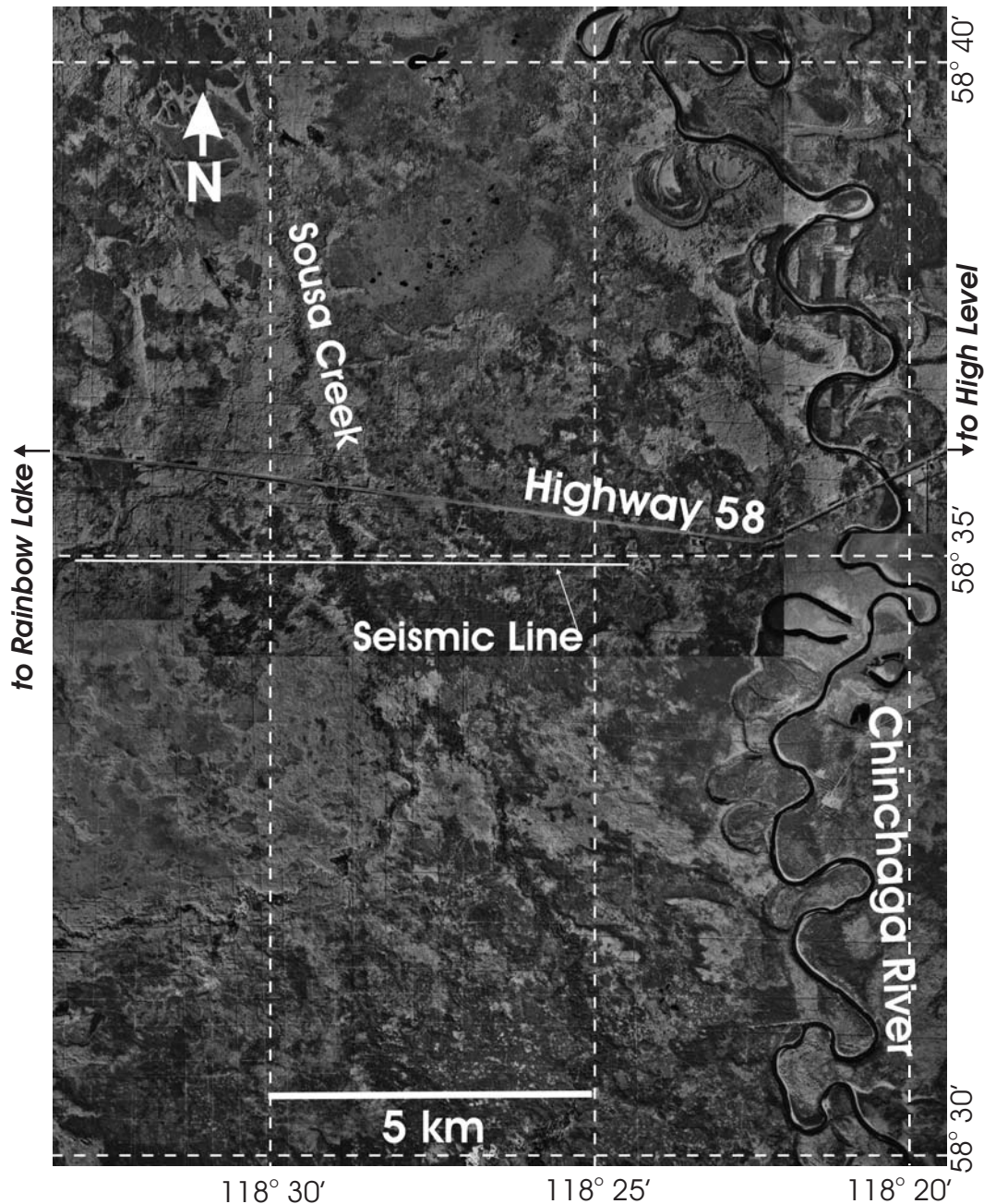


Figure 3.2: Aerial photo mosaic showing location of seismic line and surface physiographic features i.e., road, creek and river. Details of aerial photographs are; year, 1974; original scale, 1:50,000; NTS number, 84L; photograph number LN46-AS1430-126 to 129 and LN47-AS1430-164 to 167. Aerial photographs are scanned and digitally merged and annotated in Adobe Photoshop®. Topographic sheets numbers 84L-5 & 6 are used to locate and mark physiographic features. Total 8 photos used to create above image. Paper copies of Aerial photographs courtesy of 'Air Photo Distribution', Edmonton.

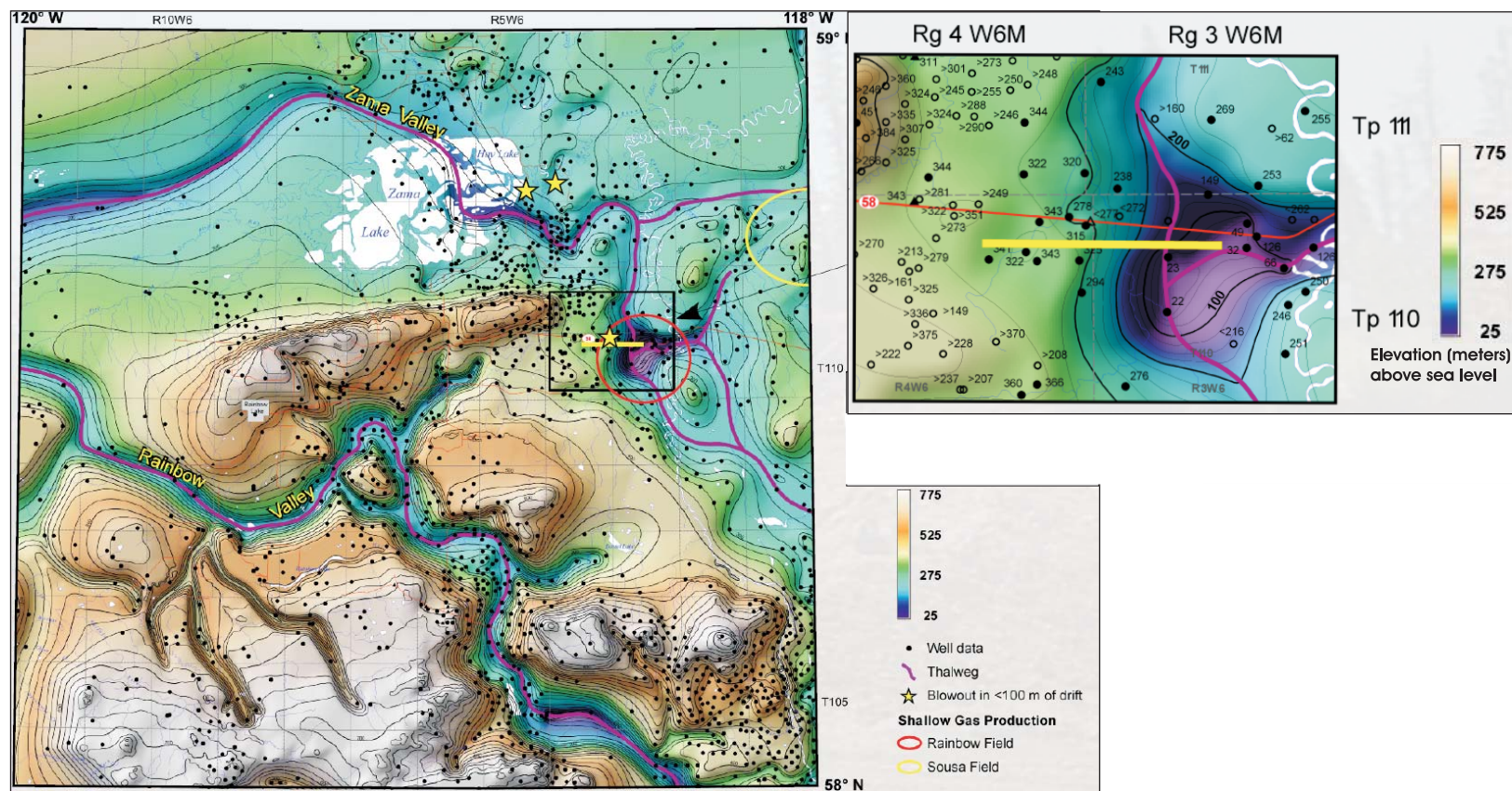


Figure 3.3: Bedrock topography map modified from Pawlowicz et. al. (2005c) showing location of seismic line, incised valleys and thalweg of paleo-drainage patterns. Original map from Pawlowicz et. al. (2005a). Permission is granted for use via the non-commercial reproduction policy of the Alberta Geological Survey (<http://www.aggs.gov.ab.ca/legal.shtml>).

Generalized Stratigraphic Column

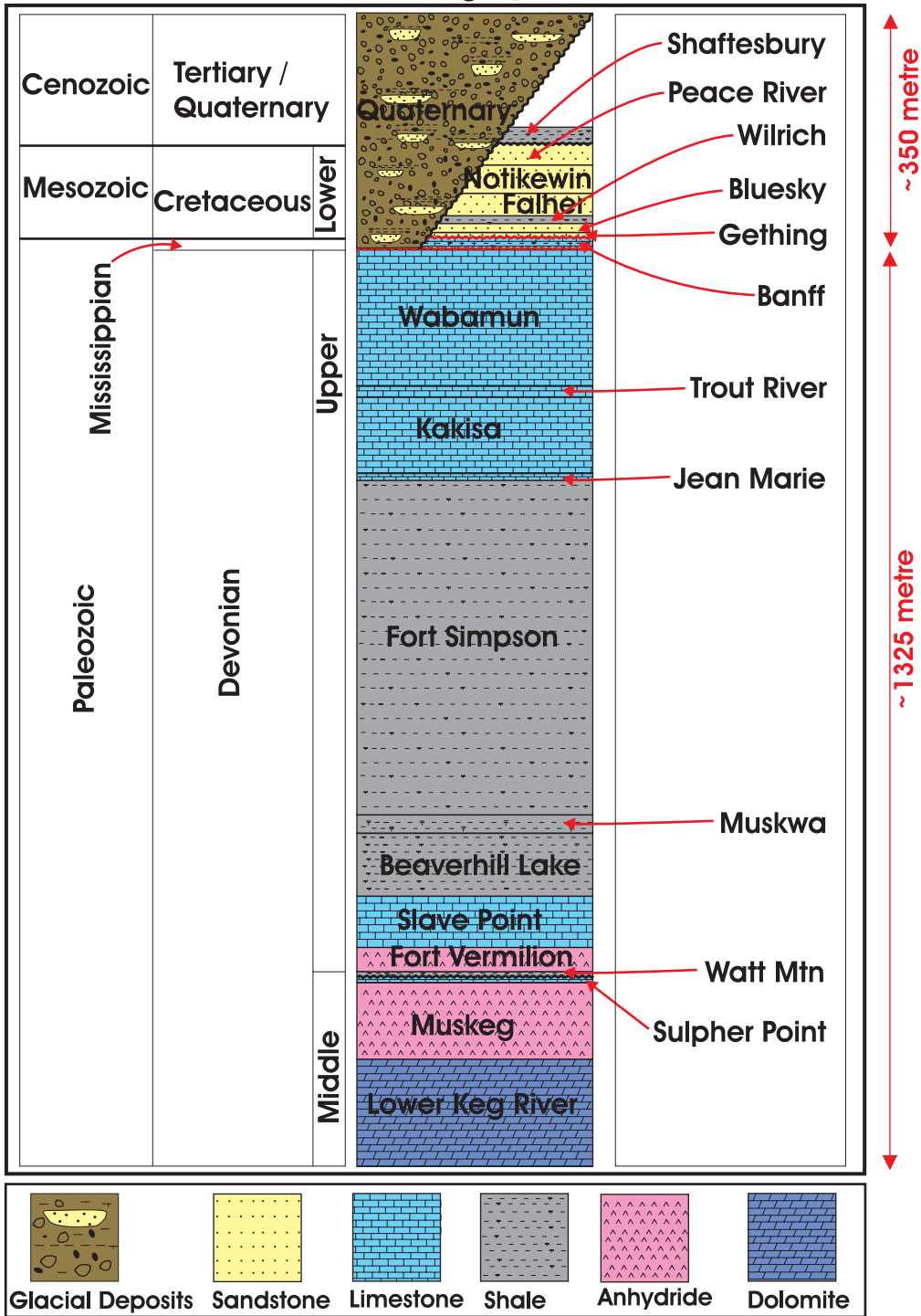


Figure 3.4: Stratigraphic column based on wells and regional correlation. Generalized Stratigraphic column is based on well: 00/01-20-110-03W6-0 and well: 00/08-29-110-03W6-0.

2.2. Gas in the Quaternary Sediments

Shallow Quaternary gas has been explored and produced in Canada since the early 50's, after the first discovery of Pointe-de-lac gas field (3.2 BCF), Québec, in 1955 in Quaternary unconsolidated sediments (~70 m) (Kelly et. al., 1994). It was not until 1988, that shallow Quaternary gas at only about 48 m depth was accidentally discovered by a water well blowout in the Zama/Rainbow Lake area, northwest Alberta (Clare and Hardick, 1988) (Figure 3.5). Later on such Quaternary gas was explored by oil companies working in that region. This was a highly attractive resource given the relatively low capital cost associated with drilling and completing such shallow wells. The commercial production from these shallow prospects was started in mid 1990's with a maximum of 5 MMscfd¹, and cumulative maximum of ~ 3.2 BCF², from one well (Table 3.1). The major Quaternary gas fields in northern Alberta are Rainbow and Sousa gas fields (Figure 3.1).

In the Rainbow/Sousa area shallow gas is believed to have migrated from bedrock formations and trapped in the porous fluvial glaciofluvial sediments. These sediments are capped by interbeds of clay and glacial lake sediments which form a seal preventing further loss of the gas. Evidence for this comes from the Carbon isotope values of Bluesky (Cretaceous) gas and from a natural gas seep ~100 km northeast of project area, named as 'Hot Pot' natural gas seep³ (Jim et. al., 2000). Carbon isotope values of both are almost similar, which supports the idea of gas migration from Cretaceous bedrock to the Quaternary sediments (Jim et. al., 2000). Carbon isotope values also confirm that Quaternary gas, at least in Rainbow Lake area, is from thermally mature (thermogenic) source with a trace of biodegradation (Karlis Muehlenbachs, personnel communication).

¹ MMscfd is 10⁶ cubic foot of gas. Mcf is 10³ cubic foot of gas

² One BCF means Billion (10⁹) cubic foot (cf). 1 cubic foot gas = 0.0010872 GigaJoule(gJ). 1 cubic foot of gas = 1030.5 British Thermal Units (BTU).

³ The 'hot pot' is known as such due to the fact that it has continuously burned (nearly) as long as anyone can remember. The local aboriginals refer to the hot pot as *kudadekune* or 'burning fire'.

This shallow, pressurized gas is a safety hazard in drilling and is associated with well blowouts in the past as recently as one in early 2005 (Alain Plouffe, personal communication) (Figure 3.6). This advises us a potential need for shallow hazard surveys prior to drilling on land environments, similar to the surveys for detecting gas chimneys in offshore environments.

Throughout the rest of the dissertation, the term ‘Quaternary gas’ will be taken to mean gas produced from or stored within near surface Quaternary deposits. The term should not be used to infer the initial source of the gas which may be from much older formations.

Quaternary gas has been produced from different parts of China since long ago. Major Quaternary bacterial gas fields are in Qaidam Basin and the Yangtze River delta near Shanghai (Jianyi et. al., 1999). ‘Sebei’ is the biggest and geologically youngest Quaternary gas field in China, and its complete ‘petroleum system’⁴ is within the Quaternary sediment (Jianyi et. al., 1999). The depth of the reservoir is > 500m in this gas field. Recently, several Quaternary shallow (30 - 55m) gas pools have also been discovered and produced in China in the province of Zhejiang (Lin et. al., 2004). These gas pools are generally in deeply incised valleys filled with fluvial sediments having high porosity. In a recent but brief abstract, An et. al. (2006) described a direct gas finding technique on seismic reflection data using low frequency component of the data. The technique is successfully applied in Chaidam basin, China for Quaternary gas exploration. Seismic signatures (i.e., bright spots, gas blanking and seismic pull down) as a shallow gas indicator in an offshore environment along with complete bibliography are mentioned in Anders et. al. (1987). For extensive review on shallow hydrocarbons i.e., case histories, development strategies and logistics refer to Meyer et. al., (1984). Shallow gas described in scientific literature in the offshore environment is; 1) biogenic gas produced in the seabed due to microbial activity; 2) thermogenic gas from leaking deeper reservoirs and trapped at ultra

⁴ A petroleum system consists of a hydrocarbon source, a reservoir, a cap or seal rock and a migration pathway from the source to the reservoir.

shallow depth and; 3) shallow ultra high pressure gas that migrates upwards and produces a gas chimney. On the other hand on the land, unconventional shallow gas resources are mostly biogenic in origin created in the shallow environment due to bacterial activity. At some places especially in the path of updip petroleum migration, bacteria may degrade petroleum to form heavy oil and biodegraded gas, and at other places dry gas may be leaking from deeper source through faults and conduits and become biodegraded as it reached near surface. The generation, migration and trapping mechanism of biogenic or 'swamp' gas is described in detail in the review article by Shurr et. al. (2002). Other than these, the shallow gas described here is onshore, thermally mature and hence highly indicative of a much deeper source, is migrated from leaking deeper reservoirs, and is trapped in Quaternary channel sands at depths of only 60 m or less from the surface.

* Well-07-25-110-04W600

Date: 15 Feb. 1996

Company: O.R.T. Energy Inc.

Field: Rainbow

Casing: 114.3 mm x 46.8 m x 4 Tonnes

Spudded: 13 Feb 1996 20:10 hrs

Rig released: Feb 14 1996

KB.: 380.66 m

G.L.: 379.56 m

Driller Depth: 55m

Depth (metre)	Porosity				Lithology	Crystal or Grain Size				Geological Description
	>20 %	12-20 %	6-12 %	1-6 %		Silt	Very Fine	Fine	Medium	
5										Surficial soil and mud brown Soft silty in parts
10										Clay grey soft pasty plastic, silty in parts sandy in places
15										Shale grey-dark grey slightly hard, blocky, fissile in places
20										Conglomerates variegated colored pebble and gravels of quartz, Arkozic, Granitic lithic fragments with sandstone quartzic matrix
25										
30										
35										Clay grey soft, plastic, sandy, silty in parts
40										Conglomerates vari-coloured pebbles and gravels of quartz, Arkozic carbonate rock fragments some of them are coated with heavy oil
45										
50										
55										Shale dark grey-black, silty slightly hard
										Sandstone white-light grey translucent very fine grained subrounded-subangular grains, loose unconsolidated
										TD 55 metre

Remarks: Surface hole was drilled by Gel-clean mud to the depth 46.8 m, at the depth 50.5 m gas started to flow through pipe to the burning pit after 1.30 hours of burning the gas the well was shut down. (the second hole to the TD was drilled by air)

Figure 3.5: Geological log redrawn from paper copy of well: 07-25-110-04W-6 showing lithological description of till and Quaternary channel sands. (Data courtesy of John Pawlowicz)



(a)



(b)



(c)

Figure 3.6: Photographs showing blow out wells in the Quaternary strata (<100 m). Photographs from Canadian Wellsite website (Canadian Wellsite, 2006); According to the website; a) 'Trail Blazes 11, blowout drilling surface in Rainbow Lake'; b & c) 'Nabors 29, January 2005, drilling surface hole @ 140 m tripping at time of blowout'. As per the website disclosure, no copyright is assigned to these photographs provided by unknown photographers. Photographs show high pressure gas that is significant drilling hazard as well as it is highly economical because of its shallow depth.

Well ID	Completion depth (m) Open Hole (OH) / Perforation (Perf) / Liner	Cumulative Production		Status of Production		Final rate of Production		Pool	
		10 ³ cubic metre	BCF ⁵ (Billion cubic ft.)	On Production	Shut Down	10 ³ Cubic metre/ day	MMscfd ⁶ Million cubic ft. / day		
08-36-110-04W6	44.5-57 (OH)	40977	1.45	07/1998	09/2001	51	1.8	Glacial Drift 'A'	
07-25-110-04W6	47-55 (OH)	53808	1.9	11/1998	On Production	-		Glacial Drift 'A'	
10-24-110-04W6	58-76 (Perf.)	71811	2.53	04/2000	03/2004	3	0.1	Glacial Drift 'A'	
10-13-110-04W6	71.5-74 (OH)	9291	0.32	04/2000	01/2004	3	0.1	Glacial Drift 'A'	
01-17-110-03W6	64-82.5 (Perf.)	12941	0.45	05/2001	03/2004	6	0.2	Glacial Drift 'A'	
10-18-110-03W6	50.7-74.3 (Liner)	24155	0.85	05/2000	03/2004	4	0.14	Glacial Drift 'A'	
11-30-110-03W6	68.7-70 (OH)	8176	0.29	10/2001	11/2001	1	0.04	-	
08-32-110-03W6	71.5-74 (OH)	8176	0.29	01/1999	07/2002	1	0.04	Glacial Drift 'B'	
05-33-110-03W6	68-74.1 (OH)	6800	0.24	03/2002	On Production	-		Glacial Drift 'B'	
Glacial Drift 'A' Pool									
Gas Composition:	He	N ₂	C ₁	C ₂	CO ₂	H ₂ S			
	0.02%	0.99%	98.98%	0.01%	N/A	N/A			
Reserves									
OGIP: (Original gas in place)		Producible:		Mean Depth:	Zone:	Initial Pressure		Porosity	Net Pay
10 ⁶ Cubic metre	BCF	10 ⁶ Cubic metre	BCF	Metre		kPa ⁷	PSI ⁸	% age	Metre
496.0	17.5	248.0	8.8	60.30 m	Glacial Drift	600	87	0.3	3.7

Table 3.1: Table showing gas properties in different Quaternary gas pools. Data compiled by Dr. C. D. Rokosh from Accumap[®] exported late 2004.

⁵ One BCF means Billion (10⁹) cubic foot (cf). 1 cubic foot gas = 0.0010872 GigaJule(gJ). 1 cubic foot of gas = 1030.5 British Thermal Units (BTU).

⁶ MMscfd is 10⁶ cubic foot of gas. Mcf is 10³ cubic foot of gas.

⁷ kPa is kilo Pascal.

⁸ PSI is Per Square Inch.

2.3. Geophysical Log Response of Quaternary Sediments

Geophysical logs provide measures of the physical properties of subsurface rocks at in-situ conditions. Different wireline tools have been developed and successfully used to observe subsurface rock properties in petroleum and hydrogeological boreholes. The most commonly used logs in the petroleum industry are the natural gamma ray (GR), self potential (SP), a variety of electrical resistivity measurements, the mass density (RHOB), and compressional wave (sonic or DT) logs. Each of the responses of the tools is briefly described below to help place the log interpretations in context. However, much more extensive details of the physics of such logging tools can be found in text such as Hearst et. al. (2000) or Ellis (1987), with numerous additional texts focusing on the interpretation of such logs such as Darling (2005).

The GR tool measures the natural radioactivity of rocks. This log is usually used to differentiate shales and clays from sands. Shales are usually more radioactive than quartz sands and easily differentiated on this log. GR log is displayed in 'gamma ray API' units which is an arbitrary, but calibrated standard in which a value of 200 is indicative of relatively highly radioactive marine shales that formed from small clays deposited in deep ocean environments. Nearly all the natural radioactivity detected by these tools is produced by the decays of various isotopes of U, Th, or K. The clays in the marine shales, for example, are more radioactive because of the propensity of natural uranium to adsorb to their surfaces. In contrast, pure quartz grains typically contain only small amounts of those elements and hence are not radioactive. Hence comparison of the levels of radioactivity can often be an indicator of 'clean' sands versus 'tight' shales. This is also perhaps one of the simplest technical logs run and it is almost always run in tandem with other tools to allow for proper correction of depth particularly if multiple logging runs are made.

The SP tool measures natural currents in the borehole mud which results from the movement of ions from the subsurface formations through the borehole fluid. Although making such log measurements is relatively simple, requiring only that an electrode be lowered into the wellbore with the changes in the voltage correspondingly measured; the physics behind this log can be quite complex. The unit for SP log is milli-volts. This log in conjunction with GR log used to differentiate shale and sand and in particular can reveal some information about the permeability of a formation because the mobility of ions through a porous medium will be dependent on the quality of the pore network which serves as the path for both fluid flow and ion motion through the rock.

The wireline resistivity tool measures the natural electrical resistivity of subsurface formations. Three common resistivity logs are shallow, medium and deep resistivity logs. The classification is based on the depth of penetration of signal that is a few centimetres to a few metres. Resistivity logs are used to identify hydrocarbon or water in the subsurface formations. In the presence of highly resistive hydrocarbons, the resistivity of the rock containing these fluids can rise substantially over the same rock containing water. The resistivity of the rock can further be controlled by the salinity of the water as brines can be highly electrically conductive. In contrast to electrical conductivity in metals where the current is carried by electrons, in rocks the predominant electrical current is carried by slower moving ions. The unit for resistivity log are Ohm-metre ($\Omega \cdot m$). Resistivities are usually presented in a logarithmic scale as they can vary by many orders of magnitude within a given formation dependent on the saturating fluids. Clays, however, also allow for substantial surface conduction and this can sometimes complicate the interpretation of such curves.

Density logging tool consists of radioactive sources (usually ^{137}Cs which gives off γ -rays as part of a β decay) and detector which record the Compton-scattered gamma rays returned to the tool. This intensity of the back-scattered gamma radiation to the tool is indicative of density of electrons in the formation which in

turn is a proxy measurement for the mass density of the formation. This log is calibrated for sandstone and limestone in order to approximately correct for bulk density values, but an interpreter of such logs need be aware that the values given will consequently contain some error. Bulk density calculated with this log is displayed in kg/m³.

Sonic tools measure the acoustic properties of rocks. Usually the term ‘sonic’ is reserved for measurements of the transit-times ‘DT’ of the compressional P-wave along the wellbore wall given in units of µs/m. The P-wave material velocity V_p is an indication of the competition between the stiffnesses and rigidity against the mass density via:

$$V_p = \sqrt{\frac{K + \frac{4}{3}\mu}{\rho}} \quad (3.1)$$

Where K and μ are the bulk and shear moduli, respectively. Typical sonic tool consists of transmitters and receivers that records travel time per unit distance and a variety of corrections to these ‘compensated’ tools attempt to account for irregularities in the borehole. Sonic log records interval transit time (ITT) which is the slowness or the reciprocal of the velocity and is usually supplied in units of µs/m. Typically soft formations i.e., sand and clays, gives low sonic velocities and hard formations i.e., Carbonate, give higher velocities.

Together with the density tool, one may calculate the acoustic impedance $Z = \rho V_p$ which is essentially a measure of the resistance of the materials particles to movement by a passing wave. The calculated ‘impedance’ log is used to calculate the normal incidence seismic reflectivity R of a given interface between two layers with differing impedances Z_1 and Z_2 via:

$$R = \frac{Z_2 - Z_1}{Z_2 + Z_1} \quad (3.2)$$

The typical log characters between one key valley-fill well and one contrasting nonvalley-fill well are shown in Figure 3.7 and Figure 3.8. Both of these wells show different character on logs due to the difference in subsurface geology. Based on the resistivity log (on track-3), the Quaternary sediments in Figure 3.7 show slightly higher resistivities as compared to the older Cretaceous sediments in Figure 3.8. Cretaceous clays/shales are of marine origin and are less resistive than non-marine clays (Quaternary). Clays are usually deposited with the suspended particles load in the calm water conditions. Due to the higher salinity of sea water marine clays are more conductive (less resistive) as compared to the clays deposited in fluvial, glacial and lacustrine environment. Quaternary and non-Quaternary sediment sediments are also easily differentiated on the GR log. GR values are very high in Cretaceous sediments due to the presence of shales (track-1, Figure 3.8); whereas GR values are significantly low in the fill sediments (track-1, Figure 3.7) due to the presence of sand/silt. Some times gravel/conglomerates beds do not produce low gamma response due to the presence of feldspar sand and other radioactive elements within the sand unit. Overall gamma ray (GR) curve response is confusing in the Quaternary sediments. Quaternary sediments are transported with glaciers/ice-sheet and traveled long distance before deposition. Bednarski (1999) described the source of these more naturally radioactive volcanic erratics and high velocity and radioactivity materials that produces anomalous GR response, hundreds of kilometre away in the northeast. Figure 3.9 shows crossplot of GR and Density log that is colour coded with density porosity log values. From this figure Quaternary channel fill material is clearly differentiated with Cretaceous strata based on low GR and density values.

Different wells in the vicinity of the seismic line were used to study regional and local geology from the surface to the middle Devonian. In order to understand the local stratigraphy, lithostratigraphic log correlations are drawn (Figure 3.10, Figure 3.11). These cross-sections help understanding local geology based on the log response. Overall Quaternary deposits do not show typical log character in

wells. Characteristic features of Quaternary are; 1) low sonic velocity (high transit time); 2) lowering down of gamma ray as a whole; and 3) low density anomalies at places. Figure 3.10 and Figure 3.11 show correlations across one paleo-valley and covers the complete succession within the glaciolacustrine and glaciofluvial deposits. Few fining and coarsening upward sequences indicative of channel sand are clearly visible on GR logs along with some blocky sand features.

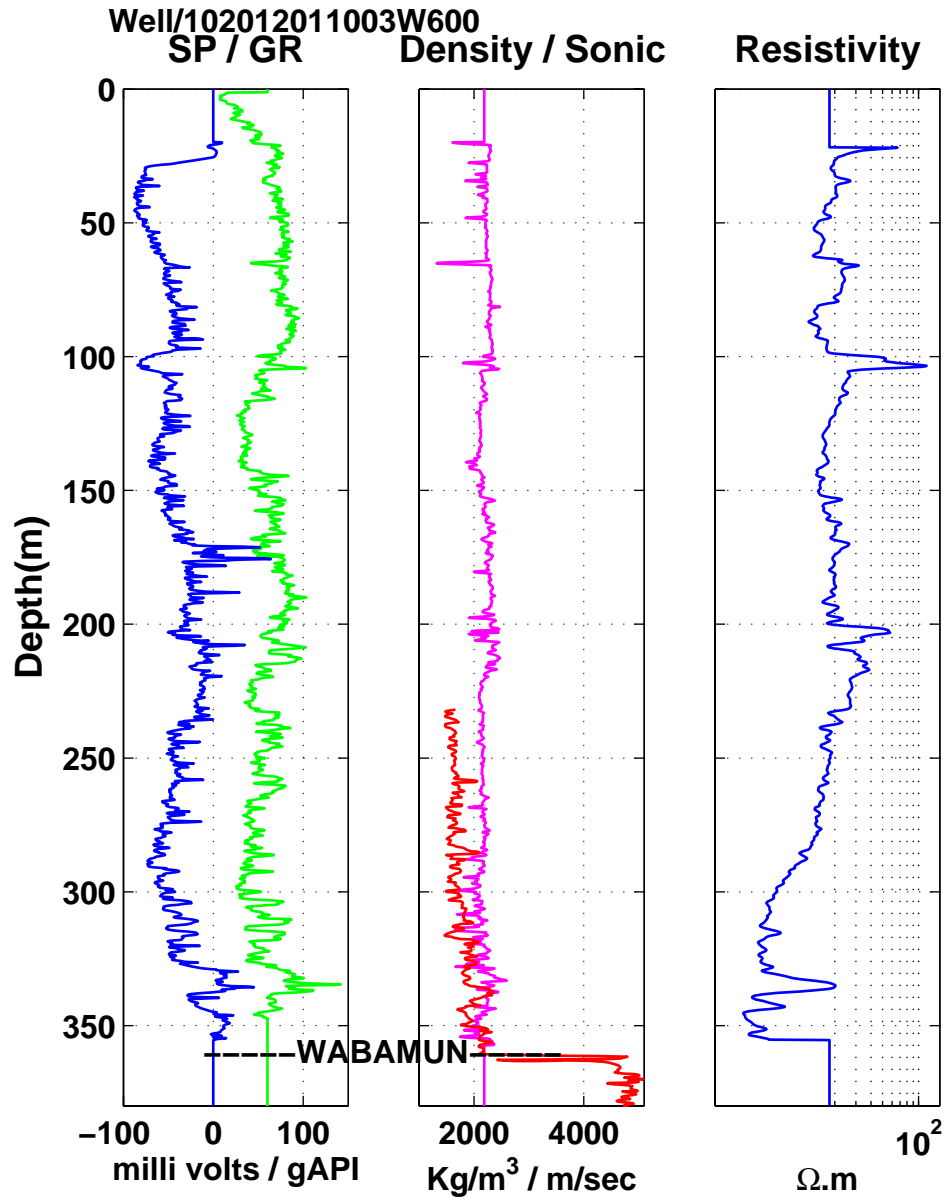


Figure 3.7: Geophysical log character of Quaternary sediments (Well: 102012011003W600). The zones 100m and 210m on resistivity log might be containing fresh water or hydrocarbons. For location of well see Figure 3.1.

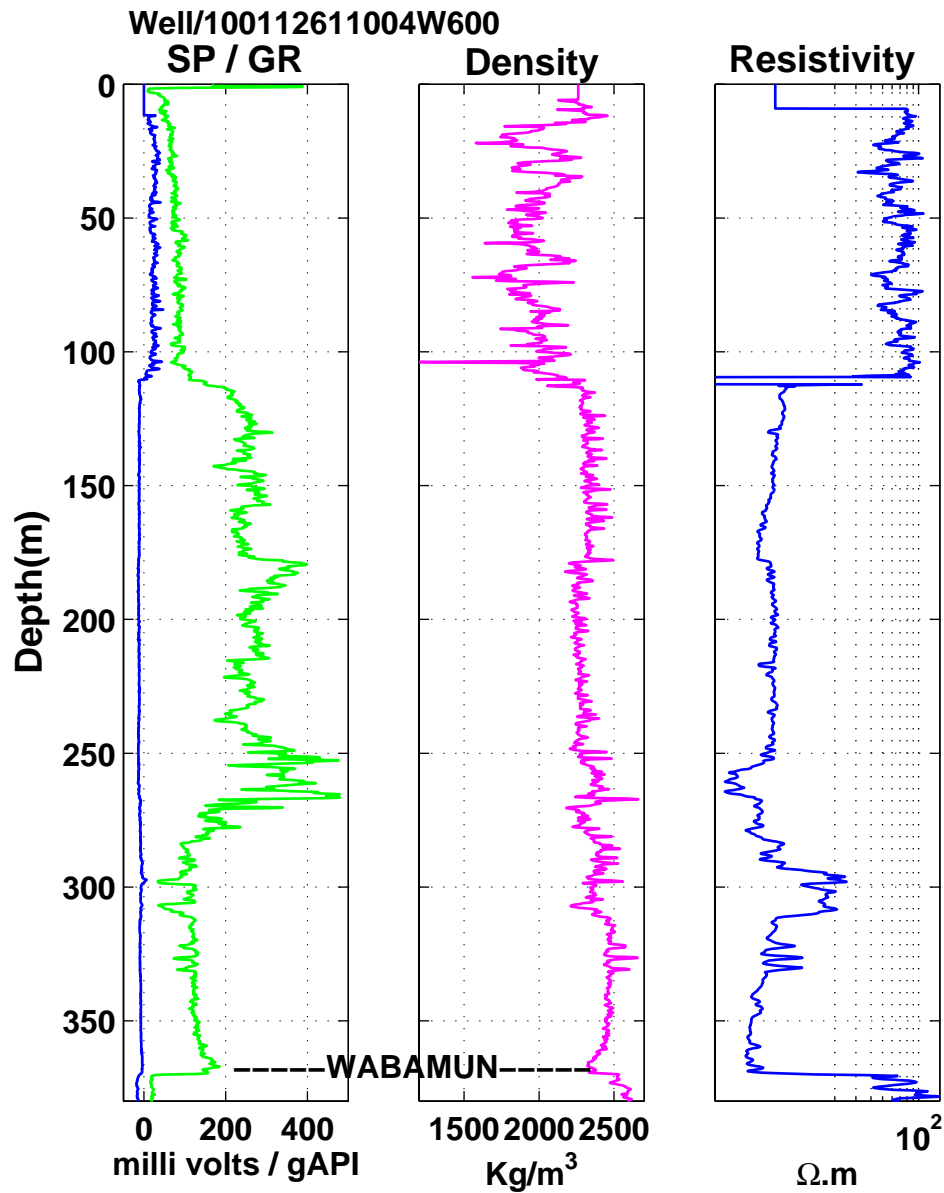


Figure 3.8: Geophysical log of non-channel well (Well: 100112611004600) showing different character as compared to channel well as shown in Figure 3.7. Logs are in cased hole from 0 to ~100m depth. Due to the casing effect resistivity values are not reliable between this depth interval. Base of Quaternary is about 60 metre as picked by Pawlowicz et. al. (2005a & b). For location of well see Figure 3.1.

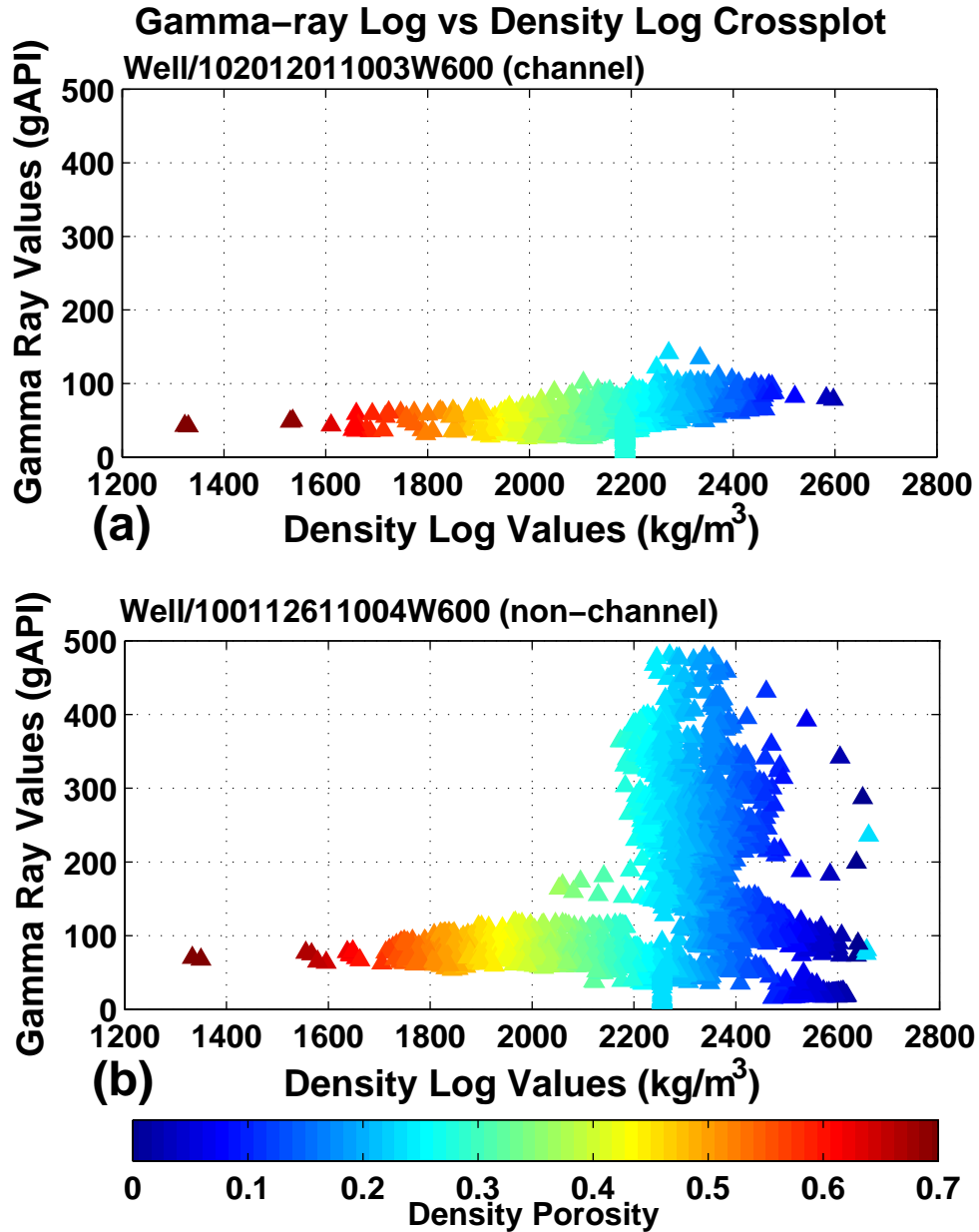


Figure 3.9: Figure showing crossplot of gamma ray (GR) and density log and colour coded with density porosity. a) Crossplot of Quaternary well displayed in Figure 3.7. b) Crossplot of non-quaternary well displayed in Figure 3.8. Valley fill sediments are clearly identified in Fig-a with low GR values whereas in Fig-b Cretaceous shale show higher GR and density values and come as separate identity. Density-porosity of both channel and non-channel wells are almost same and these cannot be distinguished based on this. Porosity log is optimized for sandstone (i.e., assumes quartz mineralogy)

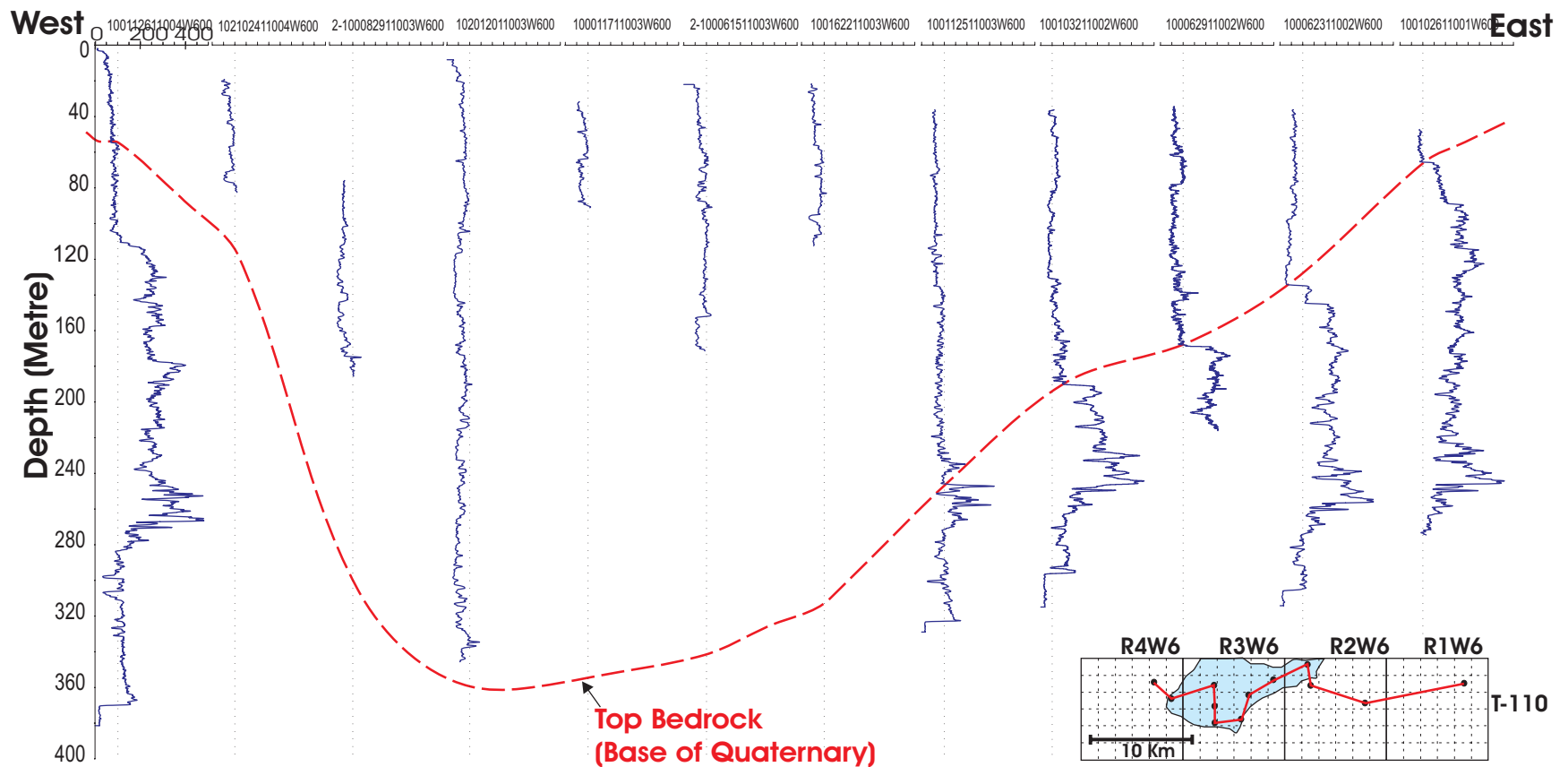


Figure 3.10: Regional scale gamma ray (GR) based crosssection showing paleo-valley and top of bedrock. Top of the bedrock picked based on the data provide in Pawlowicz, et. al. (2005a & b). High GR value in the bedrock is due to marine clays/shale. Approximate location of channel (sketched from Figure 3.3) is marked on the index map on the bottom corner of this figure.

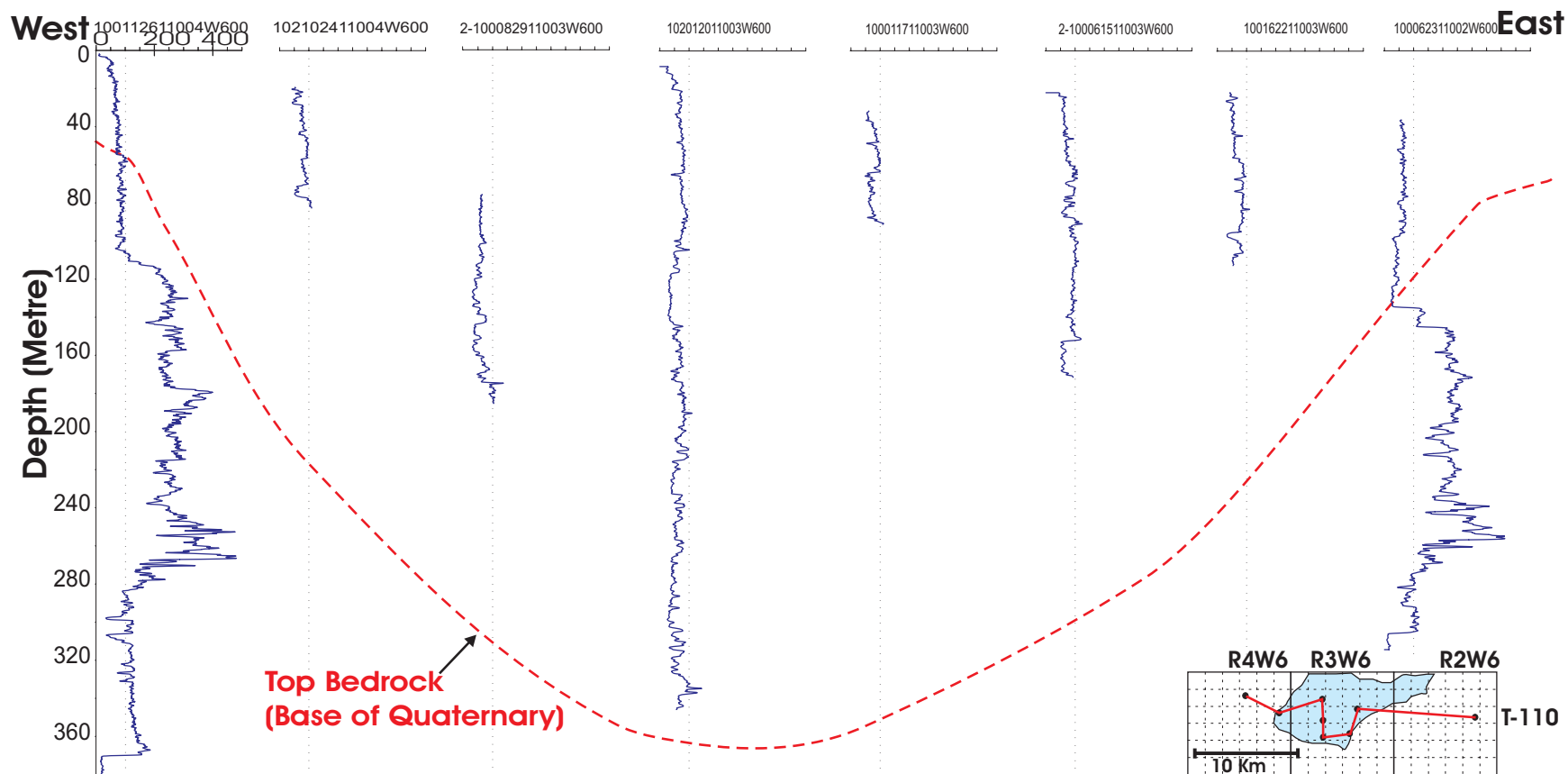


Figure 3.11: Gamma ray (GR) based crosssection showing paleo-valley and top of bedrock. Top of the bedrock picked based on the data provide in Pawlowicz, et. al. (2005b & c). Approximate location of channel (sketched from Figure 3.3) is marked on the index map on the bottom corner of this figure.

3.4. Summary

Quaternary deposits in the study area are mainly of glacial origin and were deposited during few episodes of glaciation / deglaciation. These sediments predominantly consist of glacial till, glaciolacustrine clays, and meltwater channel sand and preglacial fluvial sediments. Deeper source rock, reservoir quality sand and impermeable glaciolacustrine clay completes petroleum system and produce exploration potential in these sediments at shallow depths (<100m). Quaternary glacial deposits can easily be distinguished from Cretaceous sediments on geophysical logs based on low gamma ray and slightly high resistivity values. Paleo-valley is identified on bedrock topography map and geophysical log correlation was drawn to understand the character of the valley-fill sediments (Quaternary glacial sediments). In the next chapter seismic data acquisition and processing to image paleo-valley will be discussed. In order to differentiate valley-fill sediment with host rock and signatures of shallow gas (methane) filled within these meltwater channels, electrical resistivity tomography data was also acquired. It will be discussed following next chapter. In the chapter 6 seismic reflection signature of meltwater channels as well as shallow gas (methane) signature on the ERT profile will be seen. Joint interpretation of ERT and seismic reflection profiles will be carried out for shallow hydrocarbon bearing reservoirs and valley-fill sediments.

Chapter 4

Seismic Methodology and Results

In this chapter the seismic data acquisition and processing procedures are discussed in detail. Near surface high resolution seismic acquisition differs from that employed in standard petroleum industry exploration in that, obviously, the targets are generally much closer to the surface. This requires some special attention to the design of a program. In the present project, seismic data was recorded using University of Alberta seismic acquisition instruments with a IVI Minivib[®] seismic vibrator source providing a broad band of frequencies from 20 Hz to 250 Hz. Some seismic designing issues, particularly those related to both the vertical and the horizontal resolutions and the corresponding geophone spacing, are also discussed in this chapter. The seismic data was processed using standard near surface processing workflow. This chapter also includes some direct analysis of the raw shot gathers, the variation of which across the seismic profile are highly dependent on the changing geological structures from east to west. These observations can help in understanding the local geology and perhaps more generally in locating buried valleys in other localities.

4.1. Seismic Data Acquisition

4.1.1 Introduction

A ten kilometre east-west survey was acquired along pre-existing cut lines during March 2004. The University of Alberta IVI minivibrator, a 6000-lb force high-frequency vibrator mounted on a 3-ton truck, was used. The source operated with linear sweeps of 7 seconds duration from 20 Hz to 250 Hz at 6000 pounds (26689 N) ‘hold on’ weight with a 24 metre shot spacing and 5-7 sweeps per shot point

(Table 4.1; Figure 4.1). The monitored force level of the vibrator plate remained uniform over the entire sweep, indicating good coupling with the ground in the winter. Seismic traces were acquired using the University of Alberta 240-channel semi-distributed seismograph that consists of ten 24-channel Geometrix Geode field boxes linked via a field intranet to the control and recording computer. Standard 40 Hz geophones were placed at 4 metre intervals with one geophone per station. Two different shot gathers one in the east other in the west, is presented here for reference (Figure 4.2; Figure 4.3). Wind noise was not a big problem in this area but some times wind was shaking only a few stations (Figure 4.4). Although a lower frequency phone might be desired to improve resolution, 40-Hz was chosen in order to assist in attenuating the effects of source generated ground roll that can overwhelm the desired reflection signals particularly as geophone singles were employed. The dominant frequency of the data was > 75 Hz. Seismic data in principle contains sufficient temporal (~ 3 m) and spatial (~ 6 m) resolution to allow the imaging of small and thin geological features (e.g., sand channels) (see next sections).

SEISMIC ACQUISITION PARAMETERS	
<i>Source</i>	
Energy Source	Mini-Vibroiseis (6000 lb) peak force
Sweep Frequency	20-250 Hz.
Sweep Length	7 sec.
No. of Sweeps	5-8 Sweeps
Sweep Type	Linear
Source Point Interval	24 metre
<i>Instrument Parameters</i>	
Receding Instrument	Geometrics (Geode) 24 bit; Multiple Geode operating system (MGOS)
Dynamic Range	~110 dB
Recording Format	SEG-2
Sample Rate	0.5 msec.
Record Length	1.19 sec
No. of Channels	192-240
<i>Cable</i>	
Spread Geometry	Split Spread and end on
Group Interval	4 metre
Geophone Frequency	40 Hz
Fold	~40
No. of Geophone per group	Single

Table 4.1: Seismic acquisition parameters

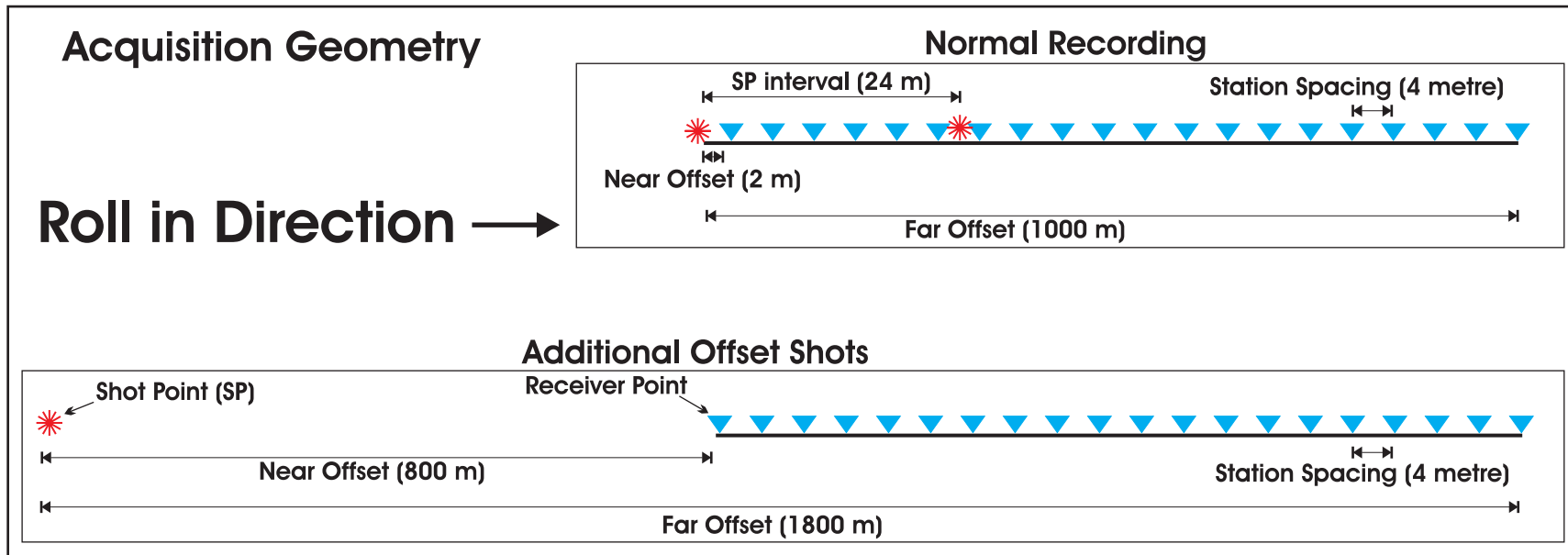


Figure 4.1: Seismic data acquisition geometry.

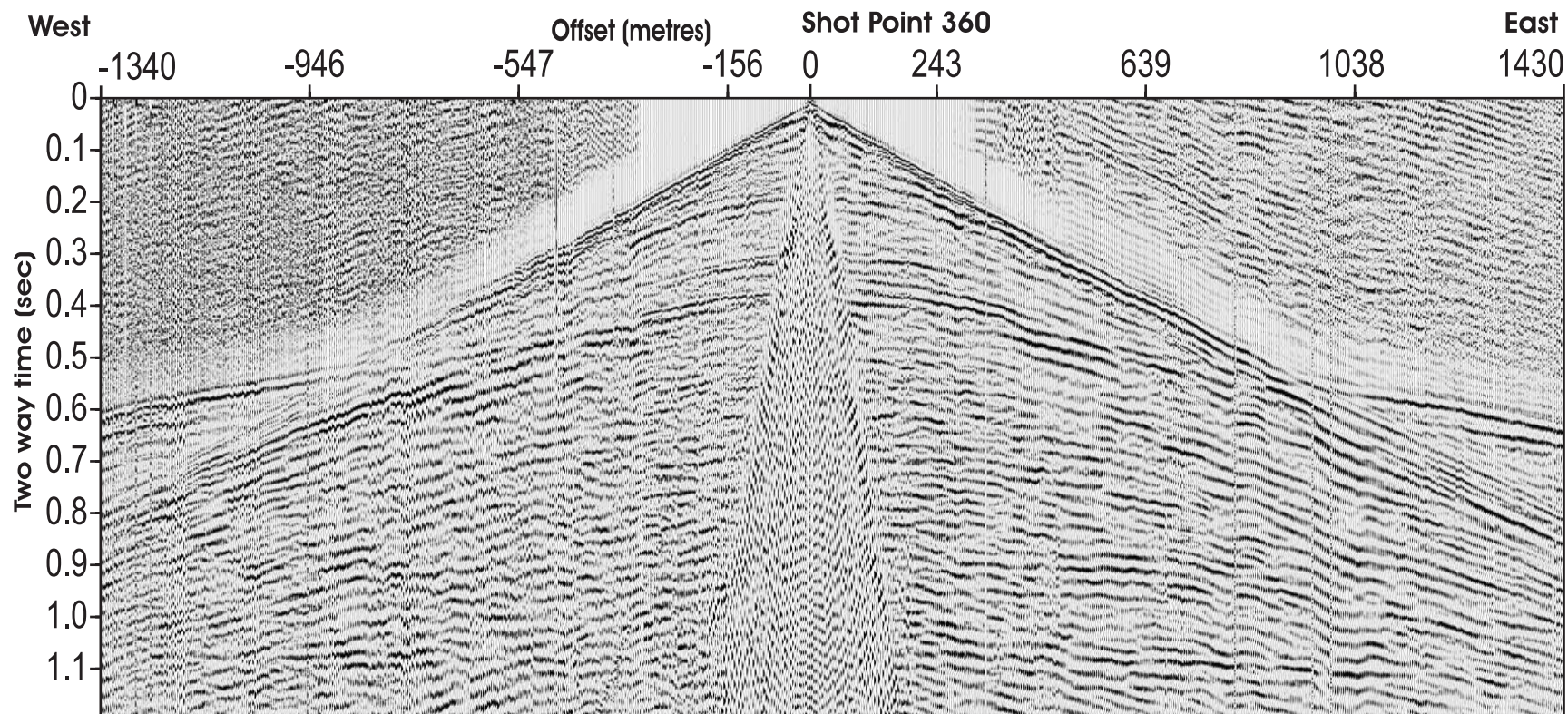


Figure 4.2: Shot point 360 showing field raw data. Shot point is in the eastern end of the seismic line.

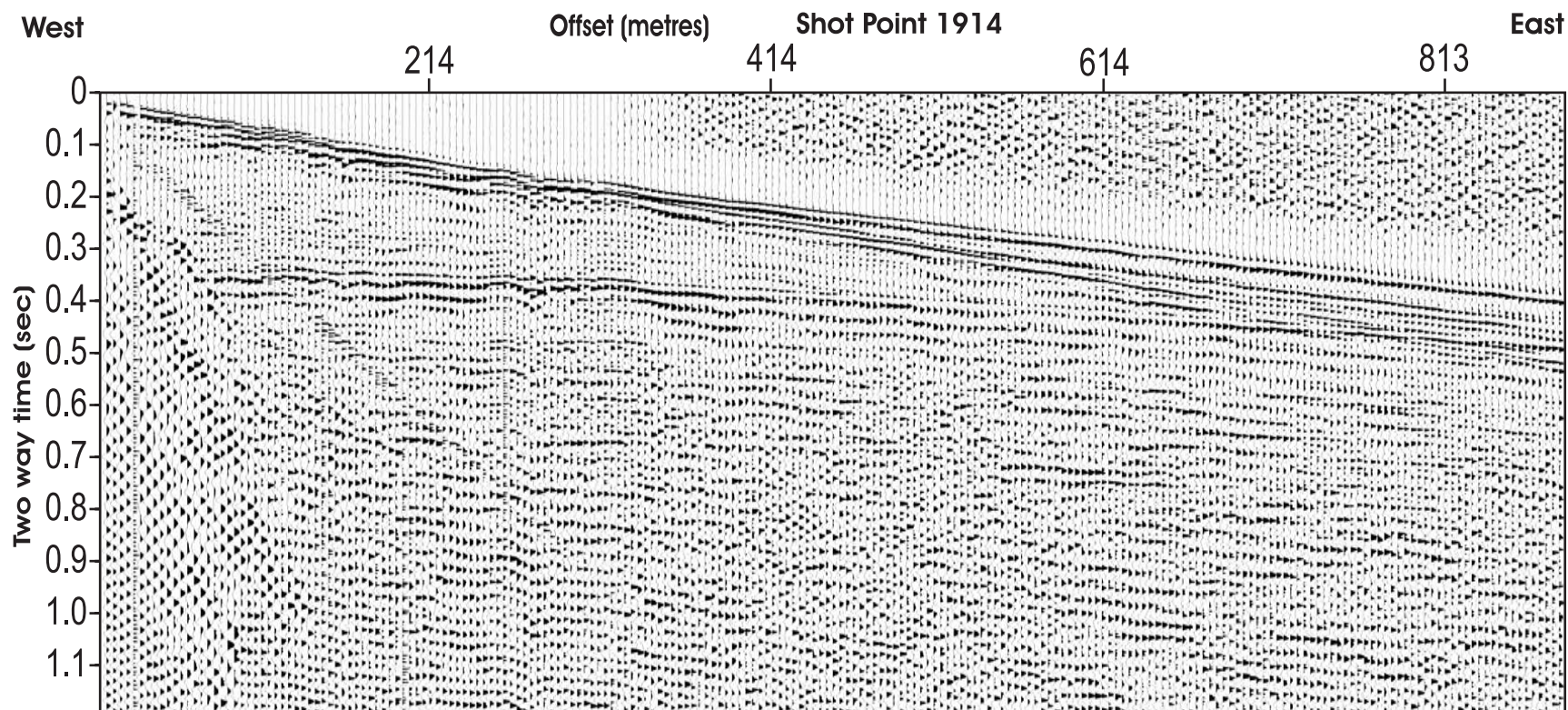


Figure 4.3: Shot point 1914 showing raw data. Shot point is in the western end of the seismic line.

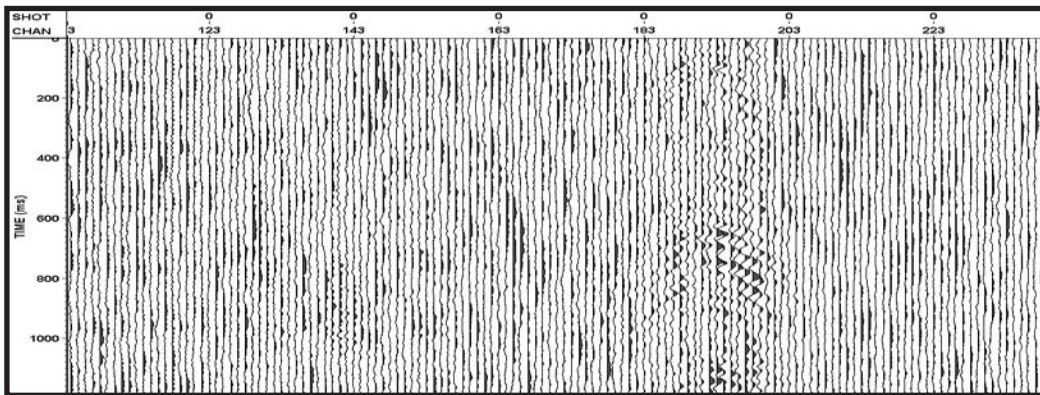


Figure 4.4 Wind noise test; also showing background noise level. Few stations are shaking due to noise; see channel 183 – 203

4.1.2. Geodetic Surveying

Geodetic surveying along the seismic profile was conducted by professional surveyors from the Alberta Geological Survey (AGS). The control points were established in the field using high precision ‘Differential Global Positioning System (GPS)’. All source points were surveyed to centimetre accuracy from the control points using an optical ‘Total Station’ with the final results reported in the Universal Transverse Mercator (UTM) coordinate system. This system places a point on the surface of the earth in terms of an easting, a northing and an elevation, with centimetre accuracy using ‘Total Station’. (Figure 4.5). Due to the severe variations in the near surface overburden structure, and hence seismic velocity, accurate measures of the elevations were required for calculating of the static corrections (see below).

Once the geodetic data was received at the U of A, coordinates of each of the receiver stations at 4 metre spacing were calculated by linearly interpolating the easting, northing and elevation between each surveyed shot point typically obtained at a 24 metre spacing except where extreme topography at Sousa Creek prevented this. In order to meet the requirement of seismic headers i.e., floating point or double, the shot and receiver points were renumbered and saved in Vista[®]

format in a text relational file containing computer file number, first and last channel number, and total number of channels. The geodetic survey data was also saved on standard SPS (shell processing support; native geodetic survey data format) format which contains three files: 1) source coordinates (.S extension); 2) receiver coordinates (.R extension); and 3) relational file (.X extension) that contains, computer file number, first and last channel, and total number of channels in recording spread.

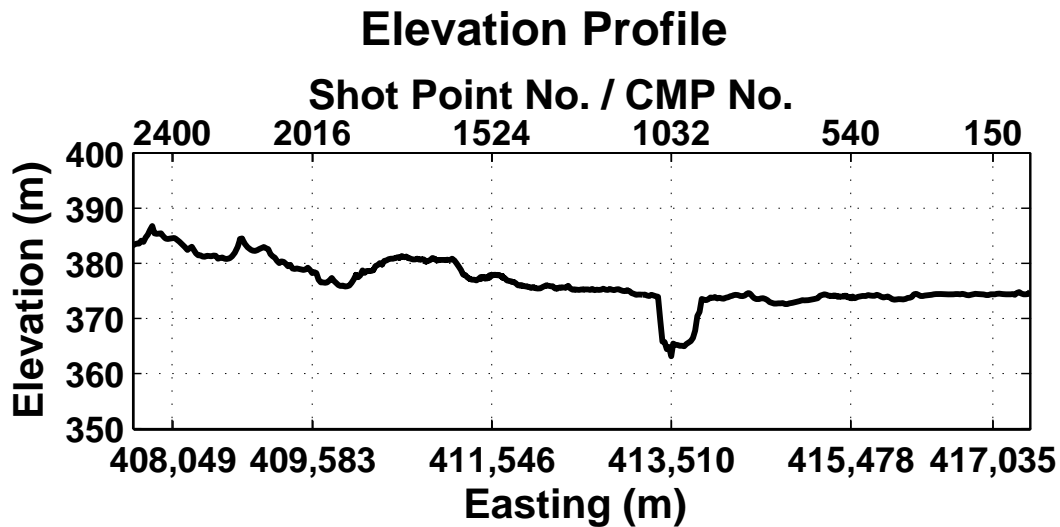


Figure 4.5: Elevation Profile along seismic line. On the top of the X-axis shot point and CMP numbers are marked. On the bottom of the X-axis easting is marked for reference. Sousa Creek crossing is at CMP 1032; see lowering of elevation.

4.1.3. Seismic Designing Considerations

Different points were kept in mind before recording seismic data. Following work will help us identifying key designing parameters for this survey.

4.1.3.1. Vertical Resolution

Seismic reflection profiles are recorded in terms of the two-way time to a given reflecting event in the earth. Consequently, the 'vertical' resolution 'in time' is, according to Sheriff (2002) the 'ability to separate two features which are very close together'. To a large degree this resolution depends on the frequency

content of the input seismic energy, optimizing the band-width of the input seismic data is of primary importance to being able to distinguish different events in the earth. Further, the higher the maximum frequencies the smaller the object that may be detected with seismic echoes. As a result, it is important to analyze the raw data to see what the ultimate bandwidth actually recorded will be, as this can depend on numerous factors such as the size of the source and the attenuation of the signal as it propagates from the source through the earth to the receivers. For this purpose, the frequency content recorded in the raw data was physically inspected; source point SP-360 is shown for example in Figure 4.2. The following observations can be made from these figures: 1) seismic signals returned from the near surface <100 msec have dominant signal time-periods of 10 msec (100 Hz) and; 2) at ~400 msec two-way travel time at the Top of the Devonian the predominant signal time-period was 17 msec (58 Hz). Consequently, a dominant frequency of 75 Hz which was assumed to be representative and used for subsequent analysis. According to Cordsen et. al. (2000) the vertical resolution is:

$$R_z = \frac{V_{int}}{4F_{dom}} \quad (4.1)$$

R_z = Vertical Resolution

The expected vertical resolutions based on both the dominant frequency and the in situ velocities will change with depth; these are estimated in Table 4.2. The question is how thin bed can be resolved with separate reflections from its top and bottom. Widess (1973) showed that bed thickness vary from $\lambda/8$ to $\lambda/4$, depending upon the incident source wavelet and signal to noise ratio. Author also showed that in the presence of thin bed reflection amplitudes are also affected.

TWT (msec)	~Depth of Target (m)	Velocity (m/sec)	Dominant frequency	Vertical Resolution (m)
<100	50	400	100	1
100 –200	100-150	800	75	2.7
~400	350	1800	50	9

Table 4.2: Table shows the subsurface vertical Resolution (metres) using Equation 4.1

4.1.3.2. Lateral Resolution

Lateral resolution on an un-migrated section is often taken as the width of the first Fresnel zone (Sheriff 2002) (Figure 4.6) which, hypothetically assumes that the source and the receiver are at the same position P in Figure 4.6, may be estimated to be:

$$F_s = 2\sqrt{(z + \lambda/4)^2 - z^2} \quad (4.2)$$

Where F_s = Radius of first Fresnel Zone, Z = depth of reflection point, and λ = dominant wavelength of the seismic signal. Note that Figure 4.6 is only a 2-D cutaway view of what is a 3-D problem, with the Fresnel zone really being a circular patch on the reflecting surface. A simple interpretation of the first Fresnel zone first begins with the assumption that each point on the reflecting interface R in Figure 4.6 will scatter energy back to P, that is the real seismic reflection incorporates energy that has traveled not just along the vertical ray from P to R and back to P (i.e. the perfect specular reflection) but also energy that travels from P to R' and is 'scattered' back from R' to P. Consequently, this simple definition of the Fresnel zone considers all the energy within the circle centred on R with radius F_s which will arrive more or less constructively with that of the primary ray path P-R-P. If a $\frac{1}{4}$ period Rayleigh assumption is employed, this means that all the energy within the radius F_s as defined by will arrive constructively; and consequently for the reflection P-R-P one cannot unambiguously define where within the circle with radius F_s the reflection has originated. If the signal has frequency f and consequently wavelength $\lambda = v/f$, then a straight-forward examination of Figure 4.6 suggests that all the waves scattered back from the circle of radius F_s will arrive within a time such that the coherent parts arrive together. This is taken as a general rule of thumb although Schmitt (1999) has recently questioned the validity of such simplifications.

Geological dip can cause further problems with the lateral seismic resolution. In general, the dips are all expected to be relatively gentle. The greatest dips anticipated are at top of the bedrock surface leading into the channel and these, as

picked on the bedrock topography map (Pawlowicz et. al., 2005), regionally dip at less 5°. However, the truncation of Quaternary against Cretaceous in the channel studied is steeply dipping $\sim 35^\circ$ (Figure 4.7). Hence, the lateral seismic resolution, as defined by the radius of the Fresnel zone, will be larger in such cases.

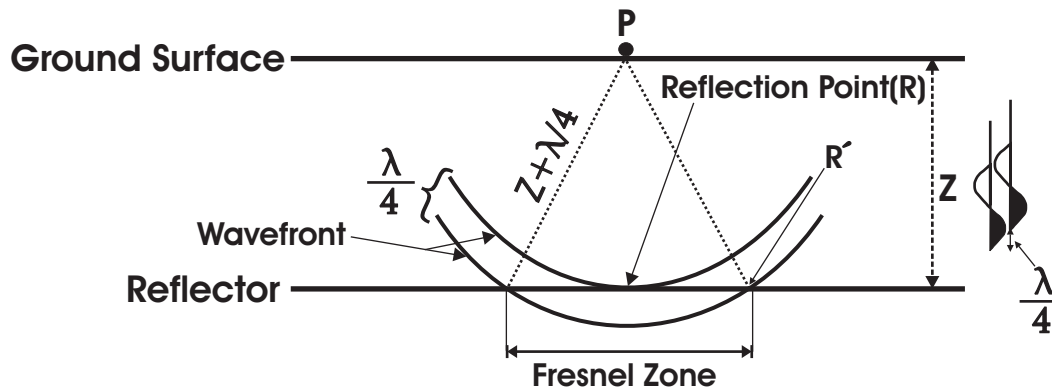


Figure 4.6: The radius of first Fresnel Zone for zero offset data i.e., source and receiver are at same location; where Z = depth of reflection point.

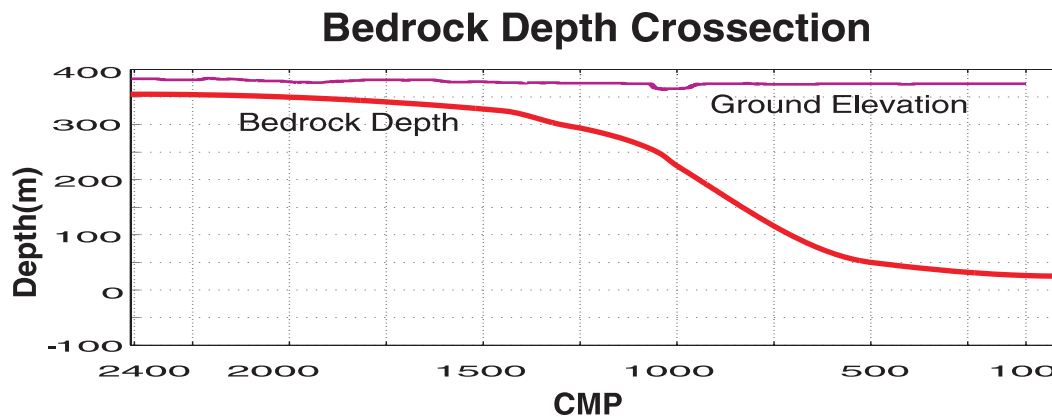


Figure 4.7: Bedrock depth crosssection based on bedrock topography map of Pawlowicz et. al. (2005) along the seismic profile

Equation 4.2 is usually used in the seismic survey designing stage where depth of target is known from well logs. Brouwer and Helbig (1998) showed horizontal resolution as $r = \frac{1}{2} \sqrt{z\lambda}$ where z is depth and λ is dominant wavelength. This equation can easily be written with respect to time, velocity and frequency

(Steeple 2004). Which is $r = \frac{v}{2} \sqrt{\frac{t_0}{f}}$ where r = radius of first Fresnel Zone, v = velocity, f = frequency, and T_0 = TWT. For simplicity, the calculation for estimates of the horizontal resolution is made using this equation. Horizontal resolution of this dataset calculated in Table 4.3 gives a general idea to the reader.

	Shallow Target	Deep Target
Velocity (m/sec)	400	1800
TWT (msec)	70	400
Frequency (Hz)	100	75
~Depth (m)	50	400
Radius of first Fresnel Zone (r); (m)	5	66

Table 4.3: Table show the horizontal resolution (radius of the first Fresnel Zone).

4.1.3.3. Receiver Station Interval to Avoid Aliasing

Proper receiver station interval is required to avoid spatial aliasing. Temporal aliasing is usually not a problem as long as the sampling period Δt is sufficiently fast that the Nyquist frequency $f_N = 1/(2\Delta t)$ is larger than the bandwidth of the signal. In this study $\Delta t = 0.5$ ms (see Figure 4.1) giving $f_N = 1$ kHz which is much larger than the maximum frequency of 250 Hz for the vibrator sweep.

Spatial aliasing with such frequencies can be more problematic and is not as easily understood. Spatial aliasing will produce false events in a final image of a shot gather or even in a processed section that dip in the wrong direction. Proper receiver station interval spacing is required to avoid spatial aliasing of a seismic arrival as it moves across the recording array. The best way to think about this is in terms of the ‘apparent’ velocity of an arrival as it moves across an array of detectors. If the wavefront of the arrival, which we assume for these purposes to be monochromatic (i.e. a single frequency f), is propagating parallel with the surface, the wave will appear to move out along the array at the wave velocity of the medium. If, however, the wave front intersects the surface at an oblique angle, then the apparent velocity as measured by tracking a certain feature of the

waveform such as an amplitude peak or trough will be given by $V_{app} = V/\sin(\theta)$ where θ is the angle of incidence. In an extreme case with $\theta = 0$ a given features of a planar wavefront will arrive simultaneously along the surface yielding $V_{app} = \infty$. The apparent spatial wavelength λ_{app} laterally is

$$\lambda_{app} = \frac{V_{app}}{f} \quad (4.3)$$

with units of metres/cycle. More usually this is put in terms of wavenumbers $\nu_{app} = \lambda_{app}/2\pi$ in units of metres/radian. The same Nyquist limits apply with the spatial sample Δx not equal to the spacing between the receiver points resulting in the Nyquist spatial frequency limit $f_{Nx} = 1/2\Delta x$ in terms of cycles/metre which equates to a limiting apparent wavelength $\lambda_{Napp} = 2\Delta x$ or to a limiting wavenumber of $\nu_N = \Delta x/\pi$. Hence, if $V_{app} > f \lambda_{Napp}$ the arrival will be insufficiently sampled laterally and hence will be spatially aliased. With the close spacing of 4 metres between receivers here, the signal could be spatially aliased at the peak $f = 250$ Hz if V_{app} only exceeds 1500 m/s. As such, it is nearly impossible to obtain data without some degree of spatial aliasing; the best that can be done is attempting to minimize the problem.

If velocity is in metre/sec and frequency is in Hz then spatial wavelength is metres. Receiver station and corresponding bin size is very important in order to avoid spatial aliasing at certain frequencies. In order to avoid aliasing we need to have 2 and preferably 3 sampling points (i.e., receiver points) for a given wave cycle across the array.

In this survey a CMP (common mid-point) bin size of 2 m (receiver spacing 4 m) was selected. In order to reduce and avoid spatial aliasing, theoretical considerations for the choice of optimum bin size are described in (Table 4.4). The highlighted values are the bin size at certain dip angle. If frequencies are more than 75 Hz at dip 25° they will be aliased. Velocity and dip angle are key factors for establishing subsurface bin size. Before the survey we had no idea

about the dips, velocity and highest frequency expected in the very shallow part. The receiver spacing of 4 metre was optimum for recording near surface reflections without aliasing. According to Cordsen et. al. (2000) theoretical considerations of bin size B in order to avoid spatial aliasing are:

$$B = \frac{v_{avg}}{4f_{max} \sin \theta} \quad (4.4)$$

where v_{avg} is average velocity of shallowest target; f_{max} highest frequency expected and ; θ is maximum dip expected. Bin size is calculated using above equation and shown in (Table 4.4).

Bin Size for Shallowest Target								
Velocity (interval) m/sec	Dips (degree)	Frequency maximum (Hz)						
		50	75	100	150	200	250	300
300.00	1.00	85.95	57.30	42.97	28.65	21.49	17.19	14.32
300.00	5.00	17.21	11.47	8.61	5.74	4.30	3.44	2.87
300.00	10.00	8.64	5.76	4.32	2.88	2.16	1.73	1.44
300.00	15.00	5.80	3.86	2.90	1.93	1.45	1.16	0.97
300.00	25.00	3.55	2.37	1.77	1.18	0.89	0.71	0.59
300.00	35.00	2.62	1.74	1.31	0.87	0.65	0.52	0.44

Bin size
in Metres*

Table 4.4: Table shows the expected bin size with varying geological dip and frequencies in order to avoid spatial aliasing. The highlighted values are the bin size in metres. The velocity chosen here the minimum velocity recorded in the data is based on refraction interpretation (see Figure 4.26 for velocities at shallow depth)

In order to image properly appropriate bin size calculations are required for particular target size. It is important that at least 2 or 3 traces pass through the target, especially we know in this study area meltwater channels have small lateral extent.

$$\text{Bin size} \leq \text{target size}/3$$

In our case bin size is 2 m, which means ~ 6 m wide anomaly can be detected on three traces in principle although in practice this might be difficult.

4.1.3.3. Fold

The jargon term ‘fold’ essentially refers to the number of traces within a given common midpoint bin that will be added together to produce a final common midpoint trace in the final seismic image¹. Fold is also important in seismic acquisition and calculation of fold at particular target is usually carried out. A CMP trace is formed by stacking traces from different midpoint location that fall in a bin. On a 2D profile bin is area with horizontal (inline) dimension depending upon survey geometry (2 m for this survey). In a bin number of traces stacked is called fold. More fold means more data volume and ultimately good data quality after processing because all CMP’s ultimately stack to give one trace - for particular CMP location. Less near offset and receiver spacing usually increase fold at shallow target level. A simple ‘back-of-the-envelope’ estimate of the expected fold can be made using

$$Fold = \frac{1}{2} \left[x \cdot \frac{\Delta x}{\Delta s} \right] \quad (4.5)$$

x = total number of receivers in spread

Δx = Receiver station interval

Δs = Shot Point interval

In the designing stage general acquisition fold was calculated using the above standard formula (Equation 4.5). According to above general formula recording fold was 20 but additional offset shots increased the fold up to ~40 (Figure 4.8). The offset shots on end-on spread were up to ~800 metres away from the receivers at either end of the line. It means for far offset shots the minimum offset (i.e., the distance between the vibrator seismic source and the first geophone) was ~800 metres and far offset ~1800m (Figure 4.1). This unique recording geometry increased acquisition fold, offset and angles for the entire line.

¹ It is useful to comment on how fold is described. In more modern practice ‘10-fold’ simply means that 10 traces will be added together. In earlier practice the terminology is a bit more confusing and this would equate to a fold of 1000%.

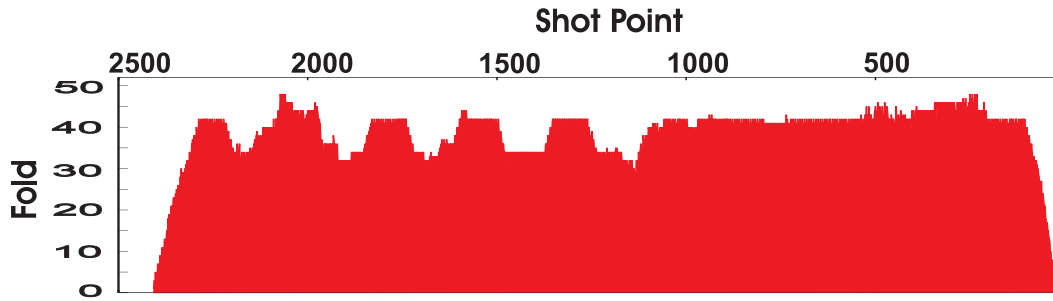


Figure 4.8: Actual final acquisition Fold

Minimum offset (X_{min}) should be small enough to sample unaliased frequencies at near offset. Usually more traces are required in the very shallow part due to the NMO stretch mute. A good rule of thumb for X_{min} is a value 1 to 1.2 times that of shallowest target (Z_{sh}) (Cordsen et. al., 2000) (Table 4.5).

Minimum offset (X_{min})	Maximum Offset (X_{max})
1 to 1.2 times depth of shallowest target	\cong depth of deepest target

Table 4.5: Table shows theoretical maximum and minimum offset limits for imaging target reflector.

As a general rule of thumb, the maximum offset is assumed to; 1) be between 1 to 1.25 times the depth of the deepest target; 2) be less than the refracted wave interference; 3) be less than where NMO stretch distortions become intolerable; 4) greater than the offset required to get the NMO $\Delta t >$ one wave length of dominant frequency (Cordsen et. al., 2000). Longer offsets are required for AVO and first break refractions for good velocity analysis in shallow high resolution seismic (< 0.5 sec two way travel time) and also in conventional deep reflection ($\sim 3-4$ sec two way travel time) surveys. In high resolution shallow seismic profiling particularly at very shallow part (< 0.2 sec), reflections strongly interfere with both refractions at far offsets and with deeper high velocity reflections having little move out. The shallow reflections also lose resolution due to NMO stretch at large offsets (Brouwer et. al., 1998). This depends upon the velocity of near surface material and bedrock or any consolidated material underlying the surface sediments.

4.1.4. Vibrator Source

Seismic energy sources are always problematic in high resolution surveys as workers must find a balance between the frequency content and the energy output. Other issues depend on the cost, damage to the environment, and, for explosives, even security questions. Seismic vibrators are often used as the source in shallow high resolution seismic surveys. Other available sources are explosives, weight drops, sledge hammers, and Betsy and buffalo guns, etc. The detailed field source signature of a portable mini-vibrator is described in Ghose et. al. (1998). That portable non-hydraulic mini-vibrator consists of small base-plate weighting 65 kg (500 N force) and able to generate sweeps from frequency range 20 to 1500 Hz. Comparison of rest of seismic sources (i.e., sledgehammer, explosives, weight drop, projectile impacts and various buffalo guns) are described in Miller et. al. (1992). Whereas, Feroci et. al., (2000) describes different sources and their comparison of frequency spectra and S/N ratio for various acquisition geometries recorded using different frequencies of geophones. In conventional deep reflection (~3-4 sec) surveys, arrays of heavy seismic vibrators (> 60,000 lb; 266,893 N) peak force are commonly used. For modest depths in the 'near surface' (< 0.5 sec) studies a single IVI minivib[®] (6000 lb; 26389 N) peak force show good results. The frequency range achieve with this vibrator is 10 to 500 Hz that is enough for shallow targets as shallow as 50 m.

A seismic vibrator consists of three main parts: 1) a flat metal plate which makes contact with the ground; 2) sweep generation electronics and hydraulics and; 3) a mobile vehicle over which all of this is mounted. During operation, the input sweep signal is triggered from the recording instrument (i.e., computer) and transferred to the vibrator sweep generation box via radio. This signal is transformed into mechanical instruction for the hydraulic system which then generates the sweep. The sweep consists of the movement of a mass whose force is transmitted into the ground surface via the plate. The vibrator sweeps with different frequencies usually starting from low (10 Hz) frequency to high (100 to 200 Hz), although this can even go as high as 600 Hz for smaller portable

vibrators (Ghose et. al., 1998). While the input sweep recipe is theoretical, a pair of accelerometers are mounted on the vibrating plate in order to obtain a true representation of the actual signal input at the surface. The signal from these accelerometers, averaged together, is called the ‘pilot’. The time duration for sweep is usually few seconds (~5 to ~15 sec). A ‘pilot trace’ is generated after autocorrelation of input sweep signal. This pilot sweep is further used to crosscorrelate saved data in order to get final raw data, which is afterward recorded on the tape/hard drive or any digital media.

In this study, the University of Alberta 6000 lb (26689 N), peak force ‘T-15000 minivib[®]’, (Manufactured by Industrial Vehicles International of Tulsa, Oklahoma) was used (Figure 4.9). Before selecting the optimum sweep parameters a number of tests were made in the field. A test sweep of 30 Hz to 250 Hz is presented here for purposes of illustration (Figure 4.10) but a sweep with frequencies from 20 Hz to 250 Hz was finally employed (Table 4.1). Theoretically a linear sweep has constant amplitude and frequency varies over desired bandwidth. The instantaneous amplitude of the uncorrelated sweep along with its power spectrum is presented in Figure 4.11. The autocorrelation of pilot sweep i.e. 7 sec duration and 30 – 250 Hz frequency is a zero phase ‘Klauder’ wavelet (Figure 4.12). The amplitude spectra of the correlated pilot trace and one recorded trace are compared in Figure 4.13.

4.1.5. Seismic Recording Instrument

Seismic data was acquired using U of Alberta 240 channel semi-distributed exploration seismographs. The recording instrument comprises of 10 Geometrics Geodes[®] boxes that are linked to the central acquisition computer via Ethernet cable. Each Geode in this system houses 24 channels and combined with 10 Geodes 240 channels can be recorded at once. Each Geode is placed in the field and connected with a 12 V battery. The seismograph consists of 24 bit analog to digital A/D converter and 110 dB dynamic range.

Geometrics Geode[®] recording system differs from the standard exploration seismographs, based on the number of available channels and hardware architecture. Typical oil exploration seismographs can handle few thousand channels at once, which are usually required for 3D seismic surveys. The Geometrics system is mainly designed for near surface seismic studies and can easily be handled and used in the field with up to 1000 channels. This seismograph can also be used for recording multiple seismic lines - a typical for 3D seismic acquisition.

Seismic data was recorded with 0.5 msec sampling interval with maximum recording time 1.1 sec. In order to reduce offline highway traffic noise and the source produced surface waves, high frequency (40 Hz OYO) geophones were selected. The overall bandwidth was reduced due to these high frequency phones, but past field experience shows that loss of bandwidth is further compensated by relative boost in the near surface reflections. Other common types of geophones used in near surface seismic acquisition are 10 and 100 Hz geophones. Selection of specific frequency geophone is a non-trivial problem, due to the different near surface geology among different field locations; past experience and field parameter testing can help picking the appropriate type of geophone for the entire survey (Steeple, 2004).



Figure 4.9: U of Alberta vibrator working in the field. Photographs courtesy of Marek Welz.

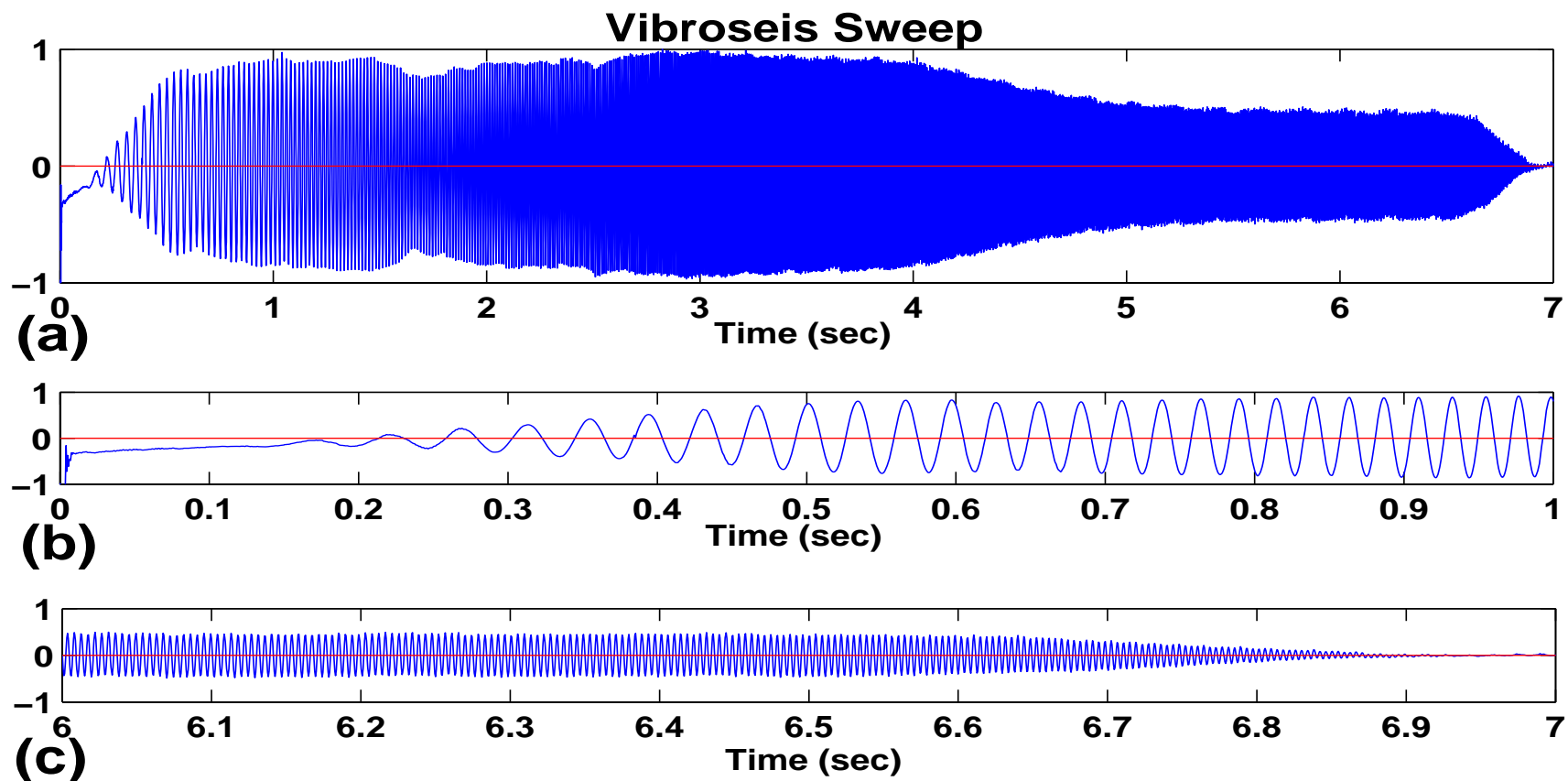


Figure 4.10: (a) Vibroseis complete sweep 30 to 250 Hz; (b) early part of the sweep (see horizontal axis); (c) late part of the sweep. Amplitudes are normalized. Sweep recorded at SP 2408.

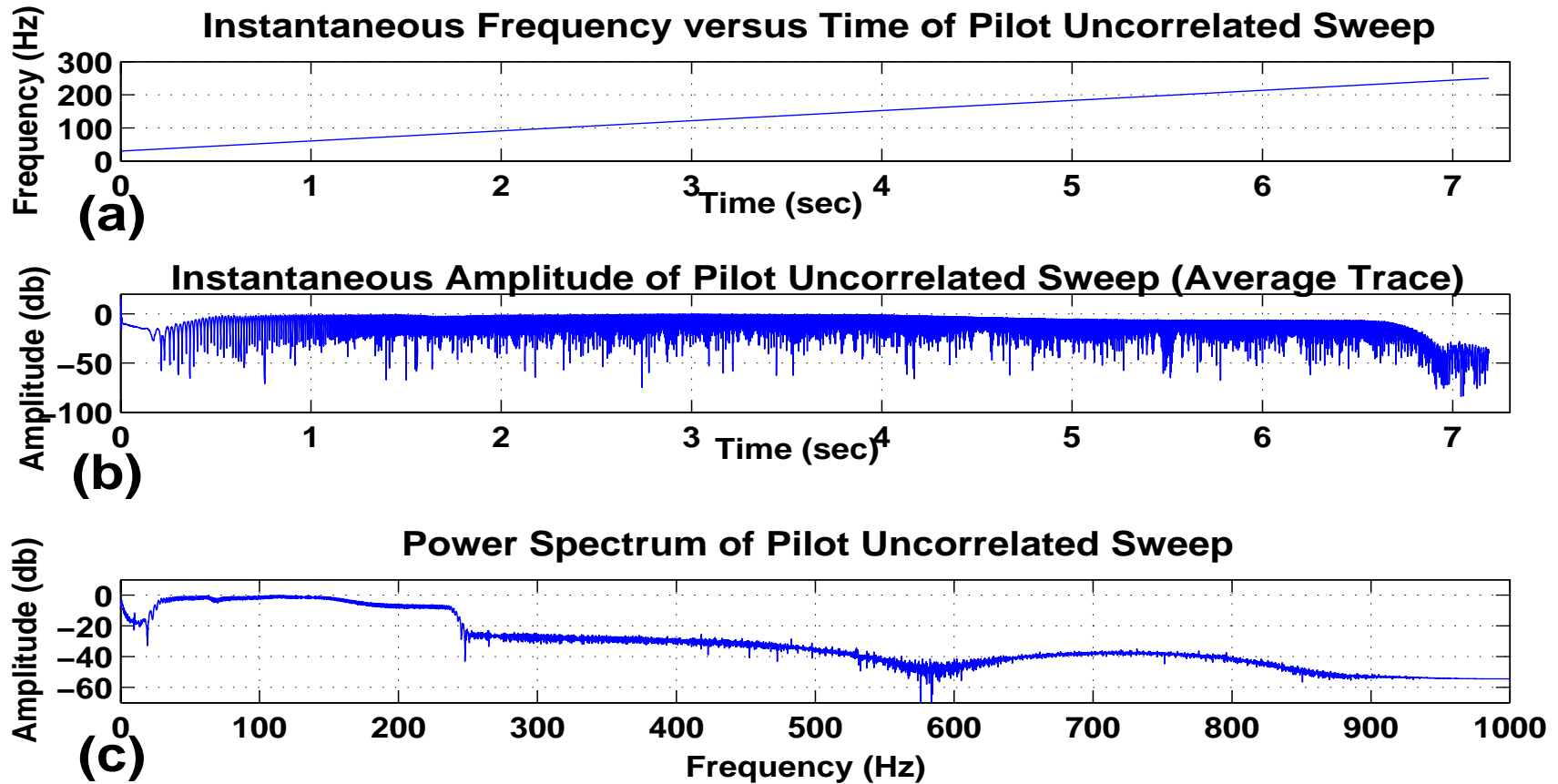


Figure 4.11: Analysis of pilot sweep; (a) frequency versus time during the linear sweep; (b) Amplitude distribution with respect to time showing slightly poor coupling of Vibroseis plate with ground; (c) power spectrum of pilot sweep calculated by simply taking Fourier transform of amplitudes.

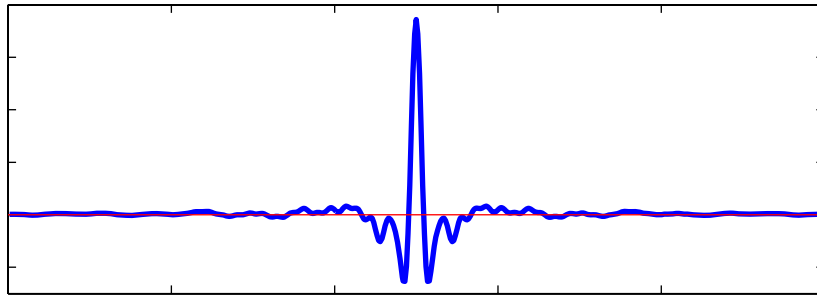


Figure 4.12: Effective source Klauder wavelet after autocorrelation of the pilot sweep, mentioned in Figure 4.10. Variation of Vibroseis force level due to poor coupling (Figure 4.11) is not a trivial problem, as after autocorrelation input signal is a zero phase spike.

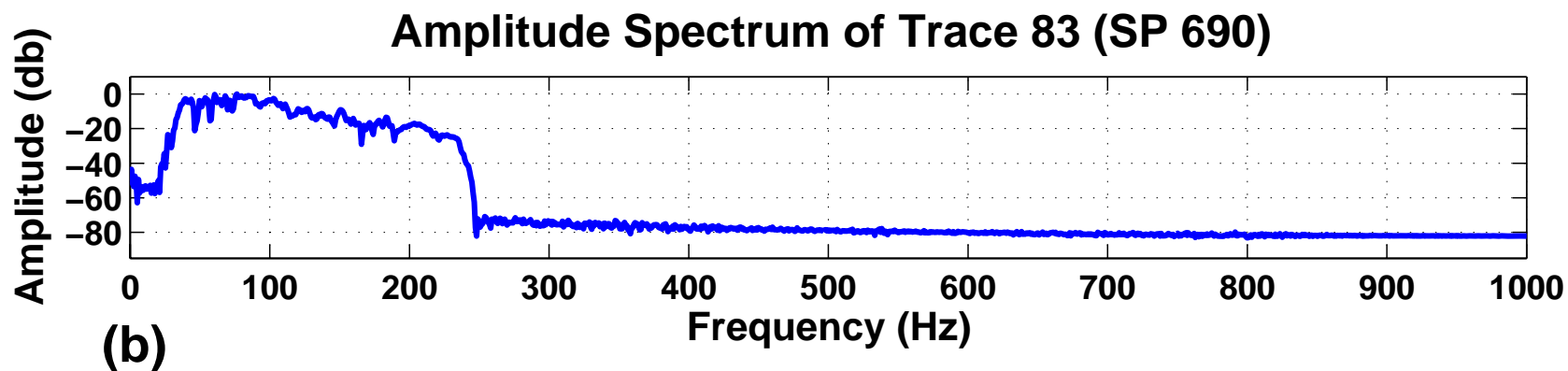
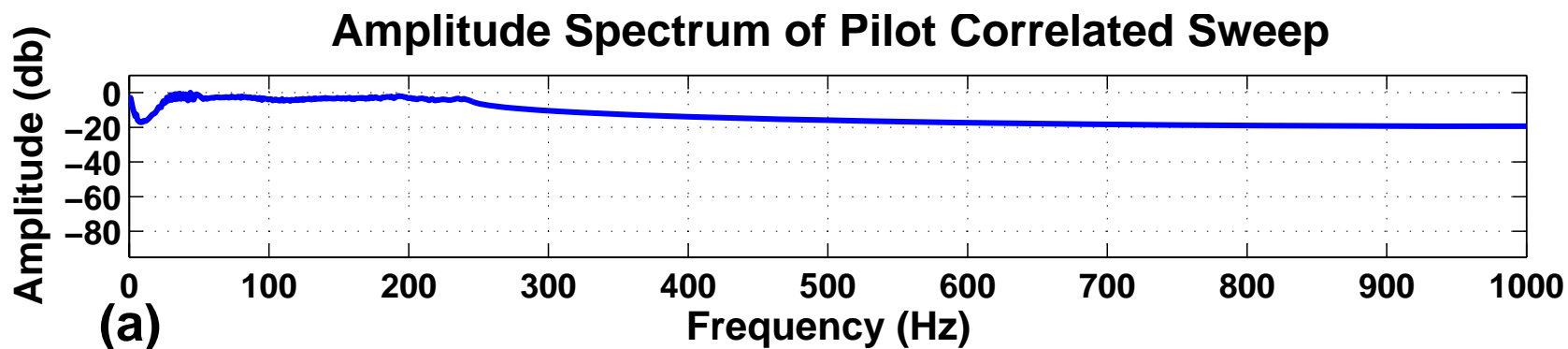


Figure 4.13: Amplitude spectrum of; (a) correlated pilot of Figure 4.10 and; (b) one trace from shot 690. In Fig-b offset of trace from source point is 216 m.

4.2. Seismic Data Processing

4.2.1. Introduction

In this section, I give an overview of how the raw data collected in the field was processed. Seismic data processing essentially refers to the digital analysis of many hundreds of the raw shot gathers, as for example given in Figure 4.2 and Figure 4.3 above, by rearrangement and suitable correction to produce a final seismic image. The whole purpose of seismic data processing is mostly to strengthen the extremely weak seismic reflections by adding like signals together to boost the coherent signal relative to random noise in this image. The overall method is referred to as the Common Midpoint Method; a complete description of this method is beyond the scope of this thesis and the reader is referred to texts such as Yilmaz (1987) and Yilmaz (2001) for details of particular aspects. This image is similar to a geological cross-section that may be interpreted for geological structure, although it must be remembered that the image is usually provided in terms of travel-times, not depth, and the interpreter must keep this in mind to avoid serious misinterpretations.

In this chapter, I have tried to provide descriptions of the various processes such that the nonexpert will have some feeling for the steps taken, this is in part necessary as much of the meaning of the various terms are obscured by the use of geophysics jargon. I apologize to the more expert reader.

Seismic data is processed with conventional processing flow using a commercial seismic data processing package Vista[®] - a PC based software provided by GEDCO of Calgary, Alberta running under a Windows[®] environment. Complete processing flow chart is presented in Figure 4.14 and data statistics in Table 4.6. The raw seismic trace data was saved by the acquisition units in a SEG-2 (Pullan, 1990) format and navigation data in SPS format (SEG, 1995). SPS (Shell Processing Support) format is ASCII data standard which is required to input field

geometries into the seismic trace data. This consists of three ASCII geometry files; 1) file containing coordinates of all receivers; 2) file containing coordinates of all source points and; 3) relational file that links source to receivers via acquisition geometry and also computer file number. After inputting the field geometry, the data were sorted and exported from Vista[®] to a standard SEG-Y format (SEG, 2002) with updated headers, and saved in the hard drive outside the Vista[®] as a stand-alone computer file. The procedure adopted in processing this data set is almost identical to the procedure described in Schmeltz et al., (2005), except a few steps are skipped and modified after testing.

Data Statistics	
Total Line length	10.0183 km
Total Shots	890
Total Traces	~0.2 million
Total CMP's	2400
Computer file size	1.8 G. Byte
Refractions Travel Time picks	~180,000 picks; total shots 410 after merging additional offset shots
Total TWT for processing	710 msec
Offset range for processing	-500 -12 and +12 +500 m
Processing sampling rate	0.5 msec same as raw recorded data

Table 4.6: Table showing statistics of the seismic data

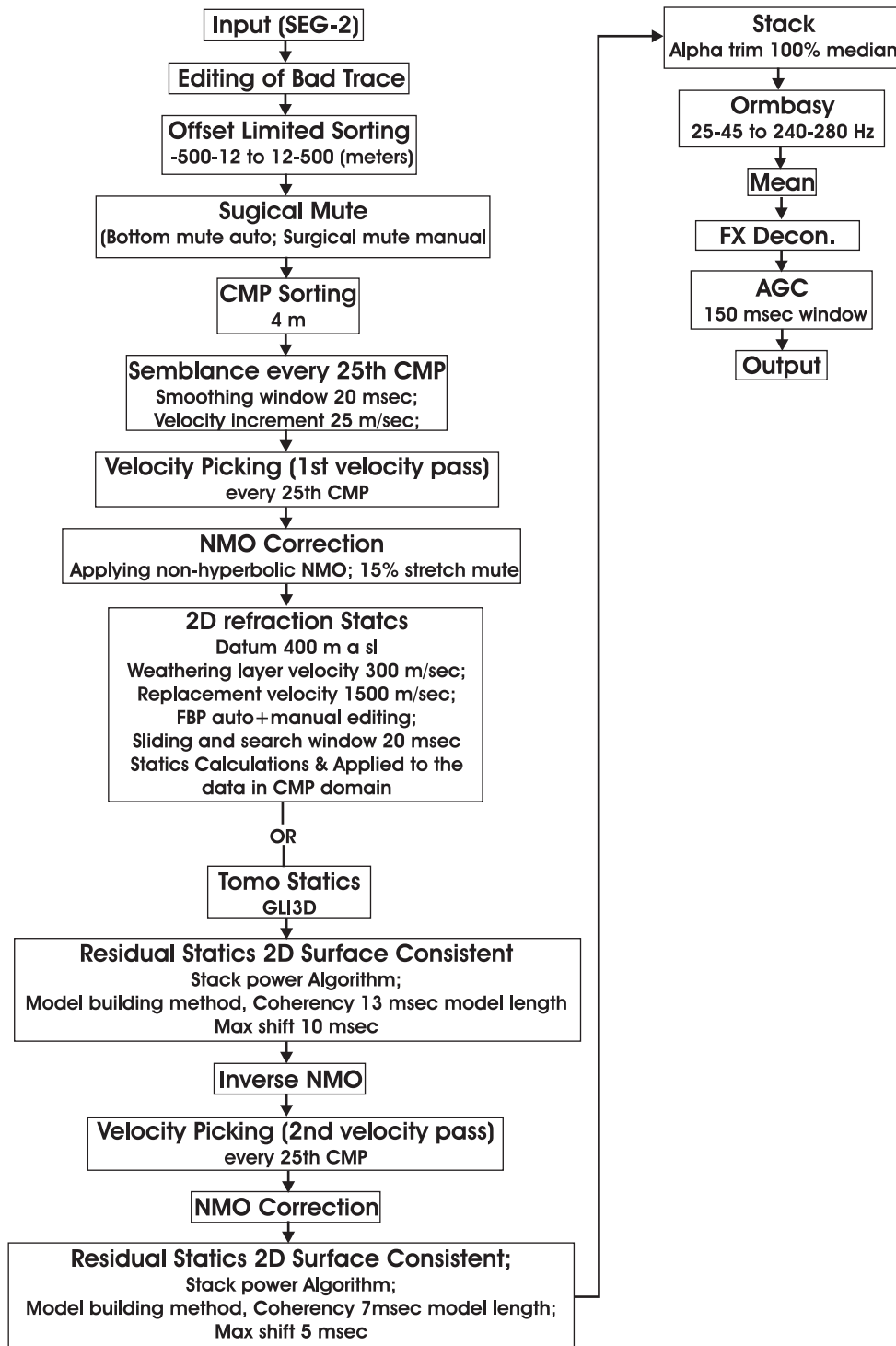


Figure 4.14: Processing flow chart for final stack

4.2.2. Editing

In the processing of shallow high resolution seismic data, the removal, or editing, of low quality signals and noise is very important. Usually such unwanted signals are muted out by ‘killing’ (i.e., removing from further use) of bad traces and muting of the noise cone that consists primarily of the slow but high amplitude surface waves (Bakers et. al., 1998; Bakers, 1999) (Figure 4.15; Figure 4.16). Refractions have high energy relative to the reflections, also significantly degrade stacking of coherent reflections and need to be removed from seismic data. In the beginning it was very difficult to remove refractions with top mute or surgical mute. So, refractions were kept in the data and removed with NMO (see below) stretch mute, later during NMO correction, as described in Miller (1992). Different values of NMO stretch mute were tested and finally 15% NMO stretch mute was selected to mute out first break refractions from every shot (Figure 4.17; Figure 4.18).

4.2.3. Sorting of seismic traces

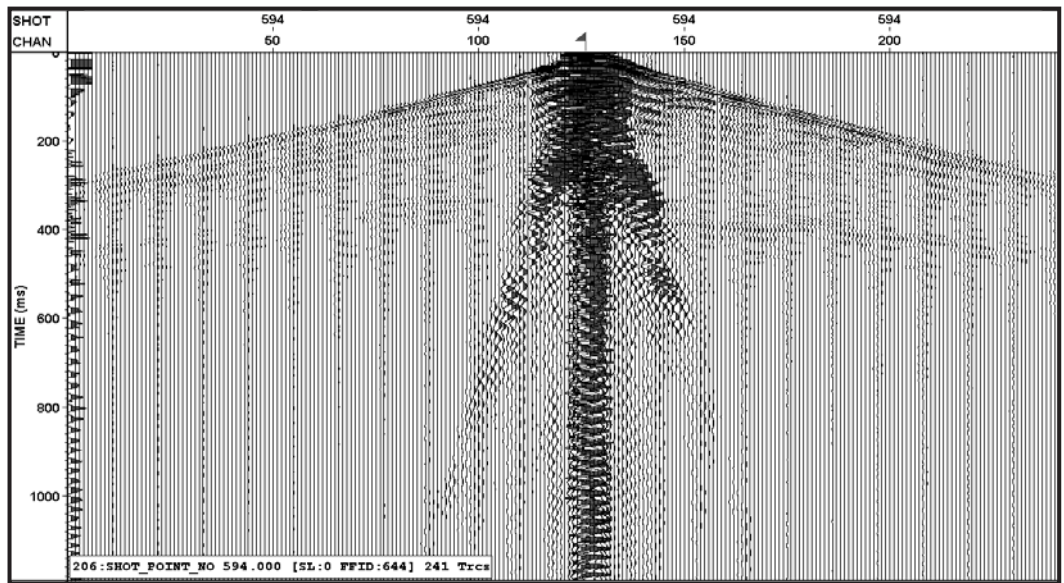
The reality of seismic imaging is that the data must be acquired one ‘shot’ (i.e., energy source position) at a time with the resulting earth response recorded at a series of receiving geophones at various offsets (i.e., distances) from the source position. However, to build the statistics (i.e., to increase the fold) to improve the signal to noise ratios in the final processed data, one desires to constructively add like information. Here this means that if one desires to image the reflection from a given point in the earth then one must selectively choose the set of seismic traces which share this same reflection point. Since this point lies mid-way between a given source and a receiver, one collects in one set all the traces that have the same midpoint – and hence the name of common mid-point (CMP) profiling². To do this, one must take the entire set of common shot gathers each consisting of

² The reader may also encounter in the seismic processing jargon the term ‘Common Depth Point’ or CDP which essentially has the same meaning as CMP in more common usage today.

hundreds of seismic traces and re-sort this set into new groupings of ‘common mid-point gathers’. How this is done will depend on what the processor deems the size of a common midpoint to be.

Here, initially seismic data was sorted according to the minimum 2 m CMP interval which derives from the 4 m receiver spacing, but the signal/noise ratio, the fold and the consequent quality of very shallow reflections were deemed not to be acceptable. In order to enhance the fold and S/N ratio in the very near offsets data was sorted again with 4 m CMP interval. The result of this is that the final seismic image will have half the processed number of traces but these traces should be less contaminated by noise. This reduction should not be a problem as the 4 m CMP trace spacing is still relatively small and remains adequate relative to the expected lateral seismic resolution of the survey as discussed above. The remainder of the processing was carried out with this 4 m CMP interval.

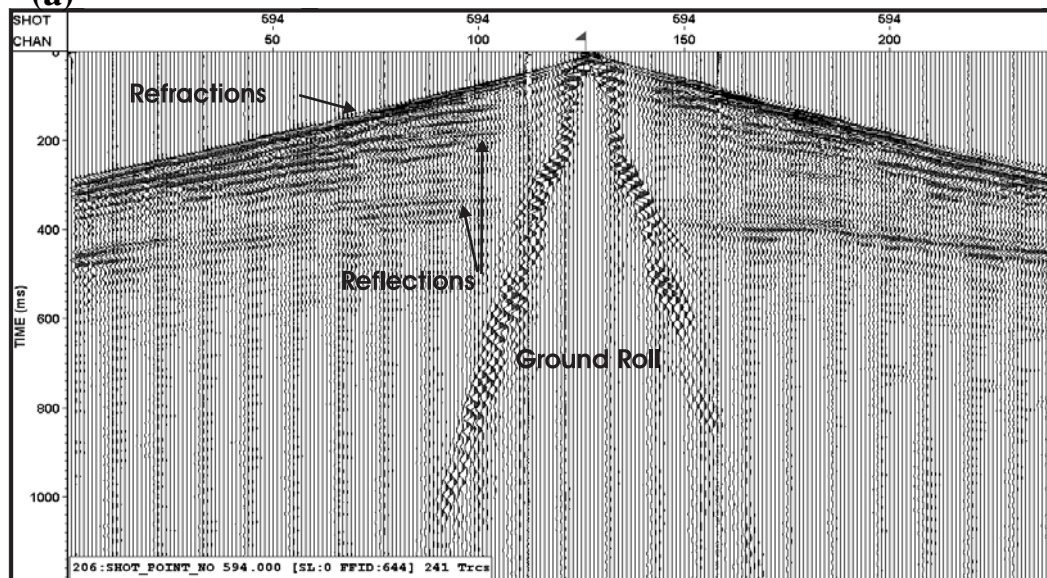
Refractions from Top of the Devonian carbonates completely masked the reflections from this same geological interface beyond offsets of ~800 m. Further, shallower refractions interfered with the desired reflections beyond offsets ~500m although this would vary from shot to shot along the line. As the near surface reflections of interest from the zone above the Devonian carbonates were then essentially obscured, only traces within 500 m of a given source position were included in the data processing. Similarly, traces within ~12 m of the source were overwhelmed by source induced noise (i.e., the diesel engines) and were also not included in the final data processing.



Without Scaling

SP 594

(a)

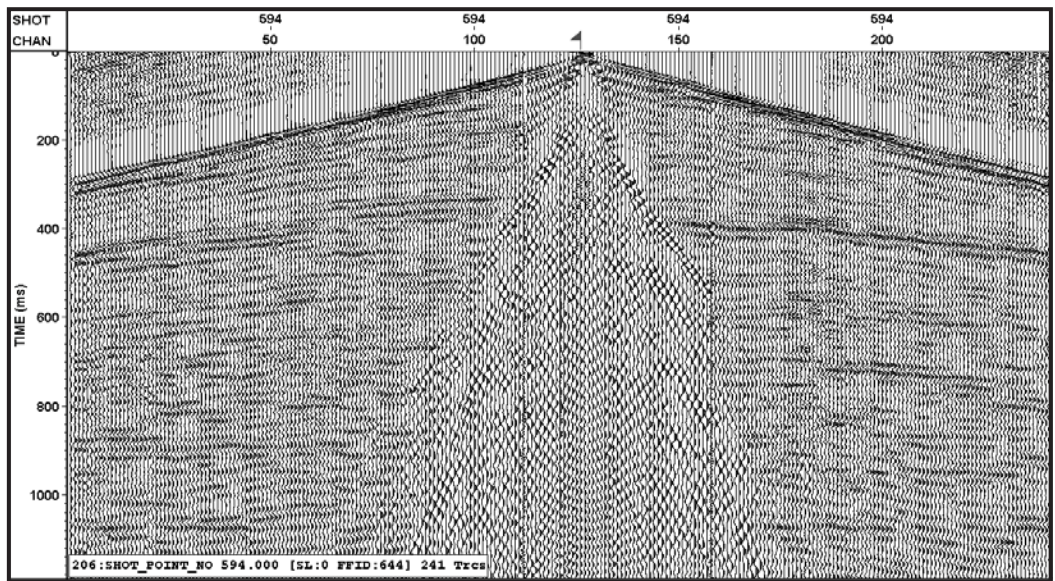


RMS Scaling

SP 594

(b)

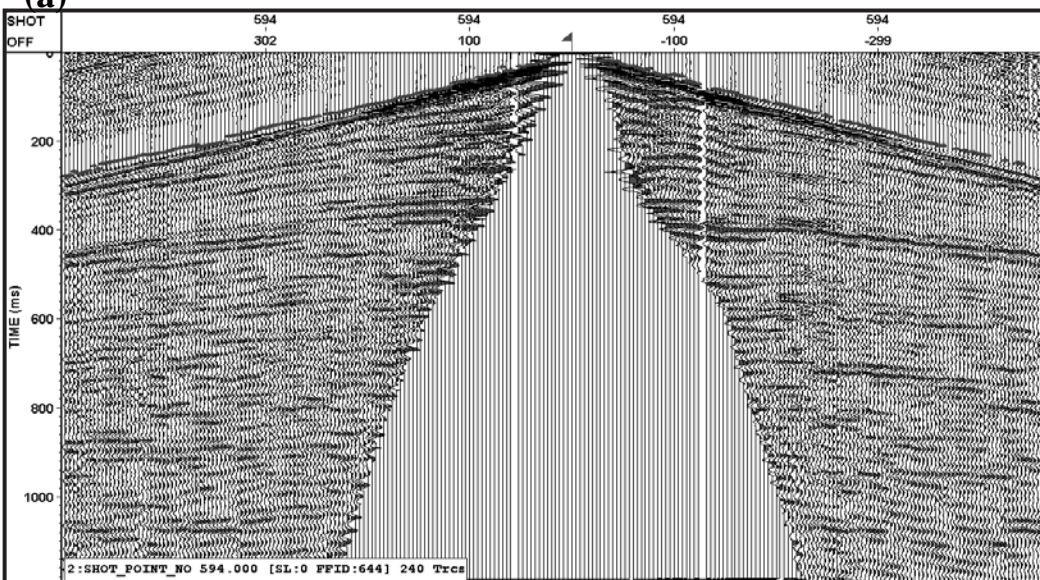
Figure 4.15: (a) without scaling; (b) with RMS scaling. Correlated pilot trace is visible in extreme left (1st channel) of Fig-a. Different events are marked on the gather i.e., refractions, reflections and ground roll.



AGC 150 msec

SP 594

(a)

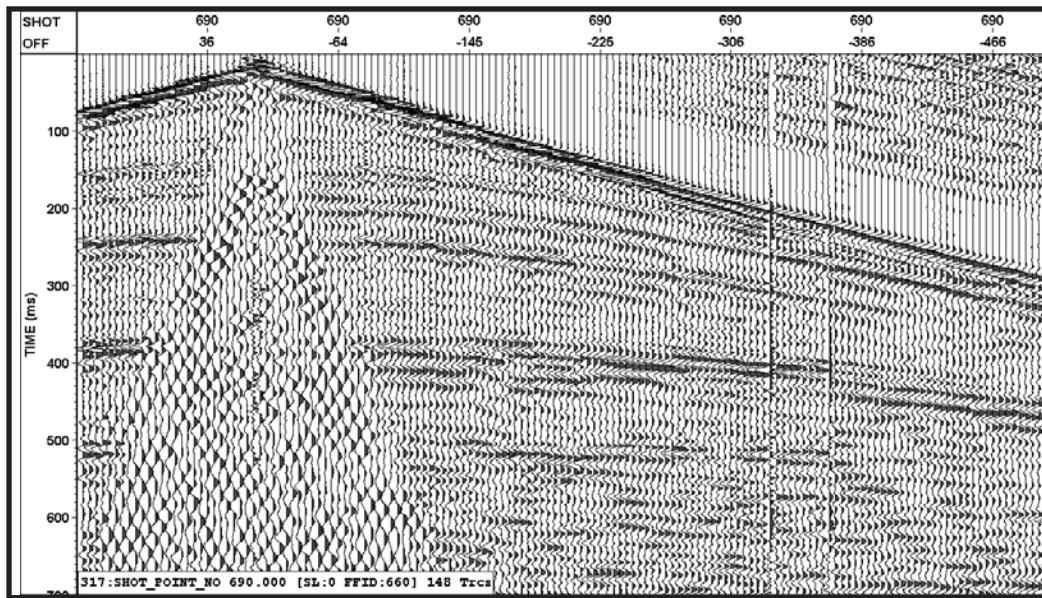


Ground Roll surgically muted; Bad trace killed; First break picked

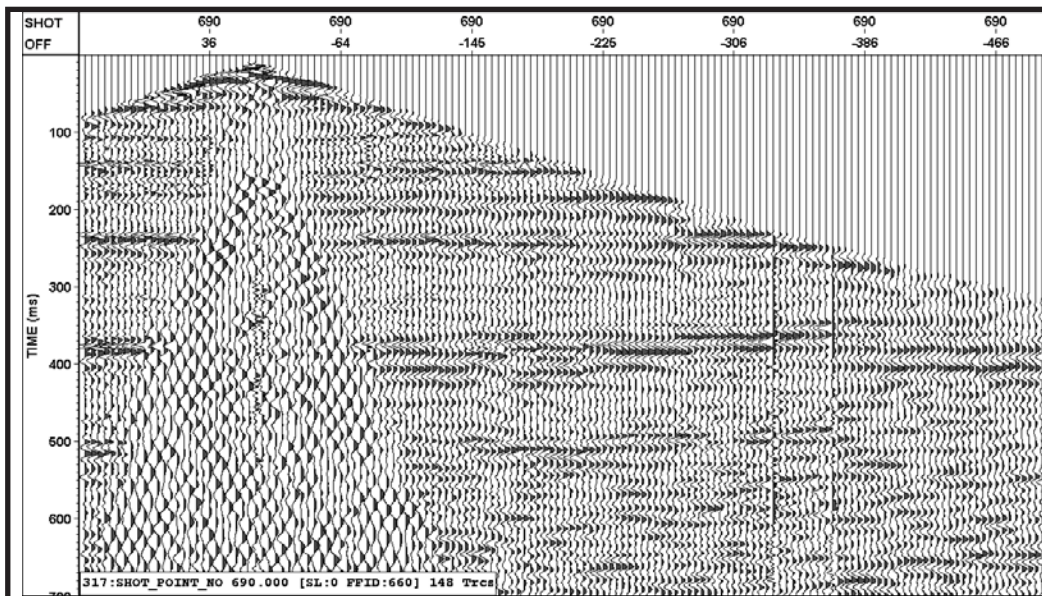
SP 594

(b)

Figure 4.16: (a) after AGC 150 msec window, (b) bad traces are killed and ground roll is surgically muted. First break refraction pick is also visible in Fig-b.

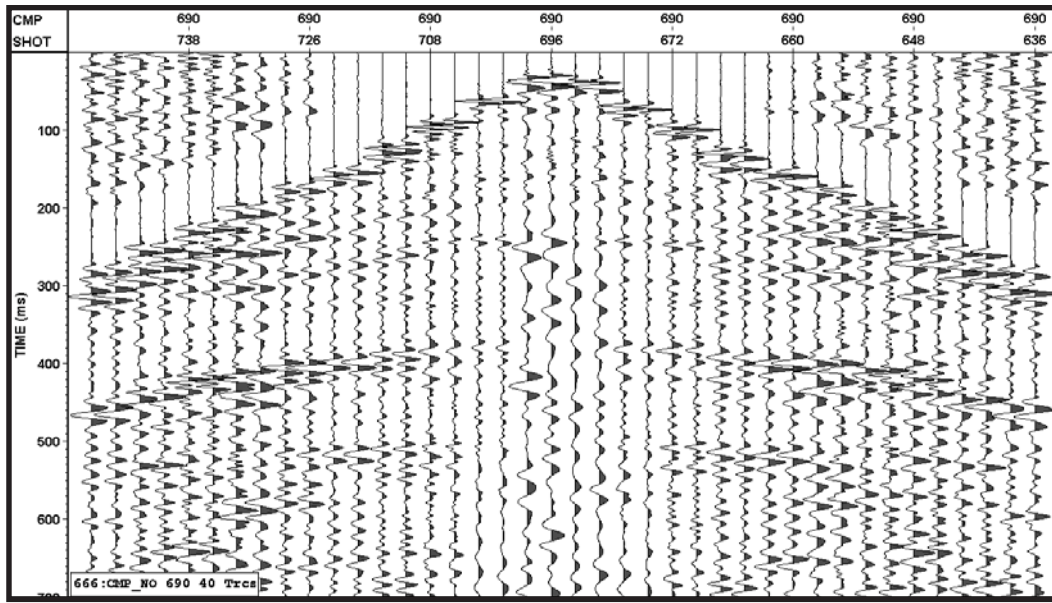


(a)

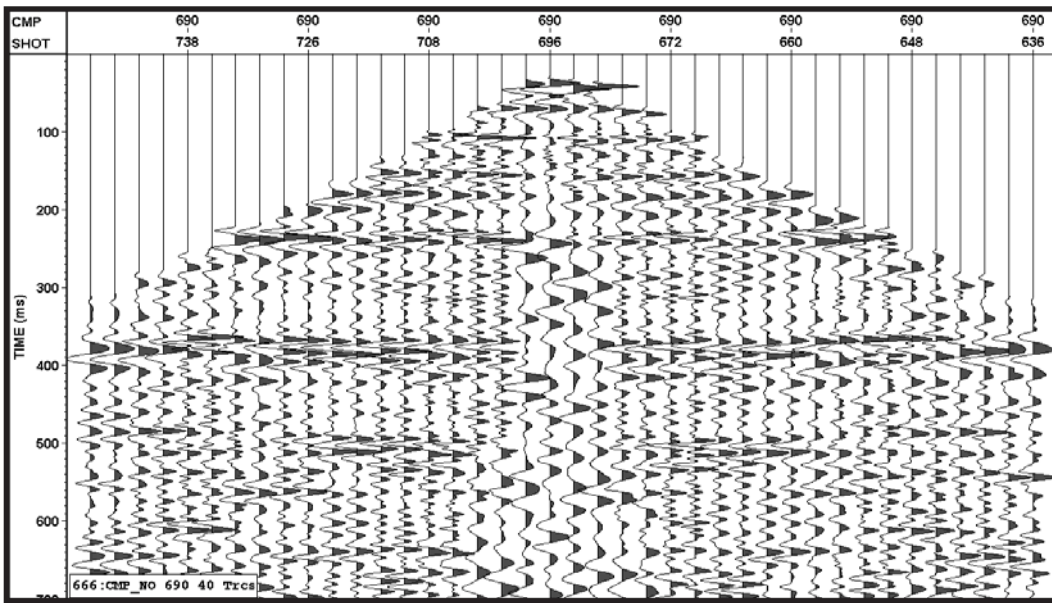


(b)

Figure 4.17: First arrival stretch mute is very important in shallow data processing but not very important in deep reflection. (a) Shot Gather without mute and; (b) same shot gather showing NMO stretch (15% stretch mute)



(a)



(b)

Figure 4.18: (a) CMP gather without stretch mute and; (b) CMP gather with NMO stretch (15% stretch mute).

4.2.4. Velocity Analysis and the Normal Moveout (NMO)

An important part of seismic data processing is carrying out the correction of the reflection travel times, which follow along nearly hyperbolic trajectories in x-t space, to what is their normal incidence travel time t_o , i.e., the time it takes for the seismic wave to propagate from the surface to the reflector and back to the same source point under the assumption that the reflecting layer is horizontal (Figure 4.19). The traveltime $t_x(t_o)$ of the same reflecting interface is approximately given by what is called the normal moveout equation:

$$\Delta t_{NMO} = t_x - t_o \quad (4.6)$$

$$\Delta t_{NMO} = t_o \left[\sqrt{1 + \left(\frac{x}{v_{rms} t_o} \right)^2} - 1 \right] \quad (4.7)$$

t_x = two way time at given offset

t_o = two way time at zero offset

v_{rms} = root mean square velocity

x = source receiver offset

Where the V_{rms} is the root mean square average velocity:

$$v_{rms}^2 = \frac{1}{t_o} \sum_{i=1}^N v_i^2 \Delta t_i \quad (4.8)$$

Δt_i = two way travel time at i^{th} layer

v_i = velocity at i^{th} layer

Of a stack of N layers each of interval (i.e., material) velocity V_i and thickness h_i . Note that in general we rarely know what the interval velocities or their thicknesses in the real earth are. However, by examination of the hyperbolic travel times, referred to as the moveout, one is able to estimate V_{rms} with time. This may then be used to determine the offset dependent traveltime shifts that need to be applied in order to ‘flatten’ the reflections so that they may easily be ‘stacked’ (i.e., added together to increase the signal to noise level).

A variety of methods are employed to obtain $V_{rms}(t_o)$ from the moveout hyperbolas and there is insufficient room to review all of these here. The ‘semblance’ method, first developed by Taner and Fulton (1969), was primarily employed. Briefly, this could be considered a brute force method in which the statistical quality of the moveout is tested for a large number of trial V_{rms} values over the expected range. The semblance is calculated as:

$$S_c(k) = \frac{\sum_{j=k-N/2}^{k+N/2} \left[\sum_{i=1}^M f_{ij} \right]^2}{M \sum_{j=k-N/2}^{k+N/2} \sum_{i=1}^M (f_{ij})^2} \quad (4.9)$$

f_{ij} = is the j^{th} sample (amplitude value) on the i^{th} trace

S_c = semblance coefficient

N = window length centered at k

M = number of traces in CMP

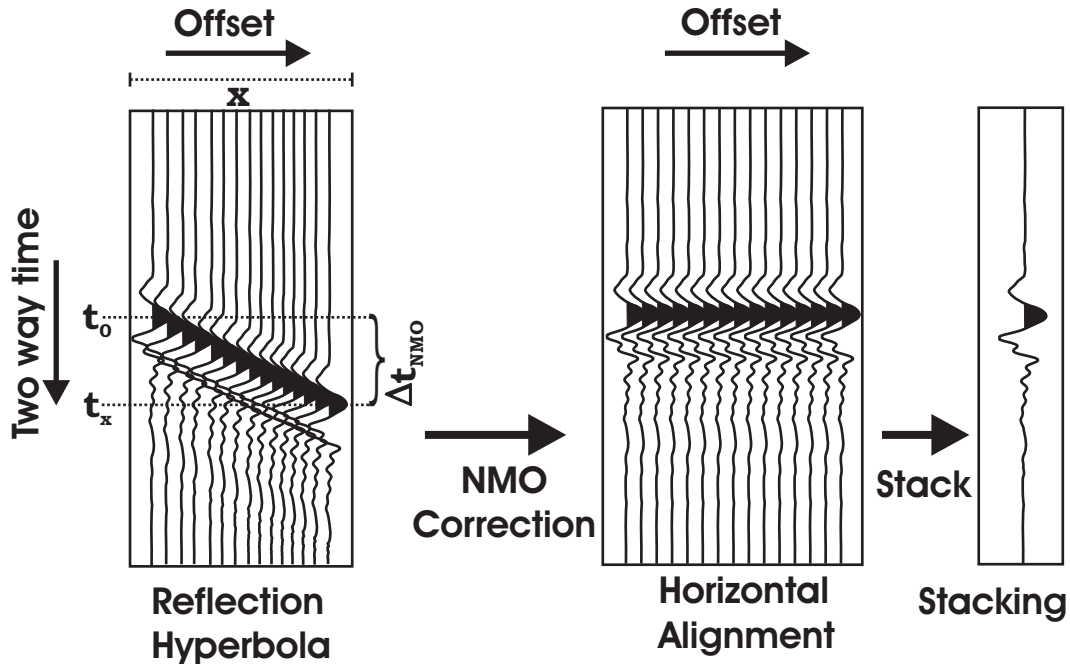


Figure 4.19: NMO (Normal moveout correction) principle on CMP gather. NMO hyperbolas are corrected using correct velocity and then reflector become flat and all traces summed to give stacked trace.

For a given constant t_o , trial values of V_{rms} are tested with this until a peak in the

value of the semblance is found. This peak provides the ‘best’ value of the V_{rms} required to find the ‘dynamic’ offset dependent correction $\Delta t_x(t_o)$.

One problem with the NMO dynamic correction is that it changes the frequency content of the traces because the offset traces will be ‘stretched’ (i.e., lengthened in time relative to the original trace) with a corresponding lowering of the frequency. Schmitt (1999) provides a formula for this frequency shift:

$$f' = f \left(1 + \frac{d(\Delta t)}{dt_o} \right) \quad (4.10)$$

f' = distorted frequency

f = original frequency

t_o = normal incidence two way time

Δt = moveout time

This stretching problem is most severe for small t_o and far offsets but at short offsets and longer times it is nearly negligible. As such, the portions of the traces most susceptible to this stretching are highly distorted and because of this these portions of the data are also discarded. In practice this is done on the basis of a percentage mute with typical ranges from 5 to 20%.

In the current study, although the raw CMP gathers are of very good quality, the stacked seismic data quality was deteriorated due to severe vertical and lateral velocity variations in the shallow part which make proper NMO correction difficult. Usually, severe velocity gradients due to the presence of near surface water table effectively degrade the quality of CMP stack (Miller et. al., 1998). In the present case, much of this variation may come from differing thicknesses of the overburden material and variation of this material between mineral soils and muskeg. Such vertical velocity variations were observed during semblance velocity analysis. Effects of lateral velocity variations are also discussed in the section on ‘static correction’.

Conventional velocity analysis was carried out interactively within the processing software with a $V_{rms}(t_o)$ function picked every 25th CMP (100 m) on a standard semblance display within the processing software (Figure 4.20). Semblance is a measure of coherency of stacked amplitudes across a set of traces (Yilmaz, 1987). The colour-coded contour plots of velocity verses time were made at each 25th CMP for velocity picking. The root mean square velocities were picked manually from the semblance plots and converted into interval velocities using Dix's (1955) formula:

$$V_n^2 = \frac{V_n rms^2 t_n - V_{n-1} rms^2 t_{n-1}}{t_n - t_{n-1}} \quad (4.11)$$

V_n = Interval velocity of nth layer

$V_n rms$ = root mean square velocity of nth layer

t_n = two way travel time to the bottom of nth layer.

Figure 4.21 shows the interval velocity profile. This profile clearly shows the variation of velocity at the Top Devonian level (~300 msec) in the western part. Based on the variation in the velocity, two different types of geological formations can be interpreted on the profile. Low velocity material in the eastern half of profile is indicative of the fill material in the buried valley/channel. At this stage, these are just observations and further details of these will be provided in the later chapters.

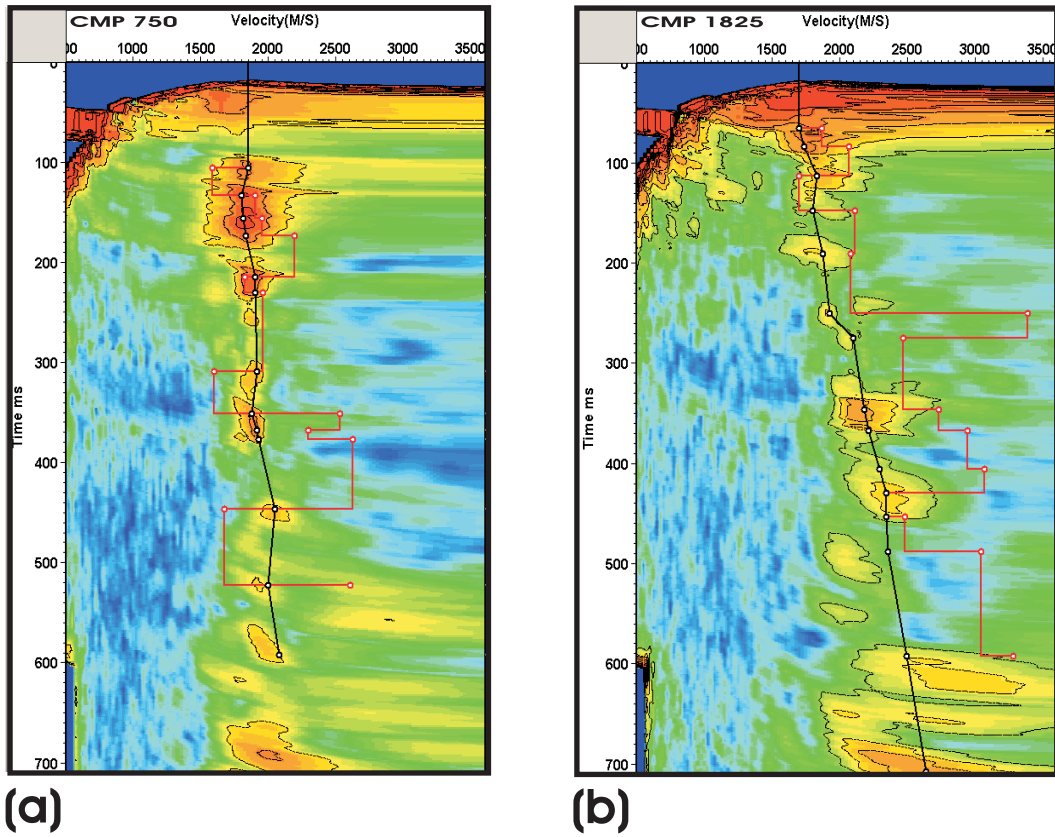


Figure 4.20: Semblance display of; (a) CMP 750 and; (b) CMP 1825 showing picked velocities (black) and Dix interval velocities (red). Both of these plots are produced from Vista[®] software.

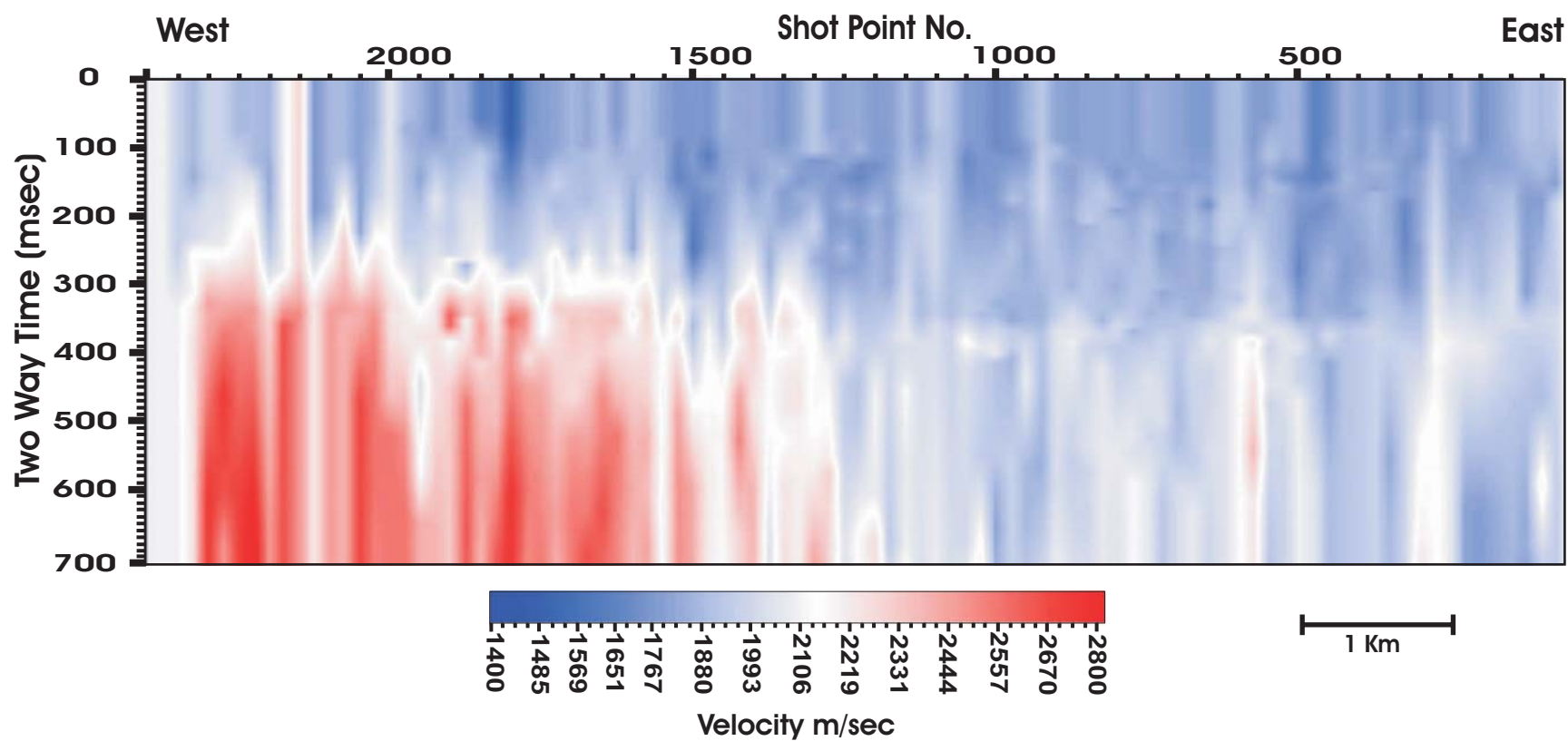


Figure 4.21: Interval velocity 10 km east-west profile. See text for details.

Because refractions show different move out velocities than the reflections and can be muted out with NMO stretch mute (Steeple et. al., 1998). Fold is reduced during processing due to the NMO stretch mute (Figure 4.22; Table 4.7). Different values of stretch mute were tested and optimum stretch mute value of 15% was selected which significantly muted out refractions. Some problems associated with severe velocity anomalies in shallow seismic data and their solutions are described in Miller et. al. (1998).

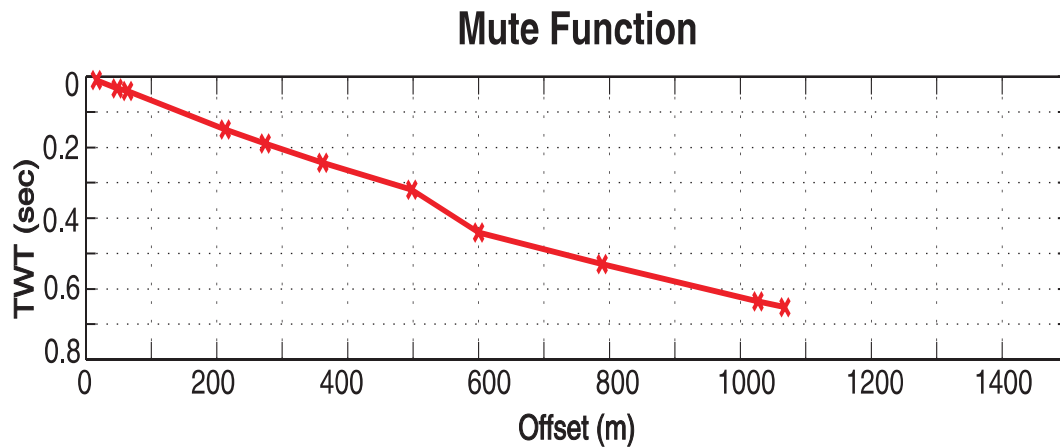


Figure 4.22: Mute function; values picked from NMO mute of shallow reflectors (< 200msec) and Top Devonian (~400msec). Beyond 400 msec values are picked on visual inspection of shot gather 690.

TWT (sec)	Offset (m)	Fold (Observed at particular TWT after NMO mute)*	~Depth based on stacking velocities
0.5	75	4	53
0.1	145	8	105
0.15	213	12	160
0.2	292	20	205
0.25	372	28	255
0.28 (~Base of Quaternary)	427	32	290
0.38 (Top Devonian Level)	548	40	365
0.4	565	40	390

Table 4.7: Table showing fold with respect to mute. *Fold increased due to 4 m CMP sorting. Fold values are based on CMP 690 and may vary along the seismic line. With these offsets i.e. 565m at ~Top Devonian level and depth 390m, data falls in wide azimuth survey.

4.2.5. Static Corrections

A ‘static’ correction is a time shift given to the traces in order to compensate for effects of the lateral variations in elevation, weathering layer thickness, and velocity. During seismic wave propagation from the seismic source to the receivers the waves must pass through low velocity near surface materials. Seismic waves travel slower in the low velocity material and their travel times are increased. Because the velocities of the near surface materials can be substantially lower than the underlying bedrock, the time of a reflection from depth will also vary due to these lateral variations in traveltimes. In short, the problem with such variations is that after the application of the dynamic NMO correction, a given event will still not line up at the same value of t_o . Hence, the quality of the final stack will be degraded because the coherent parts of the dynamically corrected seismograms will not appropriately align. Consequently, there is a need to calculate the thickness and the velocities of weathering layer in order to allow estimation of the travel time shifts for each individual trace that will remove much of the problematic shifts. One way to think about these shifts is if one were to essentially strip off the top parts of the earth making the surface of the earth now on bedrock and with no topography. This ‘new’ surface of the earth is called the datum elevation to which all of the seismic traces are corrected. Then static correction is applied and data is shifted into certain datum. Figure 4.23 schematically shows the static correction procedure

Correct static correction is a key factor in shallow seismic data processing. This is complicated by the presence of very low velocity material in the near surface which lengthens the travel time of a given seismic event, and this needs to be corrected before stacking or else the quality of the stack will be substantially degraded. Quaternary deposits present in the near surface contain both high and low velocity material. Loose muskeg³ is present at the ground surface in the

³ Muskeg is a Canadian term that refers to a peat bog filled with sphagnum moss plant material in varying states of decay. This covered much of the ground surface over which the survey was conducted. This material can only be crossed easily during winter when it is frozen. Such material also presents a formidable challenge in seismic processing as it has a very low velocity.

project area, which has very low seismic velocity.

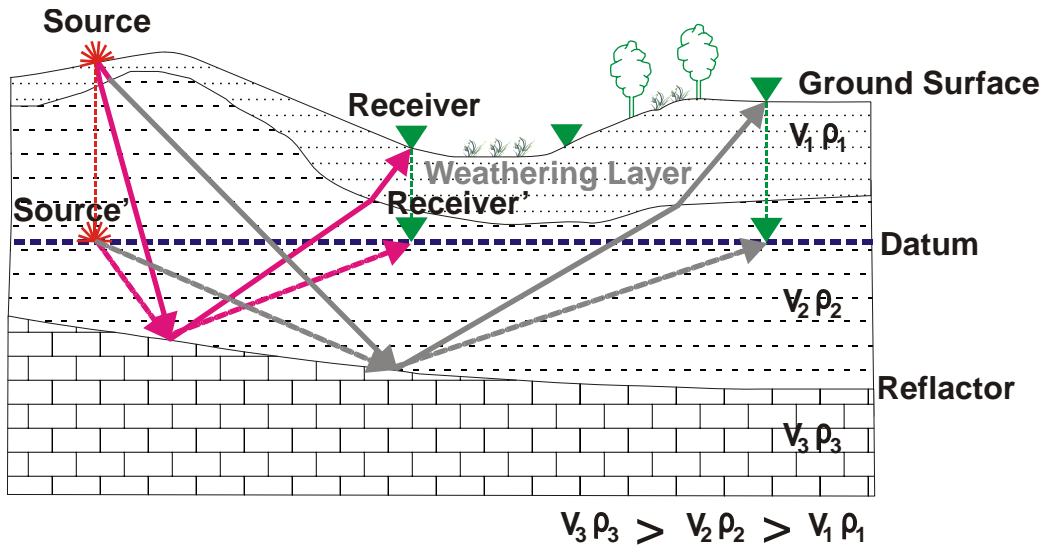


Figure 4.23: Cartoon showing static correction procedure. After calculating weathering layer thickness and velocity, static correction i.e., time shift to source and receiver, is calculated. Static correction is applied by moving ‘source’ to the datum (source) as well as receiver to the datum (receiver).

First break travel times (FBP) were picked manually in the shot domain in Vista[®]. These FBP’s were used for calculating the static correction. The refraction static correction was calculated using the plus-minus method first developed by Hagedoorn (1959). Final static values are presented in Figure 4.24. Whereas weather layer thickness and velocity used to calculate static correction is presented in Figure 4.25. Weathering layer velocity is lower in the eastern part of the line where as it is slightly higher in the western end of the line. Whereas weathering layer thickness is variable throughout the line with slightly increasing at two different places in the western half of the line. Slight increase of weathering layer velocity in the western half of the line is also noticeable on the tomographic velocity profile – discussed below (Figure 4.26), which confirms the validity of the refraction based statics analysis. More advanced techniques to determine the statics were attempted that employed the algorithms of tomo-statics. However, these techniques failed partly for technical reasons but primarily, we believe, due to the fact that the spacing of our data acquisition is

much smaller than industry norms for which the algorithms may not have been optimized. Near velocity model obtained by using tomo-statics algorithm is displayed in Figure 4.26.

After NMO and static correction the data still needs minor corrections due to misalignment of seismic amplitudes in CMP domain. In order to do this, static time shifts are calculated for each receiver and source position. In this method assumption is made that time delays are not due to the complex raypath geometry (i.e., rays that pass through weathering layer) but only due to source and receiver surface locations (Yilmaz, 1987). Different residual statistics can be adapted. But all of these techniques use some kind of statistical procedure to calculate the best fit of particular reflectors on NMO corrected CMP gather and provide time shifts for source and receiver. These time shifts are then applied in the CMP domain to best align the reflectors. Residual static corrections are applied in the pre-stack domain.

Surface consistent residual static corrections were also applied after each velocity analysis and NMO cycle. The method available in Vista[®] for surface consistent residual static correction estimation is stack power optimization that is based on Ronen et. al. (1985). In residual statics calculations the maximum residual static shift allowed was less than one wavelength (i.e., <10 msec) and it effectively improved the coherency of events. Usually higher residual time shifts smooth reflectors which further hide small scale geological features i.e., faults, pinchouts etc.

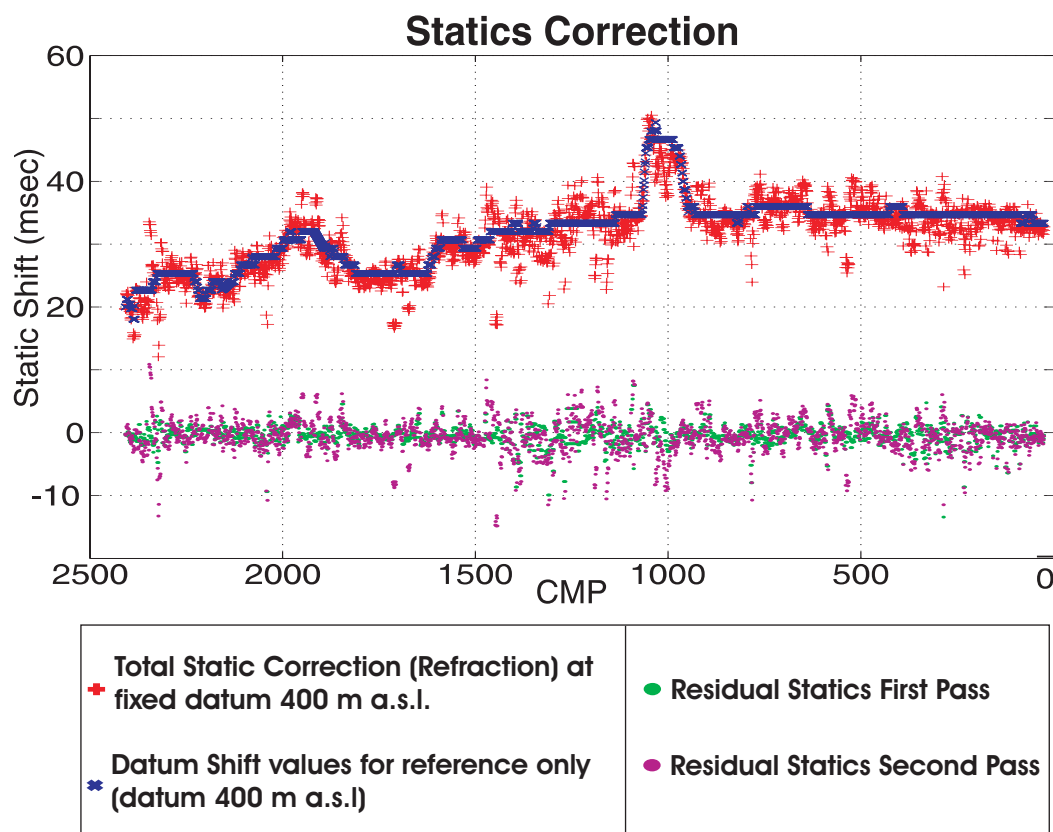


Figure 4.24: Refraction static correction calculated in Vista[®] with fixed datum using plus-minus method. Surface consistent residual static corrections 1st and 2nd pass are also shown here. Total datum shift is presented for reference only. Actual static values are very small and major shift is due to fixed datum. The elevation ranges from 360 to 385 m above sea level (see Figure 4.5). This figure is created in Vista[®].

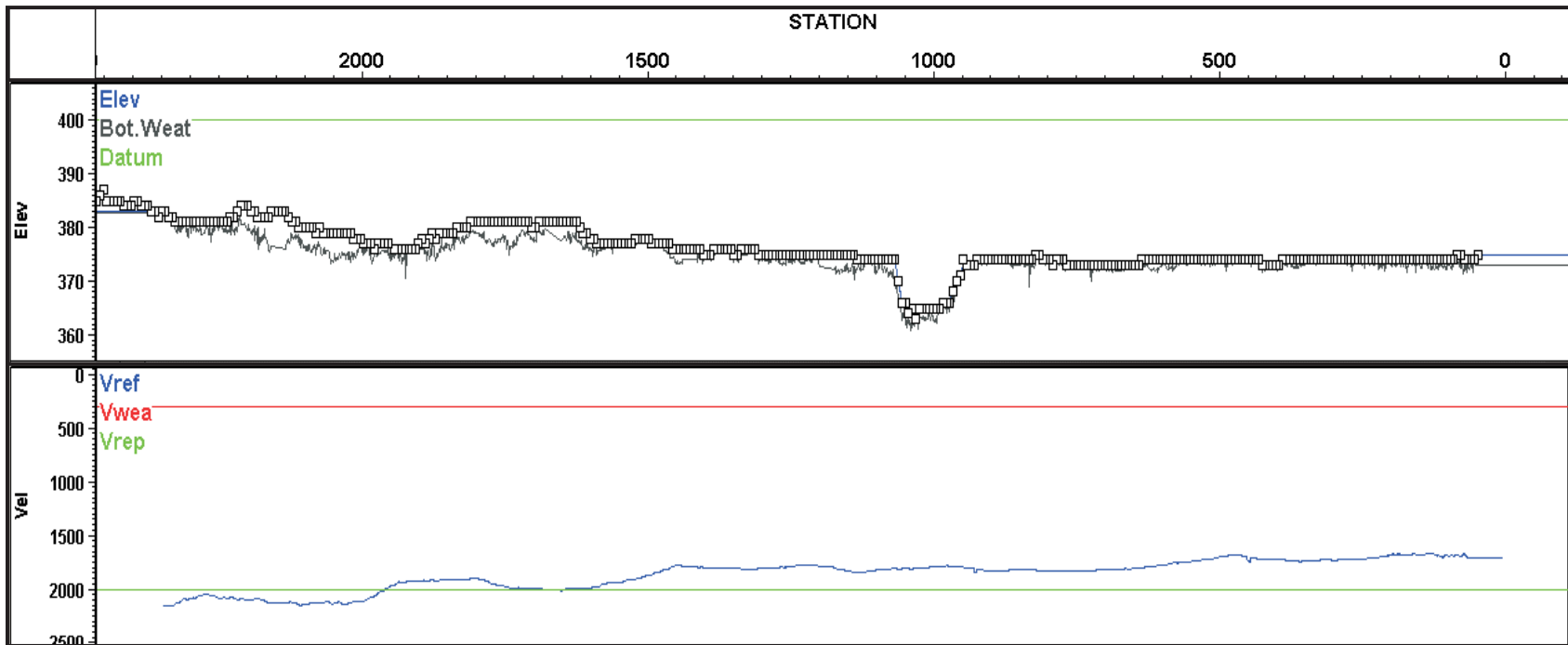


Figure 4.25: Showing (top) weathering layer thickness and (bottom) refraction velocity of weathering layer. Replacement velocity 2000 m/sec; weathering velocity 300 m/sec; and datum 400 m a.s.l. This figure is created in Vista[®].

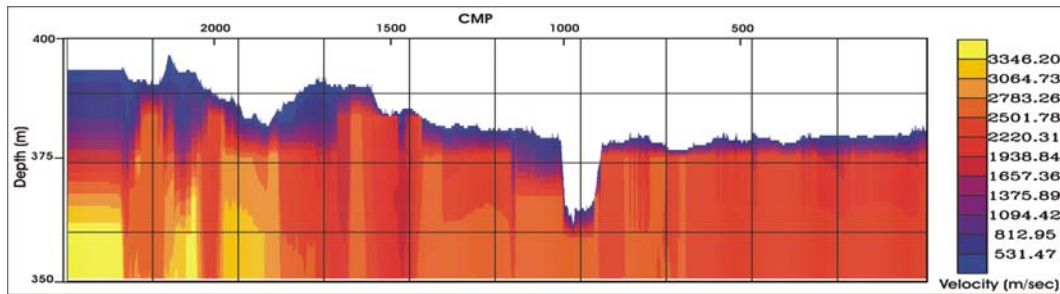


Figure 4.26: (<50 m) velocity profile based on turning ray tomography calculated in GLI3D[®]. The input parameters are FBP's as mentioned in Table 4.6. This figure is created in GLI3D[®].

4.2.6. Processing Pitfalls

High resolution seismic data processing is not only just scaled down from conventional standard exploration seismic or crustal studies but also differs in many additional points (Steeple et. al., 1998) and in many ways is much more difficult to process correctly than is surface land and especially deeper marine exploration profiling. A few of the problems encountered during data processing and subsequent solutions found from scientific literature search are presented here for reference.

Automatic gain control (AGC) scaling is often used to display seismic data after processing. AGC is usually used to balance and enhance/amplify seismic amplitudes especially for late arrivals i.e., arrivals coming on higher two way time. This procedure effectively improves visual display of seismic section. Special care must be given while selecting AGC window in shallow seismic because improper window will produce artifacts (Steeple et. al., 1998). A portion of the final stack calculated with three different AGC averaging windows of 50, 150 and 250 msec is presented in Figure 4.27. After testing different AGC windows, a 150 msec window was selected for the entire line because it gave balanced seismic amplitudes for both near surface and Top Paleozoic reflections (i.e., Top Carbonate).

The preamplifier gain of the recording instruments was set to 24 dB to boost weak reflections during acquisition. Because of this at very near offsets few traces were clipped i.e., the final amplitudes exceeded the dynamic digital range of amplitudes allowed in the computer and as such appear a phenomenon known as ‘dynamic range clipping’ (Figure 4.28). As identified by Don Steeples (personnel communication, 2004) after looking at one of the shot gathers; the near offset clipped traces were muted out by offset reject sorting.

Avoiding the stacking of strong refractions, which do not contain information on the reflections, is also a challenging problem in near surface seismic studies. These are usually removed directly by muting and since these are the first arrivals this is referred to as a top mute. However, this top mute is very hard to put in high resolution seismic data because it can be difficult to differentiate between the direct, the refracted and the reflected waves (Steeple et al., 1998). A few of the stacked refractions in brute stack are shown in Figure 4.29, which were removed later on by NMO stretch mute (see section 4.2.4).

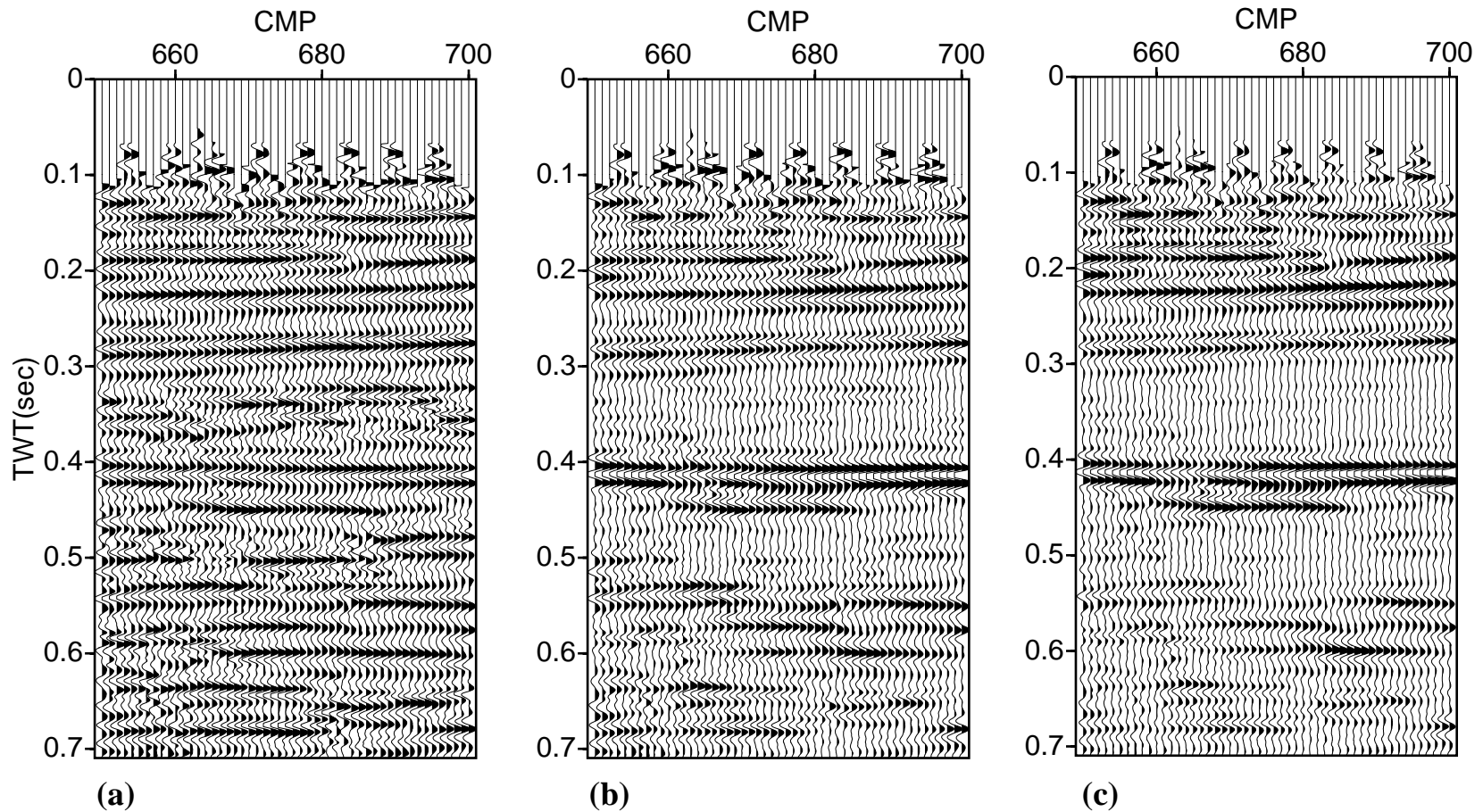
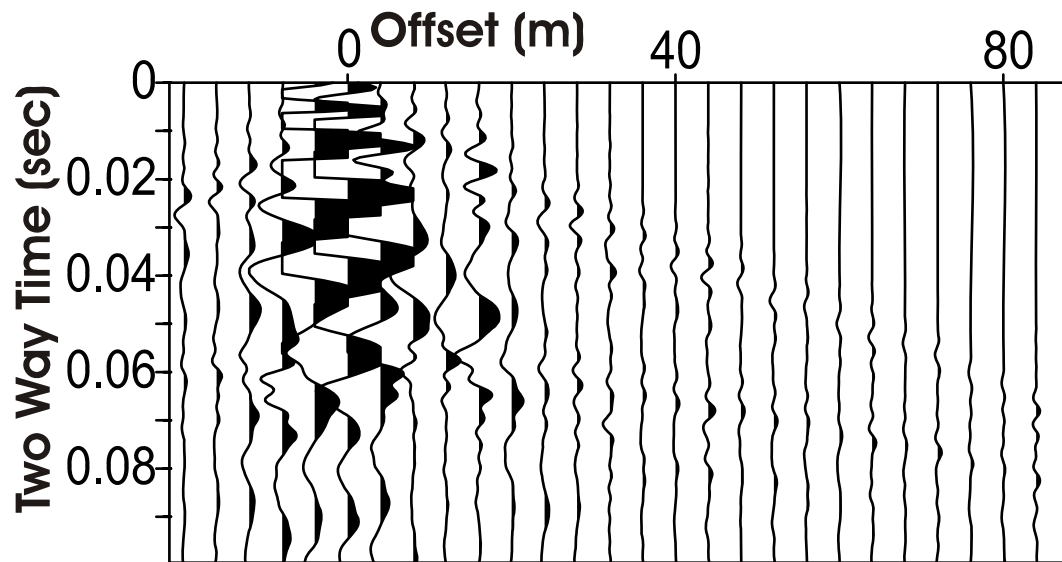
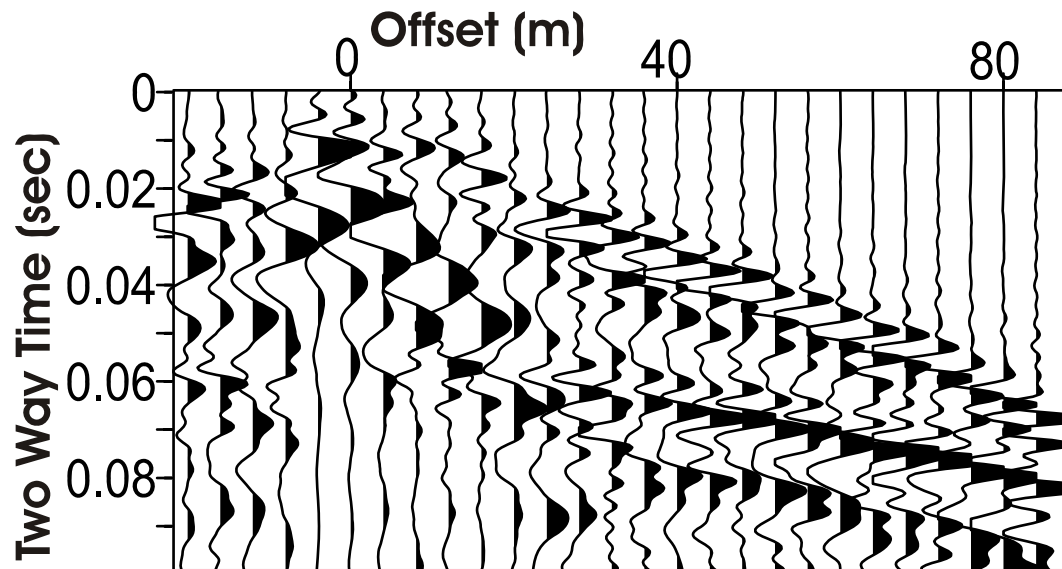


Figure 4.27: Part of brute stack with; (a) 50 msec AGC; (b) 150 msec AGC; (c) 250 msec AGC window. Correct AGC window is important to see real geological features. With 150 msec AGC window (Fig-b) the amplitudes at 0.4 sec reflector is higher than the 0.25 sec reflector which is real because 0.4 reflector is top of carbonate. 150 msec AGC window was selected for the complete line for final display purposes.



(a) No Scaling



(b) Mean Scale

Figure 4.28: (a) shows clipping at very near offset traces. The preamplifier gain was set to 24 dB to boost weak reflections at far offsets. Data was later on sorted offset limited with rejected offsets -12 to $+12$ m. (b) shows same with mean scale. SP 540; Field Record Number 635; Channels 173-205

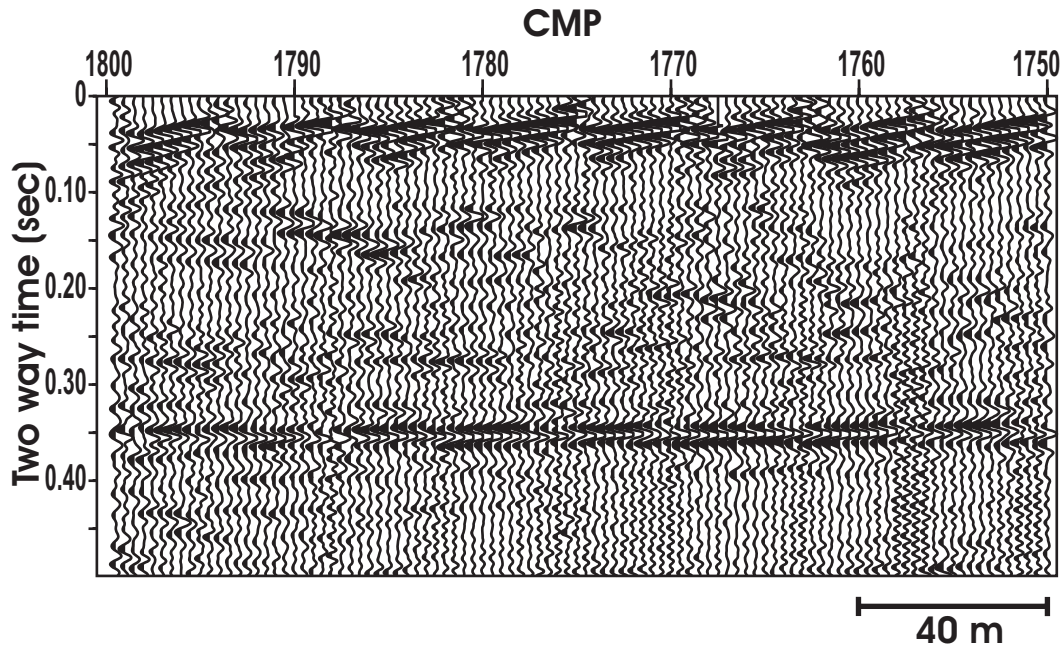


Figure 4.29: Part of the brute stack showing stacked refractions as a result of improper first arrival mute. Stacked refractions are visible at two way time < 0.1 sec on all CMP locations. Stacking of refractions is one of the main processing pitfalls for near-surface data.

4.2.7. Additional Processing Steps

In addition to the above mentioned ‘standard’ processing steps, other processes were also tested and they are briefly mentioned here although not all of these were successful and were not implemented in the final processing stream. However, the experiences gained in these exercises may be useful for later workers.

4.2.7.1. Pre-Stack

Seismic data can be displayed in frequency wavenumber (FK) domain. In FK domain different seismic events i.e., ground roll, air blast, reflections and refractions etc., are separated and usually easily be distinguished. Noise can be rejected in FK domain by simply selecting polygons of noise cone. But in this dataset signal and noise were not easily distinguishable in FK space because ground roll was masking shallow reflections. This was not clear until FK filtering was tried to remove noise from the data. Different attempts were made to remove

air blast and ground roll from the data using different FK band pass and reject polygons. The air blast was removed with little success affecting reflections in the output. Efforts for rejecting air blast along with surface waves also affected the actual reflections which were partially muted out. After different attempts the idea of FK filtering to remove noise was dropped and surgical mute was selected instead. By selecting surgical noise cone mute ground roll was easily removed. Danger of losing signal i.e., shallow reflections, using FK filtering are also described by Steeples (2000).

Pre-stack surface consistent ‘spiking deconvolution’ was also applied in processing stream to enhance frequencies. The real purpose of this is to increase the vertical resolution of the traces by broadening the frequency content as, according to Fourier theory, a signal with broad frequency content will be sharp in the time domain. Different parameters were tested prior to the application of the deconvolution to the whole dataset. This ‘decon’ somewhat increased the frequency content of the data with the quality of the stack improved in some locations but overall it was deemed to not provide additional information and was not included in the final image presented later. One reason for this may be related to the difficulties of obtaining a sufficiently long time window to give a reasonable statistical representation necessary for the spiking deconvolution algorithm to function properly. Another reason is that the waveforms used in this study use the autocorrelated Klauder ‘zero-phase’ wavelet which is not the ‘minimum phase’ wavelet specified by the spiking deconvolution algorithm. Indeed, some companies prefer explosive sources over vibrators because of this problem with deconvolution.

Another tested step was ‘DMO 2D Radon Transform’ in pre-stack domain to remove effects of geological dip. Parameters were selected and tested carefully. But it did not improve the quality of stack so the idea was also dropped.

4.2.7.2. Post-stack

The frequencies and amplitudes of seismic traces decay with time; and amplitude and frequency balancing process is required to allow later events to be viewed. Spectral balancing is a signal enhancement technique and is done by; 1) calculating series of gain functions for each frequency band and; 2) calculating envelop of narrow band-pass filtered traces. The inverse of gain function is then applied to the calculated frequency band and then summed (Yilmaz, 1987). One of the controlling parameter in spectral balancing is the maximum frequency cut off – higher the cut off more the vertical resolution is (i.e., high frequency section). In order to average out and enhance the frequency content of data in post stack domain ‘Time variant spectral balancing’ was applied. This process improved the frequency content of data but the visual look of complete stack was judged to have been degraded on the basis of identification and lateral continuity of reflections. So, the final stack was made without this.

The seismic data was also post-stack migrated using three different available algorithms in Vista[®] of Kirchhoff time, Finite difference (FD) time, and frequency wavenumber (FK) time and depth migration. But the stacking velocity solution was not appropriate for migration. Some of the issues related to post stack migrating shallow high resolution seismic data in CMP processing are described in Black et. al. (1994) and the authors concluded that migration will not change much geological interpretation of the seismic section and not required for most of the cases. The proposed solution for getting correct subsurface seismic image is pre-stack depth migration using accurate velocity model obtained from refraction and reflection tomography.

4.3. Summary

In order to image near surface geological target and perhaps shallow gas, high resolution seismic was acquired and processed at the University of Alberta. This chapter discusses all technical issues related to seismic data acquisition i.e.,

resolution, vibrator energy source, and processing i.e., challenges in near surface reflections, statics correction and processing pitfalls etc. In general, near surface seismic data processing is a challenging task and differs a substantially from conventional exploration seismic processing. Interpretation of the final results i.e., processed seismic section along with velocity profile, will be discussed in Chapter 6. In the raw data i.e., shot gathers, seismic refractions in the eastern part of the line, are more distinct than expected. These refractions may be coming for large velocity contrast between buried valley/channel and underlying bedrock i.e., Top Paleozoic. Seismic refractions will be incorporated into the seismic reflection interpretation and will be discussed in Chapter 6.

Chapter 5

Electrical Resistivity Tomography (ERT) Methodology and Results

In this chapter electrical resistivity tomography (ERT) data acquisition, inversion and interpretation are discussed. Here the ERT line was recorded at the same profile with seismic discussed in the previous chapter. ERT profile gives apparent resistivities of the subsurface that are converted into true subsurface resistivities by apply inversion procedure. Cold field condition did not stop data acquisition rather it provided excellent acquisition conditions for electrical imaging i.e., good coupling of electrodes with cold ground. The ERT data was inverted to obtain the true resistivities of subsurface formations. Cretaceous bedrock in the western half of the profile is clearly visible because of its lower resistivity values i.e., marine clays/shale has slightly lower resistivity values as compared to non-marine clays. Whereas the buried valley mainly consists of glacial material in the eastern half of the ERT profile that show slightly higher resistivities then Cretaceous bedrock and easily be distinguished. Two high resistivity anomalies that are most likely associated with free gas or fresh water in porous sands are also identified on the profile.

5.1. Introduction

Electrical and EM methods have been used in oil and gas exploration for many decades despite the prominence of seismic methods. The most common use of electrical methods in exploration likely lies in the standard electrical resistivity log which, at the simplest level of interpretation, can distinguish water saturated from oil or gas saturated porous rocks on the basis of the electrical conductivity of these materials. Essentially, water or brine saturated rocks are much more highly conductive due ionic diffusion conduction through polar water. Such ionic

conduction does not occur in (mostly) nonpolar hydrocarbons and cannot occur in free gas. Spies (1983) has provided an extensive publication regarding history and development of these methods.

Here ‘Electrical Resistivity Tomography’, or ERT, is applied along the same profile as the seismic line described in the previous chapter. The method of 2D DC (direct current) ERT imaging and inversion has been first described in Griffiths and Barker (1993). Essentially, this method is an extension of standard DC resistivity measurements i.e., Wenner or Schlumberger profiling or sounding described in earlier chapter (section 2.2.2)

ERT surveying can be accomplished in a variety of ways using different electrode arrays such as the Wenner or the Schlumberger configurations. The relative advantages, responses, and inversions to the true resistivities of these differing geometries are described by Nassir et. al. (2000). The results of a different case study on ERT imaging using pole-dipole array for detecting complex geological structures i.e., faults and graphite minerals, at the depth of 4 km are presented in Storz et. al. (2000).

5.2. ERT Acquisition

An Electrical Resistivity Tomography (ERT) survey was acquired on the same cutline as the seismic data in order to delineate the Quaternary Channels and to seek both high and low resistivity anomalies, which can be used to detect gas, fresh water and geological formations such as fluvial or marine clays and sand (Table 5.1 and Figure 5.1). The ERT data was acquired commercially by Komex Inc. in January 2005 with personnel from the Alberta Geological Survey and the author (Figure 5.2).

ERT Acquisition Parameters		
	Shallow	Deep
Electrode Spacing	15 m	30 m
Spread length	600m	1200m
Instrument	ABEM, Terrameter SAS 1000	
Total number of electrodes per spread	40	
Array type	Wenner	
Booster	No	

Table 5.1: Acquisition parameters for ERT survey.

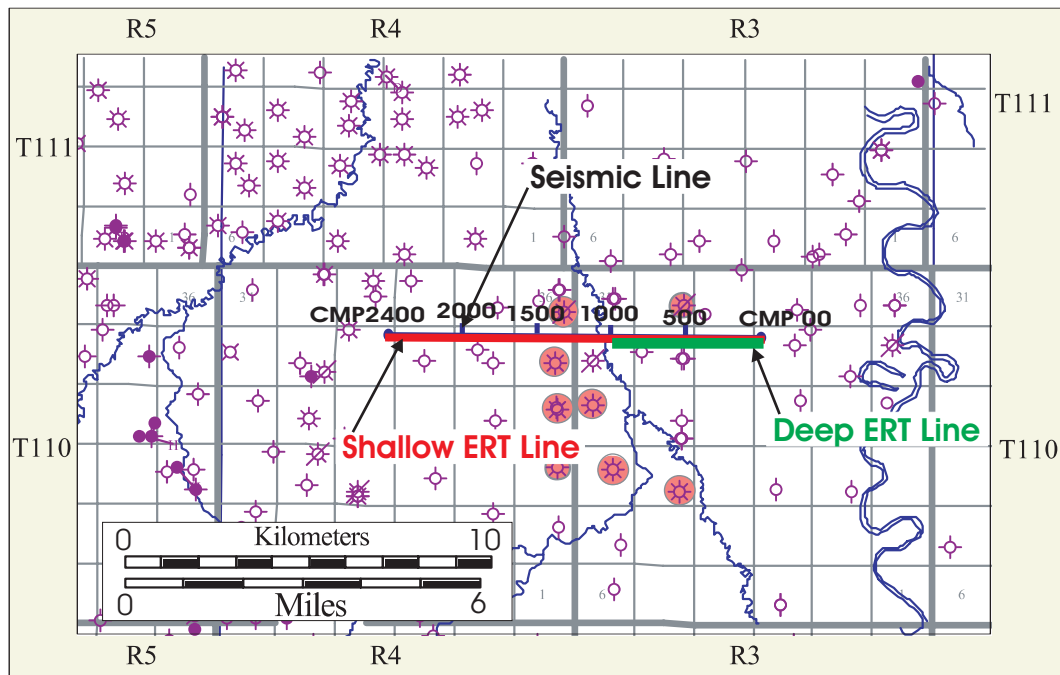


Figure 5.1: Map showing locations of two ERT profiles. Deep ERT profile is about 4 km long, whereas shallow ERT profile is 10 km long with same location as seismic line.

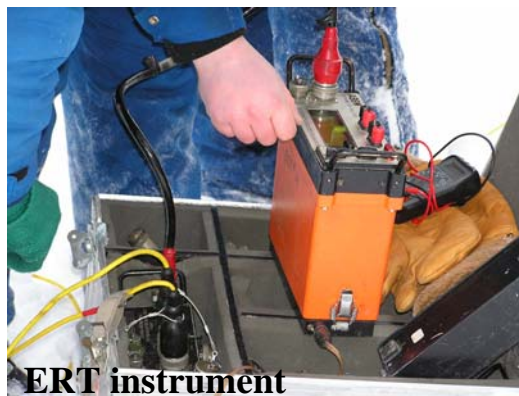
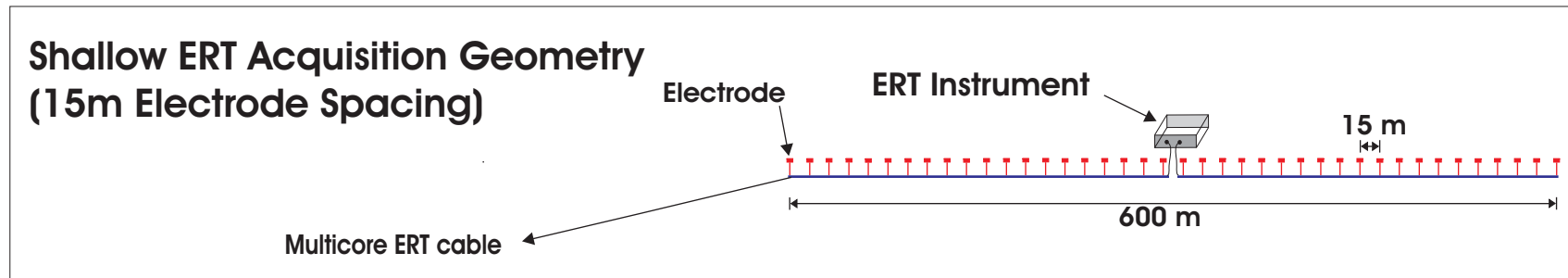


Figure 5.2: ERT field photographs, author standing of right. Cold weather conditions made working conditions difficult but provided good coupling of electrodes with the ground. Difficult to pull electrode due to hard snow (left bottom panel). Electrical resistivity tomography instrument (right bottom panel).

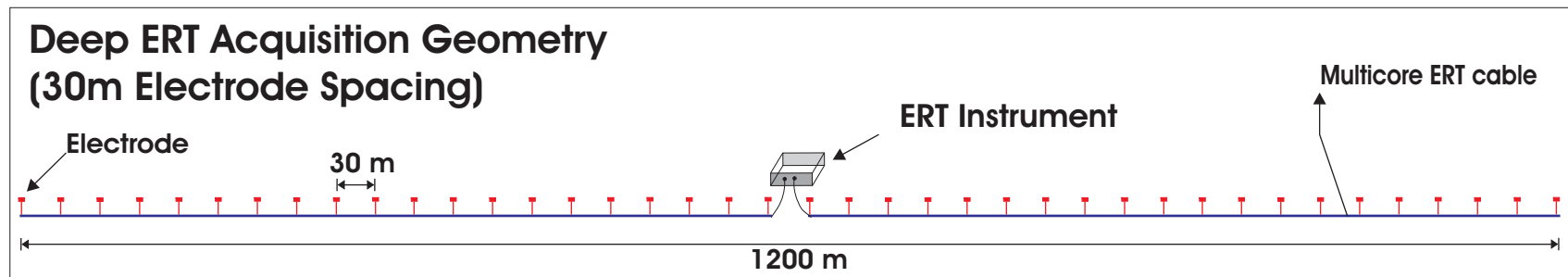
Some known problems associated with ERT data acquisition such as electrode mislocations which significantly contaminate data and reconstructed electrical resistivities as explained by Olbenborger et. al. (2005) were overcome in the field by taking accurate location measurements by GPS at every cable-end every 300 m. The electrode take-outs (outlet in the cable to attach electrode) in the cable were every 16m and electrodes were placed every 15m where additional 1m was for cable stretch. The denser seismic geodetic survey data was further used to calculate the individual electrode positions and to allow the complete ERT line to be well registered in positions with the seismic profile. Coupling of electrodes with ground is also a problem especially in dry areas as well as in soft surface soil. Poor coupling may yield current leakage and breakage of circuit between two current electrodes resulting error in the instrument which stop acquiring data. Cold winter conditions ($< -35^{\circ}\text{C}$) with deep hard snow provided excellent coupling of 1 m steel electrode to the ground, and also helped making uninterrupted supply of current between electrodes and ultimately excellent data quality (Figure 5.2).

Electrical resistivity tomography is fairly new technique in geophysical imaging. Technically, it uses a multiple electrode connected to the instrument with multi-core cable, and source receiver position switches automatically through a programmable acquisition geometry module in the instrument. Different arrays can be used in ERT imaging with particular advantage to each. The choice of array depends upon the complexity of the expected geological structure, the electrical conductivity of the near surface, the depth of the target, and the expected conductivity of the particular objective sought whether it be ground water, hydrocarbons, or subsurface contamination. Different available conventional arrays for sounding or profiling are Schlumberger, Wenner, Wenner-Schmullberger, Pole-pole, or Pole-dipole. Each array has its own particular acquisition geometry i.e., source receiver distance and combination during recording, depth of penetration, and advantage over each other in a theoretical perspective.

The Wenner array was used in this survey for ERT acquisition. Two different ERT lines were recorded; 1) with 15 m electrode spacing that would sense to depths of ~200 m and; 2) with 30 m electrode spacing that would sense to depths of ~400m (Figure 5.3). In Wenner profiling the distance between the current and the potential electrodes remains the same and a large number of measurements are taken in a sequence to make a 'pseudosection' (Figure 2.5). One potential advantage of the Wenner array is that the effect of any shallow conductive body is reduced as measurements are taken at different positions by moving complete array along the profile.



(a)



(b)

Figure 5.3: Shows two acquisition geometries of ERT survey; a) shallow ERT profile with a 15 m electrode spacing that would sense to ~200 m and; b) a deep ERT profile with 30 m electrode spacing that would sense to ~400 m.

5.3. ERT Inversion

The data was inverted using a commercially available software package 'Resis2dinv', by Geotomo Software, Malaysia (Loke, 2004) which uses a non-linear smoothness constrained least square inversion technique (Loke and Baker, 1996). A finite element subroutine was used to calculate the forward modelling operator, a Jacobian Matrix, which was then used to calculate modeled true resistivities (Table 5.2). Different parameters were tested to choose the best possible solution to meet particular geological objective. As this inversion procedure is smoothness constrained and some kind of smoothing is required in input parameter in inversion algorithm. Moderate horizontal flatness and minimum vertical flatness was allowed during inversion. Due to this, chance of smearing of any anomaly in the vertical direction was minimal. The good choice of different input parameters during inversion process boosted fine details, but overall major features were remained present in the section with slight change of shape and size of anomalies. However, it must always be kept in mind that geophysical inversion is an inherently nonunique process, i.e., there are usually a range of different possible solutions that can mimic the real observed response. The block/cell size in the ERT inversion is linearly increasing with depth. At the ground surface the horizontal and vertical dimensions of the cell is half the electrode spacing i.e., 7 m for shallow profile and 15 m for deep profile. Linear increase of the cell size in the vertical direction is dependent on the acquisition array and subsurface conductivity or chargeability. At the maximum depth the cell size for shallow profile was 20m x 25m; and for deep profile was 45m 40m. In radial direction, total 14 layers for both shallow and deep profiles were used in inversion (Table 5.2).

The ERT section was finally displayed after a careful selection of the logarithmic scale colourbar (i.e., the minimum and the maximum cutoff resistivities ($\Omega\cdot m$) values, and the colourbar interval). The choice of different cutoff resistivity values and interval affects the features in the profile that are enhanced in both

regional and fine scales. Selection of appropriate colourbar was also a matter of visualization for interpretation and suitable colourbar was selected to enhance all possible features along the profile such as the bedrock Cretaceous shales in the west, the fluvial channel in the east, and potential gas saturated zones or aquifers within the channel.

ERT Inversion Parameters		
Inversion		
Inversion Method	Smoothness constraint non-linear least square inversion (l_2 norm)	
Type of Optimization	Standard Guass-Newton	
Forward Model		
Model Discretization	Model block can exceeds number of data points	
Jacobian matrix estimation	Quasi-Newton method; calculated after every second iteration	
Mesh Parameters	Finite element method for topographic modeling	
Inversion Parameterization and Data Statistics		
	Shallow	Deep
Total no. of data points	4867	781
Total no. of Electrodes	661	281
Model Layers	14	14
Model Blocks	8842	1527
Iterations	5	4
RMS error	2.85	4.49
~Model block Size at the end of inversion	7m (horizontal) x 7m (depth) at surface; 20m x 25m at deepest level	15m (horizontal) x 10m (depth) at surface; 45m x 40m at deepest level

Table 5.2: Final parameters used to invert ERT data. These parameters were selected after number of trial inversions with different combinations. CPU time for inversion of complete dataset; 15 m electrode spacing, 10 km; on P-III PC, 1.0 GHz, was 5-15 hours depending upon choice of parameters.

5.4. ERT Interpretation

Interpretation of the ERT section is presented in detail in the following sections. The issues related to the true depth of the inverted section, and depth of penetrations of the particular array used in the presence of shallow conductive layers, are discussed in Oldenburg et. al. (1999). Shallow conductors are

problematic for such surveys because they prevent current flow in the deeper part and hence subsurface not properly illuminated and during inversion stage artefacts in depth are created. No highly conductive body was observed in the pseudosections, which could affect estimation of the true depth of the observed highly resistive anomalies in the ERT section. There is need for inverting seismic and ERT data simultaneously for acoustic and geoelectric properties and an attempt doing same in two-dimension using seismic refraction travel times and DC electrical resistivity data is presented in fairly recent article by Nardis et. al. (2005).

The apparent resistivity pseudosections for the shallow (15 m electrode spacing) and deep (30 m electrode spacing) are presented in Figure 5.4. The lower part of figure shows four kilometre ERT profile with 30m electrode spacing with maximum depth of penetration 400m. Section starts at eastern end and ends at Sousa Creek (4 km). Whereas upper part of the figure shows complete 10 km shallow ERT profile. The horizontal axis is showing distance in metres starting from the east and increasing towards the west. The vertical axis is depth (not true depth in this case) and data shows apparent resistivity in the pseudosection. The selection of an appropriate colourbar (i.e., the minimum and maximum $\Omega\cdot m$ values) is very important for the purpose of resistivity data plotting and displaying. In other words, upper limit cut off point (max. $\Omega\cdot m$) is very important in enhancing fine and small features. In addition to that colourbar scaling such as linear or logarithmic colour scale is also very important. This depends upon the data and the needs of the interpreter in deciding how fine the details are required? A linear scale usually enhances only regional features where as careful selection of logarithmic scale will ultimately enhance fine features.

This true resistivity section (Figure 5.5) was plotted using logarithmic colourbar scale with cutoff resistivity 140 $\Omega\cdot m$ (max. resistivity value is 173 $\Omega\cdot m$). The horizontal scale is distance in metres and vertical scale is true depth. The section shows true resistivities of the subsurface geological formations and is one best

possible solution of the inversion not 'the solution'. The sensitivity in the depth axis is dependant on the conductivity of the near surface layers. The western part of section shows lower resistivity $\sim <15 \Omega\cdot\text{m}$. This seems to be clay or shale, as these are conductive and less resistive - Cretaceous Shale. In the middle of section there is high resistive anomaly with resistivity $\sim 150 \Omega\cdot\text{m}$. This anomaly is at the western edge of Quaternary strata, In other words right at the edge of the truncation of Quaternary to Cretaceous. In the eastern part ERT shows low resistivity ~ 15 to $\sim 25 \Omega\cdot\text{m}$ which may be silty clay. In the eastern most end of profile one higher resistive anomaly with resistivity values $\sim 100 \Omega\cdot\text{m}$ is present.

While carrying out this inversion the input parameters were chosen in such a way that the fine details were kept in the section. Because any shallow gas pocket can have small horizontal and vertical extent; Quaternary gas gross pay is approximately >20 metre in this area.

Figure 5.6 shows the true resistivity of the deep section displayed with logarithmic colourbar scale and cutoff resistivity is $90 \Omega\cdot\text{m}$, which is almost maximum value in this case. The shallow (15 m electrode spacing) and the deep (30 m electrode spacing) resistivity data were recorded with different field geometry. It shows difference in resistivity values for eastern most high resistivity anomaly. In this section anomaly shows $\sim 50 \Omega\cdot\text{m}$ resistivity value. The eastern low resistivity elongated feature is also present here as low resistivity i.e., ~ 12 to $\sim 20 \Omega\cdot\text{m}$. This shows low resistive or high conductive material, which is probably silty clay or mud mixed with sand not coarse grained. The important feature in this deep profile is the high resistivity feature at the bottom of section. The increase of resistivity along the bottom of the deep profile suggests the area is underlain by high resistivity material consistent with carbonates and also with the abrupt jump in resistivity from the Cretaceous to the Paleozoic across the unconformity as seen in the well logs (Figure 3.7). Different inversion schemes show different results (not shown here) but in all cases lower end of profile shows high resistive feature (bedrock) all along the profile.

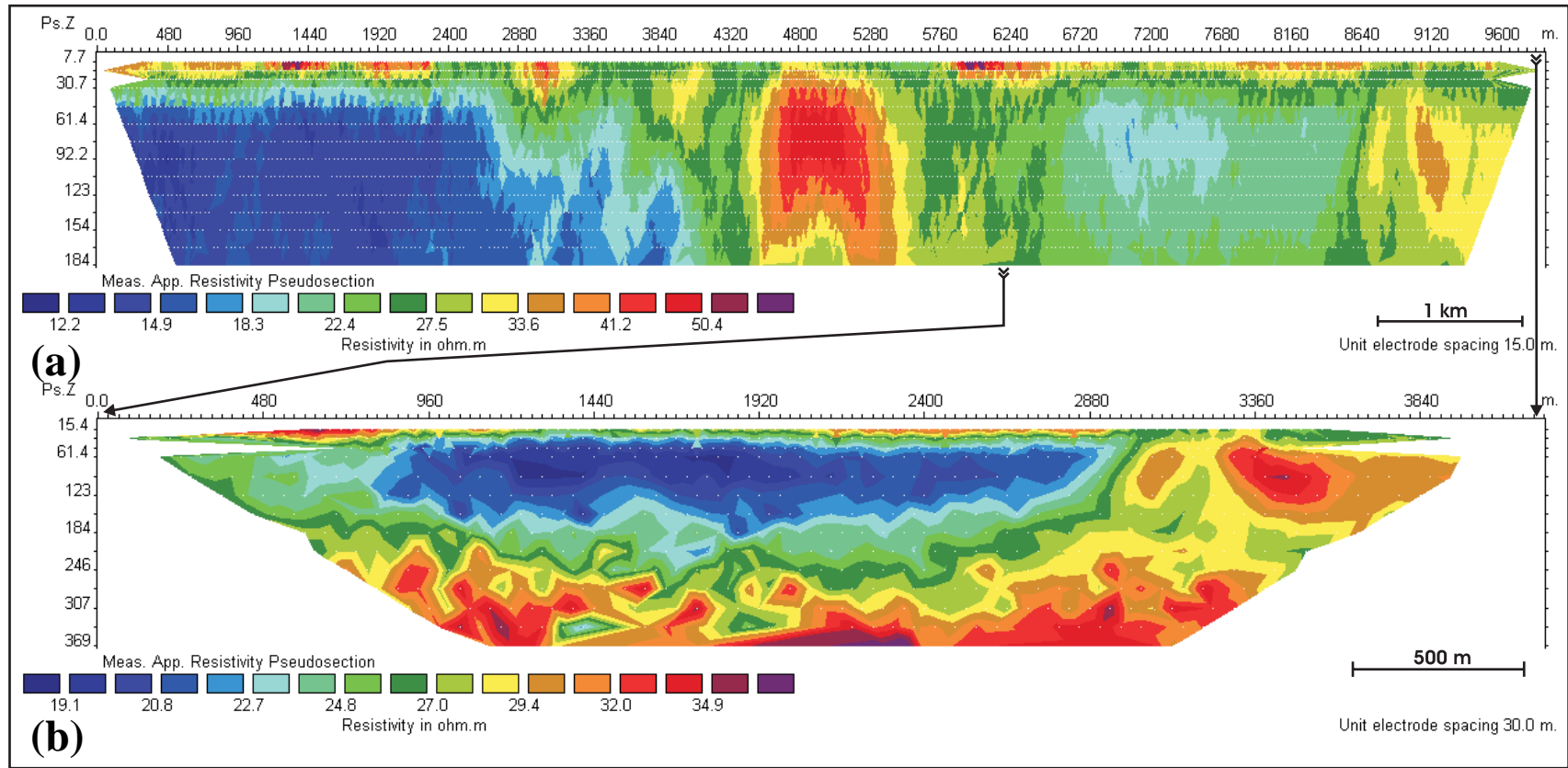


Figure 5.4: Measured apparent resistivity section. (a) 15 m electrode spacing with total length of profile 10 km. (b) 30 metre electrode spacing with total length of profile 4 km. White dots are calculated data points. Depth of the section is pseudo depth and this is non-inverted section. For shallow and deep profiles minimum contour value 9 and interval 1.22 with no high or low resistivity cutoff.

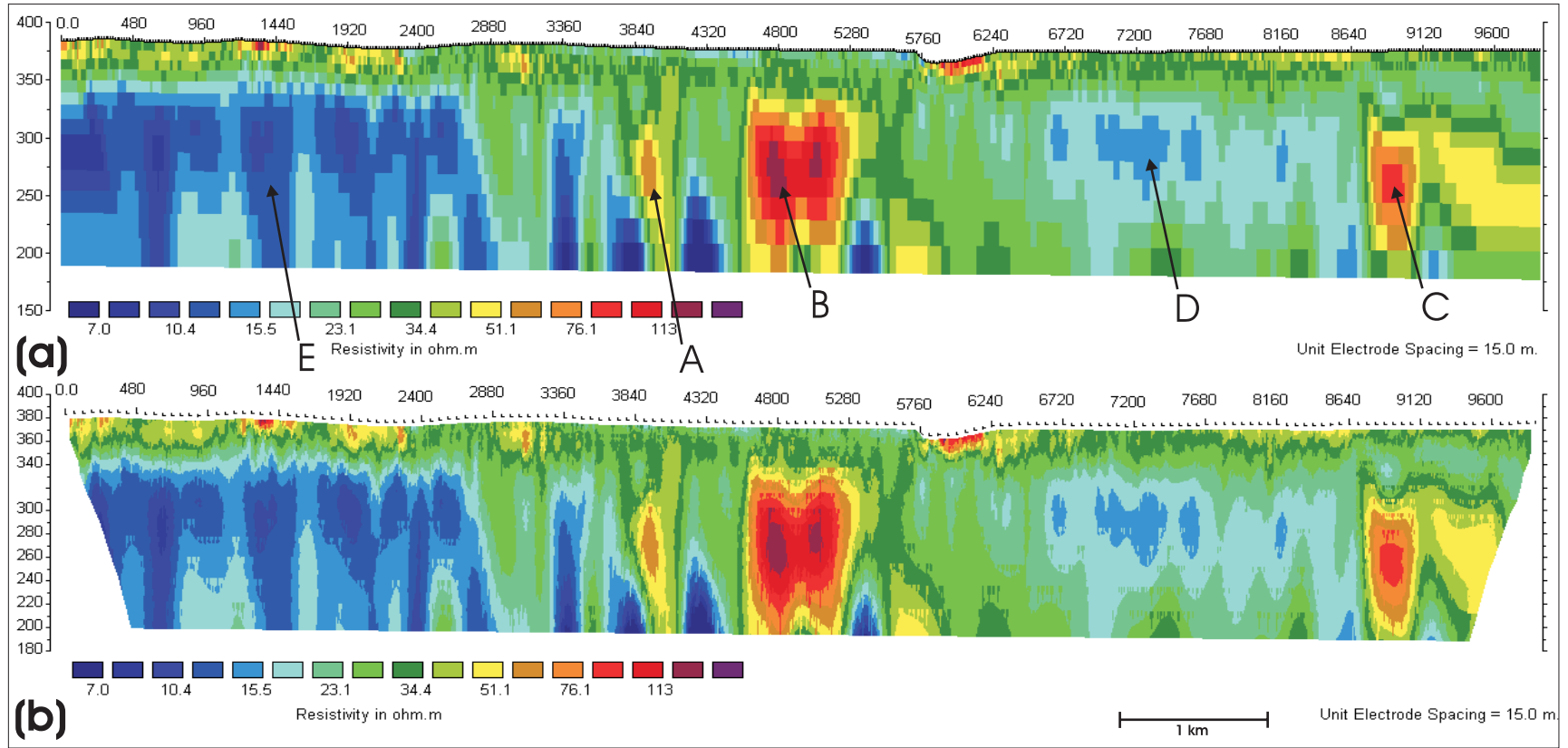


Figure 5.5: Final invested shallow ERT section with; (a) block parameterization and; (b) smooth contouring display. The logarithmic colour scaling parameters are minimum contour is 7 with interval 1.22. Minimum resistivity is $2.69 \Omega\cdot\text{m}$ and maximum resistivity is $172.98 \Omega\cdot\text{m}$. Points A, B, C, D and E marked on the profile will be discussed in chapter 6.

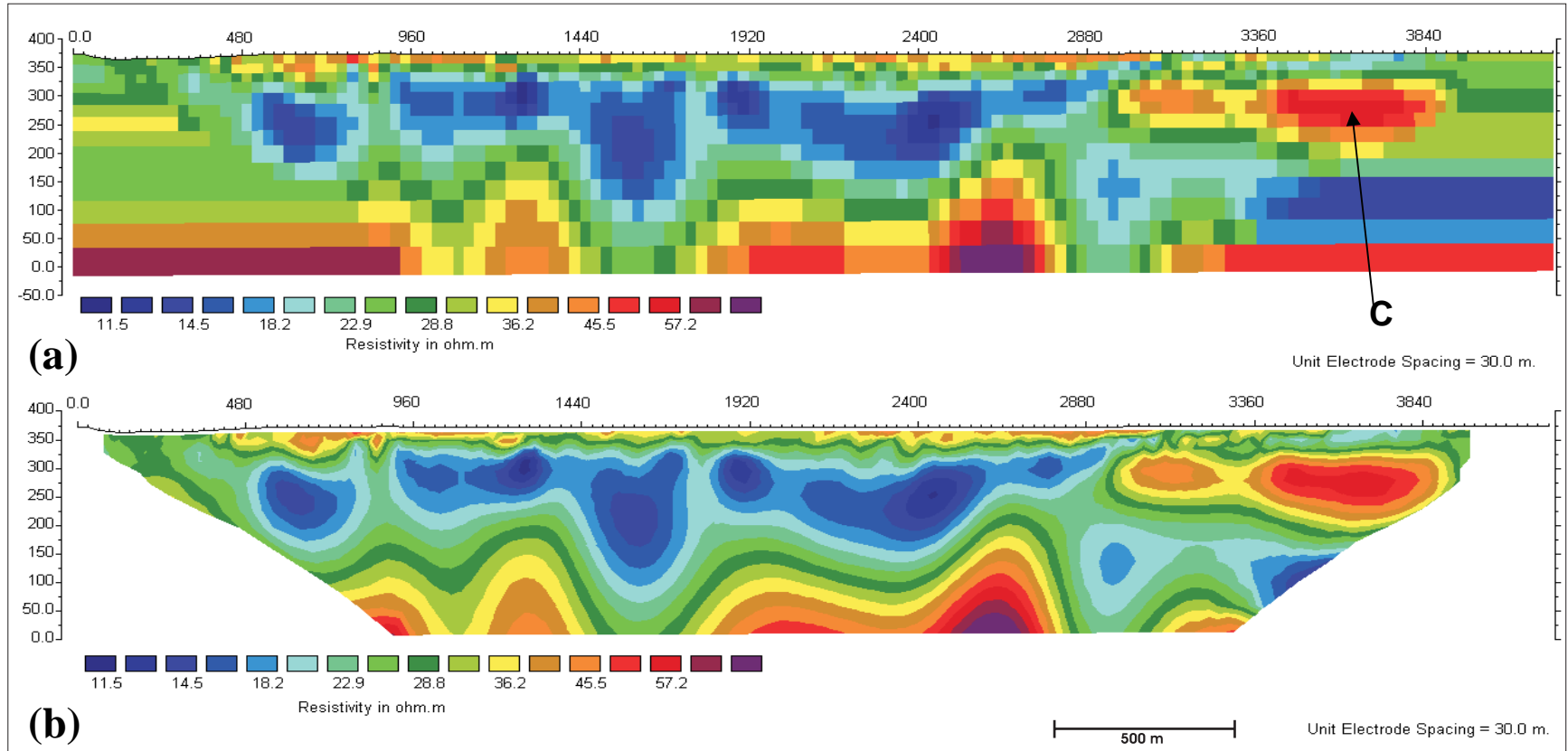


Figure 5.6: Final invested deep ERT section with; (a) block parameterization and; (b) smooth contouring display. The logarithmic colour scaling parameters are minimum contour 11.5 with interval 1.122. Minimum resistivity is 10.85 $\Omega\cdot\text{m}$ and maximum resistivity is 76.24 $\Omega\cdot\text{m}$. The marked arrow with point C will be discussed in chapter 6.

5.5. Summary

ERT data acquisition, processing and interpretation are discussed in this chapter. ERT acquisition conditions in the field were ideal because of the cold weather and snow that gave good coupling of electrodes with ground and ultimately excellent raw data quality. ERT data was inverted using standard commercially available inversion software 'resistinv2d'. The buried paleo-valley was easily identified on the profile with its slightly low resistivities then Cretaceous bedrock in the western end (shallow ERT profile) and major difference of resistivities with Devonian bedrock below it (deep ERT profile). Two high resistivity anomalies are also identified on the ERT profile. In the next chapter the ERT, seismic reflection and refraction results will be interpreted jointly. The two high resistivity anomalies identified in the ERT profile will be discussed and interpreted in detail.

Chapter 6

Interpretation

In this chapter the seismic refraction and reflection interpretations, synthetic seismograms, and the geophysical signature of shallow gas are discussed. The buried valley was imaged using conventional refraction interpretation approach with anomalous refraction character even seen in the raw data. A preliminary refraction tomography provided detailed image of the subsurface and is also used here to see details within the buried valley/channel. The seismic reflection profile provided a detailed image of the internal structure of the channel. The base of the buried valley/channel is clearly evident on the reflection profile, and the channel itself contains a number of high amplitude reflections. Synthetic seismograms were calculated using the available, but limited, geophysical logs. Synthetic traces of the buried valley/channel display different character relative to the surrounding Cretaceous bedrock sediments. High amplitude reflections are visible in the synthetic trace of the channel fill Quaternary sediments. Electrical resistivity tomography (ERT), refraction tomography, and seismic reflection data were all interpreted jointly. It is observed that high resistivity anomaly corresponds to; 1) a bright reflection in the raw reflection data and; 2) low velocities on tomographically inverted velocity profile. This anomaly corresponds to the known hydrocarbon gas reservoir of nearby shallow industry gas wells.

6.1. Seismic refraction analysis

Seismic refractions provide valuable information of the subsurface. Typically refractions are used to calculate the velocity and thicknesses of the near surface weathering layers and give a simple indication of the geological structure on this basis. This information may also be valuable later in estimating the static

corrections. But in a typical long offset seismic reflection surveys, refractions are used to obtain the velocity structure of the subsurface. Cox (1999) provides a detailed description of all refraction interpretation techniques and serves as an excellent reference in geophysics.

The basic theory and method related to seismic refraction technique was described in section 2.2.1. In the seismic refraction method the travel times of refracted waves, traveling from the source through a velocity contrast boundary and refracted back to the surface, are recorded over a set of receivers. When the seismic energy (wavefront) impinges the velocity contrast boundary at an angle of incidence equal to the critical angle it travels along that boundary and is refracted back from this boundary again at the angle of incidence back to the surface. The critical angle θ_c is defined as:

$$\sin \theta_c = \frac{V_1}{V_2} \quad (6.1)$$

where V_1 and V_2 are velocities of first and second layers.

Seismic refraction data can be acquired using different field acquisition techniques that include: 1) classical reversed profiles, 2) single ended profiles, 3) synthetic reversed profiles from CMP data, and 4) classical fan shooting technique that was used to detect salt domes (Steeple, 2004). Seismic refraction data consists of travel time picks of the first arrivals/impulses (Figure 4.16b). One travel time pick consists of travel time value at particular receiver and corresponding offset of that receiver from source. Refraction data is plotted and displayed as time – distance graph. On a time-distance graph where the slope of the first arrival curve changes that distance is called the crossover distance (Figure 6.1). The slope on the travel time graph is equal to the reciprocal to the velocity ($1/V$).

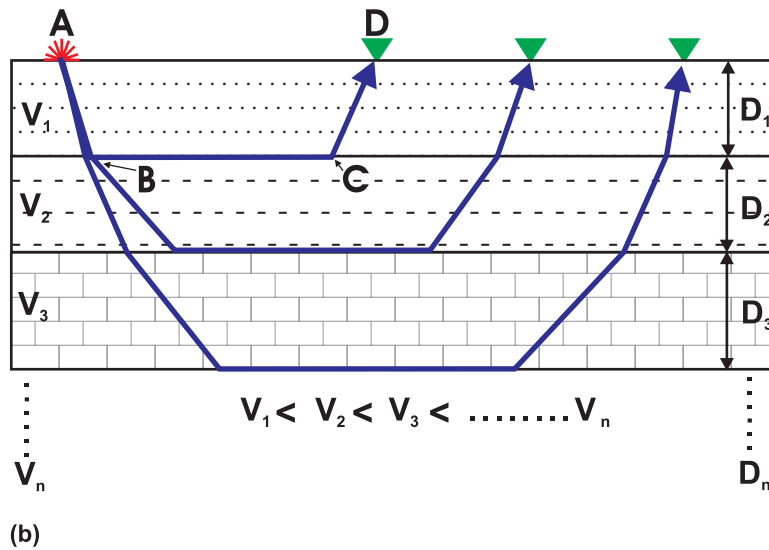
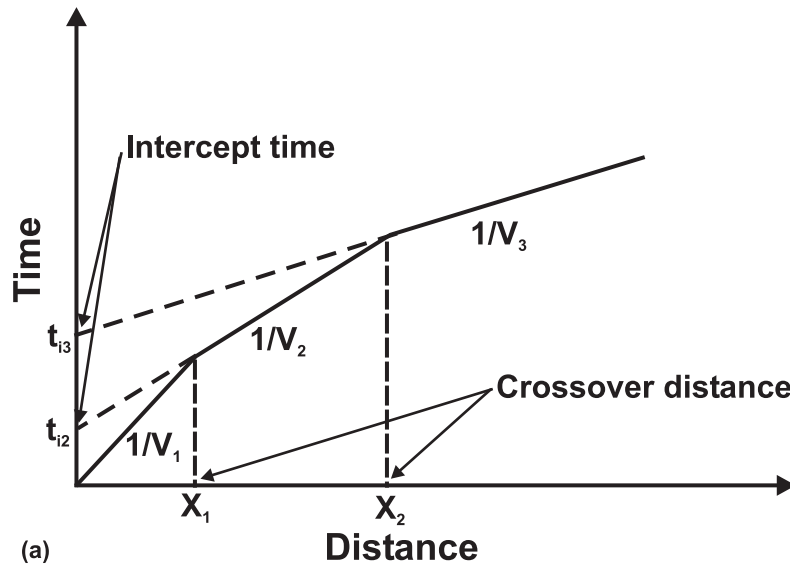


Figure 6.1: Cartoon showing refractions and time distance curve. b) Refractions from three horizontally stratified layers of different velocities. a) time distance curve of simple three layer case.

Various seismic refraction interpretation techniques are available in the literature. Each technique has advantages over each other and can be used in different expected geological situations. The choice of the type of interpretation technique is a function of the complexity of the subsurface geology. If no dipping event is present in the subsurface and beds are flat-lying then a simple interpretation technique such as the 'Intercept-time method' can be used. If the subsurface beds are dipping, at minimum one should carry out a 'reversed' refraction profile, but

one may also use more slightly advanced techniques such as the 'Generalized Reciprocal Method (GRM)'. But if subsurface is very complex and lateral velocity variations exist then none of these standard interpretation techniques are suitable. Only tomographic inversion technique is appropriate in this case. Following few paragraphs outline most commonly used seismic refraction interpretation techniques. Detail description of these methods can be found in Cox (1999).

Refraction interpretation methods are broadly grouped in three classes: 1) Intercept-time methods, 2) Reciprocal or delay-time methods, and 3) ray tracing methods. The level of difficulty and calculations required for each method is different. For example, the intercept-time method is the simplest method and only a few calculations are required. Whereas ray-tracing methods that also include tomographic inversion technique are more computer intensive.

The intercept-time method is the simplest method of seismic refraction interpretation. The direct intercept time method with its simplest form does not incorporate geological dips in the calculations but if both forward and reverse profiles are recorded geological dips can be incorporated. In this method slope and intercept time is used to calculate velocity and depth of refractors. It is the beauty of this technique that crossover distance can also be solved for depth. Usually, in refraction interpretation terms a 'forward shot' and a 'reverse shot' are used. A 'forward shot' means a shot at one end of the receiver line, while the 'reversed shot' has the seismic source along the same line of receivers but at the opposite end. The reason this is done is that if dip exists from the refracting surface then the apparent thicknesses and velocities determined from a single refraction shot will be in error. This type of acquisition geometry is typical for seismic refraction surveys. But in the case of seismic reflection surveys where refractions are also recorded this forward and reverse shot scheme might not exist. But an algorithm designed to solve these kinds of cases can sort data and create pseudo forward and reverse shot schemes. Forward and reverse shots are usually

required to calculate subsurface dip of the refractors. Interpretation using only forward shots gives apparent velocity of the 2nd, 3rd or deeper layer.

Other commonly used methods are a class of ‘reciprocal and delay time methods’ of which nearly 20 different variations are available. The term ‘reciprocal time’ is the travel time along the refractor from one end shot of the receiver for ‘forward profile’ and vice versa for the ‘reverse profile’. In this method both forward and reverse spread data should be recorded. Then the travel times from the shot to the refractor (AB in Figure 6.1), along the refractor (BC), and back to the receiver (CD) are calculated (Figure 6.1). This concept is almost same with the ‘delay time’ concept. Theoretically, both forward and reverse times should be equal if reciprocity exists. Both times are not equal because of dipping bed, undulating layers, and change in refractor velocity. In this type common refraction interpretation methods are Hagedoorn’s (1959) Plus-Minus method, the ABC method (Edge and Laby, 1931), the Gardner method (Gardner, 1939), and the Generalized Reciprocal Method (GRM) (Palmer, 1981). Details of these methods are beyond the scope of this thesis and reader is referred to the texts such as Cox (1999) and Sjögren (1984) for details.

In ‘Ray tracing’ methods, seismic ray path are traced through the input geological-velocity model; the theoretical travel times are calculated and matched against the actual first breaks. Inversion is carried out to calculate the travel time differences between actual and theoretical first breaks and input model is updated with travel time residuals for next iteration. Iterations continue until predetermined stopping criteria is matched. In this method two different varieties exist, 1) a layer based inversion, and 2) a full cell/block based tomographic inversion. Among layer based inversion methods, the Generalized Linear Inversion (GLI) method is common (Hampson and Russell, 1984). In this method the near surface geological model is proposed and rays are traced through this model. The velocity within the geological layer is assumed constant and hence under this restriction the observed travel-times are inverted for the depth and

velocity of the refractor. The constant velocities within the layer limit this method because no vertical and horizontal velocity gradients are allowed. The procedure gives good results in case of relatively simple earth models, and is used extensively in industry for assisting in the determination of static corrections.

In full tomographic inversion schemes, the velocities are allowed to vary in both the horizontal and vertical directions. The subsurface geological model is divided into blocks/cells of equal slowness which are inverted for such as in the GLI method. In the areas of severe velocity variations this method gives acceptable results. Below, I present the results of a variety of refraction analysis methods.

6.1.1. Conventional Refraction Interpretation

The delay-intercept method was adapted for refraction interpretation. The basic equations for this are as follows:

$$D_n = \left(\frac{T_{in-1} V_n V_{n-1}}{2\sqrt{V_{n-1}^2 - V_n^2}} \right) - \sum_{j=1}^{n-1} D_j \left[\frac{V_n}{V_j} \right] \sqrt{\frac{V_{n-1}^2 - V_j^2}{V_{n-1}^2 - V_n^2}} \quad (6.2)$$

D_n = depth of n^{th} refractor

T_{in} = n^{th} intercept time

V_n = velocity of n^{th} layer

This equation can easily be written in terms of crossover distance.

$$D_n = \left(\frac{X_{cn-1}}{2} \right) \sqrt{\frac{(V_{n-1} - V_n)}{(V_{n-1} + V_n)}} + \sum_{j=1}^{n-1} \frac{D_j}{V_j} \left[\frac{V_{n-1} \sqrt{V_n^2 - V_j^2} - V_n \sqrt{V_n^2 - V_j^2}}{\sqrt{V_{n-1}^2 - V_n^2}} \right] \quad (6.3)$$

X_{cn} = n^{th} crossover distance

Equations with the dip of refractor included are also available in the literature.

This first and simplest refraction interpretation was carried out using the standard “Intercept-time method”. The basic equation for a multi-layered geology is Equation 6.2. Equation 6.3 is the same equation rewritten in terms of crossover

distance and it is used to perform refraction interpretation. In this method of interpretation calculation begins from top and gradually thickness of each layer is used in downward calculations. This method assumes flat layers and above mentioned equations do not incorporate geological dip. Again, this model assumes a very simple layered geology, and to some degree the character of the observed travel-time curves are in agreement with this. However there can be problems with such a simple analysis as it does not readily account for lateral variations. Further, it cannot resolve layers in which the velocity is less than the immediately overlying stratum; such layers are said to be ‘invisible’ to the refraction analysis and it present the apparent velocity of the layer that includes it will be in error. If dip is present, this will result in a small error in the estimation of the velocities and depth. However, as the goal here was not so much determining the velocities but trying to obtain some additional low resolution information about the variations in the lateral geological structure, we deem this error to be acceptable for the current analysis.

6.1.1.2. Methodology

Long offset (wide angle) refractions (i.e., those for which the source to receiver offset is larger than the maximum depth of investigation) were present in the data. Direct examination of shot gathers in the east and the west suggest the simplest face value interpretation of 2 and 3 layers, respectively. On the shot gathers where break/turning point on refraction arrivals between first to second layer and second to third layer were prominent were selected for refraction analysis. Figure 6.2 shows a shot point in the east end of the line while Figure 6.3 and Figure 6.4 show shot points in the west. First arrivals were picked on ‘selected locations’ along the seismic line. Crossover distances were marked and picked on this first break data set. The turning points on the time distance graph were marked that gave the crossover distances for layers. This crossover distance, picked on travel time data, was further crosschecked on the original shot domain seismic trace data. Velocities for each layer were calculated from slope on the time distance graphs as illustrated in Figure 6.1 and Figure 6.5.

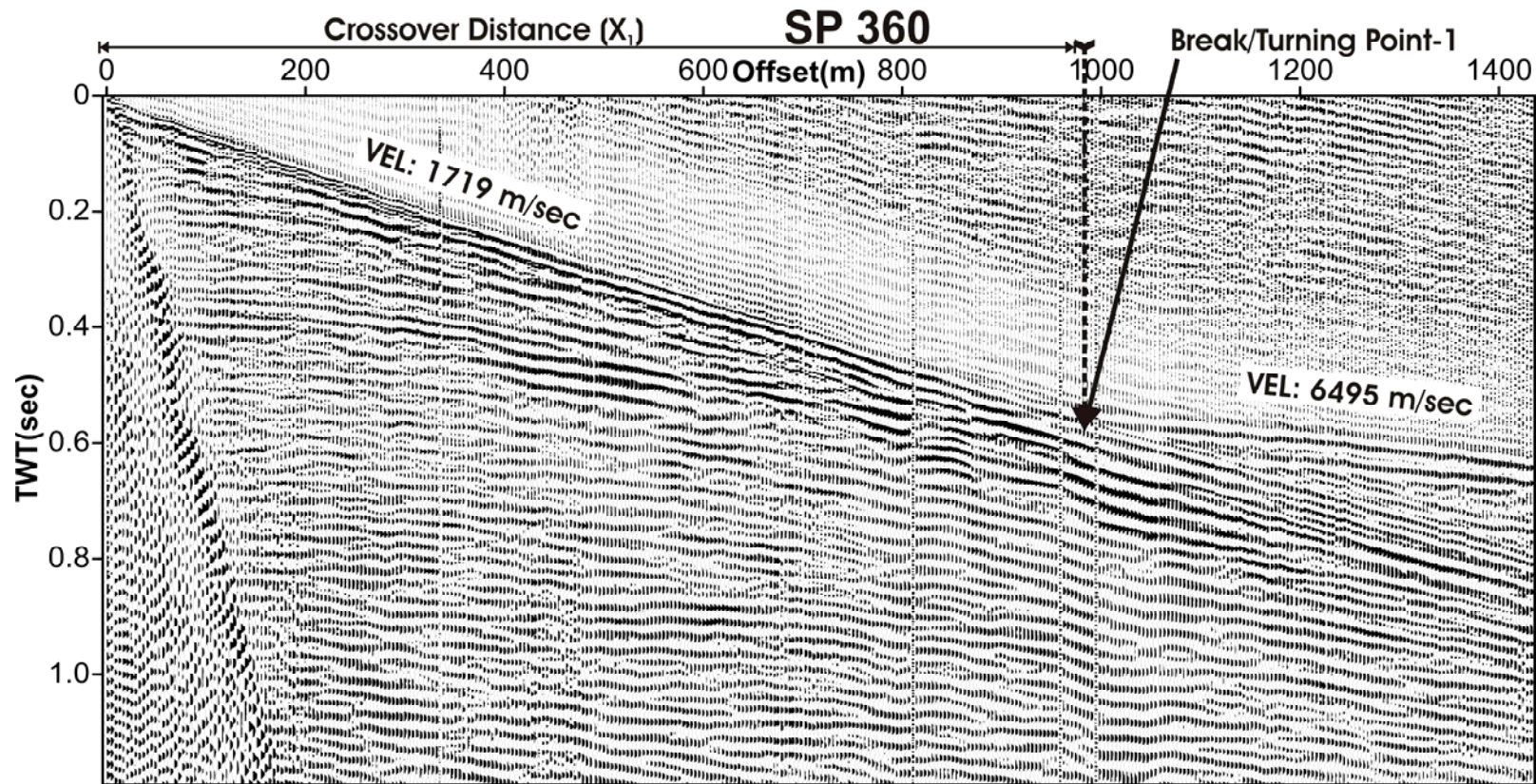


Figure 6.2: Shot point 360 showing two refraction layers. Here Quaternary strata are directly lying over Paleozoic Carbonates that gives excellent ‘textbook’ refraction that merges with the reflection from the interface. Break/turning point is also marked here for reference. Crossover distance is used to calculate depth of refractor using equation 6.3. This is a two layer refraction case.

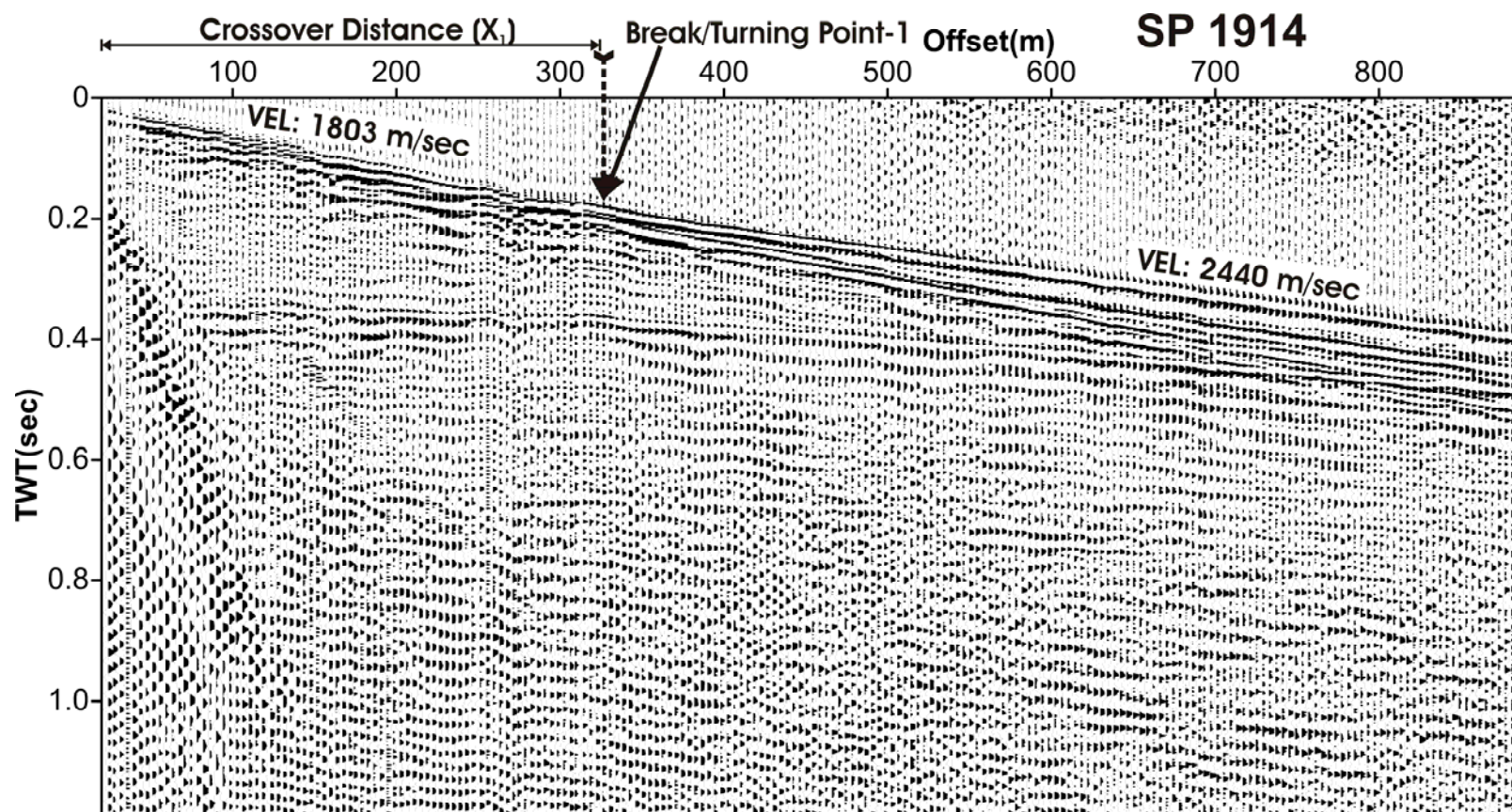


Figure 6.3: Shot point 1914 showing two layers on refraction. Here the Quaternary strata are overlies the Cretaceous bedrock sediments. Refractions for Paleozoic Carbonate are on far offsets and cannot be seen in this figure. Top Paleozoic refractions along with other are shown in Figure 6.4.

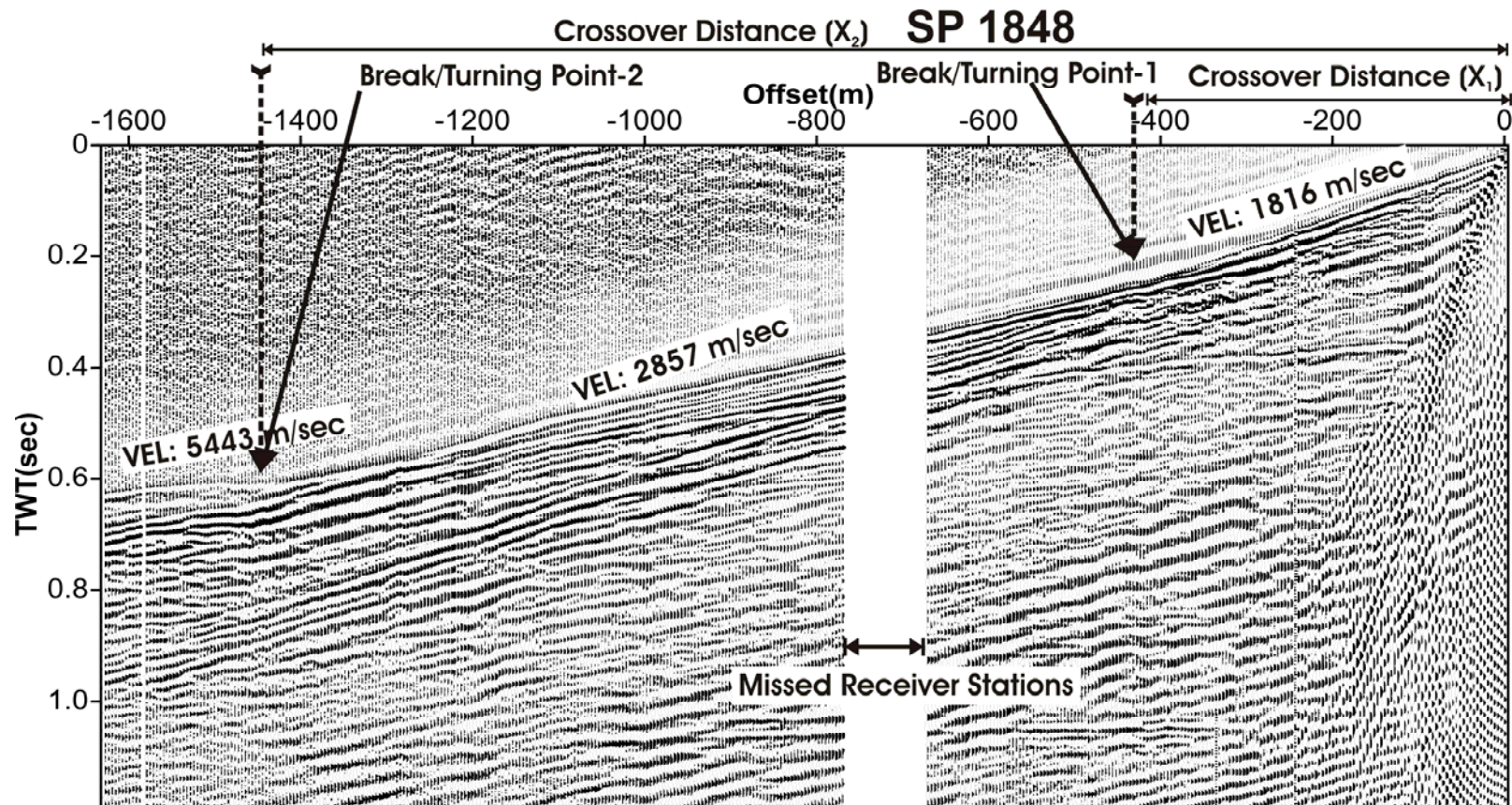


Figure 6.4: Shot point 1848 showing three layers. Here Quaternary strata are overlying Cretaceous sediments. Here the Paleozoic carbonate refractor is visible only at far offset. This is three layer refraction case. Break/turning points are also marked here for reference. Refractions from Cretaceous are more illustrative in Figure 6.3.

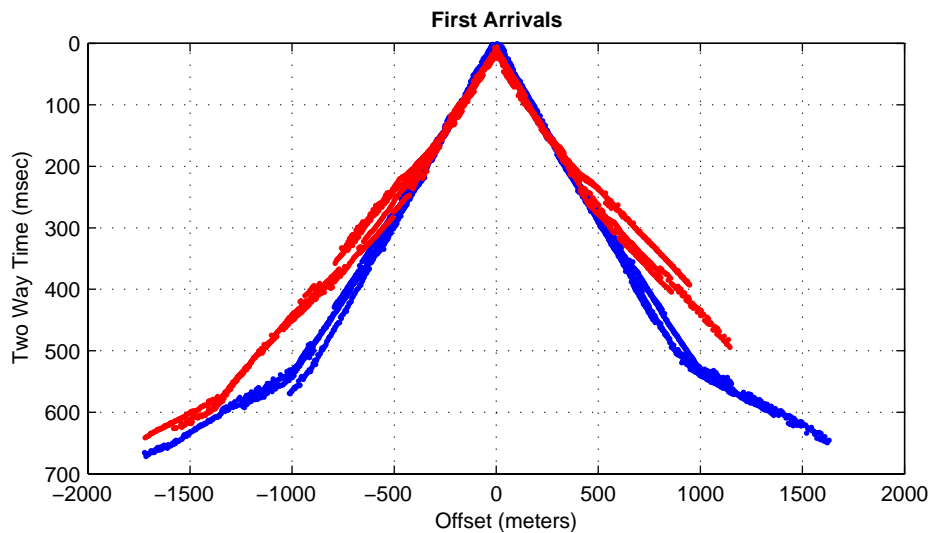


Figure 6.5: Figure shows first arrivals on selected shots. Blue color arrivals are from eastern part of line where Quaternary strata are directly overlying Paleozoic Carbonate i.e., showing two layers. Whereas red color arrivals are from western part of line and showing three layers top Quaternary then Cretaceous and then Paleozoic.

6.1.1.3. Interpretation

This conventional refraction interpretation gives a general idea about the subsurface structure in terms of the number of major layers, their velocities, and their thicknesses. This was used as added information in to the seismic reflection profile. A final velocity profile after this simple refraction interpretation is shown in Figure 6.6.

A changing ‘refraction’ structure of layers is easily identified in these nearly ‘textbook’ refraction profiles. In the eastern half of the profile, two layers of the low velocity (~ 1800 m/sec) Quaternary sediments overlying the high velocity (> 5000 m/sec) Paleozoic Carbonates. In contrast, the western half of the line shows three layers. Here, Quaternary sediments overlie the undisturbed Cretaceous sediments (~ 1800 m/sec) which then overlie the Paleozoic carbonates.

This demonstrates the utility of such simple refraction interpretations in locating low velocity channel fill deposits; it would be interesting to know whether this information has been used by industry as it could be obtained essentially for free from their existing surveys.. As in this kind of refraction interpretation where not much modeling is involved this method can be used to verify other refraction interpretation techniques; number of layers and their apparent velocity can easily be seen on raw data and interpretation was carried out for depth and thickness of layers. Whereas, in other methods such as ray tracing methods intensive modeling is involved and their results some times need to be verified from other techniques. The standard refraction interpretation can be used to identify incised valleys or depressions containing low velocity deposits i.e., lacustrine¹ or glaciolacustrine² deposits.

¹ Sediments deposited in lakes.

² Sediments deposited in glacial lake. Glacial lake is usually created at the margin of glacier or ice sheet due to its advance and retreat. Sediment input is through meltwater streams and deposition due to suspension load.

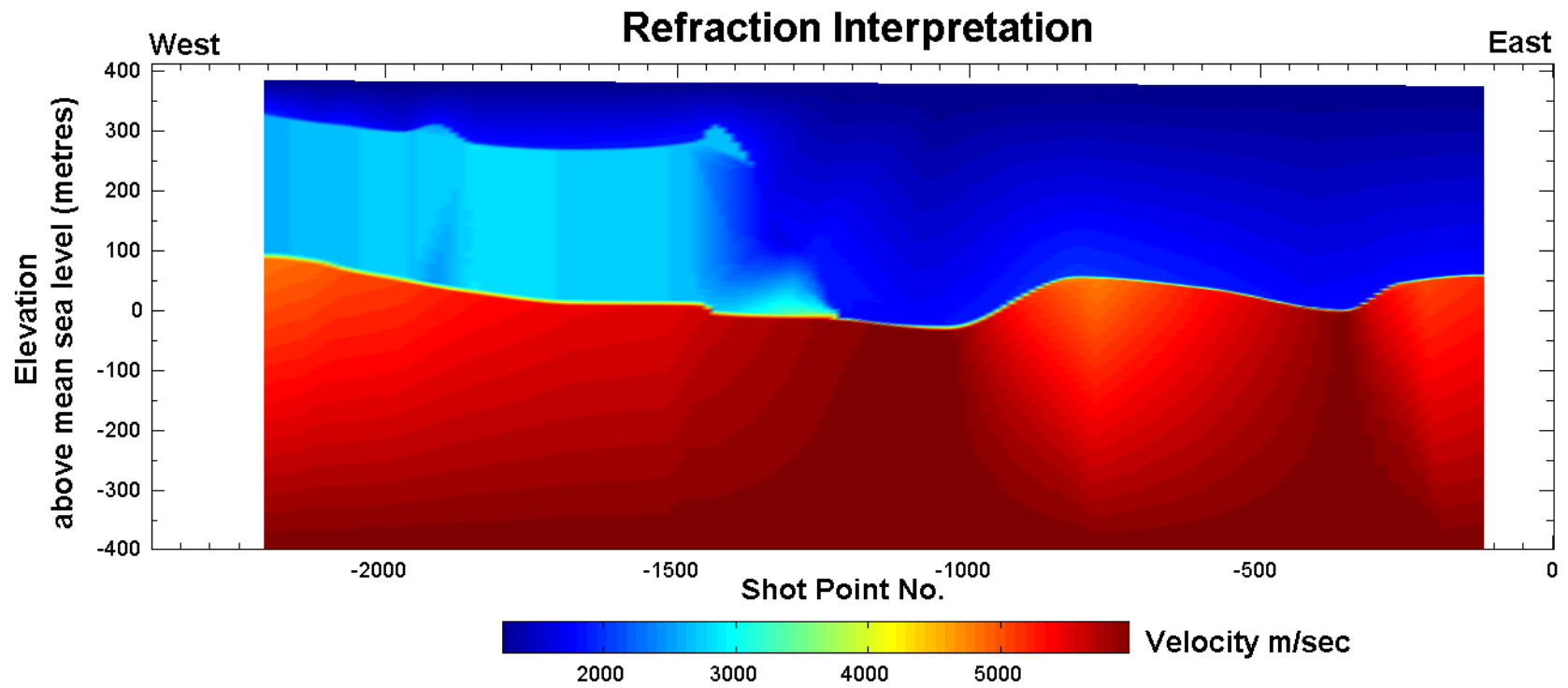


Figure 6.6: Velocity profile after conventional refraction interpretation. '0' metres on depth axis is sea level and depths are positive above and negative below this. See text for details.

6.1.2. Refraction Tomography

The original word tomography came from Greek word ‘tomos which means slice and ‘graphy’ means drawing. In geophysics, seismic tomography is used to reconstruct a velocity model of the earth from recorded travel times on seismic data. First arrival tomography is useful for estimating a geological model of the near surface in terms of its seismic velocities. First arrival tomographic inversion is also known as turning ray tomography. Turning rays are continuously refracted diving waves which follow Snells’s law but through a velocity gradient instead of discrete layers and turn back to the surface (Figure 2.3). Seismologists use these turning or diving waves to image deep earth structures. Turning ray tomography is very useful in obtaining the near surface velocity model especially where lateral velocity variations exist and used for calculating static correction i.e., tomostatics, to improve the later reflection seismic image (see section 4.2.7).

Briefly, the process begins with the construction of a starting model for the expected geological structure and put in terms of the usually lithologically dependent seismic velocities. This model should include the surface topography also. The travel times from the sources to the receivers used in the actual survey are then calculated from this model often using ray tracing or other numerical methods. These calculated travel times are then compared against those observed in the real data. The ‘error’ of the calculated to the observed provides some measure of the quality of the velocity model. This model is then updated and the latest error between the real and the modeled travel times is found. Consequently, the inversion seeks to minimize this error by iteratively updating the velocity model and calculated travel times and comparing them to the observed. Typically, this earth model is parameterized into equal size blocks/cells with constant slowness. Different researchers have explained this method in detail; Simmons and Backus (1992) explained linearized tomographic inversion method and Stefani (1995) explained turning ray tomography.

Usually, the wider the ‘aperture’³ of an acquisition geometry, the greater the depth that will be imaged. If long offset data is recorded during acquisition then tomographic velocity model gives a deeper earth image. The ratio of the maximum source-receiver offset to the depth of investigation typically ranges from 3:1 to 5:1, but depends upon the subsurface velocity gradients. Another ‘rule of thumb’ used in estimating the usable depth of the velocity model is 1/3 to 2/3 of the depth that the deepest ray penetrated (Adams et. al., 1994). If the recording aperture is wide enough then the tomographic velocity result can be used as starting model in prestack depth migration. The final tomographic velocity model is a ‘smoothed version’ of true subsurface velocity structure. Tomography works well if there are enough rays in each cell but often this is not the case due to velocity shadows and high velocity anomalies. In poorly sampled regions (i.e., those which have few rays passing through them) the imaged blocks are smeared along the ray paths (Shearer, 1999). This is also true in case of localized velocity anomalies; resulting velocity image will be smeared along ray path that penetrated it. It also depends upon inversion smoothing parameters and smoothed travel time perturbations from moving average filters. It must also be recognized, that in general, the nonuniqueness associated with inversion procedure, especially for refraction tomography, can never be fully resolved (Ivanov et. al., 2005a). Different subsurface velocity models can converge to same solution regardless of the optimization technique employed, examples of such optimization techniques being the stationary or simultaneous iterative reconstruction technique (SIRT), the algebraic reconstruction technique (ART), or the conjugate gradient (CG) (Ivanov et. al., 2005b). Those authors described a method of quantifying the nonuniqueness / uncertainty associated with refraction inversion that may lead to different solutions of same geological model. Most commonly nonuniqueness can be ‘reduced’ by applying smoothing constraints during inversion that reject extreme results which mathematically possible but geologically not realistic. Consequently, as is always the case in earth sciences one must continue to bring as much information, both geological and geophysical, into the final interpretation

³ Means opening gate or window; in seismic acquisition spread length is considered as aperture.

in order to constrain it as much as possible.

6.1.2.2. Methodology

The algorithm used here for travel time tomography is described in Hole (1992). The algorithm is fully capable of working in both 3D and 2D geometries. The forward modeling scheme used to calculate travel times is adapted from Vidale (1990), with some modifications (Hole and Zelt, 1995). The finite difference Eikonal solver forward code used here is fully capable of incorporating sharp velocity contrasts and severe lateral velocity variations. The tomographic inversion code was received through email courtesy of Prof. John A. Hole (Univ. of Virginia) after a formal request by the author.

The first break travel times on all the 410 shot point locations were picked (180,000 traveltimes picks) in Vista[®] and exported as text files. The source-receiver offsets ranged from 5m to 2000m. For each shot point, geometry and parameter files were created in Matlab[®]. These files were required as input in tomography code. Basically, the tomographic inversion code worked in four major steps: 1) construction of an initial input velocity model; 2) travel time and ray path calculation through the model i.e., calculation of a kernel or objective function (required at inversion stage); 3) inversion (calculation of traveltimes residuals); 4) velocity updating (back projection) (Figure 6.7).

In order to allow the turning rays to return back to the surface receivers, a positive gradient velocity model was created; that is the velocities gradually increased with depth although the velocity within each cell remained constant. The interval velocity model developed during processing of the reflection data (Figure 4.21) was analyzed to obtain an appropriate vertical velocity gradient model i.e., smoothly increasing velocities from approximately 300 m/sec at the surface to 4000 m/sec at 1 km depth (velocity gradient 4 m/sec/metre). Different smooth linearly increasing velocity gradients were tested before choosing final one. The velocities that were too high at the surface and increasing rapidly with depth (0.8

km/sec at the surface to 6 km/sec at 1 km depth equivalent to a velocity gradient of 5.7 m/sec/metre) could return rays to near offset receivers but did not allow waves to reach the farther offset traces.

Special care was given to obtain an appropriate input velocity model that illuminated all the receivers as was indicated by the real data. A linearly interpolated positive gradient 2D velocity model was used as a starting model (Figure 6.8). Block parameterization was used in defining starting velocity model. Different cell sizes were tested i.e., 0.5 m to 10 m. Two points were kept in mind while selecting cell sizes: 1) the cell size must be small enough to resolve small geological features, and 2) each cell must have enough number of ray segments to avoid illumination problem. The final inversion was carried out on grid cell size 2 x 2 metres, and the final model required 3.95 million cells. The choice of proper grid cell in inversion is a trade off between resolution and inversion stability. For large cell sizes, more rays pass through each cell and it eventually produce smoothed result – because of bigger cell size. For a smaller cell size less number of rays pass through each cell and less smooth result – meaning small feature can be imaged. But as cell size decrease, at some point not enough rays can pass through each cell, and the inversion become unstable. Decreasing cell size is directly proportional to the computer CPU time. For example this code was run on Sun Blade 100[®] (UltraSPARC-IIe) 500 MHz processor (64-bit machine) with one iteration taking 3 hours. The final inversion run took approximately 70 hours of dedicated computing time.

The forward modeling and ray path calculation procedure was straight-forward. Rays were traced for one shot point with its all receivers at a time and then next shot point and so on. Once rays from source to all receivers were traced for all shots then inversion was carried out.

During the inversion stage, smoothing functions were applied, first to the inversion grid and second to the travel time perturbations, using a moving average filter. Smoothing parameters were very important in the inversion because

different parameters gave different resolution output; the best parameters were chosen after testing. All the testing carried out for calculating optimum smoothing parameters were based on the scheme described in Carney (2000). Initially, in the first iteration larger smoothing operators were chosen; say 1000 metre horizontally and 333m vertically with 3:1 ratio. In subsequent iterations smoothing size was decreased nonlinearly by ~80% in every 3rd iteration. For one smoothing parameter three iterations were carried out with ray tracing in every iteration. Carney (2000) described a scheme for tomographic inversion in the areas where very little information of subsurface velocity is known. In this procedure positive gradient velocity model is given as starting model and after tomographic inversion solution iteratively converge to the smoothed almost true velocity model.

6.1.2.3. Interpretation

Refraction tomography gave a detailed image of the subsurface. Small block size was used in parameterization that allowed seeing detailed features. Turning ray tomography is an inversion technique that gives the ‘best possible’ solution of the subsurface not ‘the solution’. Tomographic inversion gave smoothed subsurface velocity model. The final complete 10 km inverted velocity model is shown in Figure 6.9.

Tomographic inversion depends a great deal on the input velocity model; and the final solution can be biased towards this initial model. The positive gradient velocity model was given as input model and in subsequent iterations smoothing was applied regressively. This strategy gave smooth results and final solution was not biased to the input model. In the final inverted velocity profile some low velocity anomalies are present such as at the UTM location 414 km horizontal and at sea level. Channels consist of low velocity material and any low velocity anomaly at the location of incised valley can be indicative of this. However, the incised valley was not imaged in this profile as in case of conventional refraction interpretation. Tomography gives a smoothed result and probably the truly abrupt

velocity contrasts across the Cretaceous-Paleozoic unconformity and the Quaternary-Cretaceous unconformity are ‘smeared’ in the tomographic results. In the forward modeling a smooth gradient is usually required; and a sharp discontinuity may be problematic for a ‘conventional’ ray tracing forward modeling code. Attempts were also made to shoot rays from the bottom to the surface. This means that when a ray turns back from its maximum depth location (i.e., turning point) or bounces back from the discontinuity, the location of that point is saved. Rays were then shot from the point back to the surface. The result using above mentioned forward modeling procedure was same with the results using conventional approach i.e., shooting rays from surface shot location.

In the western end of the profile two discontinuities are visible, these are most likely due to some artifacts in the inversion. Figure 6.10 is a 3.5 km inverted velocity profile showing layer cake geology with some low velocity features. Isolated lenticular velocity anomalies are also visible in the profile.

Overall, refraction tomography could not provide ‘detailed’ internal structure of channel. No procedural error was observed while applying this technique. It is rational to incorporate refraction analysis in the thesis and I deem results are acceptable although at this point they are preliminary.

First Arrival Traveltime Tomography Workflow

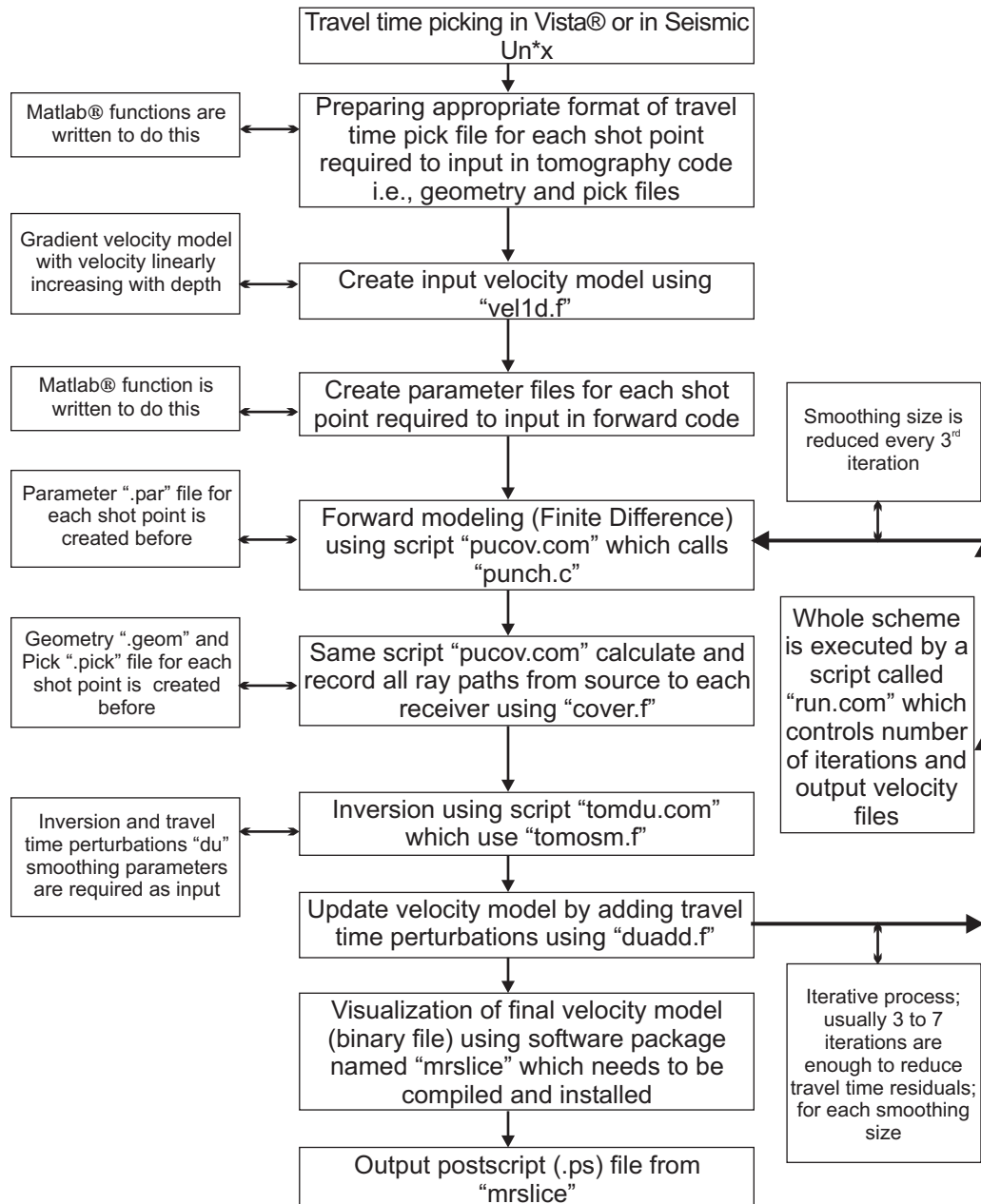


Figure 6.7: Block diagram showing complete workflow of seismic travel time tomography.

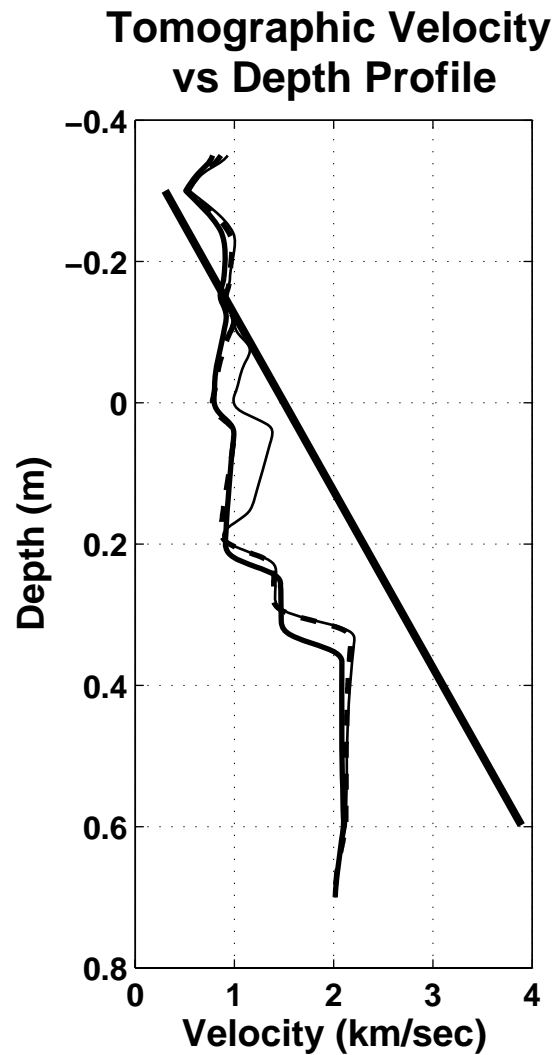


Figure 6.8: Tomographic 1D velocity profile. Thick solid line is input velocity model. Medium thick solid line is 1D velocity profile extracted at $X=15$ km. Thin line is at $X=9$ km. Dashed line is $X=9.5$ km. Tomographic velocity model is smoothed image of the true earth model. High gradient input velocity model (with velocity 7 km/sec at 0.8 km depth) was also tried but rays were not traced at surface receivers and tomographic inversion became unstable (mathematically unstable; NaN values) after second or third iteration. The input velocity model was the best guess for current geological condition.

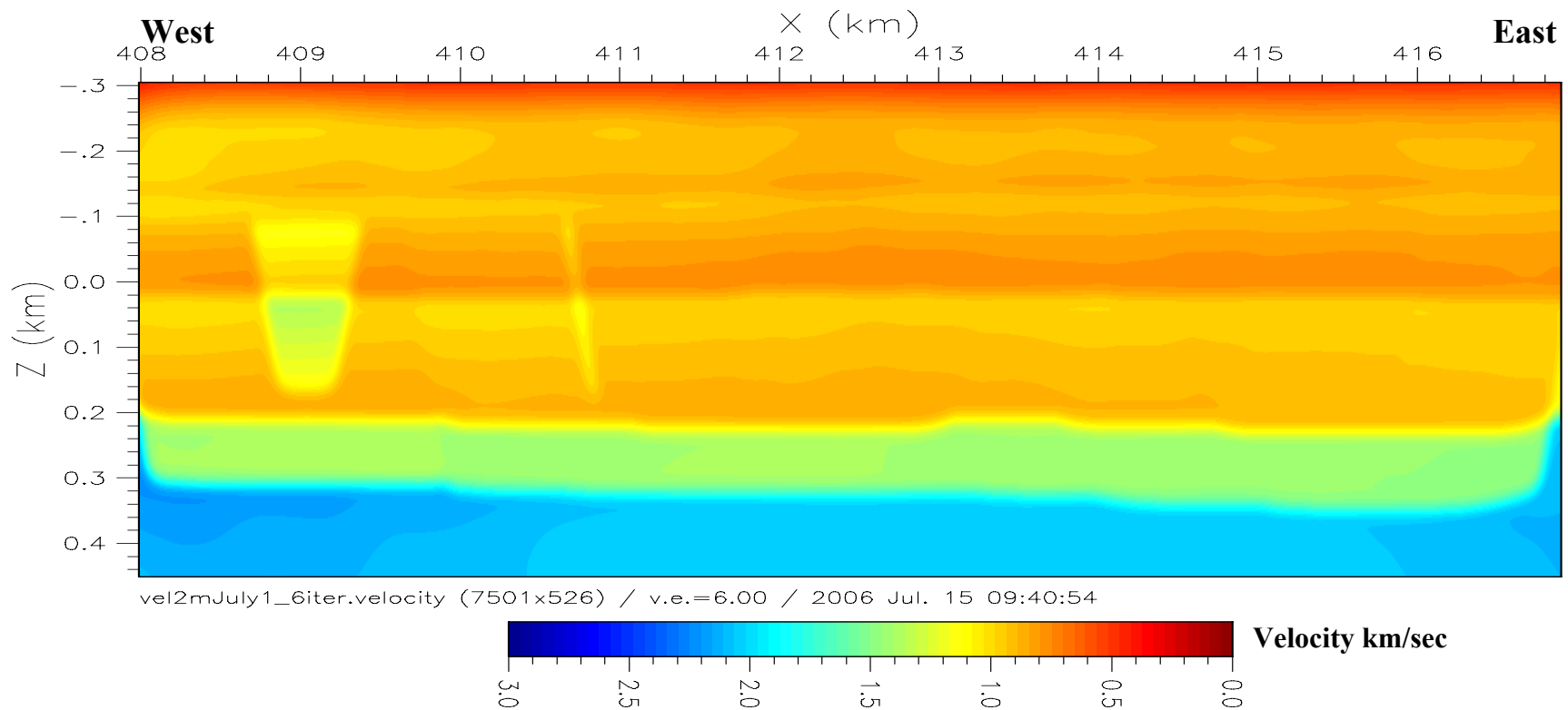


Figure 6.9: Final complete (10 km east west) velocity model after tomographic inversion. X-axis is UTM easting in kilometres. Y-axis is depth in kilometres. Depth from ground surface is increasing downward. Depth of 0.0 km. is sea level value. Discontinuities in the western part of the line might be indicative of faults but it may be an inversion artifact. See some poor reflection quality at same location in Figure 6.11.

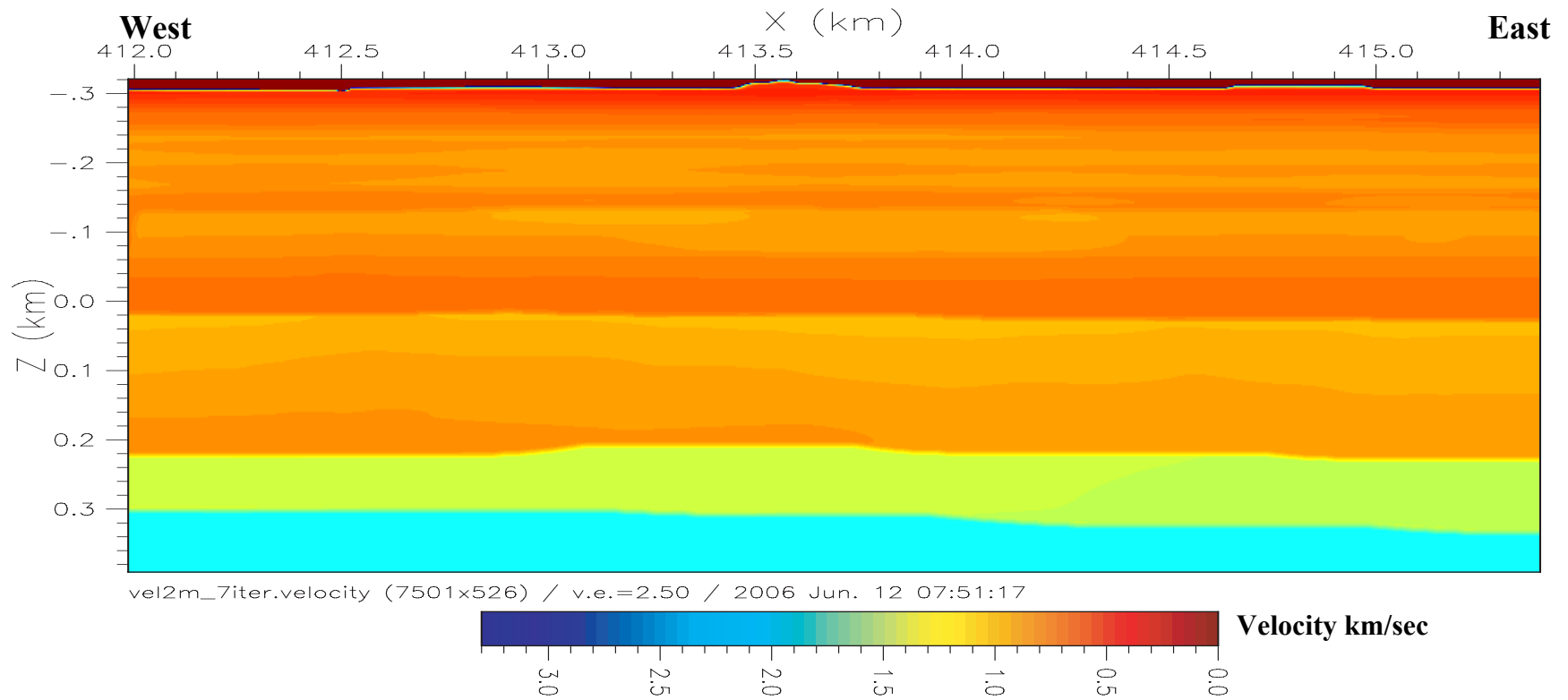


Figure 6.10: Zoomed in tomographic velocity profile showing layer cake geology. Isolated velocities anomalies are visible in the profile.

6.2. Seismic Reflection Interpretation

The final time processed reflection profile is shown in Figure 6.11. The 10 kilometre east-west seismic reflection line consists of 2400 common midpoint traces (CMP) at a 4 m spacing; this figure is highly laterally compressed in order to fit on the page. The dipping event from shot point (SP) 400 to SP-1000 at two way time (TWT) 0.3 sec to 0.2 sec is anomalous to the normal flat lying Cretaceous layers to the west and is likely the base of the Quaternary deposits (see Figure 4.5 for Easting and SP relationship). The dip of this horizon is $\sim 2^{\circ}$ to 3° . High amplitude reflections between SP-300 to 1500 in shallow region (0.05 to 0.25 sec) are also seen within these Quaternary deposits. Quaternary deposits in this area are interbeds of clay, sand and conglomerates as was suggested from the well logs that are available as discussed in previous chapters. These high amplitude reflections are most likely associated with conglomerate beds. Some of these high amplitude reflections may be associated with the near surface gas deposits.

The nearly continuous and high amplitude reflection at 0.35 sec is from the top of the Paleozoic (primary carbonate) unconformity. This Paleozoic reflection is not clearly continuous at two locations (SP 1450-1500 and SP 2050-2150) in the western part of the line. This may be due to the poor reflection quality at that level which made velocity picking difficult on semblance plots described in Chapter 4 (Figure 4.20). Or these broken reflections can be linked to the geological faults as seen in tomographic velocity profile (Figure 6.9). Figure 6.12 shows part of seismic section on larger scale. A few truncations of seismic horizons are marked on line interpretation section in this figure. Seismic horizons are truncating on the high amplitude reflections which may be top of clay or till.

Sequence stratigraphic concepts can also be applied to this dataset for interpretation. For detail descriptions of sequence stratigraphic principles refer to Catuneanu (2006). Quaternary strata in this area were mostly deposited in glacial

environment and climate was the main driving mechanism. Eustatic⁴ changes had minimal effects in deposition of glacial sediments because the area was removed from coastline. The sediment response to erosion and deposition in the valleys were ultimately the function of changes in the local 'base level'⁵. Quaternary deposits in this particular area might consists of; 1) glaciofluvial⁶ sand and gravel that were deposited through the meltwater channels and; 2) glaciolacustrine sediments that are stratified till and clay. By looking at the bedrock topography map of Pawlowicz et. al. (2005a) (Figure 3.2) and seismic character, this paleo-valley fill material can be interpreted as glaciolacustrine deposits. The size of the proglacial lake⁷ is about 8 x 8 km (see Figure 3.2). The characteristics of proglacial lake deposits are: 1) sediments were deposited in the lake environment which form deltas and; 2) lake level fluctuate due to the glacial advance and retreat or climate changes and; 3) lake was fed by meltwater channels with variable sediment load depending upon climatic conditions. Lake level has no influence of eustasy and was factor of local climatic and tectonic changes. Sometimes, proglacial lakes also preserve deltaic successions which help in interpretation. The seismic section is not perpendicular to the incoming and outgoing stream of the lake. Consequently, it is not possible to see perfect clinoforms⁸ of delta foreset⁹. But few clinoform type features are visible which downlap¹⁰ on the high amplitude horizon (may be top of clay or till). Stratified succession in the seismic section (between 0.15 – 0.25 sec) shows calm period of deposition with minimum sediment input and aggradation¹¹ due to suspension load i.e., mainly clay. The broken high amplitude reflections in the shallow part of the section < 0.15 sec are may be from isolated gravel or till beds. These broken reflections show a relatively high energy environment with abrupt sediment

⁴ Global changes in sea level.

⁵ Hypothetical datum surface provides the surface of balance between sedimentation and erosion. Usually datum surface measured from the centre of the earth.

⁶ Sediments deposited from meltwater streams coming from glaciers or ice sheets.

⁷ The lake that is formed in the frontal margin of advancing or retreating glacier or ice sheet.

⁸ Subaqueous landform similar to the continental slope of the oceans or in deltas

⁹ Gently inclined bed deposited in the frontal slope or outer margin of delta

¹⁰ Downward stratal termination.

¹¹ The build up of sedimentary succession by the deposition

supply mainly due to climatic fluctuations. This lake was probably cut from meltwater input for a long period of time and only filled during warm periods that provide a favourable deposition environment for fine-grained sediments (between 0.15 to 0.25 sec). The electrical resistivity profile (ERT) profile (see Figure 5.5 point “D”) shows low resistivity material at this location (within the Quaternary deposits) which possibly means clay or fine-grained material.

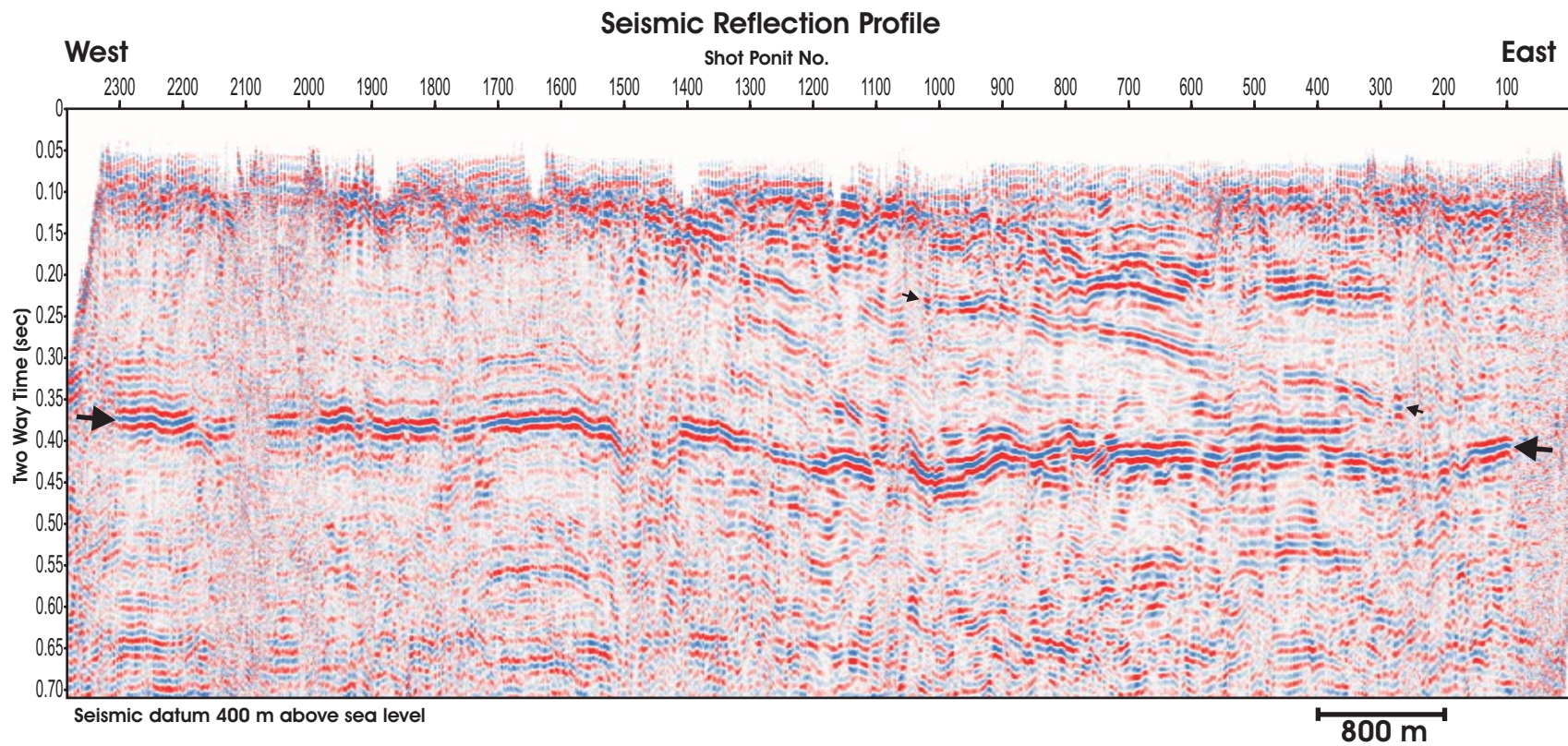


Figure 6.11: Conventional time processed seismic reflection profile. Small arrows showing base of the Quaternary deposits. Large arrows showing Top Paleozoic (carbonates). See text for details.

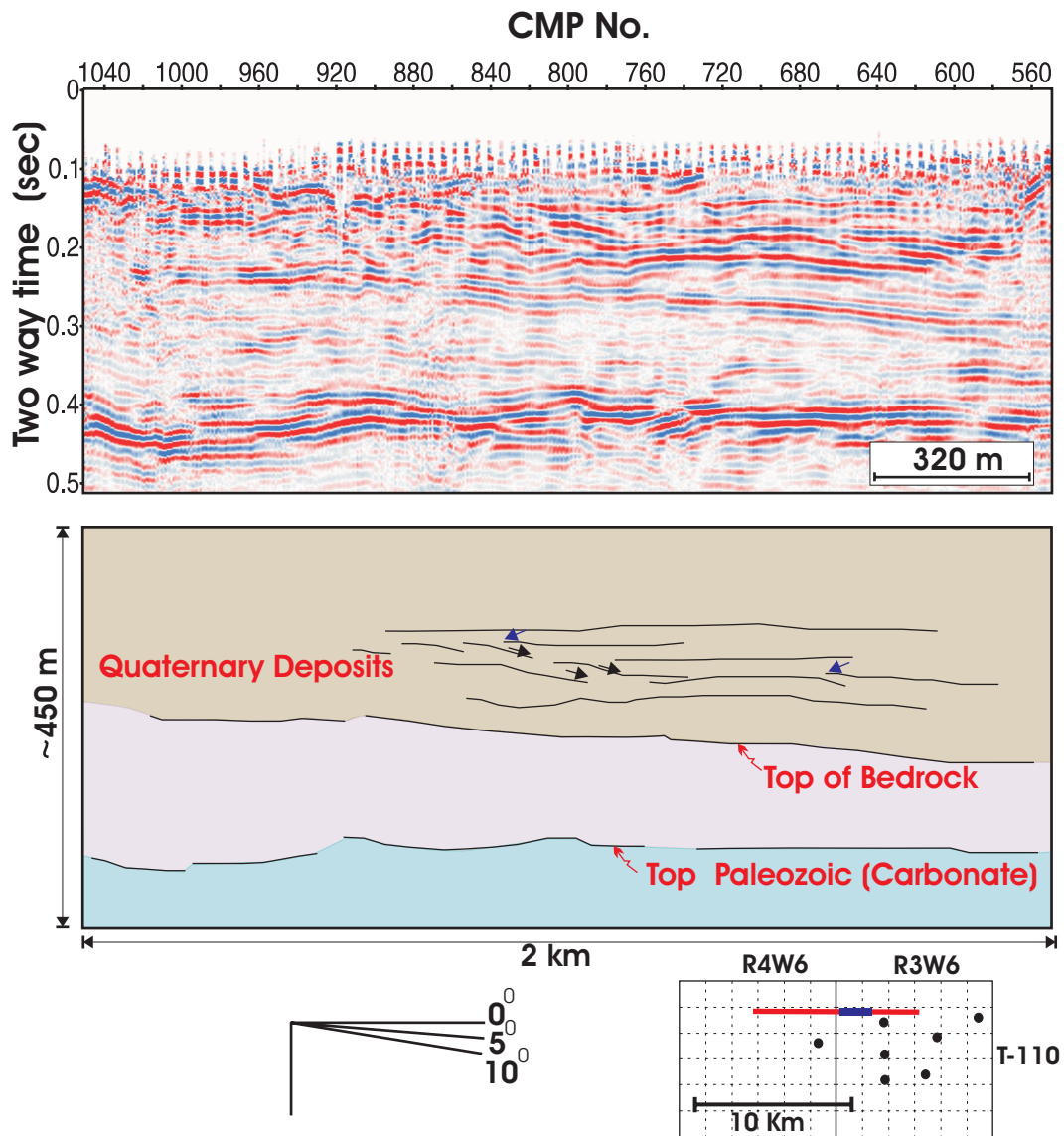


Figure 6.12: Part of the uninterpreted seismic section (top) and line drawing interpretation (bottom) (Profile from Figure 6.11). High amplitude reflections within the Quaternary strata are clearly visible. Vertical exaggeration is 1.85. The material deposited above the bedrock is of glacial origin. Marked arrows on the uninterpreted section are showing truncating strata. These truncations show the possible lateral accretion surfaces with may be indicative of point bars. Top of the bedrock pick is based on the data provided in Pawlowicz et. al. (2005a & b).

6.3. Synthetic Seismogram

A ‘synthetic seismogram’ $s(t_o)$ is a calculated one dimensional seismic response of the earth used to assist in the interpretation of seismic data. It is calculated by convolving an estimated source ‘wavelet’ $w(t_o)$ (i.e., the expected output of the seismic source) with an estimate of the earth’s reflectivity generated from density and sonic logs in a borehole. For description of geophysical logs refer to section 3.3. The basic equation used in this modeling is as follows:

$$R = \frac{V_2\rho_2 - V_1\rho_1}{V_2\rho_2 + V_1\rho_1} \quad (6.4)$$

where R is reflection coefficient/reflectivity and ρ_2 , ρ_1 and V_2 , V_1 are densities and velocities of layers below and above the interface, respectively. In application, the velocities and densities come from the sonic and density logs, respectively, although the researcher should be aware of the errors in these that will influence the synthetic seismogram. The reflectivity as a function of two-way travel time $R(t_o)$ be may then be calculated using equation 6.4 and this reflectivity is then converted to the synthetic via

$$s(t_o) = w(t) * R(t_o) \quad (6.5)$$

where ‘*’ is the symbol for convolution. When this synthetic trace is displayed against other geophysical well logs, an idea of local geology and its acoustic response can be made which helps interpreting seismic reflection data. Different central peak frequencies the standard zero-phase interpretational ‘Ricker wavelet’ (source wavelet) were tested in order to choose best matching frequency for making synthetic seismogram and that with a 75 Hz central peak frequency was selected for making synthetic seismogram. The synthetic seismogram was created in Matlab[®] with the code for creating the synthetic seismogram provided by Dr. Ulrich Theune.

It is sometimes difficult to differentiate Quaternary sediments filling buried

valleys with the surrounding geology on geophysical logs because glacial deposits do not give any specific signature on logs. Glacial tills usually have higher P-wave velocity than surrounding glacial deposits (i.e., glaciolacustrine clay, glaciofluvial sand and silt) but there is little difference of character with these on the natural gamma ray log. The results of a study in the region of less horizontally continuous reflectors, and use of synthetic seismogram to show high amplitude reflections and their comparison to the shallow high resolution seismic is presented in Adam et. al. (1998). In an article by Hunter et. al. (1998) downhole logging technique is developed to get appropriate velocity-depth control in unconsolidated overburden. In that study, borehole seismic observations successfully applied to interpret reflectors on the shallow high resolution reflection profiles.

In the past geophysical logging usually starts only after surface casing is put in place; so only few wells in this area have sonic and density logs in the very shallow part ($< 50\text{m}$). After detailed search of the Alberta well database, a few wells were selected for making synthetic seismogram and for the time-to-depth conversion. Accumap[®] was used to search and download digital geophysical logs.

Comparison of geophysical logs and the synthetic seismograms of channel and non-channel wells are presented in Figure 6.13 and Figure 6.14. Synthetic traces of different Quaternary wells were created (only one is shown in Figure 6.13). In each well the character of the synthetic trace within the Quaternary was different, probably due to the isolated and laterally limited pockets of till, gravel and sand within these types of deposits. However, the common feature is that all such synthetics from the Quaternary showed zones of high reflectivity. This may be contrasted with the nearby undisturbed Cretaceous section where the layering is more consistent, but the variations in acoustic impedance from layer to layer are smaller such that only weak reflectivity results (Figure 6.14). The geological log of a nearby well (Figure 3.5) shows repeated successions of gravel and silty clay. These gravel beds have good impedance contrast and show high amplitude

reflections in the seismic. Comparison of the synthetic trace and final processed seismic profile is given in Figure 6.15. High reflectivity above the Paleozoic unconformity (Top Wabamun) is clearly visible both in the synthetic and seismic trace.

Time to depth conversion is almost always a problem in seismic interpretation. Different techniques used are: 1) vertical seismic profile (VSP); 2) check-shot survey; 3) pre-stack depth migration (PSDM) in the areas with enough well control; and 4) sonic logs. Sonic log in conjunction with marker bed such as the top Paleozoic (carbonate) was used as control point for time/depth conversion. The top Paleozoic (carbonate) was clearly identified on the sonic logs because of the abrupt increase in velocity across the major pre-Cretaceous unconformity. The low sonic velocity in the Quaternary sediments as compared to the Cretaceous is observed which effectively increased two way time (TWT) in the wells penetrated in the Quaternary (see time/depth conversion Figure 6.13). This is in likely also evident in the complete time seismic profile which displays an apparent thickening above the pre-Cretaceous unconformity which most likely results from the lower seismic velocities in the channel fill materials to the east. Overall the Quaternary sediments show low sonic velocity with increased travel time.

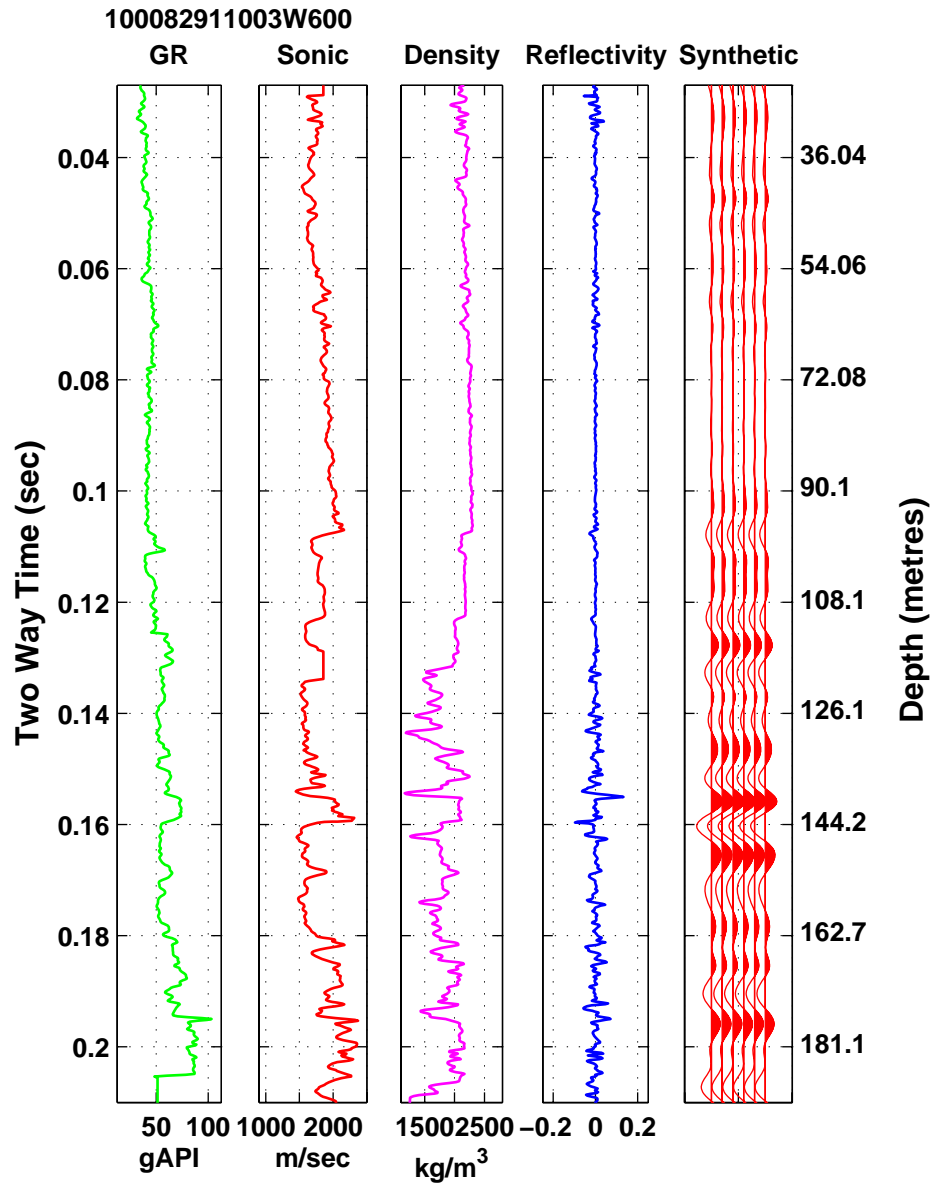


Figure 6.13: Log and synthetic seismogram of a Quaternary well (Well/100082911003W600). Synthetic trace is displayed after fix gain. Synthetic seismogram was created using 75 Hz Ricker wavelet. Time to depth conversion was carried out using sonic log and tied with the Top Paleozoic (Carbonates). Top Paleozoic is a regional unconformity and can be used as marker bed. It has high sonic velocity and easily distinguished on sonic log. Due to low velocity in the Quaternary deposits the travel time of seismic waves are higher that creates pull down of Top Paleozoic reflection in the eastern part of the seismic profile (Figure 6.11).

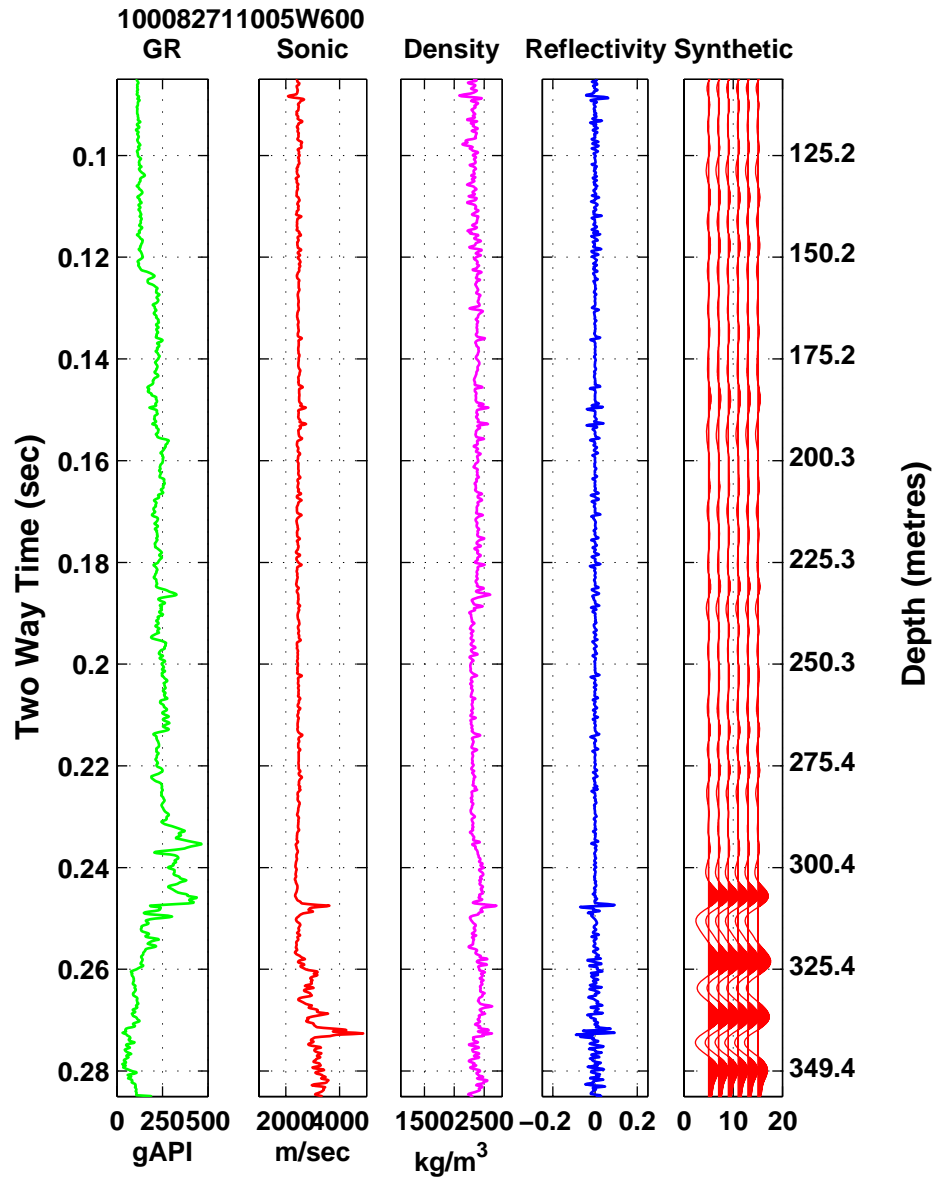


Figure 6.14: Log response along with synthetic seismogram of non-Quaternary (Cretaceous) well (Well/100082711005W600). Synthetic seismogram was created using 75 Hz Ricker wavelet. Synthetic trace is displayed after fix gain. Time to depth conversion was carried out using sonic log and tied with the Top Paleozoic (Carbonates). Top Paleozoic is a regional unconformity and can be used as marker bed. It has high sonic velocity and easily distinguished on sonic log. The Cretaceous section has very little reflectivity and almost no response in the shallow part. Also, see high GR values in the Cretaceous.

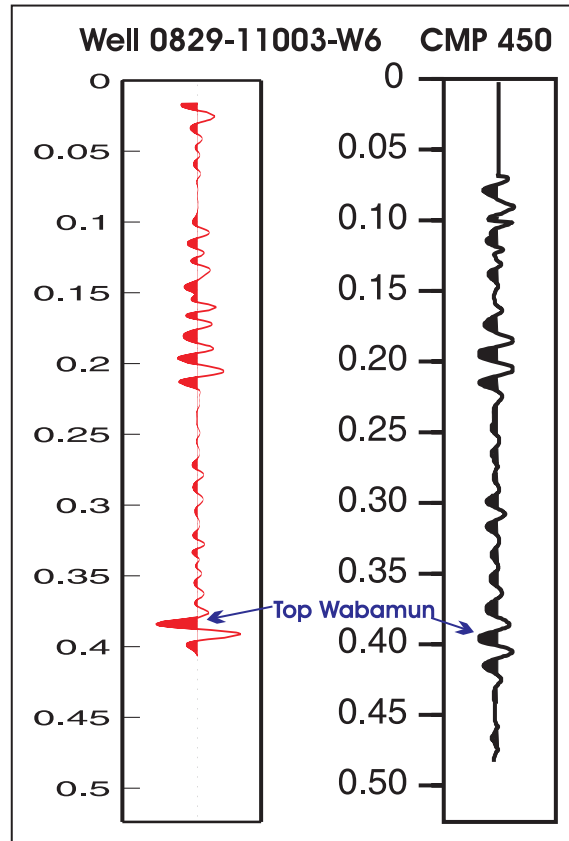


Figure 6.15: Comparison of Synthetic trace (well/0829-110-W6 (600 m away from line) and seismic (CMP-450). Seismic trace is displayed after scaling. Synthetic trace is created using both density and sonic log; but no density log was recorded below the depth of 190 m. This is the only representative well close to the seismic line (within the paleo-valley) which has sonic log recorded. Reflections above Top Devonian (Wabamun L. St.) are almost similar in synthetic and seismic trace, which confirms that lithological contacts are the main cause of reflections. These reflections are from the paleo-valley filled Quaternary deposits. Base of the Quaternary here is ~0.3 sec based on seismic and well log interpretation.

6.4. Integration of Electrical Resistivity Tomography and Seismic

The electrical resistivity tomography (ERT) technique described in Chapter 5 measures the apparent resistivity of the subsurface rocks which after inversion provides a geological model in terms of the true resistivity ($\Omega \cdot m$). High resistivity anomalies can be used as direct hydrocarbon indicator (DHI). Analysis of the high resistivity anomalies was carried out carefully and shown below (Table 6.1).

	Depth from ground surface	Gross Thickness (m)	Net Thickness (m) @ depth	Peak Ω Value	Horizontal Extent (m)
Western most anomaly (A)	80	35	5 @ 100	50-70	290
Central Anomaly (B)	50	75	20 @ 95 15 @ 85	80 ->100	780
Eastern Anomaly (C)	50	80	10 @ 96	60-80	360

Table 6.1: Table showing statistics of resistivity anomalies observed in Figure 5.5

The conventionally processed seismic profile (Figure 6.11) is indicative of the impedance response of the subsurface. That impedance response is associated with different subsurface horizons. The seismic reflection profile gives us the shape and the location of various subsurface structures some which may contain fluids. However, with conventional seismic profiling estimating the fluid content information of subsurface rocks is difficult. Joint interpretation/visualization of ERT and seismic reflection profile is good approach to get clear subsurface picture.

The central (B) and eastern (C) high resistivity anomalies (Figure 5.5) have different seismic signatures. The eastern anomaly C is distinguished by broken reflectors at <0.15 sec two way time while at the central anomaly B the seismic reflectors are vertically piled (see Figure 6.11). Therefore, the location of central anomaly B which appears at the boundary between the Quaternary fill and the

Cretaceous bedrock does not appear to be a simple co-incidence and needed further attention. Truncations across geological boundaries are usually important as these zones may indicate likely structures for that can trap fluids, or conversely also suggest zones that might allow for fluid movement.

6.4.1. Gas Anomaly

The central ERT anomaly 'B' has anomalously high values of resistivity ($> 100 \Omega \cdot m$) that are suggestive of free gas and hence may be of economic interest. This anomaly is in the vicinity of well 07-25-110-04W-6 that is producing gas at a depth of only 50 to 55 metres (Figure 3.5; Figure 6.16). The depth of the resistivity anomaly 'B' at 50m closely matches with the producing horizon of that shallow Quaternary well and, consequently, it is likely that the anomaly 'B' indicates free gas saturating the porous sands. Figure 6.17 shows seismic reflection, ERT and tomographic velocity profiles. The ERT profile shows this anomaly 'B' in the central part of the seismic profile but just to the immediate east of where the seismic reflection and tomographic velocity profiles show the dipping reflector that has been interpreted as the base of the Quaternary. The tomographic velocity profile shows channel like feature with low velocities in the middle part and high velocities at bottom. On the ERT profile gas anomaly appears slightly bigger in size because of the smearing effects associated with the resistivity inversion. Like seismic tomographic inversion, ERT inversion also gives smooth results and high resistive anomaly is temporally and spatially smoothed. But the actual size i.e., horizontal and lateral extent, of the gas pocket associated with this anomaly cannot exactly be calculated. The gross pay for a shallow gas pool is ~20m and net pay is ~4 m (Table 3.1). The block/cell size at the place of anomaly 'B' is ~15 m horizontally x ~13 m vertically. Whereas block cell size imaged on anomaly 'C' on deep profile (Figure 5.6) is ~20 m x ~15 m. This anomaly is not an artifact of inversion because it was also present in the raw data (Figure 5.4). ERT – seismic reflection and tomographic velocity – seismic reflection profiles are overlaid with each other and displayed in Figure 6.18. This figure gives good comparison of two different geophysical methods. The high

resistivity anomaly is also associated with a bright reflection. But only bright reflection on the raw seismic data can not give clue of fluid contents associated with it. Not all bright reflections are associated with hydrocarbons. Combined with ERT, seismic bright reflections can be interpreted and potential zones of hydrocarbons can be marked.



Figure 6.16: Photograph of producing Quaternary gas well 07-25-110-04W-6. Well number is clearly visible in the photograph. Compressor is attached with the well in order to pump gas in the gathering pipe lines. Compressor is seen the top left of the figure. This well is 700 metre south of the seismic and ERT line. Photograph taken by the author in January 2005.

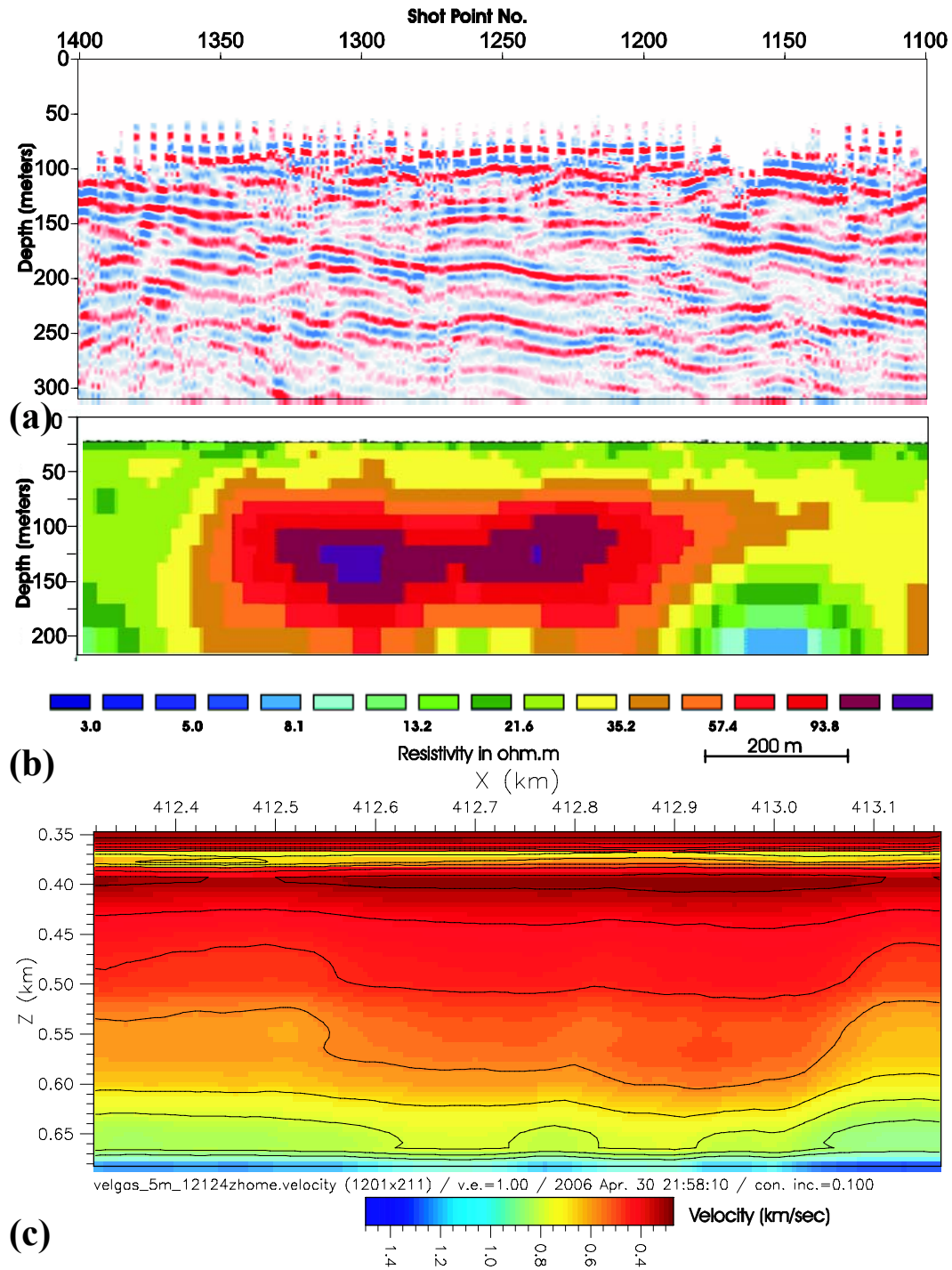


Figure 6.17: (a) Depth converted seismic section; (b) Electrical Resistivity Tomography (ERT) Profile showing high resistivity anomaly 'B'; (c) tomographic velocity profile showing low velocity anomaly. Profile is created using 5m x 5m cell/block size. The depth (Fig-c) is increasing downward from ground surface. On Fig-c 0.35 km is equal to 50m depth on Fig-a & b. Figures are at datum 400 m above sea level means 0 m on depth scale on Fig-a & b is 400m above sea level.

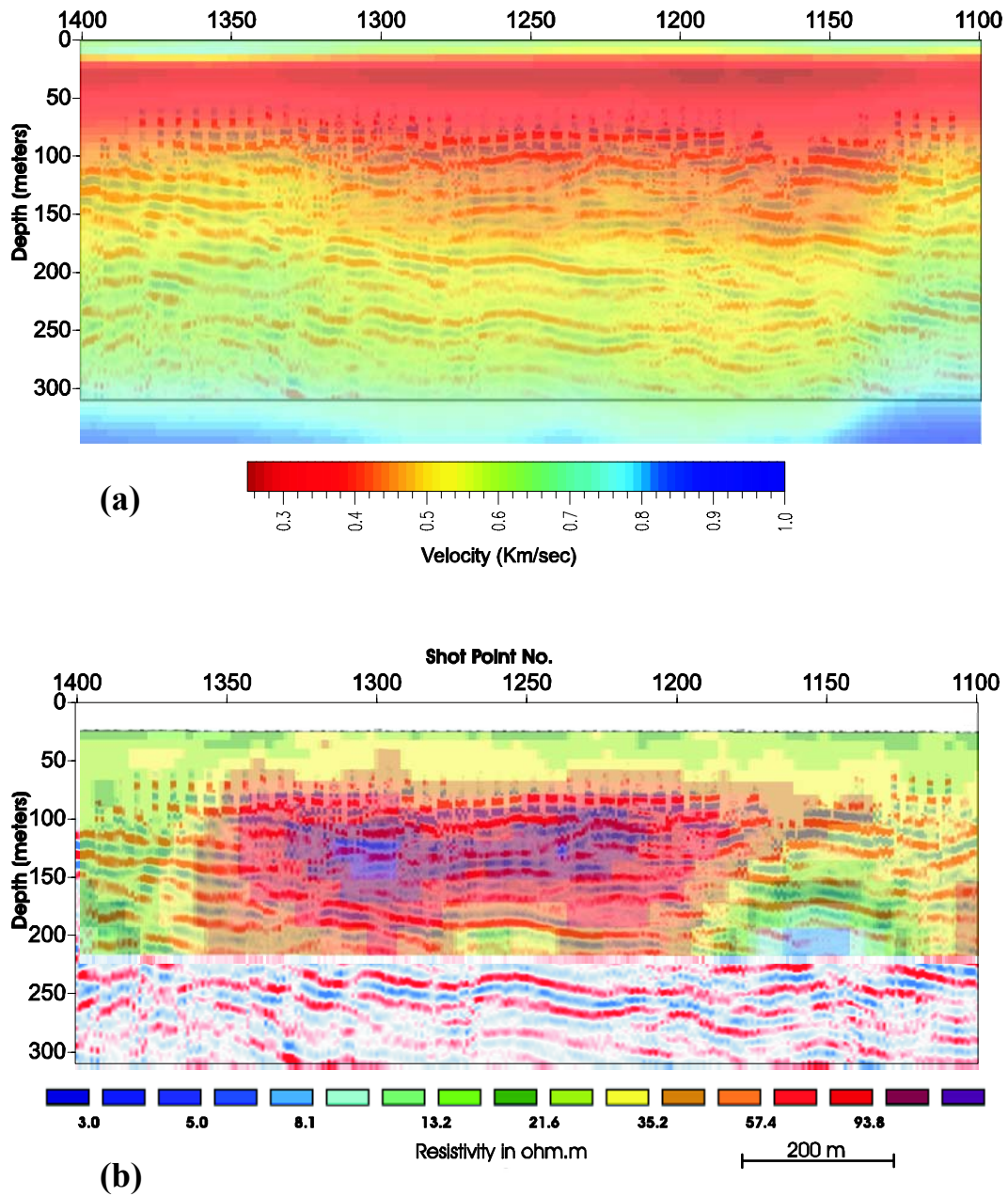


Figure 6.18: (a) Seismic – tomographic velocity overlay; (b) seismic and ERT overlay showing channel and associated high resistivity anomaly 'B' respectively, which might be indicative of gas. In both figures; 1) seismic and tomographic velocity profile and; 2) seismic and ERT profile are graphically merged and overlaid. Figures are at datum 400 m above sea level means 0 on depth scale is 400m above sea level.

6.4.2. Specialized Processing

The results of specialized processing for enhancing shallow gas anomaly are described in Ahmad and Schmitt (2006).

Seismic data was processed using standard industry flow and discussed in Ahmad and Schmitt (2005a) and Chapter 4. Seismic data showed few high amplitude reflections in shot gathers at the preliminary processing stage but none of the bright reflection was continuous after stacking. The static time shifts apparent in this data set were severe and caused considerable degradation of the final seismic section relative to the quality of the original input shot gathers. The idea of looking on the bright spots as a potential indicator for gas zones was dropped at the initial stage because; 1) it was very difficult to differentiate between reflections and refractions on shot gathers especially at near offsets and; 2) after stacking these reflections were not continuous, so it was assumed that they were stacked refractions and they were removed by muting (Steeple and Miller, 1998). After encouraging results of seismic survey, Electrical Resistivity Tomography (ERT) profile was recorded at same place to see resistive gas anomalies and to compare both imaging techniques for shallow targets. As noted above, the ERT data showed the high resistivity anomaly 'B' which further confirmed as gas reservoir due to its location in the vicinity of industry producing gas well (Ahmad and Schmitt, 2005a).

6.4.2.1. Conventional Re-processing Approach

In order to analyze seismic signature of shallow gas, key portions of the seismic data were re-examined and a part was reprocessed carefully. This occasion data was processed with 2m CMP spacing. In this second round of processing only those portions of the seismic shot gathers above was 510 msec and within ± 300 m offset were employed. One tantalizingly, 'bright' reflection is visible in the raw shot gathers at times < 100 ms (Figure 6.19). This strong reflection likely

corresponds to the gas saturated zone encountered in nearby well and also seen as high resistivity anomaly 'B' on ERT profile. This bright reflection merges with the refraction beyond the offset of only 125 metre; that was the practical offset limit for this reflection. Due to fine spatial sampling interval (4 metre) this reflection was able to be imaged on number of field receiver stations and ultimately produced enough fold (~10) at two way time (~50 msec). During reprocessing care was given to this and associated reflections - especially during velocity picking. Velocity picking was very difficult because common mid point (CMP) spacing was 2 metre and any picking errors on the semblance plot can deteriorate the CMP stacking. The initial estimate of stacking velocities was made by making constant velocity stacks on a central CMP with the contribution of all CMP's that are adjacent to the central CMP. By doing this, the complete seismic line was displayed at a chosen stacking velocity interval. Once initial estimate of stacking velocities was determined (~1800 m/sec for complete section) then semblance plots and constant velocity stacks were produced with very fine velocity increment (10 m/sec). At every 25th CMP (50 metre) location the stacking velocities were determined using both semblance plots and on constant velocity stacks within the velocity analysis module of Vista[®]. The data was also passed through a surface consistent residual statics algorithm in order to better align the reflections. This final reprocessed seismic profile is presented in Figure 6.20

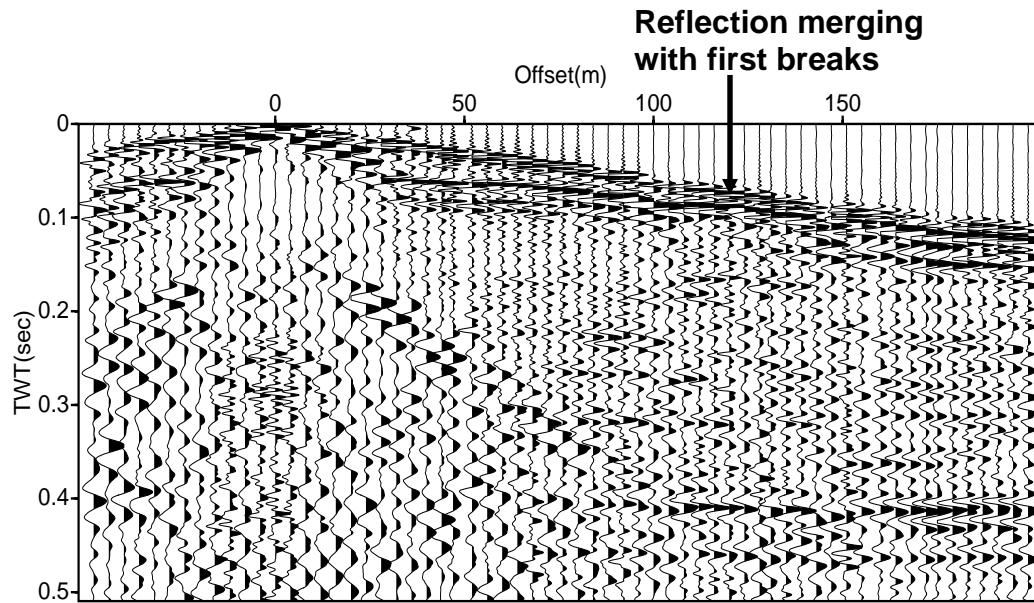


Figure 6.19: Shot gather showing bright reflection at ~0.05 sec and offset 40 – 50 m. This reflection is from shallow gas reservoir encountered in nearby well. Reflection at ~0.4 sec and 150 m offset are from Sub-Cretaceous unconformity (Carbonate)

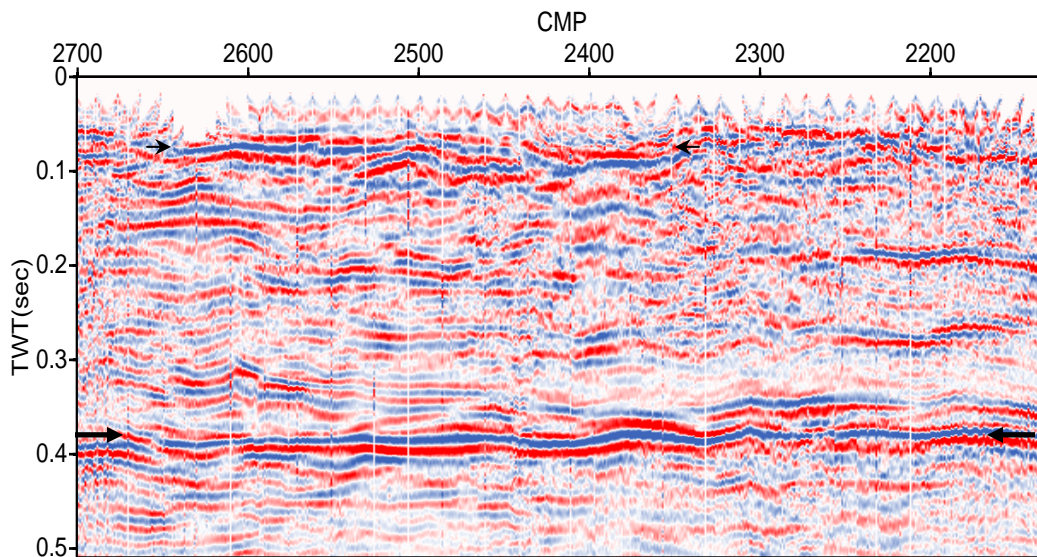


Figure 6.20: Conventional (NMO stack) reprocessed seismic section showing high amplitude reflections at <0.1 sec (small arrows). These high amplitude reflections are associated with gas reservoir encountered in nearby well. Reflection at 0.4 sec (large arrows) is from top of the sub-Cretaceous unconformity (Carbonate).

6.4.2.2. Shift Stack Processing Approach

The shift stack technique was developed to assist in the imaging of near surface reflectors in a similar geological situation in Northern Alberta and is described in detail in Schmitt (1999) and used here to identify high amplitude reflection associated with gas reservoir. Due to slight velocity picking error data was not stacked properly and interpretation of gas zone was not clear in the conventional NMO reprocessed seismic profile. The methodology to create shift stack is described as follows. As high amplitude reflection was clearly visible on shot gathers its travel time was picked carefully. The reflection on shot gather at almost zero offset (<20m) was at ~55 msec. All the traces where reflection was not present, weak or ambiguous were muted out. The traces that were left contain bright reflections. Once these traces were edited, the remaining good ones were statically shifted such that the observed reflecting event lined up at 55 msec (almost zero offset time). Figure 6.21 shows clear picture from shot gather to muting and to shifting traces at certain time. The shift-stacked section is shown in Figure 6.22. It is clear in this figure that bright amplitudes are at the zone of gas. As we move away from gas zone amplitudes are not as bright as in the gas zone.

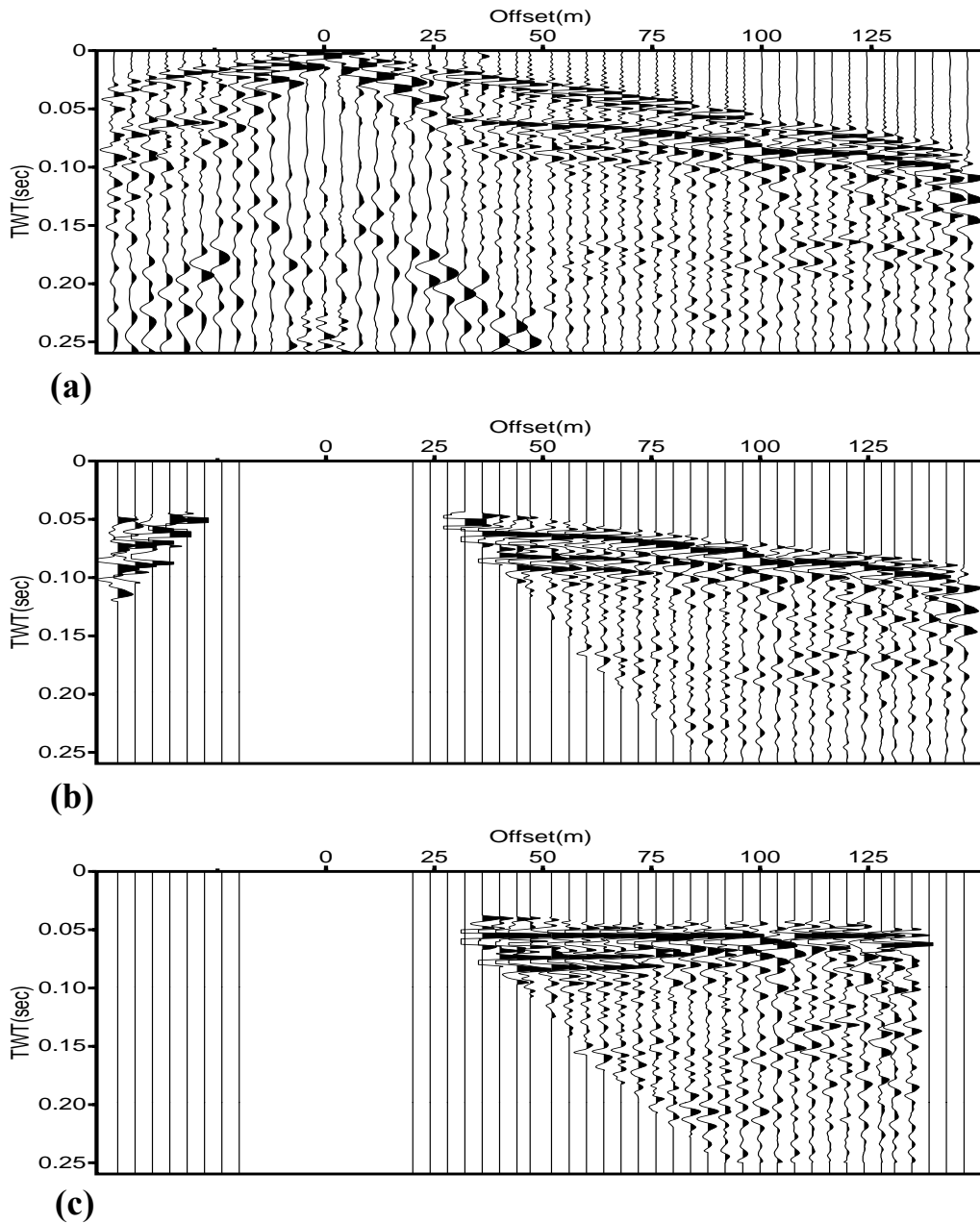


Figure 6.21: Shows step by step procedure of shift – stack technique. (a) Shows shot gather with maximum offset 150 m and time 0.25 sec. (b) data after offset limited sorting (rejecting -20 to +20 m offsets) and muting first arrivals. (c) Data after applying static shift at known time (0.055 sec, in this case), which is close to the expected zero offset two way travel time to the reflector.

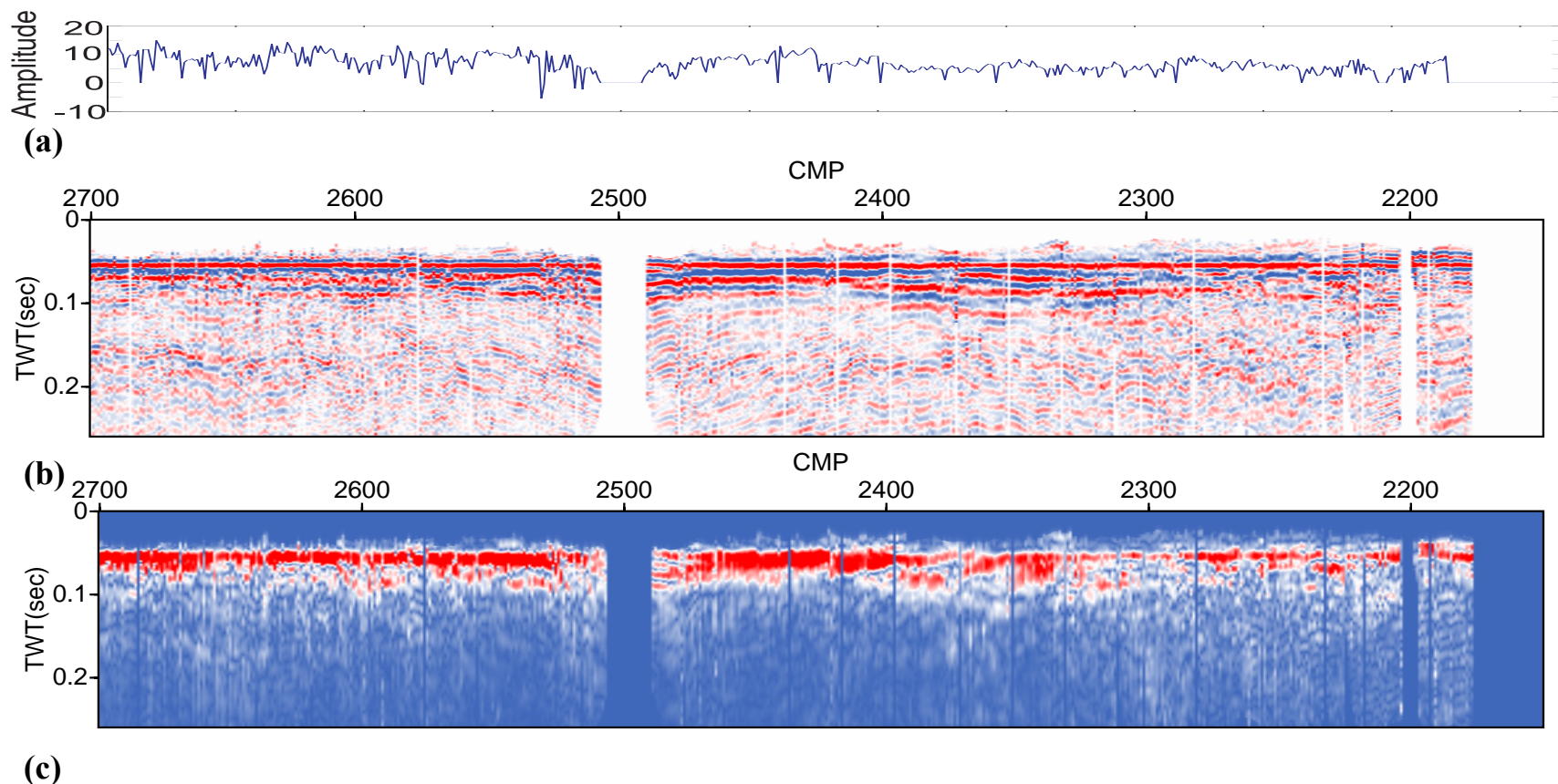


Figure 6.22: Shift-stack processed seismic section (see text for details). (a) Maximum normalized instantaneous amplitude displayed against each Common Mid Point (CMP). (b) Shift stack processed section showing high amplitude reflection giving more confidence interpreting gas reflections on conventional processed section. (c) Instantaneous amplitude section of the above mentioned (Fig-b) seismic section. Gap in the section is due to the missing receiver stations due to the instrument cable limitations. No gap in Figure 6.20 is due to the offset shots used in calculating CMP's which created traces in the gap.

6.5. Summary

Detailed analysis of geophysical data is carried out in this chapter. The seismic line was located in a well known shallow gas producing province. Different shallow gas pools are present in that area, and a few wells are producing gas in the vicinity of the seismic line. There are a number of lines of evidence that converge in this chapter:

On the bedrock topography map a large and deep depression is marked where bedrock was eroded. Geophysical logs from that area show that the depression is filled with weak, likely unconsolidated sediments. A fair amount of difference in the log character exists between surrounding host sediments and the channel fill material

The seismic data show by variety of means that the difference of geology exists. The interval velocity profile (from Chapter 4) shows that there is a change in velocities from east to the west but only in a gross sense.

Seismic refraction analysis shows a substantially different velocity structure of channel fill material, surrounding host Cretaceous sediments and underlying Paleozoic Carbonates. Based on the refraction velocities, the channel can easily be identified although such refraction analyses cannot give details of the structure particularly along the transition from the channel fill in the east to the bedrock in the west.

Refraction tomography does not provide detailed internal structure of the channel fill material as expected. But it does provide some velocity inversions with fairly low velocity in the shallow part.

The seismic reflection profile highlights the existence of the filled channel in the east and the undisturbed Cretaceous sediments in the west. A ramp, or series of

ramps, is seen near midline which likely represents the unconformity produced on the Cretaceous bedrock when the channel was incised. Smaller scale lateral structure is seen within the valley fill material that is consistent with the expected fluvial and lacustrine type glacial deposits. There is some possibility too that anomalously high reflectivity could be indicative of gas saturated near surface zones.

On the electrical resistivity tomography (ERT) profile high resistivity anomaly is identified and it likely also associated with the gas deposits. This resistivity anomaly is at the western margin of the base of channel as seen in the seismic reflection profile (Fig. 6.11). As well, the ERT profiles display the grosser features of the higher resistivity channel fill sediments in the east and the undisturbed more conductive Cretaceous bedrock to the west. The deeper profile hints at the existence of the ubiquitous underlying Paleozoic carbonates, that are expected to also be highly resistive, but these are likely at the edge of applicability of the method and may smear the smoothed results of the tomography.

Carbon isotope values of the gas of one Quaternary well and the Cretaceous well are almost same which further confirms that both are from same source rock (Karlis Muehlenbachs, personnel communication; section 3.2). Further, the concentration of heavier hydrocarbons in this gas indicates a deeper thermogenic origin. Consequently, the co-incidence of the valley wall as seen in the reflection seismic profile with the highly resistive near surface anomaly as seen in the ERT profile, suggests that this gas has migrated into the valley fill sands from the Cretaceous.

Due to the shallow depth of these gas reservoirs and associated low drilling cost these are highly economical. Although it is very difficult to see this gas on the reflection seismic due to problems associated with the processing of such data, it appears that the gas zone too may be associated with a strong seismic reflection which is apparent in the raw shot gathers but substantially muted in the final

processed reflection profile.

Although there is room for improvement in the work here, as will be discussed in the next and final chapter, the joint interpretation of the various kinds of data from well logs through refraction seismic analysis to seismic reflection profiling and finally ERT studies appears promising. The author does know of cases where industrial concerns have used either ERT or reflection seismic or both. Unfortunately, these studies are to the author's knowledge all proprietary with the data eventually lost and the author has not been able to benefit from the work that has gone on independently. What is not known, but is not likely given current industry practices, is whether industrial exploration has taken advantage of the refraction data to help add value to the interpretations. Here, a substantial amount of information was gained with only a small added investment during the analysis of the data with no additional data acquisition costs. Further, while the focus on the likely gas filled zone here was partially successful, the fact that this anomaly is so evident in the raw data directly suggests a simple approach to the analysis of such data might also yield benefits. Indeed, processing of the data into reflection profiles may do more harm than good if the goal is to find gas saturated zones using seismic profiling.

Chapter 7

Conclusions and Future Work

7.1 Conclusions

The main purpose of the work in this thesis is to carry out a geophysical case study of a buried channel in Northern Alberta. The study sought to provide additional information about the position, the geological setting and internal structure, and possibly the saturating fluids of one Quaternary buried channel. Buried channels are former valleys that were filled in with glacial materials. Porous zones in these glacial deposits sometimes contain methane and fresh water, both of which are economic resources.

Two different geophysical methods were employed to achieve the goal. First, high-resolution seismic reflection data was acquired and processed to image and characterize the Quaternary channels. Second, electrical resistivity tomography (ERT) data was acquired and inverted to image and characterize channels based on their resistivity contrast with surrounding rocks and possibly to get fluid content information based on the electrical resistivities of the rocks. In addition to this, based on available geophysical well logs, synthetic seismic modeling was carried out to understand the acoustic response of the Quaternary channels and the less disturbed surrounding sedimentary bedrock.

In the first stage a buried valley was identified on the published bedrock topography map and a prospective location for the seismic line marked. Then high-resolution seismic reflection/refraction data were acquired using the University of Alberta recording instruments and seismic vibrator energy source.

Seismic data was processed using a conventional seismic processing flow. On the final processed section the base of the buried valley was identified as an eastward dipping event which matched with the much sparser well data. Within this buried valley, high amplitude reflection events were identified which are likely related to the internal structure of the fill zone and may in some cases be related to the gas saturation.

Seismic refraction analysis was also carried out using conventional and tomographic inversion methods. Refraction interpretation clearly reveals the presence of the paleo-valley with its low velocity contained within the flanking higher velocity Cretaceous formations and the underlying Sub-Cretaceous carbonates. An attempt to obtain more detailed internal velocity structure of the channel fill material using travel time tomography was not successful. Tomographic inversion delivered slightly flat and smooth results with layers of varying velocity.

The seismic data displayed by variety of means the differences in the geology as between the channel fill material and the undisturbed host bedrock. The Dix's interval velocities derived as part of the reflection velocity analysis indicated that the velocities vary from the east to the west sides of the line, but in only a gross sense. More refined, but still simple, seismic refraction analysis shows a substantially different velocities of the channel fill material (<1800 m/sec), surrounding host Cretaceous sediments (~2600 m/sec) and the underlying Paleozoic Carbonates (>5000 m/sec). Based on the refraction velocities, the channel can easily be identified, although such refraction analyses cannot give finer details of the structure particularly along the transition from the channel fill in the east to the bedrock in the west.

Synthetic seismograms were calculated using available geophysical sonic and density logs. Synthetic traces calculated from the Quaternary deposits differed substantially from the surrounding Cretaceous formations. High reflectivity within the Quaternary sediments may be due to isolated bodies of till and gravel,

whereas Cretaceous synthetics show low reflectivity in good agreement with the observed seismic reflection profile. In resistivity logs, however, the Quaternary sediments were substantially more resistive than the surrounding shale-rich Cretaceous formations. This is also observed in the ERT profile.

In the second stage, ERT data was acquired along the seismic profile. The final ERT profile shows the channel fill material to be substantially more resistive ($10 - 25 \Omega \cdot m$) than the flanking Cretaceous formations ($<10 \Omega \cdot m$) and allowed the channel to be detected on this profile on this basis. ERT profile also highlighted potential gas bearing zone based on its high resistivity relative to the surrounding formations which corresponds to the known producing horizon in the nearby well. The channel fill materials have generally lower seismic velocities and are more resistive than the flanking undisturbed Cretaceous formations. These contrasts allow the channel to be detected on the basis of both refraction and resistivity analysis, and both are consistent with the lower resolution picture of the area from earlier well log interpretations.

The ERT profile contained a number of interesting highly resistive $>100 \Omega \cdot m$ values and shallow (~ 50 m) anomalies. The strongest of these is likely a methane saturated zone based on the high resistivity as well as the fact that a number of nearby wells have been producing gas from this depth. Once this potential gas bearing zone was identified on the ERT profile, the reflection seismic data were re-examined and partially reprocessed. Sections of the data in the vicinity of the resistive anomaly were carefully reprocessed using conventional processing flow and using the specialized shift stack approach. After this reprocessing, the near surface high amplitude reflections were present in the final section. Shift stack section gave more confidence in interpreting conventional reprocessed seismic section. Although it is difficult to see high amplitude reflections and their correspondence to gas reservoir due to the problem associated with processing of such data, it appears gas zone too may be associated with strong seismic reflection.

As noted, the buried valley is identified on both seismic reflection and refraction data. The detailed internal structure of the valley fill material is seen only on the seismic reflection profile. Electrical resistivity tomography profile clearly showed the difference of valley fill material and surrounding host rocks based on the resistivity values. The valley fill material has higher resistivities than the surrounding Cretaceous rocks. Synthetic seismogram of Quaternary valley fill sediments shows high reflectivity than the undisturbed Cretaceous sediments. The resistivity log of the Quaternary sediments shows high resistivity than the Cretaceous shale-rich sediment. High resistivity anomalies on the resistivity profile and bright amplitude on the seismic reflection raw data corresponds to the gas reservoir in the nearby well. That gas may originate from the deeper Cretaceous or even Paleozoic reservoirs as it contacts with the Quaternary valley-fill material at the margin of the channel. The geochemistry of this gas has shown that it is of thermogenic origin.

Refraction analysis may be a good and a relatively inexpensive approach to identify such buried channels at least for initial reconnaissance. Refraction data is recorded in conventional reflection seismic for free and normally only used for static correction. This information can be used to get low resolution structural images including buried channels.

This is first detailed geophysical study, at least in public domain of which we are aware, in which high resolution seismic and electrical resistivity tomography was used to better delineate the structure of a filled valley. Before this study, the buried valley in question was located from the analysis and interpolation of well logs. These techniques are used on a known location of buried valley and however, provide reference for other exploration possibilities. These techniques can be used to identify and locate buried valleys and perhaps locate shallow gas reservoirs.

7.2. Future Work and Recommendations

This study, while finding many interesting aspects of the geophysical behaviour of buried channels in Northern Alberta, should be considered as still preliminary work. In the course of the analysis a number of new points arose that are worthy of additional study.

First, the results of the refraction ‘turning ray’ analysis here were somewhat disappointing. The reasons for this are not known, but it may be that the algorithm employed including the assumption of the geology used may not have been appropriate. A different tack, taken recently by Domes (2004) using the similar codes developed by C. Zelt (Rice University) may be one approach that could yield additional detailed information but this of course comes at the cost of greatly increased effort through the iterative construction of the velocity model. However, the data set acquired here is somewhat unique and should allow for additional testing both to refine the lateral velocity model and to possibly assist in finding better values of the static corrections that could improve the seismic imaging.

Once an improved velocity model has been developed, the reflection processing carried out here can still be carried further. This is suggested because the raw data itself shows considerable structure in the buried channel that actually diminished by the ‘noise-reduction’ inherent to the common midpoint processing methods employed to create the final stacked section. In order to improve the subsurface images, the seismic data could be reprocessed using different and more advanced processing algorithms, particularly pre-stack depth migration techniques that are likely, within the next decade, to supplant the more conventional seismic processing routines now used for upwards of 40 years. As noted above, it may be useful to attempt this jointly with turning ray tomography, the initial results of which presented here were not satisfying. Someone can try other algorithm to invert first arrivals and possibly buried valley and even low velocity anomalies associated with gas can be identified. This data

was processed using normal moveout processing (NMO) processing approach. It is common in the near surface seismic studies that velocity might increase few times at the transition from dry or partially saturated to fully saturated unconsolidated overburden. Under these conditions for shallow dataset NMO velocity analysis is very difficult and at some place might fails to give proper velocities for stacking. The alternative scheme is pre-stack depth migration (PSDM) processing approach. PSDM is iterative process and velocities are calculated using tomographic inversion technique. PSDM position reflectors at their original location, increase spatial resolution and provide data is depth domain. Bradford and Sawyer (2002) successfully applied PSDM processing technique to image <100m aquifers in different geological settings. The problem in PSDM is the availability of algorithm and expertise in velocity model building. The PSDM processing approach is recommended for this dataset.

Ground roll and noise generated by the seismic source was big problem in the acquired data. This can be reduced by using a low energy seismic source. As source energy is decreased the depth of penetration of the seismic waves is also decreased. It is a trade off between depth of imaging and a reduced amount of noise in the shallow data. But if area of interest is <100m deep, which is usually the case for shallow gas prospects, than mini-vibrator with reduced peak force (<2000 lb or 8896 N) can be used. Other seismic sources such as accelerated weight drop method can also be tried (~200 lb or 890 N), which may give low noise and possibly enough deep penetration of signal for shallow targets. The explosive energy source such as dynamite can be used but it does create safety and logistic issues. Once buried valleys are identified on the conventional industry seismic data than above mentioned strategy can be employed which may improve signal to noise ratio for shallow data. In addition to that low natural frequency (10 or 14 Hz) geophones can also be used to increase the bandwidth of the data which, if ground roll is suppressed during acquisition, will definitely increase signal to noise ratio.

In order to better understand petroleum system in Quaternary sediments, an extensive hydrocarbon potential study¹ is recommended. The Quaternary gas in the study area is from thermally mature source and perhaps migrated from deeper reservoirs. Additionally, there is potential for biogenic gas in the Quaternary sediments in Canada. In China, several Quaternary biogenic gas pools have been discovered in near surface as well as >500 m depth. Petroleum source, reservoir and cap rock are within the Quaternary sediments. Shallow gas exploration in Canada is confined to only one location. But Quaternary sediments are deposited almost everywhere in Canada and might contain hydrocarbons at certain places. If commercial quantities of biogenic gas can be produced from Quaternary deposits as shallow as 50 m in China then why not from Canada.

Finally, it would be interesting to attempt to use a variety of other tools to assist in such studies. These additional measurements might include:

- Simple gravity and magnetic surveying now can be carried out with great precision such that small variations in character can be seen. Examples of this occur in Alberta where relatively fine variations of the stratigraphy may be mapped on the basis of their aero-magnetic signatures (e.g., Lyatsky et. al., 2004). The possibility that gravity may be used to assist in delineating such buried channels is also not unexpected as the weakly or unconsolidated fill materials are less dense than the bounding undisturbed and indurated bedrock sediments. This prospect is being attempted over the next few years by the U of Alberta geophysics field school whose studies are focusing on a similar buried channel in Southern Alberta.
- It is expected that airborne EM surveys could also assist in both the reconnaissance and delineation of such channels. Such proprietary data sets are believed to exist in the private domain and it would be a useful

¹ Hydrocarbon source, migration pathways, reservoir and cap rock are usually analyzed in petroleum geology studies.

exercise to contrast that type of measure of electrical conductivity with our surface based measurements.

- Further seismic field tests would be interesting. For example, carrying out a full 3D seismic survey, either at the scale of the shallow gas deposits (over $\sim 1 \text{ km}^2$ or over the scale of the buried channel $\sim 10 \text{ km}^2$) would assist in the delineation of various structures. Having better values of the in situ seismic velocities would be useful. To that end obtaining Vertical Seismic Profiling (VSP) data in a series of wellbores both within and outside of the buried channel would provide additional constraints on the velocity structure in this area that would fruitfully be available to the processing of the seismic data. Finally, it might also be interesting to attempt either a full 3D- 3 component or at least a 2D- 3 component survey to allow for mapping of the shear wave structure of the subsurface. The shear waves will have the advantages of shorter wavelengths (and hence higher resolution) as well as having a different overall response than the P-waves. The contrast between the two types of surveys can yield additional information on the state of fluid saturation in the sands.

References

- Adam, E., Milkereit, B., and Mareschal, M., 1998, Seismic reflection and borehole geophysical investigation in the Matagami mining camp: *Can. J. Earth Sci.*, **35**, 686 – 695
- Adams, D., C., Miller, K. C., and Baker, M., 1994, Application of first break turning-ray tomography to shallow reflection data processing and interpretation: *Soc. Expl. Geophys.*, expanded abstracts, 587 – 590
- Ahmad, J., Schmitt, D. R., Rokosh, D., Pawlowicz, J. G., Fenton, M. M., and Plouffe, A., 2005a, Seismic Imaging of Quaternary Channels, Rainbow Lake, Northern Alberta, Canada: Expanded Abstract, *Can. Soc. Expl. Geophys.*, 2005 annual conference
- Ahmad, J., Schmitt, D. R., Rokosh, D., Pawlowicz, J. G., and Plouffe, A., 2005b, Seismic Imaging of Quaternary Channels for Shallow Gas at Rainbow Lake, Northwest Alberta, Canada: Expanded Abstract, *Can. Soc. Expl. Geophys.*, 2005 annual conference
- Ahmad, J. and Schmitt, D. R., 2005a, Seismic and Resistivity imaging for Quaternary Channels: Rainbow lake, Northwest Alberta, Canada: *Can. Soc. Expl. Geophys.*, Recorder, **30(9)**, 40 – 43
- Ahmad, J., and Schmitt, D. R., 2005b, Seismic and DC resistivity imaging of a buried channel: Poster Presentation (S23B-0261), American Geophysical Union (AGU), 2005 Fall Meeting
- Ahmad, J., and Schmitt, D. R., 2006a, Reservoir Characteristics of a Quaternary Channel: Incorporating Rock Physics in Seismic and DC Resistivity Surveys: Expanded Abstract, *Can. Soc. Expl. Geophys.*, 2006 annual conference
- Ahmad, J., and Schmitt, D. R., 2006b, High Resolution Seismic Imaging of a Shallow Gas Reservoir, Alberta, Canada: Expanded abstract, 76th Ann. Internat. Mtg., *Soc. Expl. Geophys.*
- An, P., Wei, G., Li, Q., Zhang, D., and Zhu, Z., 2006, The practice of directly finding Quaternary gas by seismic method in Chaidam Basin: Poster Presentation (S21B-0048), Western Pacific Geophysical Meeting

- Anders, S., and Larsson, F. R., 1987, Seismic indications of shallow gas in the Northern Barents Sea, Nr. 36: Norwegian Polar Research Institute, P.O. Box 158, N-1330 Oslo Lufthavn, Norway
- Andriashek, L. D. and Fenton, M. M., 1989, Quaternary stratigraphy and surficial geology of the Sand River area 73L: Alberta Research Council, Bulletin – 57
- Andriashek, L. D., Pawlowicz, J. G., Fenton, M. M., and Ranger, I. M., 2001, Bedrock topography and drift thickness, Athabasca oil sands (in-situ) areas and adjoining areas: Alberta Geological Survey Information series – 124
- Baines, D., Smith, D. G., Froese, D. G., Bauman, P., and Nimeck, G., 2002, Electrical resistivity ground imaging (ERGI): a new tool for mapping the lithology and geometry of channel-belts and valley-fills: *Sedimentology*, **49**, 441 – 449
- Baker, G. S., 1999, Processing near-surface seismic reflection data: A primer: Young, R. A., Series Editor, Soc. Expl. Geophys., Tulsa, Oklahoma
- Bakers, G. S., Steeples, D. W., and Drake, M., 1998, Muting the noise cone in near surface reflection data: An example from southeastern Kansas: *Geophysics*, **63**, 1332 – 1338
- Bednarski, J. M., 1999, Quaternary geology of northeastern Alberta: Geological Survey of Canada Bulletin – 535
- Benjumea, B., Hunter, J. A., Aylsworth, J. M., and Pullan, S. E., 2003, Application of high-resolution seismic techniques in the evaluation of earthquake site response, Ottawa Valley, Canada: *Tectonophysics*, **368**, 193 – 209
- Black, R. A., Steeples, D. W., and Miller, R., 1994, Migration of shallow seismic reflection data: *Geophysics*, **59**, 402 – 410
- Boyce, J. J., and Koseoglu, B. B., 1996, Shallow seismic reflection profiling of waste disposal sites: *Geoscience Canada*, **23**, 9 – 21
- Bradford, J. H., 2002, Depth characterization of shallow aquifers with seismic reflection, Part I – The failure of NMO velocity analysis and quantitative error prediction: *Geophysics*, **67**, 89 – 97

- Bradford, J. H., and Sawyer, S. D., 2002, Depth characterization of shallow aquifers with seismic reflection, Part II – Prestack depth migration and field examples: *Geophysics*, **67**, 98 – 109
- Brouwer, J., and Helbig, K., 1998, Shallow high-resolution reflection seismic: vol 19, Series Handbook of Geophysical exploration, seismic exploration, series editors Helbig, K., and Treitel, S., Elsevier Publishing
- Büker, F., Green, A. G., and Horstmeyer, H., 1998, Shallow seismic reflection study of a glaciated valley: *Geophysics*, **63**, 1395 – 1407
- Butler, D. K., 2005, Near-surface Geophysics: Soc. of Expl. Geophys., Tulsa, Oklahoma
- Canadian Wellsite, 2006, Available from <http://www.canadian-wellsite.com/Gallery/gallery.htm> [Cited July 23, 2006]
- Canadian Discovery Digest, 2004, Quaternary gas in Northern Alberta: Can. Soc. of Pet. Geologist, Reservoir, **31(5)**, 57 – 58
- Carney, B., J., 2000, Building velocity models for steep-dip prestack depth migration through first arrival traveltimes tomography: Unpublished MSc Thesis, Virginia Tech University
- Carr, B. J., and Hajnal, Z., 1999, P and S-Wave characterization of near surface reflectivity from glacial tills using vertical seismic profiles: *Geophysics*, **64**, 970 – 980
- Catuneanu, O., 2006, Principles of Sequence Stratigraphy, Elsevier Publishing
- Clare, S., and Hardick, R. C., 1988, Water well test drilling and Natural gas blowout – Zama Lake south observation well project: Alberta Environment, Environment Protection Services, Earth Science Division, Hydrogeology Branch; Alberta Department of Environment Library.
- Cordsen, A., Galbraith M., and Peirce J., 2000, Planning land 3D seismic surveys: Edited by Hardage B. A., Series editor: Hill, S. J., Geophysical Development Series No. 9: Soc. of Expl. Geophys. Tulsa, Oklahoma
- Cox, M., 1999, Static Corrections for seismic reflection surveys: Geophysical reference series 9: Soc. of Expl. Geophys., Tulsa, Oklahoma

- Daily, W., Ramirez, A., Binley, A., and LaBrecque, D., 2005, Electrical Resistivity Tomography - Theory and Practice: *In* Near Surface Geophysics, Edited by Butler D. K., Soc. of Expl. Geophys., Tulsa, Oklahoma, pg. 525 – 561
- Darling, T., 2005, Well logging and formation evaluation: Gulf Professional Publishing
- deBoer, J. Z., Hale, J. R., and Chanton, J., 2001, New evidence for the geological origins of the ancient Delphic oracle (Greece), *Geology*, **29**, 707 – 710
- Diogo, L. A., Diagon, L. F. M. M., and Prado R. L., 2004, Bedrock imaging using post-critical shallow seismic reflection data: *Journal of Applied Geophysics*, **57**, 1 – 9
- Dix, H. C., 1955, Seismic velocities from surface measurements: *Geophysics*, **XX**, no. 1, 68 – 86
- Domes, F., 2004, 2-D travelttime inversion of near surface refractions and reflections in support of hydrogeological studies, (supervisors, D.R. Schmitt (U of Alberta) F. Wenzel (Uni-Karlsruhe)), Diplomarbeit, research at U of Alberta with defence at Geophysikalisches Institut der Universitat Karlsruhe, pp. 123
- Edge, A. B., and Laby, T. H., 1931, The principles and practice of geophysical prospecting: Cambridge University Press, 339 – 341
- Ellis, D. V., 1987, Well logging for earth scientists: Elsevier Publishing
- Fennell, J. W., Sikstrom, C., and Lukie, T., 2001, A multidisciplinary approach to resolving complex hydrogeologic systems (Extended Abstract): *In*, An Earth Odyssey, 2nd The Canadian Geotechnical Society (CGS) and International Association of Hydrogeologists (IAH) joint conference
- Fenton, M. M., Schreiner, B. T., Nielsen, E., and Pawlowicz, J. G., 1994, Quaternary geology of western plains; *in* Geological atlas of western Canadian basin, G. D. Mossop and I. Shetson (comp.), Canadian Society of Petroleum Geologists and Alberta Research Council, Calgary, Alberta
- Fenton, M.M., Pawlowicz, J.G., Prior, P. G. J., and Olson, R. A., 2003, Quaternary geology of northern Alberta: Implications for Kimberlite exploration: (Expanded Abstract): *In* 8th International Kimberlite Conference Long Abstract.

- Fenton, M. M., Schreiner, B. T., Nielsen, E., and Pawlowicz, J. G., 1994, Quaternary Geology of Western Plains; in Geological Atlas of the Western Canada Sedimentary Basin, G.D. Mossop and I. Shetson (comp.), Canadian Society of Petroleum Geologists and Alberta Research Council, Calgary, Alberta, URL
<http://www.ags.gov.ab.ca/publications/ATLAS_WWW/ATLAS.shtml>,
[July, 15 2006].
- Feroci, M. L., Balia, O., Bosman, R. C., Cardarelli E., and Deidda, G., 2000, Some considerations on shallow seismic reflection surveys: Journal of Applied Geophysics, **45**, 127 – 139
- Forel, D., Benz, T., and Pennington, W. D., 2005, Seismic data processing with Seismic Un*x: A 2D seismic data processing primer: Gochioco, L. M., Series Editor, Course Notes Series No. 12, Soc. of Expl. Geophys., Tulsa, Oklahoma
- Francese, R., Guidici, M., Schmitt, D. R., and Zaja, A., 2005, Mapping the geometry of an aquifer system with a high-resolution reflection seismic profile: Geophysical Prospecting, **53**, 817 – 828
- Francese, R., Hajnal, Z. G., and Prugger, A., 2002, High-resolution images of shallow aquifers – A challenge in near-surface seismology: Geophysics, **67**, 177 – 183
- Froese, D. G., Smith, D. G., and Clement, D. T., 2005, Characterizing large river history with shallow geophysics: Middle Yukon River, Yukon Territory and Alaska: Geomorphology, **67**, 391 – 406
- Fulton, R. J., 1989, Quaternary Geology of Canada and Greenland: Minister of Supply and Services Canada
- Gardner, L.W., 1939, An areal plan of mapping subsurface structure by refraction shooting: Geophysics, **4**, 247 – 259
- Ghose, R., Nijhof, V., Brouwer, J., Matsubara, Y., Kaida, Y., and Takahashi, T., 1998, Shallow to very shallow, high-resolution reflection seismic using a portable vibrator system: Geophysics, **63**, 1295 – 1309
- Griffiths, H. D., and Barker, R. D., 1993, Two dimensional resistivity imaging and modelling in areas of complex geology: Journal of Applied Geophysics, **29**, 211 – 226

- Hall, H. D., and Hajnal, Z., 1962, The Gravimeter in studies of buried valleys: *Geophysics*, **6**, 936 – 951
- Hagedoorn, J.G., 1959, The plus-minus method of interpreting seismic refraction sections: *Geophysical Prospecting*, **7**, 158 – 182
- Hampson, D., and Russell B., 1984, First-break interpretation using generalized linear inversion, *J. Can. Soc. Expl. Geophys.*, **20**, 40 – 50
- Hobson, G. D., Hunter, J. M., A., and Scott, J. S., 1970, A shallow seismic survey, elastic constants studies and surficial geology of part of defence research establishment Suffield (Dres), Suffield, Alberta: Geological Survey of Canada, paper 69 – 13
- Holzschuh, J., 2002, Low-cost geophysical investigations of a paleochannel aquifer in the Eastern Goldfields, Western Australia: *Geophysics*, **67**, 690 – 700
- Hole, J. A., 1992, Nonlinear High-Resolution three-dimensional seismic travel time tomography: *Journal of Geophysical Research*, **97**, 6553 – 6562
- Hole, J. A., and Zelt, B. C., 1995, 3D finite difference reflection traveltimes: *Geophysical Journal International*, **121**, 427 – 434
- Hunter, J. A., Pullan, S. E., Burns, R. A., Good, R. L., Harris, J. B., Pugin, A., Skvoetsov, A., and Goriainov, N. N., 1998, Downhole seismic logging for high-resolution reflection surveying in unconsolidated overburden: *Geophysics*, **63** 1371 – 1384
- Huuse, M., and Anderson, H. L., 2000, Overdeepened Quaternary valleys in the eastern Danish North Sea: morphology and origin: *Quaternary Science Reviews*, **19**, 1233 – 1253
- Huuse, M., Piotrowski, J. A., and Anderson, H. L., 2003, Geophysical investigation of buried Quaternary valleys in formerly glaciated NW European lowland: significance for groundwater exploration, Editorial: *Journal of Applied Geophysics*, **53**, 153 – 157
- Iaco, D. R., Green, A. G., Maurer, H. R., and Horstmeyer, H., 2003, A combined seismic reflection and refraction study of a landfill and its host sediments: *Journal of Applied Geophysics*, **52**, 139 – 156

- Ivanov, J., Miller, R. D., Xia, J., Steeples D., and Park, C. B., 2005a, The inverse problem of refraction travel times, Part I: Types of geophysical nonuniqueness through Minimization: *Pure and Applied Geophysics*, **162**, 447 – 459
- Ivanov, J., Miller, R. D., Xia, J., and Steeples, D., 2005b, The inverse problem of refraction travel times, Part II: Quantifying refraction nonuniqueness using three layer-model: *Pure and Applied Geophysics*, **162**, 461 – 477
- Jianji, H., Lirong, D., and Qiming, L., 1999, The Geology of Natural Gas in the People's Republic of China: A Review: *Journal of Petroleum Geology*, **22**(2) 191 – 213
- Jim, L., Miller, R., Muehlenbachs, K., and Rostron, B., 2000, Stable isotope geochemistry of some natural gas macroseeps in Alberta: Extended abstract, In 2000 Annual Conference of Can. Soc. of Expl. Geophys.
- Joseph, H. R., Nelson, P. H., and Paillet, F. L., 2000, Well logging for physical properties: a handbook for geophysicists, geologists, and engineers; 2nd edition: Wiley Publishers
- Junlin, C., Palm, H., Müllern, C. F., and Wållberg, B., 2002, Imaging of groundwater resources in glacial deposits using High-resolution reflection seismics, Sweden: *Journal of Applied Geophysics*, **51**, 107 – 120
- Kelly, R. G., Dupere, S., Adel-Mauuel, M., Lizotte, A. H., and Hugolt, B., 1994, Le developement des stockages souterrains de gaz naturel au Québec (in French): Internal Report, Hydro- Québec Pétrole et Gaz, Place Iberville II, 1175, rue Lavigerie, Bureau 050, Sainte-Foy (Québec) G1V 4P1
- Klassen, E. W., 1989, Quaternary geology of the southern Canadian Interior Plains. In Chapter 2 of Quaternary geology of Canada and Greenland, R. J. Fulton (ed.), Geological Survey of Canada, Geological of Canada, no. 1 (also Geological Society of America, The Geology of North America, v. K-1) p. 138 – 174
- Kuhn, O., 2004, Ancient Chinese drilling, Can. Soc. Expl. Geophy., Recorder, June, 39 – 43
- Lennox, H. D., and Carlson, V., 1967, Geophysical exploration for buried valleys in an area north of two hills, Alberta: *Geophysics*, XXXII, No. 2, 331 – 362

- Lin, C.M., Gu, L. X., Li, G. Y., Zhao, Y. Y., and Jiang, W. S., 2004, Geology and formation mechanism of late Quaternary shallow biogenic gas reservoirs in the Hangzhou Bay area, eastern China: AAPG Bulletin, **88**(5), 613 – 625
- Loke, M. H., 2004, Tutorial: 2D and 3D Electrical Imaging Surveys. Geotomo Software: Penang, Malaysia. Available from <http://www.geoelectrical.com/> [Cited July 22, 2006]
- Loke, M. H., and Barker R. D., 1996, Rapid least-squares inversion of apparent resistivity pseudosections by a quasi-newton method: Geophysical Prospecting, **44**, 131 – 152
- Lyatsky, H.V., Pana, D., Olson, R., and Godwin, L., 2004. Detection of subtle basement faults with gravity and magnetic data in the Alberta Basin, Canada: a data-use tutorial; The Leading Edge, **23**, 1282 – 1288
- Mathews, W. H., 1980, Retreat of the last ice sheets in northeastern British Columbia and adjacent Alberta: Geological Survey of Canada, Bulletin – 331
- McKercher, R. B., and Wolf, B., 1986, Understanding Western Canada's Dominion Land Survey System. Saskatoon: Division of Extension and Community Relations, University of Saskatchewan.
- Meyer, R. F., 1984, Shallow oil and gas resources, Proceedings of the first international conference, United Nations Institute for training and research (UNITAR), Current development in exploration, production, economics, and legal issues
- Miller, R. D., Pullan, S. E., Steeples, D. W., and Hunter, J., 1992, Field comparison of shallow seismic sources near Chino, California: Geophysics, **57**, 693 – 709
- Miller, R. D., 1992, Normal moveout stretch on shallow-reflection data: Geophysics, **57**, 1502 – 1507
- Miller, R. D., and Xia, J., 1998, Large near-surface velocity gradients on shallow seismic reflection data: Geophysics, **63**, 1348 – 1356
- Miller, R. D., Markiewicz, R. D., Merey, C., Xia, J., and Maples, C. G., 1995, Improvements in shallow high-resolution seismic reflection through PC-based systems: Computers and Geoscience, **21**, 957 – 964

- Mossop, G.D., and Shetsen, I., 1994, Geological atlas of the Western Canada Sedimentary Basin: Canadian Society of Petroleum Geologists and Alberta Research Council, Calgary, Alberta, URL <http://www.ags.gov.ab.ca/publications/ATLAS_WWW/ATLAS.shtml>, [13 June, 2006].
- Moret, Geoff J. M., Knoll, M. D., Barrash, W., and Clement, W. P., 2006, Investigating the Stratigraphy of an alluvial aquifer using crosswell seismic travelttime tomography, *Geophysics*, **71**, B63 – B73
- Musil, M., Maurer, H., Green, A. G., Horstmeyer, H., Nitsche, F. O., Mühill, D. V., and Springman, S., 2002, Shallow seismic surveying of an Alpine glacier: *Geophysics*, **67**, 1701 – 1710
- Nardis, D., Cardarelli, R., E., Dobroka, M., 2005, Quasi-2D hybrid joint inversion of seismic and geoelectric data: *Geophysical Prospecting*, **53**, 705 – 716
- Nassir, S.S.A., Loke, M. H., Lee, C. Y., and Nawawi, M.N.M., 2000, Salt water intrusion mapping by geoelectrical imaging surveys: *Geophysical Prospecting*, **48**, 647 – 661
- Oldenbrger, G. A., Routh, P. S., and Knoll, M. D., 2005, Sensitivity of electrical resistivity tomography data to electrode position errors: *Geophysical Journal International*, **162**, 1 – 9
- Oldenburg, D. W., and Li, Y., 1999, Estimating depth of investigation in dc resistivity and IP surveys: *Geophysics*, **64**, 403 – 416
- Olsen, H., Ploug, C., Nielsen, U., and Sorensen, K., 1993, Reservoir characterization applying high resolution seismic profiling, Rabis Creek, Denmark: *Ground Water*, **31**, 84 – 90
- Palmer, D., 1981, An introduction to the generalized reciprocal method of seismic refraction interpretation: *Geophysics*, **46**, 1508 – 1518
- Pawlowicz, J. G., Hickin, A. S., Nicoll, T. J., Fenton, M. M., Plouffe, A. and Smith, I.R. 2004, Shallow gas in drift: northwestern Alberta; Alberta Energy and Utility Board, EUB/AGS Information Series – 130
- Pawlowicz, J. G., Hickin A. S., Nicoll, T. J., Fenton, M.M., Paulen, R.C., Plouffe, A. and Smith, I. R., 2005a, Bedrock topography of the Zama Lake area, Alberta (NTS 84L); Alberta Energy and Utility Board, EUB/AGS Map 328, scale 1:250,000.

- Pawlowicz, J. G., Hickin A. S., Nicoll, T. J., Fenton, M.M., Paulen, R.C., Plouffe, A. and Smith, I. R., 2005b, Drift thickness of the Zama Lake area, Alberta (NTS 84L); Alberta Energy and Utility Board, EUB/AGS Map 329, scale 1:250,000.
- Pawlowicz, J. G., Nicoll, T. J., Fenton, M. M., Ahmad, J., Schmitt, D. R., Rokosh, D., and Plouffe, A., 2005c, Bedrock topography and drift thickness mapping show potential for shallow gas, Northwestern Alberta, Canada: AAPG, Search and Discovery article # 10086 (2005), [pdf], [Cited, July, 15 2006]
<http://www.searchanddiscovery.com/documents/2005/pawlowicz/images/pawlowicz.pdf>
- Pugin, A., and Rossetti, S., 1992, Acquisition of land based high resolution seismic profiles in glacial basins, two case studies in the Alpine foreland of Switzerland: *Eclogae Geol. Helv.* **85/2**, 491 – 502
- Pugin, A., and Pullan, S. E., 2000, First arrival alignment static corrections applied to shallow seismic reflection data: *Journal of Environmental and Engineering Geophysics (JEEG)*, **5**, 7 – 15
- Pullan, S. E., and Hunter, J. A., 1985, Seismic model studies of the overburden-bedrock reflection: *Geophysics*, **50**, 1684 – 1688
- Pullan, S. E., 1990, Recommended standard for seismic (/radar) files in the personal computer environment: *Geophysics*, **55**, 1260 – 1271
- Ronen, J., and Claerbout, J. F., 1985, Surface consistent residual statics estimation by stack-power maximization: *Geophysics*, **50**, 2759 – 2767
- Safety bulletin 2005-01, 2005, Energy Utility Board (EUB), [html, pdf]. Available from <http://www.eub.gov.ab.ca/BBS/requirements/safetybulletins/2005-01.htm> [Cited August 11, 2005]
- Schlumberger, 1989, Log Interpretation Principles / Applications: Schlumberger, [pdf] Available from, <http://www.slb.com/content/services/resources/books/index.asp?> [Cited July 15 2006]
- Schmelzbach, C., Green, A.G., and Horstmeyer H., 2005, Ultra-shallow seismic reflection imaging in a region characterized by high source-generated noise: *Near Surface Geophysics*, **3**, 33 – 46

- Schmitt, D. R., 1999, Seismic attributes for monitoring of a shallow heated heavy oil reservoir: A case study, *Geophysics*, **64**, 368 – 377
- SEG Technical Standards Committee, 2002, SEG Y rev 1 Data Exchange format: Soc. Expl. Geophys., Tulsa, Oklahoma
- SEG Technical Standards Committee on Ancilliary Data Formats, 1995, Shell Processing Support Format For Land 3-D Surveys: *Geophysics*, **60**, 596 – 610
- Sharpe, D. R., Pugin, A., Pullan, S. E., and Gorrell, G., 2003, Application of seismic stratigraphy and sedimentology to regional hydrogeological investigations: as example from Oak Ridges Moraine, southern Ontario, Canada: *Can. Geotech. J.*, **40**, 711 – 730
- Sheriff, R. E., 2002, *Encyclopedic Dictionary of Applied Geophysics*, 4th edition: Soc. of Expl. Geophys., Tulsa, Oklahoma
- Shearer, P., 1999, *Introduction to seismology*: Cambridge University Press, pg. 82
- Shurr, G. W., and Ridgley J. L., 2002, Unconventional shallow biogenic gas systems: *AAPG Bulletin*, **86**, 1939 – 1969
- Simmons, J. L., and Backus, M. M., 1992, Linearized tomographic inversion of first-arrival times: *Geophysics*, **57**, 1482 – 1492
- Sjögren, B., 1984, *Shallow refraction seismics*: Publisher, Chapman and Hall
- Stalker, A. M., 1960, Buried Valleys in Central and Southern Alberta: *Geological Survey of Canada*, paper 60 – 32
- Stea, R. R., and Pullan, S., 2001, Hidden Cretaceous basins in Nova Scotia: *Can. J. Earth Sci.*, **38**, 1335 – 1354
- Storz, H., Storz, W., and Jacobs, F., 2000, Electrical resistivity tomography to investigate geological structures to the earth's upper crust: *Geophysical Prospecting*, **48**, 455 – 471
- Spies, B. R., 1983, Recent developments in the use of surface electrical methods for oil and gas exploration in the Soviet Union: *Geophysics*, **48**, 1102 – 1112
- Steeple, D., 2004, *Near Surface Seismology: A Short Course*: Soc. of Expl. Geophys., Tulsa, Oklahoma

- Steeple, D. W., Miller, R. D., and Black, R. A., 1990, Static corrections from shallow-reflection surveys: *Geophysics*, **55**, 769 – 775
- Steeple, W. D., and Miller, R. D., 1998, Avoiding pitfalls in shallow seismic reflection surveys: *Geophysics*, **63**, 1213 – 1224
- Steeple, D. W., Green, A. G., McEvilly, T. V., Miller, R. D., Doll W. E., and Rector, J. W., 1997, A workshop examination of shallow seismic reflection surveying: *The leading Edge (TLE)*, **16**, 1641 – 1647
- Stefani, J. P., 1995, Turning-ray tomography, *Geophysics*: **60**, 1917-1929
- Taner, T. M., and Koehler, F., 1969, Velocity spectra – digital computer derivation applications of velocity functions: *Geophysics*, **34**, 859 – 881
- Telford, W. M., Geldart, L. P., and Sheriff R. E., 1991, *Applied Geophysics*, 2nd edition: Cambridge University Press
- Vidale, J. E., 1990, Finite-difference calculation of traveltimes in three dimension: *Geophysics*, **55**, 521 – 526
- Widess, M. B., 1973, How thin is a thin bed: *Geophysics*, **38**, 1176 – 1180
- Wiederhold, H., Buness, H. A., and Bram, K., 1998, Glacial structures in northern Germany revealed by a high resolution reflection seismic survey: *Geophysics*, **63**, 1265 – 1272
- Whiteley, R. J., Hunter, J. A., Pullan, S. E. and Nutalaya, P., 1998, “Optimum offset” seismic reflection mapping of shallow aquifers near Bangkok, Thailand: *Geophysics*, **63**, 1385 – 1394
- Yilmaz, Ö., 1987, *Seismic Data Processing*: Soc. of Expl. Geophys., Tulsa, Oklahoma
- Yilmaz Ö., 2001, *Seismic data processing: inversion, and interpretation of seismic data*: Soc. of Expl. Geophys.,
- Zhu, X., Sixta, D. P., and Angstman, B. G., 1992, Tomostatics: Turning-ray tomography + static correction: *The Leading Edge (TLE)*, **11**, 15 – 23
- Zonge, K., Wynn, J., and Urquhart S., 2005, Resistivity, Induced Polarization, and Complex Resistivity, *In Near Surface Geophysics*, Edited by Butler D. K., Soc. of Expl. Geophys., Tulsa, Oklahoma, pg. 265 – 300.